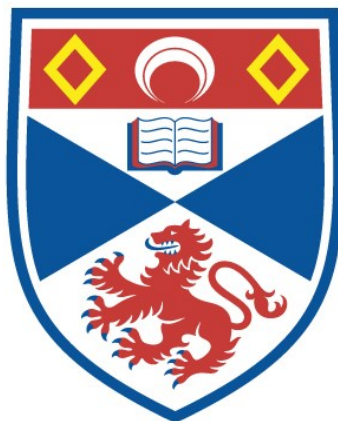


OPTICAL AND MASS SPECTROMETRIC STUDIES OF  
MICROWAVE DISCHARGES

Janet A. Hewitt

A Thesis Submitted for the Degree of PhD  
at the  
University of St Andrews



1986

Full metadata for this item is available in  
St Andrews Research Repository  
at:  
<http://research-repository.st-andrews.ac.uk/>

Please use this identifier to cite or link to this item:  
<http://hdl.handle.net/10023/13754>

This item is protected by original copyright

UNIVERSITY OF ST. ANDREWS

Thesis Copyright Declaration Form.

A UNRESTRICTED

"In submitting this thesis to the University of St. Andrews I understand that I am giving permission for it to be made available for public use in accordance with the regulations of the University Library for the time being in force, subject to any copyright vested in the work not being affected thereby. I also understand that the title and abstract will be published, and that a copy of the work may be made and supplied to any bona fide library or research worker."

B RESTRICTED

"In submitting this thesis to the University of St. Andrews I wish access to it to be subject to the following conditions:

for a period of **5** years [maximum 5] from the date of submission the thesis shall be

a) withheld from public use.

b) made available for public use only with consent of the head or chairman of the department in which the work was carried out.

I understand, however, that the title and abstract of the thesis will be published during this period of restricted access; and that after the expiry of this period the thesis will be made available for public use in accordance with the regulations of the University Library for the time being in force, subject to any copyright in the work not being affected thereby, and a copy of the work may be made and supplied to any bona fide library or research worker."

Declaration

I wish to exercise option **Bb** [i.e. A, Ba or Bb] of the above options.

Signature

Date 25/4/86

ProQuest Number: 10167411

All rights reserved

INFORMATION TO ALL USERS

The quality of this reproduction is dependent upon the quality of the copy submitted.

In the unlikely event that the author did not send a complete manuscript and there are missing pages, these will be noted. Also, if material had to be removed, a note will indicate the deletion.



ProQuest 10167411

Published by ProQuest LLC (2017). Copyright of the Dissertation is held by the Author.

All rights reserved.

This work is protected against unauthorized copying under Title 17, United States Code  
Microform Edition © ProQuest LLC.

ProQuest LLC.  
789 East Eisenhower Parkway  
P.O. Box 1346  
Ann Arbor, MI 48106 – 1346

Optical and Mass Spectrometric Studies of  
Microwave Discharges

A thesis presented by  
J A Hewitt, BA  
to the  
University of St Andrews  
in application for the degree of  
Doctor of Philosophy  
January 1986



### Declaration

I hereby certify that this thesis has been composed by me, and is a record of work done by me, and has not previously been presented for a higher degree.

This research was carried out in the Physical Sciences Laboratory of St Salvator's College, in the University of St Andrews, under the supervision of Dr A Maitland.

J A Hewitt

Certificate

I certify that J A Hewitt BA has spent nine terms at research work in the Physical Sciences Laboratory of St Salvator's College, in the University of St Andrews, under my direction, that she has fulfilled the conditions of Ordinance No 16 (St Andrews) and that she is qualified to submit the thesis in application for the Degree of Doctor of Philosophy.

A Maitland

Research Supervisor

### Author's Career

The author was born in Belfast in 1961. Primary education was at Glengormley, Co Antrim. Secondary education was at Belfast Royal Academy. A BA in Physics and Theoretical Physics was obtained at the University of Cambridge (1979-1982). From October 1982 the author has been working on microwave excitation of gases at the University of St Andrews. The research was sponsored by English Electric Valve Co Lincoln.

### Acknowledgements

I wish to thank Dr A Maitland for his help, encouragement and advice throughout this work. Thanks are also due to Dr J Broadhead of EEV, for his help and supervision of my work at Lincoln. I gratefully acknowledge many helpful discussions on various aspects of the work with my colleagues, both at St Andrews and Lincoln. Thanks too, to my parents and friends for their encouragement and support.

Finally, I wish to thank English Electric Valve Co, Lincoln for their sponsorship of this work.

### Abstract

The structure, operation and performance characteristics of the TR cell and its role in microwave duplexing in a radar system are discussed. Theory of the microwave discharge is discussed, and the mathematics of microwave transmission along a waveguide examined. Two computer models are established; one to model the transfer of heat from the microwave discharge in the cell to the cell window, and one to model the operation of the TR cell, in terms of the reaction kinetics of the gases within. The results of both models are compared with experimental observations. Finally, the gas in the cell is analysed throughout the manufacturing procedure of the cell and during its operation.

Study of the mathematics of microwave transmission along a waveguide leads to expressions for the conductivity, and reflection and transmission coefficients for an ionized gas, resulting in calculations of the electron density in the ionized gas as a function of input power.

A computer program to model the heat transfer from the microwave discharge in the TR cell to the cell window has been written. Good agreement with experimental results has been obtained. The temperatures at selected points on the TR cell window, frame and flange are calculated, using the finite difference method. The power incident on the window is input to the program together with the window dimensions and materials selected. The output from the program is in the form of

temperatures at selected points across the TR cell window, frame and flange. The temperature at which a window is likely to fail is estimated from the results of the program.

Three different techniques are used in the analysis of the gas in the TR cell during its manufacture and operation. They are the study of relative changes in peak heights in the microwave-excited optical emission spectrum of the gas, using an optical spectrum analyser with a recording facility, measurement of the performance of the cell when subject to high power microwave pulses and finally, mass spectrometry of the gases in the cell. Several batches of cells were studied. Using the results from these different analytical techniques, the manufacturing procedure and the operation of the cell are discussed. The batch of cells analysed using mass spectrometry contained traces of oxides of carbon and nitrogen, which were shown to have a negative influence on the performance of the cells.

Finally, a computer model of the operation of the TR cell is established. The reaction rates and cross sections of the species likely to be present are calculated from the available literature. The model predicts the number densities of the species present as a function of the operating time of the cell and is used to predict the useful lifetime of the cell. The partial success of the model is due in part to the scarcity of reaction rate data for the microwave discharge.

## Contents

1	Introduction
3	Chapter 1 The TR Cell
3	1.1 Introduction
3	1.2 The TR Cell in the Radar System
6	1.3 Duplexer Systems
6	1.3.1 The Branched Duplexer System
7	1.4 TR Cell Components
7	1.4.1 Body
8	1.4.2 Glass Window
8	1.4.3 Gas Filling
9	1.4.4 Resonant Structures
11	1.5 Performance Characteristics of the TR Cell
11	1.5.1 Insertion Loss
12	1.5.2 Voltage Standing Wave Ratio
12	1.5.3 Arc Loss
13	1.5.4 Leakage Power
13	1.5.4 (1) Introduction
13	1.5.4 (2) Spike Leakage Energy
14	1.5.4 (3) Flat Leakage Power
14	1.5.5 Low Power Breakthrough
14	1.5.6 Recovery Time
16	1.6 Cell Lifetime
17	1.7 Pre-TR Tube
18	References
19	Chapter 2 The Microwave Discharge and Microwave Transmission
19	2.1 Introduction
19	2.2 Microwave Breakdown and Microwave Transmission

23	2.3 Collision, Diffusion, Attachment and Recombination
23	2.3.1 Collisions
24	2.3.2 Diffusion
26	2.3.3 Attachment
27	2.3.4 Recombination
28	2.4 Electron Energy Distribution Function
30	2.5 Microwave Transmission
30	2.5.1 Maxwell's Equations
31	2.5.2 Derivation of the Wave Equation for a Non Conductor
31	2.5.3 Radiation in a Waveguide and the Waveguide Equation
33	2.5.4 Power Transmitted along a Waveguide- no Attenuation
34	2.5.5 The Wave Equation for a Good Conductor
35	2.5.6 Attenuation along a Waveguide and Skin Depth
38	2.6 Glass
39	2.7 Characteristics of an Ionized Gas
42	2.8 Critical Electron Density
43	2.9 Transmission, Reflection and Refraction at a Boundary
46	2.10 Theory of the TR Cell Recovery Period
49	References
51	Chapter 3 The Heat Transfer Computer Program
51	3.1 Introduction
52	3.2 Heat Transfer Theory
52	3.2.1 Conduction
53	3.2.2 Convection
53	3.2.3 Radiation
54	3.2.4 Derivation of the Heat Transfer Equation
55	3.3 Glass
55	3.3.1 Introduction
56	3.3.2 Viscosity and Temperature

57	3.4	The Computer Model
57	3.4.1	Introduction
59	3.4.2	Finite Difference Method
61	3.4.3	Establishment of the Model
62	3.4.4	Calculation of the Frame and Flange Temperatures
63	3.5	Results
63	3.5.1	Results of the Computer Program
66	3.5.2	Comparison with Experimental Results- EEV Co Data
69	3.6	Further Consideration of the Approximations
69	3.6.1	Radiation and Convection Losses
70	3.6.2	Variation of Specific Heat and Thermal Conductivity with Temperature
72	3.6.3	Arc Loss
73	3.7	Conclusions
75		References
76	Chapter 4	Analysis of the TR Cell using Emission Spectra and Microwave Measurements
76	4.1	Introduction
78	4.2	Emission Spectra
78	4.2.1	Introduction
78	4.2.2	Atomic Spectra
80	4.2.3	Molecular Spectra
84	4.3	Emission Spectra Measurements
84	4.3.1	Introduction
84	4.3.2	Operation of the OSA
86	4.3.3	Spectral Analysis of the TR Cell Discharge
87	4.3.4	Experimental Technique
88	4.4	Microwave Measurements
88	4.4.1	Introduction

89	4.4.2	Low Power Measurements
89	4.4.2 (1)	VSWR
90	4.4.2 (2)	Insertion Loss
91	4.4.3	High Power Measurements
91	4.4.3 (1)	Keep-Alive Current
91	4.4.3 (2)	Spike Leakage Energy
92	4.4.3 (3)	Total Leakage Power
93	4.4.3 (4)	Recovery Time
93	4.4.3 (5)	Low Power Breakthrough
94	4.5	TR Cell Experiments
94	4.5.1	Manufacturing Procedure
94	4.5.1 (1)	Hot Exhaust
95	4.5.1 (2)	Age Stand
95	4.5.1 (3)	Ageing
95	4.5.1 (4)	Cold Refill
96	4.5.2	Experimental Procedure
97	4.6	Discharge in a Pre-TR Tube
97	4.6.1	Introduction
99	4.6.2	Impurities in Pre-TR Tubes
101	4.7	Results of TR Cell Experiments
108	4.7.1	Effect of Keep-Alive Discharge on Life
109	4.8	Results for the Experimental Batch of Cells
116	4.9	Cells which Fail
119	4.10	Summary and Conclusions
125		References
126	Chapter 5	Mass Spectroscopic Analysis of the Gas in the TR Cell
126	5.1	Introduction
126	5.2	Quadrupole Mass Spectrometer
130	5.3	Experimental Apparatus

131	5.4	Experimental Procedure
135	5.5	Effect of Keep-Alive Discharge on Cell Life
135	5.5.1	Introduction
136	5.5.2	Results of Microwave and Emission Spectra Measurements
139	5.5.3	Mass Spectra Results
141	5.5.4	Conclusions
142	5.6	Cells Tested at Intervals Throughout Life
142	5.6.1	Introduction
143	5.6.2	Results of Microwave and Emission Spectra Measurements
145	5.6.3	Mass Spectra Results
146	5.6.4	Conclusions
147	5.7	Summary and Conclusions
149		References
151	Chapter 6	Computer Model of the TR Cell Discharge
151	6.1	Introduction
151	6.2	Reactions of Argon
153	6.3	Water Vapour
155	6.4	The Microwave Discharge in Argon and Water Vapour
158	6.5	The Model
158	6.5.1	Introduction
159	6.5.2	The Microwave Pulse
160	6.5.3	The Recovery Period
162	6.5.4	The Period Between Pulses
163	6.6	The Computer Program
164	6.7	Results of the Computer Program
164	6.7.1	Number Densities of Species Created Throughout a Cycle
165	6.7.2	Variation of the Ionization Rate of Argon
166	6.7.3	Variation of the Recombination Rate of O, H and OH Radicals
167	6.7.4	Variation of Input Electron Density

167	6.7.5	Variation of the Initial Number Density of the Species
168	6.7.6	Comment on the Results
170	6.8	Surface Reactions
170	6.8.1	Chemisorption
170	6.8.2	Absorption
170	6.8.3	Adsorption
171	6.8.4	Outgassing
171	6.8.5	Cleanup in TR Cells
173	6.8.6	Discussion of the TR Cell Manufacturing Procedure
174	6.9	Surface Recombination
177	6.10	Conclusions
179		References
183		Conclusions
187	Appendix 1	Physical Properties and Dimensions of the Materials in the TR Cell
189	Appendix 2	Heat Transfer Computer Program
192	Appendix 3	Magnetron
194	Appendix 4	The t-Test
196	Appendix 5	Computer Program to Analyse the Mass Spectra Data
200	Appendix 6	The Computer Program to Model the TR Cell Discharge

## Introduction

In a pulsed radar system a microwave duplexer, containing a TR cell, is required to enable the same antenna to be used for both transmission and reception by protecting the receiver from the high power transmitted signal and allowing the low power reflected signal to reach the receiver with the minimum attenuation. Ideally, the gas in the cell should break down immediately the high power microwave pulse reaches it and it should deionize as soon as the high power pulse ends, to allow reception of the low power reflected signal. The TR cell is designed to optimise these conflicting requirements.

The TR cell was designed during the Second World War, in the development of radar. However, the complexities of the microwave discharge utilised in its operation require fuller understanding than previously achieved in order to meet the requirements for the modern radar system.

Developments in computerised instrumentation now provide measurement facilities which have not been available hitherto. One of the most sensitive indicators of change in gas discharge systems is its optical spectrum. The optical spectrum can be displayed within seconds on an Optical Spectrum Analyser and stored on computer. The Optical Spectrum Analyser utilises a diffraction grating and a vidicon detector. The spectra may be displayed on a screen or output to a pen recorder or to a computer. From the

spectra, atoms and molecules present in the microwave discharge in the cell may be identified. In the past, such information could only be obtained by microdensitometric measurements of spectrographic plates in a total process from exposure to chart recording which typically required several hours. As a result, optical spectra have been generally neglected in the investigation of TR cell performance.

Mass spectrometric studies of the gas in the TR cell provide information on the cell performance, for example during its life. Along with measurements of the performance of the TR cell when subjected to high power microwave pulses, it is the aim of this work to provide additional information on the TR cell, with the aim of improving performance and/or life.

## Chapter 1 The TR Cell

### 1.1 Introduction

The TR cell is a component in a radar system. In this chapter, the basic radar theory will be introduced and the role of the TR cell in radar explained. The construction of the TR cell is described and the various terms used in conjunction with the TR cell to describe its construction and performance are listed and defined.

### 1.2 The TR Cell in the Radar System

A radar system consists of a signal transmitter, a receiver and duplexer and an antenna for the transmission and reception of signals. A signal in the form of a microwave pulse is transmitted by the antenna and the reflected or reradiated signal from the target is analysed in the receiver. To achieve good resolution in range, a short pulse of energy is required. For good resolution in direction very narrow angled beams of very short wavelength are necessary. It is found that microwave radiation of typically 3 cm or 10 cm is used.

The radar equation is

$$P_r = P_t (G/4\pi r^2) (A/4\pi r^2) \quad (1.1)$$

where  $P_r$  is the received power,  $P_t$  is the transmitted power,  $G$  is the antenna gain,  $r$  is the target distance,  $A$  is the effective area

of the antenna and  $\sigma$  is the target scattering cross section.

The technical difficulties involved in aligning two scanning antennae geometrically to sufficient accuracy are avoided by combining the transmission and reception antennae into a single antenna. The system cost and weight are also reduced thereby. Transmitted power can be of the order of megawatts. Since the received power is likely to be in microwatts and since the transmitter and receiver both use the same antenna, it is necessary to protect the receiver input from the transmitted pulse when the radar system is in transmission. The microwave duplexer with a TR (Transmit-Receive) cell is the device normally employed to protect the receiver. Basically the TR cell is a high frequency switch, switching the receiver out of circuit when the radar system is in transmission and switching it back into circuit in time to accept the reflected signal.

The operating requirements for a TR cell are listed below.

- (1) When the radar is in transmission, the cell must connect the transmitter to the antenna and disconnect the receiver.
  
- (2) The cell must protect the receiver input from the transmitted power when the system is in transmission.

(3) After transmission, the cell must rapidly disconnect the transmitter and connect the receiver to the antenna.

(4) The cell must introduce minimum attenuation to the received signal.

The TR cell also performs the important function of passive protection of the receiver against high power signals reaching the antenna from other radar systems. These signals may easily damage the receiver input, even when the radar system is switched off.

A typical radar system operates at a pulse repetition frequency (prf) of 1 kHz, with a microwave pulse length of 1 microsecond. The activation time for the TR cell switch must therefore be about 0.01 microseconds.

The TR cell consists of a sealed length of rectangular waveguide containing two resonant structures at a predetermined separation and filled with a gas mixture. A glass window, also a resonant structure, is sealed onto each end of the cell. The cell is constructed of metal, which minimises the resistive loss of the microwave power travelling through it and reduces energy loss by radiation. When a high power (transmitted) pulse enters the cell, the gas inside is ionized and the discharge, which approximates to a short circuit across the waveguide, reflects almost all of the transmitted power, preventing it from reaching the receiver. When a low power (reflected or re-radiated) pulse enters the cell, it

passes through to the receiver since it has insufficient power to ionize the gas.

### 1.3 Duplexer Systems

There are many types of duplexer system, for example one type employs a circulator to direct the transmitted power to the antenna and the received power to the receiver. The balanced duplexer employs two 3 dB hybrid couplers, which couple power between two adjacent waveguides, connected by a TR cell. Transmitted power enters via the first coupler and is reflected by the fired TR cell to the antenna. Received power travels via the antenna through the unfired TR cell and the second coupler to the receiver. In this thesis, the branched duplexer system, described in section 1.3.1 below, has been used; for convenience of operation, ease of the access of the discharge in the TR cell and consistency of power measurements.

#### 1.3.1 The Branched Duplexer System

In the branched duplexer radar system (see fig (1.1)), the transmitter and antenna are connected by a length of waveguide and the receiver is connected to this waveguide by another section of waveguide perpendicular to the first. The distances between this junction, the transmitter and the receiver are all calculated according to the wavelength of microwave radiation used. The TR cell is situated in front of the receiver at a distance  $n\lambda_g/2$  from the junction, where  $\lambda_g$  is the wavelength of the microwave radiation

in the waveguide and  $n$  is an integer. The portion of the transmitted pulse which travels down the waveguide towards the receiver is reflected by the TR cell in phase with the radiation travelling from the transmitter to the antenna. The distance from the transmitter to the junction is calculated such that the portion of the received signal which travels along the waveguide to the transmitter is reflected to the receiver in phase with the portion which travels directly to the receiver, ensuring that the maximum possible signal received by the antenna reaches the receiver. The branched duplexer system is simple and compact but the bandwidth over which it is designed to operate is small.

#### 1.4 TR Cell Components

##### 1.4.1 Body

The body of the cell, a length of rectangular waveguide (shown in fig (1.2)), is constructed in mild steel. A flange, also made of mild steel, is brazed onto each end of the cell. The whole body is copper plated to minimise resistive losses in the cell. A glass window in a kovar frame is brazed into the flange using a eutectic alloy of copper and silver.

#### 1.4.2 Glass Window

The windows in a TR cell are made from a borosilicate glass. The physical properties of the glass are listed in Appendix 1. This type of glass is used partly because its expansion characteristics match those of the kovar window frame over the whole range of temperatures encountered during the manufacture and use of the cell. The size and thickness of the window are calculated to allow maximum transmission of a low power signal of a given frequency through the cell. The window is a resonant element of a precise Q and frequency and is part of the multielement resonant system of the TR cell. An increase in window height requires a decrease in the window thickness for maximum transmission of a signal of a given frequency (EEV Co data).

#### 1.4.3 Gas Filling

The gas filling in a TR cell is a low pressure mixture of gases; one with a low ionization potential and one with a high electron capture cross-section. The gas pressure in the cell is chosen to minimise the breakdown and sustaining voltages of the discharge and to minimise the leakage of power through the cell (see section 1.5.4 for a fuller discussion of leakage power). Low ionization potential gases commonly used include  $H_2$ , Ar,  $N_2$  and He. In the early investigations, as described by Smullin and Montgomery (1948), it was discovered that argon was the most suitable. When a transmitted pulse enters the cell, the argon is

cell, the argon is ionized; the discharge then reflects the microwave pulse. At the end of the pulse there is no further ionization of the gas. The ionized gas then decays by recombination, diffusion to the walls and electron capture. A gas with a high electron capture cross-section is added to accelerate the process of electron removal and reduce the recovery time of the cell (see section 1.5.6 for a fuller discussion of the recovery time of the cell). Water vapour is the gas most commonly added to reduce the recovery time of the cell. Other gases which may be added include  $O_2$ , NO and  $SO_2$ .

#### 1.4.4 Resonant Structures

The cell contains two resonant structures, separated by a distance  $\lambda_g/4$  (see fig (1.2)). Each structure consists of an iris at right angles to a pair of cones forming an adjustable gap. The irises and cones are tuned to give the required bandwidth for low power signals. One cone, the one farthest from the input window of the cell, is provided with an electrode, the keep-alive electrode. The keep-alive discharge is generally a low current, dc glow. The keep-alive current is large enough to limit the spike leakage energy (described more fully in section 1.5.4) to a safe level, but low enough that the resultant electron density at the electrode has the minimum effect on the received signal. The electron density is of the order of  $10^{14} \text{ m}^{-3}$  (Harvey (1960)).

When the transmitter pulse begins, the electron density at the keep-alive electrode is low. When the electrons gain sufficient energy from the pulse to cause ionization, the electron density increases very rapidly. At the critical electron density the discharge creates a short-circuit of the cone gap at the keep-alive electrode. The second pair of cones is at a distance  $\lambda_g/4$  from the keep-alive electrode. Between the input window of the cell and the keep-alive electrode. Almost all the incident power is reflected from the keep-alive electrode and a standing wave with its voltage maximum at the second pair of cones is established. A discharge now forms at this cone gap; it reflects almost all of the power incident on it. The input window is situated at a distance approximately  $\lambda_g/4$  from the second pair of cones. A standing wave is set up with its voltage maximum at the window. If the input power level is sufficient, ionization occurs at the window and the discharge finally transfers to the region just inside the input window.

There are several advantages in having the discharge at the input window; the short-circuit created by the discharge across the window is more effective than the short circuit at the cone gaps, resulting in less leakage; the recovery time is reduced, since the discharge is more diffuse and electrons are captured more easily and, finally, the cones are protected from the discharge; bombardment by the ions damages the surface of the cones and the spike leakage may be increased thereby.

## 1.5 Performance Characteristics of the TR Cell

### 1.5.1 Insertion Loss

The insertion loss of the TR cell is a measure of the attenuation of the device to the received signal. This measurement is carried out at a power level below that required for breakdown of the gas in the cell. The insertion loss  $L$  of the cell is defined as

$$L = 10 \log_{10} (P_i / P_t) \quad , \quad (1.2)$$

where  $P_i$  is the power incident on the cell and  $P_t$  is the power transmitted through the cell. The magnitude of the loss depends on the dimensions and materials of the windows and on the locations and geometries of the resonant structures in the cell. Insertion loss comprises two components; reflection loss and dissipative loss. The reflection loss is the power reflected back towards the transmitter by the windows and the resonant structures. The windows and resonant structures are designed to minimise the reflection loss, which is of the order of -20 dB. The dissipative loss is the power absorbed by the windows and the cell body. A typical value for the insertion loss of a cell is 0.8 dB.

Experiments performed by Fiske (1945) during the development of the TR cell show that the insertion loss of the window increases as the height of the window decreases. As the thickness of the glass in the window is reduced, the insertion loss decreases. The insertion loss of the window is also reduced by decreasing both the

real and imaginary parts of the dielectric constant of the glass of the window (see Chapter 2 for a calculation of the power absorbed by the TR cell window).

### 1.5.2 Voltage Standing Wave Ratio

The voltage standing wave ratio or VSWR is the ratio of the incident to the reflected voltage when a low power signal is reflected by a TR cell. The bandwidth of the cell is the range of frequencies over which the VSWR does not exceed the maximum acceptable value.

### 1.5.3 Arc Loss

The arc loss is the power dissipated in the microwave discharge in the TR cell. This power represents a loss of transmitted power. The total arc loss is the sum of the power absorbed by the discharge and by the input window of the cell. The relationship between the arc loss  $P_{arc}$  and the power incident on the cell is given by

$$P_{arc} = 10 \log_{10} P_i / P_{ref} \quad , \quad (1.3)$$

where  $P_{ref}$  is the power reflected by the cell. Heat is transferred from the discharge, situated behind the input window of the cell, to the input window. If sufficient heat is transferred, the window will be damaged. In Chapter 3 a computer model of the variation of window temperature with input power is described. The model is used to predict power failure levels for a TR cell. For a pure argon discharge, the arc loss is very low. Adding water vapour

increases the arc loss. Arc loss increases with increasing partial pressure of water vapour. The arc loss decreases for decreasing window height (Smullin and Montgomery (1948)).

#### 1.5.4 Leakage Power

##### (1) Introduction

The leakage power includes all the microwave power incident on the receiver during the transmitting period. It comprises two components, the spike leakage energy and the flat leakage power (fig (1.3)). The total leakage power is the average leakage power during the transmitter pulse. The leakage power of a TR cell is limited to a value low enough to protect the receiver. The leakage power varies with the gas pressure in the cell.

##### (2) Spike Leakage Energy

The spike leakage energy is the energy transmitted to the receiver during the time interval between the beginning of the transmitter pulse and the establishment of the microwave discharge. The time interval is about  $10^{-8}$  seconds. The receiver input will be damaged by an energy level of about  $5 \times 10^{-8}$  Joules over this time period so the keep-alive electrode was introduced to limit the spike leakage energy to about  $10^{-8}$  Joules. The spike leakage energy is reduced by the presence of electrons at the keep-alive electrode, since the time for the establishment of the microwave discharge is so decreased. Hence, less transmitted power

reaches the receiver. The keep-alive discharge by its presence also helps to minimise statistical variation from pulse to pulse. The spike leakage energy increases with increasing cone gap.

### (3) Flat Leakage Power

The flat leakage power is composed partly of transmitter power leaking through the discharge and partly of microwave energy radiated by the discharge. The magnitude of the flat leakage power depends on the total pressure and partial pressures of the gas fill. In practice, the flat leakage power of a typical TR cell is of the order of 100 mW.

#### 1.5.5 Low Power Breakthrough

The low power breakthrough is the maximum power which can be transmitted through the TR cell without actually creating a discharge in the cell when the power is progressively increased from zero.

#### 1.5.6 Recovery Time

The recovery time of a TR cell is the time taken for the cell to deionize after the end of the transmitted pulse. It is normally measured in terms of the time taken for the attenuation through the cell to decrease from 60-70 dB, when the radar system is in transmission, to within 3 dB of the passive insertion loss. Typically, recovery times of 3 microseconds are required for

satisfactory system performance. The shorter the recovery time, the shorter is the minimum range. There are three possible mechanisms for reducing the electron density in the discharge; diffusion, recombination and electron attachment. The detailed mechanisms operating during the recovery time will be considered more fully in Chapter 2. Margenau et al (1946) have shown that the time necessary for the electrons to diffuse to the walls and recombine there is of the order of thousands of microseconds and that electron-ion recombination takes times of the order of 1 second. Electron attachment is thus the mechanism by which the required rate of deionization of the gas in the cell is achieved. A gas with a high electron attachment cross-section is added to the TR cell to decrease the recovery time. Water vapour is the gas most commonly added, other gases being  $\text{SO}_2$ ,  $\text{O}_2$  and  $\text{NO}$ .

Measurements made by Smullin and Leiter (1944) of the transmission through a cell 6 microseconds after the end of the transmitter pulse as a function of partial pressure of water in the cell show that transmission and hence recovery time are decreased as the partial pressure of water is increased. The recovery time increases with increasing rf pulse energy, since greater ionization occurs with greater peak powers and a longer pulse duration.

## 1.6 Cell Lifetime

The life of a TR cell is determined by the rate at which the gaseous constituents of the cell change. The end of the cell life is usually indicated by an excessive increase in either the recovery time or the leakage power. The recovery time increases as the partial pressure of water in the cell decreases. Due to the presence of the dc current at the keep-alive electrode and also due to the high power microwave pulses, a continuous modification of the gas content of the cell occurs, through sputtering and by chemical reactions between the gases in the cell and between the gases and the cell materials.

Sputtering is a process whereby the cathode of the keep-alive electrode is heated by positive ion bombardment; particles leave the cathode and condense on the anode or on the cell walls. On their way the particles may collide with gas molecules and carry them to the walls, where the gas is trapped. The rate at which sputtering occurs is a cause of the rate of decrease of the partial pressures of the gases in the cell, resulting in the rate of increase of the leakage power. The cell is copper plated to minimise resistive losses. Under the action of the microwave discharge and the dc glow discharge, some  $\text{OH}^-$  ions are created. These ions may then react with the copper plating on the cell walls to give



The above process reduces the partial pressure of water in the cell

and increases that of hydrogen. A more detailed account of the reactions of the gases in the cell is given in Chapter 6. Typical lifetimes for TR cells are of the order of several hundred hours, the minimum for practical use of a cell.

### 1.7 Pre-TR Tube

In a high-power radar system a pre-TR tube is often needed to protect the TR cell. At high power, the discharge at the input window of the TR cell may transfer sufficient heat to the window to damage it. A pre-TR tube is inserted between the transmitter and the TR cell to reflect a proportion of the power incident on it (the function of the pre-TR tube is to protect the TR cell and not the radar receiver). One design of pre-TR tube, used in several experiments in this thesis, is the gas-filled cylindrical quartz tube which is inserted in a waveguide mount. This design has the advantages of simplicity, large bandwidth and long life. Desirable characteristics for a pre-TR tube include high reflection and low arc loss when ionized, short recovery time, low insertion loss and the ability to withstand high incident powers. The gas filling is usually a low-pressure mixture of argon and water vapour.

References

- M D Fiske (1945) Resonant Windows for Vacuum Seals in  
Rectangular Waveguides, G E Research Lab Report, Feb 10
- A F Harvey (1960) Duplexing Systems at Microwave Frequencies,  
IRE Trans Microwave Theory and Tech 8, 415
- H Margenau, F L McMillan, I H Dearnley, C S Pearsall and  
C G Montgomery (1946) Physical Processes in the Recovery of  
TR Tubes, Phys Rev 70, 349
- L D Smullin and H A Leiter (1944) The 1B27 TR Tube, R L Report  
No. 594, Oct 4
- L D Smullin and C G Montgomery (1948) Microwave Duplexers,  
McGraw-Hill Book Co. Inc, USA

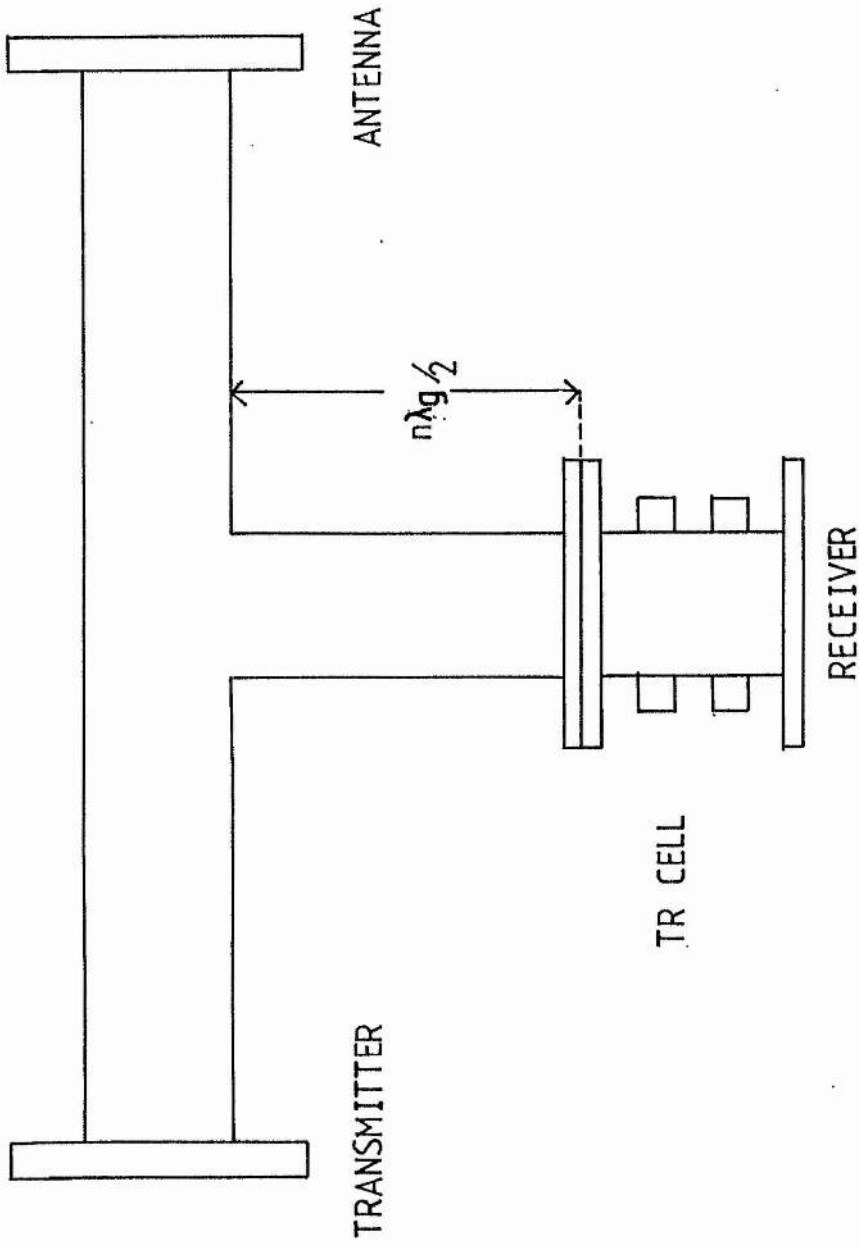


Fig 1-1 Branched Duplexer System

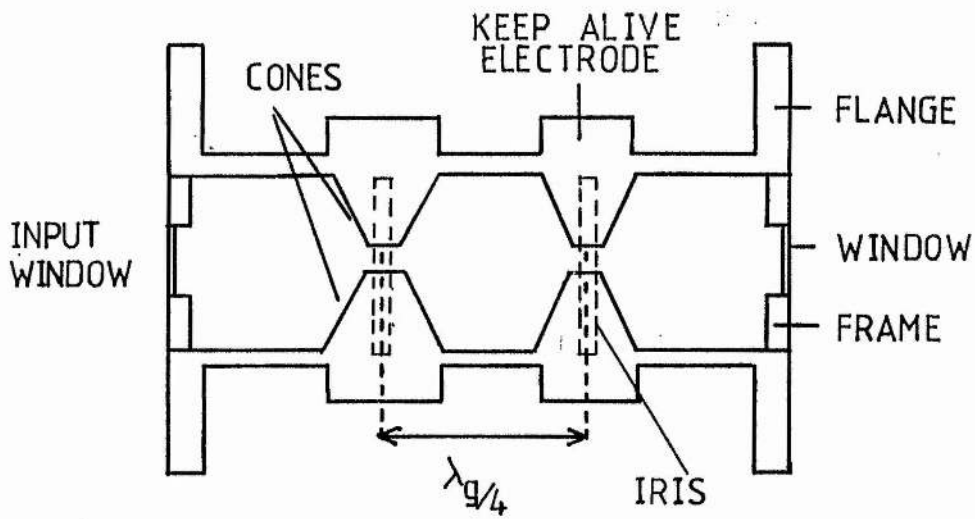


Fig 1:2 TR Cell

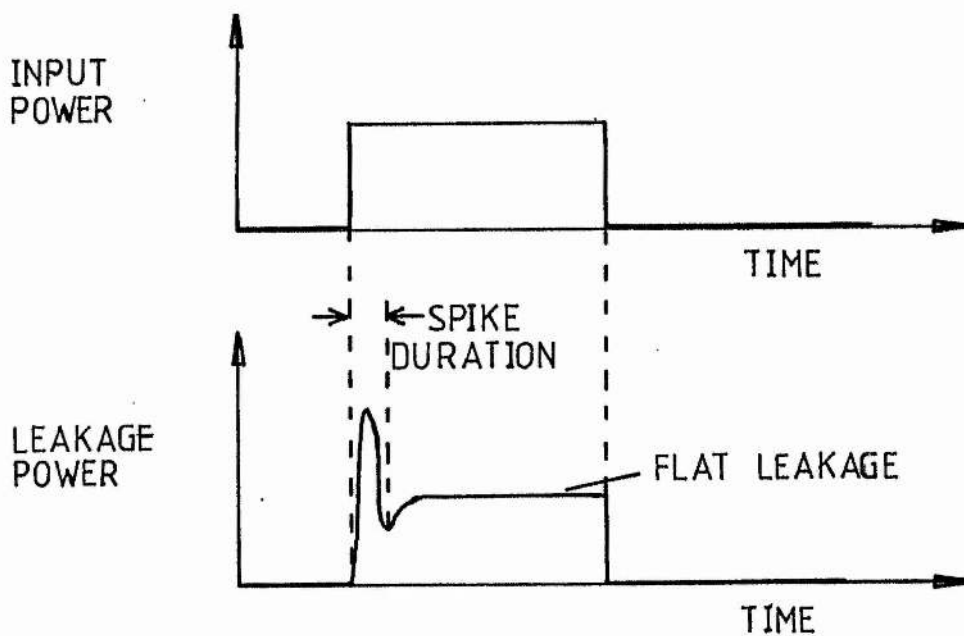


Fig 1:3 Leakage Through a TR Cell

## Chapter 2 The Microwave Discharge and Microwave Transmission

### 2.1 Introduction

Microwave discharges have been investigated since the Second World War, during the development of radar. Much of the experimental and theoretical work was carried out by professors Allis and Brown at the Massachusetts Institute of Technology. Recent reviews of microwave discharges include those by Marec et al (1983) and Zander and Hieftje (1981).

### 2.2 Microwave Breakdown and the Microwave Discharge

When an electric field at a microwave frequency is applied across a gas, energy is transferred to charged particles in the gas. Electrons, due to their much smaller mass, are accelerated to a greater extent than the ions by the applied field. When the direction of the field changes, the direction of the force on the electrons changes. The electrons oscillate within their container provided its walls are sufficiently far apart, and are not swept out of the discharge region by the electric field. Energy is transferred to the atoms and molecules in the gas by collision with the electrons. If an electron has sufficient energy to exceed an excitation level of an atom or molecule, their collision results in transfer of energy from the electron to the atom, sending it to an excited state. The energy absorbed by the atom is subsequently radiated and the atom returns to a lower energy state. If the

electron possesses sufficient energy to ionize an atom by collision, then a second electron is created. At the same time, electrons are being lost from the discharge region by diffusion to the walls, recombination with positive ions and electron capture.

The rates of electron production and loss are functions of the gas pressure and type, the magnitude and frequency of the electric field and the container geometry. The energy transfer to the electrons from the microwave field is a function of the electric field vector of the microwave radiation to the gas pressure; this determines the energy gained between collisions. The Townsend criterion for breakdown of a gas is that the loss rate by diffusion, attachment or recombination should equal the production rate. Herlin and Brown (1948) have shown the applicability of the Townsend breakdown criterion to microwave breakdown.

The Townsend criterion was originally formulated for breakdown in low frequency or dc discharges. The difference between the low and high frequency discharges is that in the low frequency discharge the electrons strike the walls of the container at high speed, producing secondary electrons which are an important source of electrons for the discharge. For the high frequency discharge the direction of the applied field changes before the electrons strike the walls of the container. Thus the only source of electrons for the high frequency discharge is through ionization by collision.

Breakdown electric fields have been reported in the literature for different gases and different microwave frequencies and cavities eg Krasik et al (1949) (argon) and Tetenbaum and Weiss (1979) (water vapour). The breakdown criterion is a particle balance equation, requiring the distribution function of electron energy and position. The electron energy distribution function will be discussed further in section 2.4; here we consider briefly an average electron model. The energy gain by an electron,  $\xi$ , is

$$\xi = eE\bar{v} = (e^2 E^2 / m \nu_m) (\nu_m^2 / \nu_m^2 + w^2) \quad , \quad (2.1)$$

where  $E$  is the amplitude of the electric field vector,  $\bar{v}$  is the mean electron drift velocity,  $\nu_m$  is the collision frequency for momentum transfer and  $w$  is the angular frequency of the microwave field. For a gas at high pressure, where  $\nu_m$  is very much greater than  $w$ , the energy transferred from the electric field to the electrons in the gas is dissipated through elastic collisions between the electrons and the gas atoms and molecules. At equilibrium, the energy dissipated per collision by an electron is equal to its average energy gain. The electron collision frequency for momentum transfer is so large that electrons gain insufficient energy between collisions to ionize an atom. At low pressures, where  $\nu_m$  is very much less than  $w$ , the electrons make many oscillations per collision and little power is transferred from the field. The energy transfer from the electric field to the electrons at a given value of  $E/p$ , where  $p$  is the gas pressure, is shown to be the most efficient when the pressure is high enough or the frequency low enough to result in many collisions of electrons with gas molecules per cycle.

An ionized gas or plasma is said to be in a state of Local Thermodynamic Equilibrium (LTE) if it obeys all the thermodynamic distribution laws. Then the energy and velocity distributions of the particles in the plasma are governed by the Maxwell-Boltzmann relations and the Saha-Eggert equation gives the yield of ionization products. Collisional excitation and de-excitation rates for some or all of the excited levels are much higher than the radiative decay rates. The plasma can be described by one temperature for the electrons, ions and neutral particles. Plasmas near atmospheric pressure, high current arcs and discharges in shock tubes are all in a state of LTE but lower pressure plasmas and low current gas discharges are not. At lower pressures the collision rates are lower, reducing the likelihood of proper partitioning of energy between excited states. The equilibrium population is determined by a balance between excitation by electrons and decay by radiative and collisional processes. Detailed information on the electron collision cross sections and electric dipole transition probabilities is required before the number densities in each state can be calculated.

The microwave discharge is similar to that in the positive column of a dc glow discharge, having similar values of electron density and electron energy. Maksimov (1967) investigated the microwave discharge in helium and compared it to that in the positive column of a glow discharge. He found that, in the microwave discharge, the electron temperature  $T_e$  and the ratio of the effective electric field to the gas pressure,  $E_e/p$  were larger

than in the positive column of the dc glow discharge, for the same power input. Avni and Winefordner (1975) have measured electron temperatures in microwave discharges at 2450 MHz and 200 W for rare gases and rare gas-metal impurity mixtures. They found that the electron temperature decreased with increasing pressure over the range 1-4 torr, then levelled off at temperatures between 30,000 K and 60,000 K. At 4 torr, it is likely that the electron collision frequency is just sufficient that the energy imparted to the electrons by the microwave field is largely transferred by collision and not retained. They also found that the electron temperature increased with increasing power.

## 2.3 Collision, Diffusion, Attachment and Recombination

### 2.3.1 Collisions

For a two-body elastic collision between an electron and an atom there is no change in the internal state of the atom; only kinetic energy is exchanged. In a three-body elastic collision the third body usually removes excess energy. The third body may be a gas particle or the walls containing the gas. An inelastic collision may occur if an electron has energy in excess of a threshold value characteristic of the gas before colliding with a gas atom or molecule. Some of the energy lost by the electron is spent in internal rearrangement of the atom or molecule, which subsequently returns to the ground state or a lower energy state by radiation of energy or by losing an electron. The mean free path  $l$  of an electron is the average distance between collisions. It is

defined as

$$l = 1/N\sigma \quad , \quad (2.2)$$

where  $\sigma$  is the electron-atom collision cross-section and  $N$  is the atom number density. The collision frequency  $\nu_c$  is given by

$$\nu_c = \bar{v}/l \quad , \quad (2.3)$$

where  $\bar{v}$  is the mean electron velocity. It is generally a function of electron velocity. Similarly, a collision frequency for electron attachment,  $\nu_a$ , and a collision frequency for ionization,  $\nu_i$ , are defined, where

$$\nu_a = \nu_c h_a \quad \text{and} \quad (2.4)$$

$$\nu_i = \nu_c h_i \quad , \quad (2.5)$$

with  $h_a$  and  $h_i$  the probabilities of attachment and ionization per collision, respectively. The rate  $k$  of a reaction is the product of the cross-section for the reaction and the relative velocity of the colliding particles

$$k = \sigma v \quad . \quad (2.6)$$

The collision cross section is usually a function of velocity.

### 2.3.2 Diffusion

Diffusion is a process which leads to an equalization of concentrations of particles within a single phase. Fick's law of diffusion relates the diffusion current  $J$  and the concentration  $C$  of the diffusing substance by

$$J = -D \text{ grad}C \quad , \quad (2.7)$$

where  $D$  is the diffusion coefficient. From the kinetic theory of gases and by allowing for the exchange of internal energy between colliding particles and the molecules not being rigid spheres, we

obtain an expression for  $D$ , for the diffusion of non-charged particles (Jeans (1940));

$$D = 3/8(\pi KT/2[1/m_1+1/m_2])^{0.5}/(\sigma[n_1+n_2]) \quad , \quad (2.8)$$

where  $m_1$  and  $m_2$  are the masses and  $n_1$  and  $n_2$  the number densities of the two diffusing gases.

In a plasma the charged particles diffuse via ambipolar diffusion. The electrons tend to diffuse out to the walls of the container. The excess of positive ions left in the plasma volume gives it an overall positive charge. The negatively charged electrons remaining in the plasma volume are attracted by the net positive charge of the volume and their diffusion is impeded. If the plasma is contained in a volume of dimensions greater than  $l_D$ , the Debye length, the positive ions and electrons diffuse at the same velocity, linked together by the attractive force between them. Since the Debye length is a measure of the distance over which the electric field of an individual electron extends before it is effectively shielded by oppositely charged particles, individual interactions between particles are important only over distances less than  $l_D$ ; for distances greater than  $l_D$  collective effects dominate. The Debye length is given by (McDaniel (1964))

$$l_D = [(\epsilon_0 k T_e)/(n e^2)]^{0.5} \quad . \quad (2.9)$$

If the dimensions of the plasma volume are much less than  $l_D$  then the electrons diffuse independently of the ions; free diffusion.

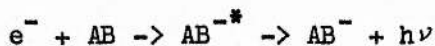
In a steady state discharge the electron losses are controlled by ambipolar diffusion, since the electron concentration in the discharge is sufficiently high. The ambipolar diffusion coefficient  $D_a$  is defined as

$$D_a = (D_+ K_e + D_e K_+) / (K_+ + K_e) \quad , \quad (2.10)$$

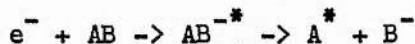
where  $D_+$  and  $K_+$  are the ion free diffusion coefficient and mobility respectively and  $D_e$  and  $K_e$  are the electron free diffusion coefficient and mobility respectively. The ambipolar diffusion coefficient is much smaller than the free diffusion coefficient, so fewer electrons are lost to the walls. The electric field required to maintain a discharge, therefore, is much smaller than that required to break down the gas.

### 2.3.3 Attachment

An electron attached to a neutral molecule in the discharge region is effectively lost to the discharge, since the very massive negative ion can gain little velocity from the applied field. Collision processes which lead to electron attachment are controlled to a large extent by conservation of energy. Radiative attachment is the simplest process, but it is not very likely.



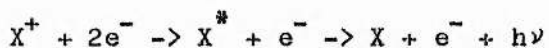
Dissociative attachment is very common.



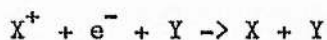
Electrons attach readily to atoms having nearly filled outer shells, such as chlorine or oxygen. A measure of the likelihood of attachment is the electron affinity energy of the atom or

#### 2.3.4 Recombination

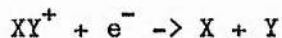
The process of electron-positive ion recombination is one method whereby electrons are removed from the discharge. Collisional radiative recombination is dominant in highly ionized plasmas at high temperatures where the electron density is of the order of  $10^{21} \text{ m}^{-3}$ .



When two bodies recombine, the presence of a third body is often required to ensure energy and momentum conservation. The third body may also promote the collisional stabilisation of an unstable state of one of the recombining particles, thus encouraging the reaction.



The third body is not altered chemically during the reaction. The third body may be a gas molecule or the surface of the container. For further details on the reactions at a surface, see Chapter 6, section 6.8. Dissociative recombination may also occur.



Two and three body positive and negative ion recombination also occurs, perhaps accompanied by the emission of radiation or dissociation of one of the products.

## 2.4 Electron Energy Distribution Function

In the presence of an electric field the electron energy distribution is no longer Maxwellian. In a noble gas discharge the electron densities are large enough, however, to lead, in a good approximation, to a Maxwellian distribution of electron energies for the bulk of the energy distribution, i.e. below the first excitation threshold. Above this threshold resonance and metastable states can be created. Hence, the fast electrons are lost rapidly and the tail of the electron energy distribution is depleted. This depletion is accounted for by using the two-electron group model, with one group of electrons below the excitation threshold and one group above it. The low density, high energy group of electrons tends to dominate the measured electron temperature. This temperature describes the energy of these electrons and serves to indicate the degree of ionization and excitation in the plasma. The second group of low velocity electrons contributes the major fraction of the electron number density. The temperature of the slow electrons may be measured from the Boltzmann slope of spectral lines corresponding to transitions between highly excited atom energy levels. The two-electron group model is applicable to noble gas and metal-doped noble gas discharges, but not to molecular discharges, such as the argon-water vapour system since these are generally dominated by many inelastic processes, each of very small energy loss.

The distribution function of the velocities and energies of the electrons in a plasma is given by the Boltzmann equation, together with boundary conditions determined by the physics of the problem. The Boltzmann equation is an expression of the continuity of electrons in phase space;

$$C = \partial F / \partial t + v \cdot \nabla F + a \cdot \nabla_v F, \quad (2.11)$$

where  $\partial F / \partial t$  is the local rate of change at the point  $s, v$ ;  $\nabla$  is the grad in configuration space and  $\nabla_v$  is the grad in velocity space;  $a$  is the acceleration;  $C$  is the change caused by collisions. There is no known general method of solution of the Boltzmann equation. MacDonald (1966) discussed the Boltzmann equation in detail and obtained a second order differential equation for the electron energy distribution function. The range of validity of the expressions used was discussed and theoretical results and experimental data for the various gases compared.

Several attempts have been made to solve the Boltzmann equation numerically, eg Smith and Thomson (1978). Also, Golant (1957) has attempted a solution of the Boltzmann equation for the electron energy distribution in argon. However, no attempt has yet been made to solve the Boltzmann equation for an equal mixture of two gases, such as argon and water vapour. So, in this thesis, we treat the electron energy distribution in the microwave discharge in argon and water vapour as being Maxwellian in the absence of information on the actual energy distribution.

## 2.5 Microwave Transmission

### 2.5.1 Maxwell's Equations

The laws governing the transmission of electromagnetic radiation is summed up by Maxwell's equations, one form of which is listed below.

$$\text{div } E = \rho_t / \epsilon_0 \quad (2.12)$$

$$\text{div } B = 0 \quad (2.13)$$

$$\text{curl } E = -dB/dt \quad (2.14)$$

$$\text{curl } B = \mu_0 J_m + (dE/dt)/c^2, \quad (2.15)$$

where  $E$  is the electric field vector,  $B$  is the magnetic induction,  $\rho_t$ , the total electric charge density, is the sum of  $\rho_f$  the free charge density and  $\rho_b$  the bound charge density,  $\epsilon_0$  is the permittivity of free space,  $\mu_0$  is the permeability of free space and  $J_m$  is the current density due to the flow of charge in matter. We can write  $J_m$  as

$$J_m = J_f + dP/dt + \text{curl } M, \quad (2.16)$$

where  $J_f$  is the current density of free charges,  $dP/dt$  is the polarisation current density and  $\text{curl } M$  is the equivalent current density in magnetised matter.

### 2.5.2 Derivation of the Wave Equation for a Non Conductor

Consider microwave radiation travelling in air. Air is an isotropic, linear and homogeneous medium with effectively zero conductivity and zero attenuation and having permeability  $\mu$  and permittivity  $\epsilon$ . The total charge density  $\rho_t$  is zero. Equations (2.12) and (2.15) now become

$$\text{div } E = 0 \quad (2.17)$$

$$\text{curl } B = \mu\epsilon(dE/dt)/c^2 \quad (2.18)$$

By taking the curl of equation (2.14) and using the vector identity

$$\text{curl curl } X \equiv \text{grad div } X - \text{del}^2 X \quad (2.19)$$

and substituting for curl B from equation (2.18) and for div E from equation (2.17), we obtain

$$\nabla^2 E = (d^2E/dt^2)/\mu\mu_0\epsilon\epsilon_0 \quad (2.20)$$

which is the wave equation for microwave radiation travelling in air.

### 2.5.3 Radiation in a Waveguide and the Waveguide Equation

Consider propagation of microwave radiation along a rectangular waveguide containing air of permeability  $\mu$  and permittivity  $\epsilon$  and having no dielectric losses. The radiation travels in the z direction and is bounded by planes at x equal to 0 and x equal to a, which have infinite conductivity. For a conductor with infinite conductivity, the tangential component of the electric field vector,  $E_t$ , is zero. Since  $E_t$  is continuous across a boundary, then  $E_t$  is zero in air. So, for the planes at x equal to zero and

x equal to a the electric field vectors in the y and z directions,  $E_y$  and  $E_z$  are zero.

The microwave radiation is constrained to travel along the waveguide in the Transverse Electric (TE) mode. In this mode, the electric field vector is perpendicular to the direction of motion of the radiation. But we have already seen that the electric field vectors in the y and z directions are already zero at the boundaries where x is equal to zero or a. The simplest solution is for  $E_x$  only to be non-zero everywhere and  $E_y$  and  $E_z$  zero everywhere. Another solution involves having  $E_x$  and  $E_z$  zero everywhere, with  $E_y$  non-zero, except at the boundaries where x equals zero or a. We shall consider the latter solution.

A wave travelling in the z direction has the form  $\exp(i\omega t - kz)$  where k is the wavenumber of the wave and  $\omega/2\pi$  is its frequency. Substituting for E in equations (2.14) and (2.18) gives a relation between  $E_y$  and the x and z components of the magnetic induction B. Since the travelling wave has the form  $\exp(i\omega t - kz)$ , we obtain, by eliminating the terms for the magnetic induction,

$$d^2 E_y / dx^2 = -(\omega^2 \mu \mu_0 \epsilon \epsilon_0 + k^2) E_y \quad . \quad (2.21)$$

The solution of the above equation is, for  $E_y$  equal to zero at x equal to zero,

$$E_y = E_0 \sin[(\omega^2 \mu \mu_0 \epsilon \epsilon_0 + k^2)^{0.5}] x \quad . \quad (2.22)$$

For  $E_y$  equal to zero at x equal to a we obtain

$$(\omega^2 \mu \mu_0 \epsilon \epsilon_0 + k^2)^{0.5} a = \pi \quad . \quad (2.23)$$

Rearranging equation (2.12) to make k the subject gives

$$k^2 = (\pi/a)^2 - \mu \mu_0 \epsilon \epsilon_0 \omega^2 \quad . \quad (2.24)$$

At low frequencies,  $k^2$  is positive, giving an attenuated wave. At high frequencies  $k^2$  is negative, giving a travelling wave which is not attenuated. For  $k^2$  negative,  $k$  can be written in terms of a complex number  $i\beta$ , giving a wave of the form  $\exp(i(\omega t - \beta z))$ . For  $k$  equalling zero, at the cut-off frequency, the wavelength  $\lambda_c$  (where  $\lambda_c$  is equal to  $2a$ ) is the shortest wavelength to be propagated without attenuation. The wavelength of radiation in an unbounded medium,  $\lambda_0$ , is given by

$$\lambda_0 = 2\pi / (\omega^2 \mu \mu_0 \epsilon \epsilon_0)^{0.5} \quad (2.25)$$

Substituting in equation (2.25) to obtain  $\lambda_0$ ,  $\lambda_c$  and  $\lambda_g$ , the wavelength in the guide (where  $\lambda_g$  is  $2\pi/\beta$ ), we obtain

$$1/\lambda_0^2 = 1/\lambda_g^2 + 1/\lambda_c^2 \quad (2.26)$$

which is the waveguide equation. For the microwave system used in this thesis, the frequency of radiation is 9.4 GHz, travelling along size 16 waveguide (inside dimensions 2.286 cm x 1.016 cm). Hence  $\lambda_g$  is 4.478 cm.

#### 2.5.4 Power Transmitted along a Waveguide- no Attenuation

Energy is associated with electric and magnetic fields. The quantity  $S$ , where

$$S = E \times H \quad (2.27)$$

is the Poynting vector and  $H$  is defined as

$$B = \mu_0 (H + M) \quad (2.28)$$

where  $M$  is the magnetization of the medium of propagation. For an isotropic, linear, homogeneous medium then

$$B = \mu \mu_0 H \quad (2.29)$$

When integrated over a closed surface,  $S$  gives the total outward

flow of energy from the surface per unit time. The vector  $S$  points in the direction of the electromagnetic wave. The time average of  $S$  can be written as (Lorrain and Corson, (1970))

$$S = 1/2 \operatorname{Re}(E \times H^*) \quad , \quad (2.30)$$

where  $H^*$  is the complex conjugate of  $H$ . Using equation (2.14) with  $E$  equal to  $E_y$  and substituting for  $E_y$  from equation (2.22) we obtain a relationship between  $E_y$  and  $B_x$  and  $B_z$ . To obtain the corresponding values of  $H_x$  and  $H_z$  we substitute for  $B_x$  and  $B_z$  in equation (2.29). By inserting the values of  $E_y$ ,  $H_x$  and  $H_z$  into equation (2.30) we obtain for  $S$

$$S = E_0^2 \sin^2(k^2 + w^2 \mu \mu_0 \epsilon \epsilon_0)^{.5} \times (k^2 + w^2 \epsilon \epsilon_0 \mu \mu_0)^{0.5} / (2w \mu \mu_0) \quad , \quad (2.31)$$

which is the energy transmitted per unit area. The average transmitted power  $W_T$  along a waveguide of height  $b$  and width  $a$  is the integral of equation (2.31) between the points  $x$  equal to zero and  $x$  equal to  $a$ , giving

$$W_T = (\pi a b E_0^2) / (2 \lambda_g w \mu \mu_0) \quad . \quad (2.32)$$

For a typical magnetron power supply for a radar system supplying 20 kW peak power with a pulse length of 1 microsecond and a prf of 1 kHz,  $E_0$  for such a pulse is calculated to be  $4.268 \times 10^5 \text{ Vm}^{-1}$ .

### 2.5.5 The Wave Equation for a Good Conductor

Consider an isotropic, linear and homogeneous conductor with conductivity  $\sigma$ . The charge density  $\rho_t$  is zero. Maxwell's equations, equations (2.12) to (2.15) become

$$\operatorname{div} E = 0 \quad (2.33)$$

$$\operatorname{div} B = 0 \quad (2.34)$$

$$\operatorname{curl} E = - dB/dt \quad (2.35)$$

$$\text{curl } B = \mu\mu_0(\sigma E + \epsilon_0 dE/dt) \quad ; \quad (2.36)$$

since

$$J_f = \sigma E \quad . \quad (2.37)$$

By taking the curl of equation (2.35) and substituting for curl B from equation (2.36) we obtain, by using the vector identity (equation (2.19)),

$$\text{del}^2 E = \mu\mu_0\sigma dE/dt + \epsilon_0\mu\mu_0 d^2E/dt^2 \quad , \quad (2.38)$$

which is the wave equation for electromagnetic radiation travelling in a good conductor. As in section 2.5.3, we consider a wave travelling in the z direction, of the form  $\exp(i(\omega t - \beta z))$ . Substituting for E in equation (2.38) we obtain

$$\beta^2 = \mu\mu_0\epsilon_0\omega^2 - i\omega\mu\mu_0\sigma \quad . \quad (2.39)$$

The wave number is complex. For a good conductor,  $\sigma$  is large and  $\beta$  can be approximated by

$$\beta = ((\omega\sigma\mu\mu_0)/2)^{0.5}(1-i) \quad , \quad (2.40)$$

which is the wavenumber for a wave travelling in a good conductor. From equations (2.35) or (2.36) E and H are related by

$$E/H = (\omega\mu\mu_0)/\beta \quad . \quad (2.41)$$

For a good conductor, E/H becomes

$$E/H = ((\omega\mu\mu_0)/\sigma)^{0.5} e^{i\pi/4} \quad . \quad (2.42)$$

### 2.5.6 Attenuation along a Waveguide and Skin Depth

Waveguides have walls of a finite, though high, conductivity; they are not perfect ideal conductors. Therefore, part of the energy transmitted along the waveguide is dissipated in the walls due to induced electric currents in the metal. For a perfect conductor, the electric field tangential to the surface is zero; for a real conductor there is a small tangential electric field in

the conductor. There will also be a tangential component  $H_t$  at the surface of the conductor. Since  $H_t$  must be continuous across an interface, we can calculate  $H_t$  in the conductor. The relationship between  $E$  and  $H$  inside a conductor is given in equation (2.42). For a wave propagating in the  $z$  direction,  $H_x$  and  $H_z$  are non-zero. Consider the  $y$ - $z$  planes of the waveguide, at  $x$  equal to zero and  $x$  equal to  $a$ . Here, the transverse component of  $H$  is  $H_z$ ;  $H_x$  is zero and  $E_y$  is non-zero. The average power transmitted is given in equation (2.30), resulting in

$$S = 1/2 \text{Re}(E_y H_z^*, 0, -E_y H_x) \quad , \quad (2.43)$$

for non-zero  $E_y$ . Following section 2.5.4, and since  $H_x$  is zero, we obtain for  $S$

$$S = 1/2 \text{Re}(E_y H_z^*) = (\pi/a)^2 [E_0^2 / \sigma^{0.5}] (w \mu \mu_0)^{-1.5} \quad . \quad (2.44)$$

The power lost per unit length,  $P_{xy}$ , in both the  $y$ - $z$  planes is therefore, for a waveguide of height  $b$ ,

$$P_{xy} = 2b (w \mu \mu_0)^{-1.5} (\pi/a)^2 [E_0^2 / \sigma^{0.5}] \quad . \quad (2.45)$$

Considering the faces parallel to the  $x$ - $z$  plane, the power transferred in the  $y$  direction,  $P_{xz}$ , is, from equation (2.30),

$$P_{xz} = 1/2 \text{Re}(E_z H_x - E_x H_z) \quad . \quad (2.46)$$

We obtain  $H_x$  using equations (2.14) and (2.18) to get

$$H_x = 2\pi / (\lambda_g w \mu \mu_0) E_0 \sin[(\beta^2 + w^2 \mu \mu_0)^{0.5}] x e^{i(\omega t - \beta z)} \quad , \quad (2.47)$$

where  $E_z$  and  $H_x$  are related according to equation (2.42). Similarly, we obtain  $H_z$  and  $E_x$ . The resulting power lost per unit length in the two  $x$ - $z$  planes, for  $y$  equal to zero and  $y$  equal to  $b$  is

$$P_{xz} = (E_0^2 / \pi (1 + (2a/\lambda_g)^2)) / [a (2\mu \mu_0 w)^{1.5} \sigma^{0.5}] \quad . \quad (2.48)$$

The total power lost in the walls per unit length,  $W_L$ , is, therefore,

$$W_L = P_{xy} + P_{xz} \quad . \quad (2.49)$$

An attenuation constant  $k_a$  is defined such that both the E and H of the transmitted wave are attenuated by a factor  $\exp(-k_a z)$  in a distance  $z$ . The average transmitted power,  $W_T$ , will decrease by the factor

$$e^{(-2k_a \Delta z)} \approx 1 - 2k_a \Delta z \quad ,$$

in a distance  $\Delta z$ . Hence, we have

$$k_a = W_L / 2W_T \quad . \quad (2.50)$$

Substituting in equation (2.50) for  $W_T$  from equation (2.32) and for  $W_L$  from equation (2.49) we obtain for the attenuation constant

$$k_a = (\pi \lambda_g / (\sigma^{0.5} 2b (2\mu\mu_0 W)^{0.5})) (2b/a + 1 + (2a/\lambda_g)^2) \quad . \quad (2.51)$$

The power lost per unit length in the copper walls (conductivity  $5.88 \times 10^7 \text{ (}\Omega\text{m)}^{-1}$ ) is calculated to be 530 W, using the values of  $a$ ,  $b$  and  $\lambda_g$  from section 2.5.3 and the value of  $E_0$  calculated in 2.5.4, for a microwave frequency of 9.4 GHz. The percentage of input power lost per metre of waveguide is therefore 2.65%. In the experimental setup there is approximately 0.8 m of waveguide. Hence the percentage of incident power lost is negligible.

The skin depth  $\delta$  is defined as the depth in a conductor at which the incident electric field reaches a fraction  $1/e$  of its value at the surface of the conductor. For a good conductor,  $\beta$ , the wave vector, is given by equation (2.40). For a wave of the form  $\exp(i(\omega t - \beta z))$ , the real part of  $\beta$  represents the travelling wave and the imaginary part represents the attenuation of the wave. Hence,  $\delta$  is given by

$$\delta = 2 / (\mu\mu_0 \sigma W)^{0.5} \quad . \quad (2.52)$$

The skin depth of copper, with which the inside of the waveguide is

plated, is calculated to be  $9.6 \times 10^{-7}$  m, for microwaves of frequency 9.4 GHz. The depth of plating in the cell is greater than this value, so all the heat dissipated by the microwaves in the waveguide wall is dissipated in the copper.

## 2.6 Glass

Since glass is a dielectric having non-zero conductivity, it obeys Maxwell's equations for a non-conductor. If the electric field vector has time variation of the form  $\exp(i\omega t)$  then equation (2.36) can be written as

$$\text{curl } B = (\sigma + i\omega\epsilon\epsilon_0)E\mu\mu_0 \quad . \quad (2.53)$$

Since a dielectric has a small conductivity, we have

$$\sigma E \ll i\omega\epsilon\epsilon_0 E \quad .$$

The current density in the dielectric,  $J_d$ , can be written as

$$J_d = (\sigma + i\omega\epsilon\epsilon_0)E = i\omega\epsilon\epsilon_0(1 - i\sigma/(\omega\epsilon\epsilon_0))E = i\omega\epsilon_0\epsilon_c E \quad , \quad (2.54)$$

where  $\epsilon_c$ , the complex dielectric constant, is written as

$$\epsilon_c = \epsilon' - i\epsilon'' = \epsilon - i\sigma/(\omega\epsilon_0) \quad . \quad (2.55)$$

The real part of the dielectric constant results in a current at right angles to the direction of the electric field. Hence, no power is absorbed by the dielectric. The imaginary part of the dielectric constant points in the direction of the electric field and therefore absorbs power. The power absorbed,  $P_D$ , per unit volume by a dielectric is given by

$$P_D = \sigma E^2 = \omega\epsilon_0\epsilon'' E^2 \quad . \quad (2.56)$$

The power absorbed by a dielectric is often described in terms of the loss tangent,  $\tan\delta$ , which is written as

$$\tan\delta = \epsilon''/\epsilon' = \sigma/(\omega\epsilon) \quad . \quad (2.57)$$

For the borosilicate glass used for the TR cell window,  $\epsilon''$  is  $4.6 \times 10^{-2}$  so the power absorbed per unit volume for an input peak power of 20 kW, having an electric field vector of  $4.268 \times 10^5 \text{ Vm}^{-1}$  is  $4.355 \times 10^6 \text{ Wm}^{-3}$ . Hence the power absorbed by the window, of approximate volume  $1.08 \times 10^{-8} \text{ m}^3$  is 47.0 mW. The mean incident power is 20 W so 0.24% of this incident power is absorbed by the window. Hence, the TR cell window is effectively transparent to incident microwave radiation.

## 2.7 Characteristics of an Ionised Gas

In a plasma (which is assumed to be electrically neutral), if the electrons were completely free to move in the medium without hindrance there would be no transfer of energy from the electrons to the surrounding heavy ions and gas molecules. The plasma would be lossless. However, elastic and inelastic collisions do occur between the electrons and other particles in the plasma, which cause the electrons to lose energy. The total loss of energy due to collisions is allowed for by introducing an effective electron collision frequency. The effective collision frequency is the equivalent number of collisions occurring per unit time which would extract the same total energy from the electrons as happens in practice. The influence of discrete positive ions and neutral molecules in a plasma can be represented to a good approximation by including a viscous damping term proportional to the velocity in the electron equation of motion. On average, an electron loses its directed momentum  $mv$ , where  $m$  is the electron mass and  $v$  its velocity, at each collision. For the electrons the current density

J is

$$J = nev \quad . \quad (2.58)$$

The equation of motion of an electron in an electromagnetic field is

$$m \frac{dv}{dt} = -m\nu_m v - e(E + v \times B) \quad , \quad (2.59)$$

where  $\nu_m$  is the collision frequency for momentum transfer ie the rate of change of velocity of an electron is equal to the sum of the force due to the stopping effect of collisions and the force due to the interaction of the electron and the electromagnetic field. If the electron velocity is a function of time and position then

$$dv/dt = (\partial v/\partial z)(\partial z/\partial t) + \partial v/\partial t \quad , \quad (2.60)$$

where  $\partial z/\partial t$  is the low frequency or steady movement of the electron through the plasma. We assume that  $\partial z/\partial t$  is zero. For an oscillating electric field with time dependence of  $\exp(i\omega t)$  we obtain

$$i\omega m v + m\nu_m v = -eE \quad . \quad (2.61)$$

By substituting for  $v$  from equation (2.58) into equation (2.61) we obtain

$$J(i\omega + \nu) = ne^2/mE \quad . \quad (2.62)$$

By substituting for  $J$  from equation (2.37) we obtain for  $\sigma$ ,

$$\sigma = [ne^2/m](\nu - i\omega)/(\nu^2 + \omega^2) \quad , \quad (2.63)$$

giving an expression for the conductivity of an ionised gas, known as the Lorentz conductivity. The plasma frequency  $\omega_p$  is defined as

$$\omega_p^2 = ne^2/\epsilon_0 m \quad , \quad (2.64)$$

giving

$$\sigma = \epsilon_0 \omega_p^2 (\nu - i\omega) / (\nu^2 + \omega^2) \quad . \quad (2.65)$$

The electrons oscillate about their equilibrium positions with

simple harmonic motion at the plasma frequency. From equation (2.42) and equation (2.14) and by using the vector identity (equation (2.19)) we obtain, for a wave of the form  $\exp(i\omega t - kz)$

$$k^2 = i\omega\mu_0\sigma - \omega^2\epsilon_0\mu_0 \quad (2.66)$$

Substituting from equation (2.63) for  $\sigma$ , the complex conductivity of an ionised gas, we obtain

$$k^2 = (\omega^2\mu_0 n e^2) / m(\nu^2 + \omega^2) - \omega^2\epsilon_0\mu_0 + i\omega\mu_0 n e^2 \nu / [m(\nu^2 + \omega^2)] \quad (2.67)$$

But the refractive index  $N$  of a material is defined as the ratio of the velocity of light  $c$  to the phase velocity in the medium  $v_\phi$

$$N = c/v_\phi \quad (2.68)$$

$$\text{where } v_\phi = \omega/k_\phi \quad (2.69)$$

For a wave of the form  $\exp(i\omega t - kz)$ , with  $k$  complex, the real part of  $k$  is the attenuation coefficient and the imaginary part of  $k$  is the phase constant, ie

$$k = k_r + k_\phi \quad (2.70)$$

(see Heald and Wharton (1965)). Hence, we have

$$N = c/\omega \operatorname{Re} k = \{ .5(1 - (\omega_p^2/\omega^2 + \nu^2)) + .5[ (1 - (\omega_p^2/\omega^2 + \nu^2))^2 + ((\omega_p^2/\omega^2 + \nu^2)\nu/\omega)^2 ]^{0.5} \}^{0.5} \quad (2.71)$$

The attenuation index  $A$  is defined as

$$A = c/\omega \operatorname{Im} k = \{ -.5(1 - (\omega_p^2/\omega^2 + \nu^2)) + .5[ (1 - (\omega_p^2/\omega^2 + \nu^2))^2 + ((\omega_p^2/\omega^2 + \nu^2)\nu/\omega)^2 ]^{0.5} \}^{0.5} \quad (2.72)$$

The graphs are plotted of the refractive index  $N$  and the attenuation index  $A$  against electron density, for varying ratios of  $\nu/\omega$  (see figs (2.1) and (2.2)).

A reasonable measure of the discharge thickness can be obtained by assuming that  $d$ , the discharge thickness, is equal to the skin depth, ie of the order of the penetration depth of the incident wave into the plasma (Gould (1961), Ward et al (1961)). Hence, we have

$$d = c/wA \quad . \quad (2.73)$$

The graphs are plotted of the variation of  $d$  with  $n$ , the electron density for varying ratios of  $v/w$  (see fig (2.3)).

## 2.8 Critical Electron Density

For a fixed frequency of microwave radiation there exists a critical electron density,  $n_c$ , such that

$$w^2 = n_c e^2 / \epsilon_0 m \quad . \quad (2.74)$$

From equation (2.72) for the attenuation coefficient,  $A$ , it can be seen that for electron densities below this critical value the medium is a nearly transparent dielectric and above, it is opaque and highly reflecting. If the attenuation index is real, then there is attenuation of a microwave signal, ie the electron density is greater than  $n_c$  and  $w_p^2$  is greater than  $w^2$ . For  $w_p^2$  less than  $w^2$ , ie for an electron density below that of the critical electron density, the microwaves are transmitted without attenuation.

For the TR cell, where the frequency of microwave radiation applied is 9.4 GHz, the critical electron density is calculated to be  $1.09 \times 10^{18} \text{ m}^{-3}$ . So, when the TR cell is fired and no signal passes through the cell, the electron density in the discharge must

exceed  $1.09 \times 10^{18} \text{ m}^{-3}$ .

## 2.9 Transmission, Reflection and Refraction at a Boundary

Maddix et al (1968) have analysed the high power properties of the input window discharge of a TR cell in terms of the transmission and reflection coefficients of a thin plasma slab, and obtained values for arc loss and leakage power as functions of collision frequency and electron density.

For a microwave pulse travelling in the z direction in a waveguide, we have already seen that the electric field vector of the radiation points in the y direction. The TR cell window is situated in the x-y plane in the waveguide, perpendicular to the direction of propagation of the radiation. The electric field vector lies in the plane of the window. Consider a wave travelling in a direction normal to a surface representing the boundary between two media with the E vector in the plane of the surface, (see fig (2.4)) and  $E_i$ ,  $E_r$ ,  $E_{tr}$ ,  $H_i$ ,  $H_r$  and  $H_{tr}$  are the incident, reflected and transmitted electric field vectors and magnetic field intensities respectively. At the surface the electric fields and the magnetic fields parallel to the surface are continuous across the surface, giving

$$E_i + E_r = E_{tr} \quad , \quad (2.75)$$

and

$$H_i \cos \theta_i - H_r \cos \theta_i = H_{tr} \cos \theta_{tr} \quad . \quad (2.76)$$

where  $\theta_i$  and  $\theta_{tr}$  are the angles of incidence and transmission respectively for H at the surface. By using equation (2.41) for

the relationship between E and H at the surface between media 1 and 2 we obtain

$$k_1/w\mu_1(E_i - E_r)\cos\theta_i = k_2/w\mu_2 E_{tr}\cos\theta_{tr} \quad (2.77)$$

Rearranging equations (2.74) and (2.76) gives

$$\frac{E_r}{E_i} = \frac{(N1/\mu_{r1}\cos\theta_i - N2/\mu_{r2}\cos\theta_{tr})}{(N1/\mu_{r1}\cos\theta_i + N2/\mu_{r2}\cos\theta_{tr})}, \quad (2.78)$$

$$\frac{E_{tr}}{E_i} = \frac{2N1\cos\theta_i/\mu_{r1}}{(N1\cos\theta_i/\mu_{r1} + N2\cos\theta_{tr}/\mu_{r2})}, \quad (2.79)$$

which are Fresnel's equations for radiation incident on a boundary with the electric field vector in the plane of a boundary. The refractive index N, is  $ck/w$ . From Snell's law we have

$$\sin\theta_i/\sin\theta_{tr} = N1/N2 \quad (2.80)$$

For a wave in the z direction, we have

$$\theta_i = \theta_{tr} = 0 \quad (2.81)$$

Now we apply Fresnel's equations to the case of microwaves incident on a TR cell. Consider microwaves incident normally on the TR cell window face. Fresnel's equations, (2.78) and (2.79), relate the incident, reflected and transmitted waves at a boundary and the refractive indices of the respective media either side of the boundary. The reflection coefficient R is defined as

$$R = (E_r/E_i)^2 \quad (2.82)$$

If T, the transmission coefficient includes the power absorbed by the medium and that transmitted through it, then we have

$$R + T = 1 \quad (2.83)$$

For the borosilicate glass of the TR cell window, N is 1.485, giving a value of R of 3.81% and of T of 96.19%. So the glass of the TR cell window can transmit almost all of the microwave power

incident on it (the TR cell window is one of several resonant elements in the device, which is tuned to allow only the transmission of radiation of a specified bandwidth).

The graphs are plotted of R and T against electron density for the microwave-excited discharge in the TR cell for varying ratios  $v/w$  (see figs (2.5) and (2.6)). From these graphs it can be seen that both the reflection and transmission coefficients are complicated functions of collision frequency and electron density. For an electron density greater than  $10^{19} \text{ m}^{-3}$  and a collision frequency greater than  $w/10$  the transmission coefficient falls sharply. For the TR cell to perform efficiently, the discharge must reflect the maximum incident power and allow the minimum of power to be absorbed or transmitted. Hence the electron density must be greater than  $10^{19} \text{ m}^{-3}$  and the collision frequency must have a value of  $w$  or greater.

A typical value for arc loss in a TR cell is 0.8 dB. Arc loss and incident electric field vector are related by

$$P_{\text{arc}} = 10 \log_{10} (E_i/E_r)^2 \quad . \quad (2.84)$$

(see Chapter 1, section 1.5.3)

So a minimum value of R of 0.8318 and a maximum of T of 0.1682 are required. These values of R and T correspond to an electron density in excess of  $5 \times 10^{21} \text{ m}^{-3}$ , for a collision frequency equal to  $w$  and to an electron density greater than  $10^{22} \text{ m}^{-3}$  for a collision frequency equal to  $10w$ .

In this Chapter we have derived expressions for the microwave radiation travelling in a waveguide and its wavelength in the guide; the power transmitted down the waveguide by the microwaves and the power lost to the waveguide walls. We have also calculated the microwave power absorbed and reflected by glass. The refractive index, attenuation index, thickness, reflection coefficient and transmission coefficient of a microwave-excited discharge have been calculated as functions of collision frequency and electron density. Much of the information gained will be used in Chapter 6, to aid the understanding of the processes occurring in the TR cell when subjected to microwaves.

## 2.10 Theory of the TR Cell Recovery Period

Some attempts have been made to understand the physical processes occurring in the recovery period, after a microwave pulse ionizes the gas in the TR cell. Among the first such attempts was that of Margenau et al (1946). First, they measured the transmission through the TR cell by applying a low power microwave pulse to the cell. The detected microwave power increases with decreasing electron density in the cell. They also include a theoretical analysis of the recovery period, which is as follows; for electron-ion recombination they write

$$dn/dt = -v\sigma_r n^2 \quad , \quad (2.85)$$

where  $n$  is the electron density,  $\sigma_r$  the recombination cross section and  $v$  the electron velocity. They obtained a time of 1 second for half of the electrons to recombine, assuming thermal electrons over

this period and a recombination cross section of  $2 \times 10^{-21} \text{ cm}^2$ .

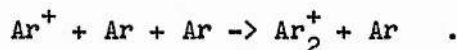
Margenau et al consider the diffusion from a slab of thickness  $d$  adjacent to the window of a pre-TR tube. They solve the diffusion equation for the electrons

$$\nabla^2 n - D_2 n / \partial t = 0 \quad , \quad (2.86)$$

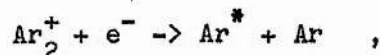
where  $D_2$ , the ambipolar diffusion coefficient, has a value of  $5 \text{ cm}^2 \text{ sec}^{-1}$  and estimate a diffusion time of several thousand microseconds when  $d$  is approximately 1 mm. Hence, they conclude that electron capture by water vapour is the method by which the TR cell recovers.

Takeda and Dougal (1960) investigated the deionization of a water vapour discharge to identify the electron loss mechanisms over the electron density range  $10^8 - 10^{10} \text{ cm}^{-3}$ , using the same measurement technique as Margenau et al. They displayed their results in the form of graphs of  $1/n$  against time, which were straight lines over the range 15-250  $\mu\text{s}$  for the above electron density. Their results indicated that electron-ion recombination was the dominant electron loss mechanism. They observed that attachment was negligible at low electron energies and concluded that "the role of electron attachment in the overall deionization process may be insignificant compared with recombination".

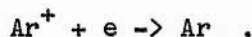
Biondi (1963) measured electron losses during the afterglow following a microwave discharge in argon and found that the electron losses in pure argon were due to dissociative recombination of  $\text{Ar}_2^+$ , created in the reaction



The  $\text{Ar}_2^+$  ion then combines with an electron, giving



with a recombination rate of  $10^{-7}$ - $10^{-6} \text{ cm}^3\text{s}^{-1}$ . However, he found that for mixtures of argon in helium, the dominant recombination reaction was



with a much lower recombination rate of at most  $10^{-10} \text{ cm}^3\text{s}^{-1}$ . Here, the electron loss mechanism was found to be ambipolar diffusion to the container walls.

The electrons slow down to thermal energies within a few microseconds. It is likely that electron attachment is the dominant mechanism for electron loss in the first few microseconds after the end of a microwave pulse, when the electrons are still energetic and at the energy corresponding to maximum electron capture. However, when the electrons have lost their energy (through collisions with the gas molecules and the container walls) and are thermal, then electron-ion recombination may be the dominant electron loss mechanism. The results of Takeda and Dougal cover the electron density range  $10^8$ - $10^{10} \text{ cm}^{-3}$ ; however we have estimated that the electron density in the discharge may be as high as  $5 \times 10^{15} \text{ cm}^{-3}$ . So the initial loss of electrons is through attachment, in the first few microseconds after the end of a pulse, then, when the cell has recovered sufficiently to allow a pulse through it, further electron loss proceeds through electron-ion recombination.

## References

- R Ayni and J D Winefordner (1975) Some Considerations on the Microwave Electrodeless Discharge, *Spectrochim Acta B* 30B, 281
- M A Biondi (1963) Studies of the Mechanism of Electron-Ion Recombination 1, *Phys Rev* 129, 1181
- V E Golant (1957) Formation of a Pulse Discharge in Argon at Very High Frequencies, *Zhurnal Tekhnicheskoi Fiziki* 27, 756
- L Gould (1961) Recent Studies in Microwave Gas Duplexers, 1961, *Proc Int Conf on Microwave Tubes*, J Wosnik (ed) New York Academic Press
- M A Heald and C B Wharton (1965) *Plasma Diagnostics with Microwaves*, J Wiley and Sons Inc, New York
- M A Herlin and S C Brown (1948) Breakdown of a Gas at Microwave Frequencies, *Phys Rev* 74, 291
- J Jeans (1940) *An Introduction to the Kinetic Theory of Gases*, Cambridge University Press
- S Krasik, D Alpert and A O McCoubrey (1949) Breakdown and Maintenance of Microwave Discharges in Argon, *Phys Rev* 76, 722
- P Lorrain and D L Corson (1970) *Electromagnetic Fields and Waves*, W H Freeman and Co, San Fransisco
- A D MacDonald (1966) *Microwave Breakdown in Gases*, John Wiley and Sons Inc, New York
- H S Maddix, J J Pergola and P Chorley (1968) Physical Processes in Duplexer Discharges in Chlorine and Oxygen, *IEEE Trans ED*, ED 15, 873
- A I Maksimov (1967) Electron Density and Energy in a Microwave Helium Discharge, *Sov Phys Tech Phys* 11, 1316
- J Marec, E Bloyet, M Chaker, P Leprince and P Nghiem (1983)

Electrical Breakdown and Discharges in Gases Part B Macroscopic Processes and Discharges ed E H Kuhardt and L H Luessen, Plenum Press, New York

H Margenau, F L McMillan, I H Dearnley, C S Pearsall and

C G Montgomery (1946) Physical Processes in the Recovery of TR Tubes, Phys Rev 70, 349

E W McDaniel (1964) Collision Phenomena in Ionized Gases, John Wiley and Sons Inc, New York

K Smith and R M Thomson (1978) Computer Modelling of Gas Lasers, Plenum Press, New York

S Takeda and A A Dougal (1960) Microwave Study of Afterglow Discharge in Water Vapour, J App Phys 31, 412

S J Tetenbaum and J A Weiss (1979) Microwave Breakdown of Water Vapour, IEEE Trans Plasma Sci PS 7, 109

C S Ward, F A Jellison, N J Brown and L Gould (1961) The Arc Loss of Multimegawatt Gas Discharge Duplexers, IEEE Trans MTT 9, 506

A T Zander and G M Hieftje (1981) Microwave-Supported Discharges, Applied Spectroscopy 35, 357

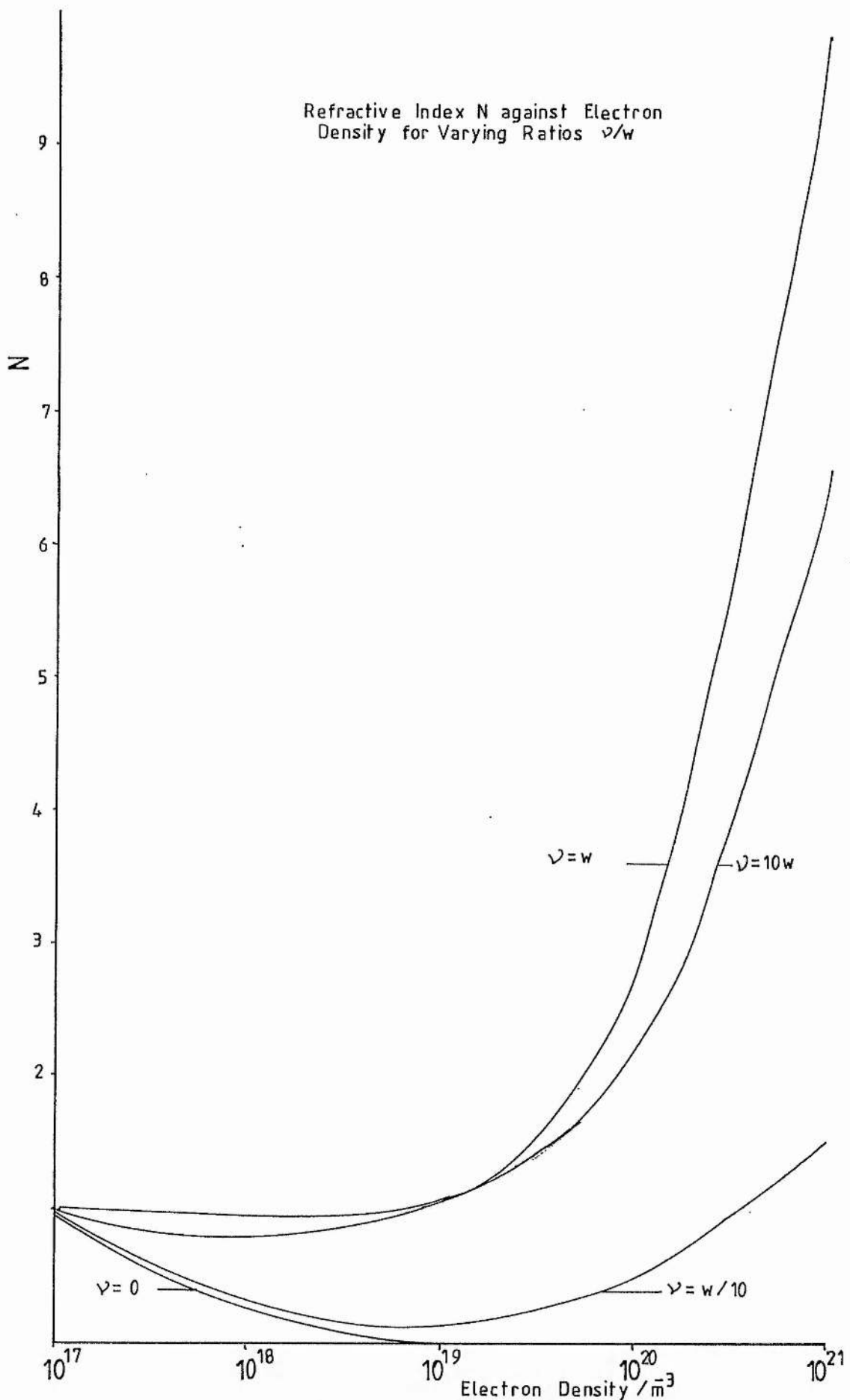


Fig 2-1 Refractive Index against Electron Density

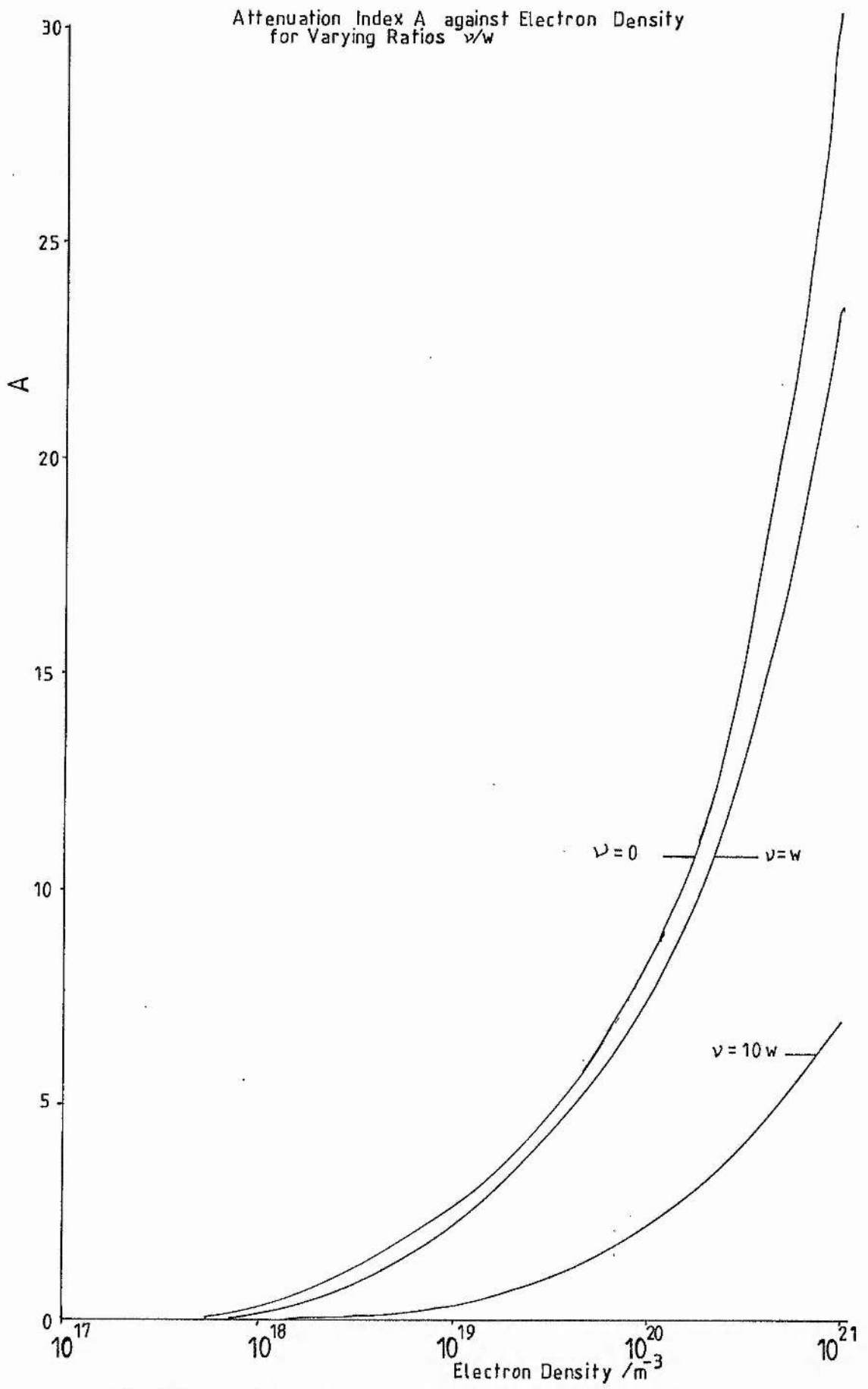


Fig 2-2 Attenuation Index against Electron Density

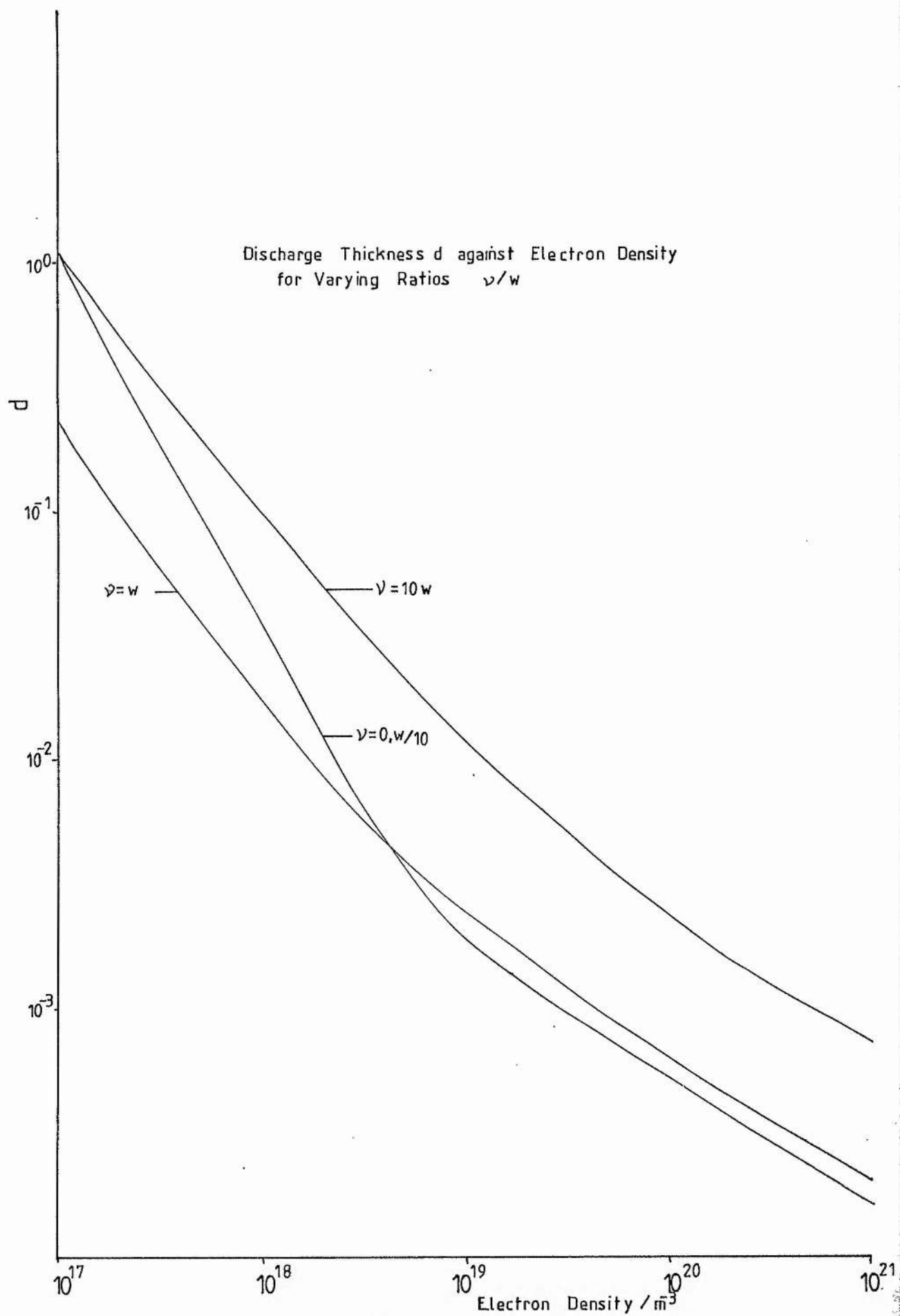


Fig 2.3 Discharge Thickness against Electron Density

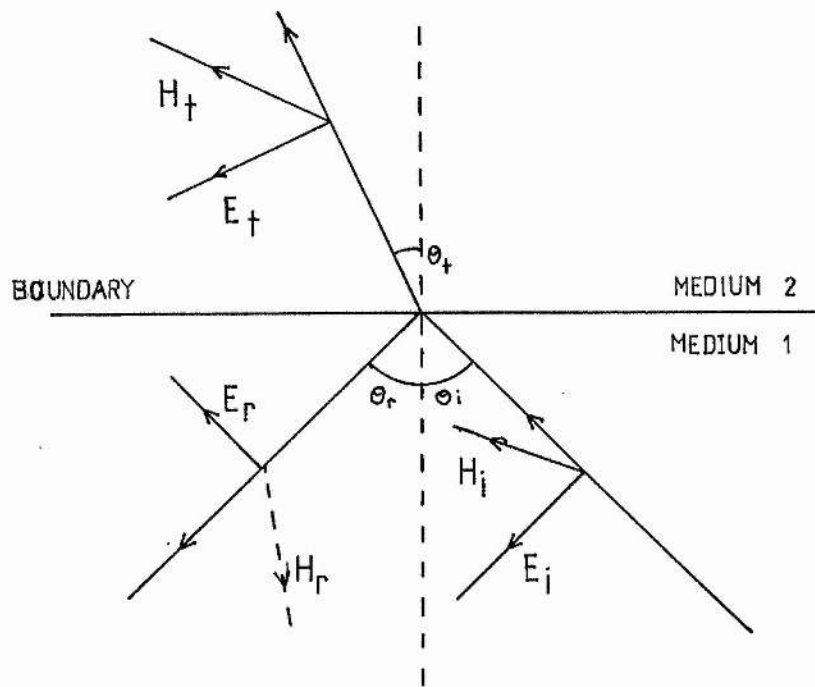


Fig 2.4 Reflection and Refraction at a Boundary

# Reflection Coefficient R against Electron Density for Microwave Discharge

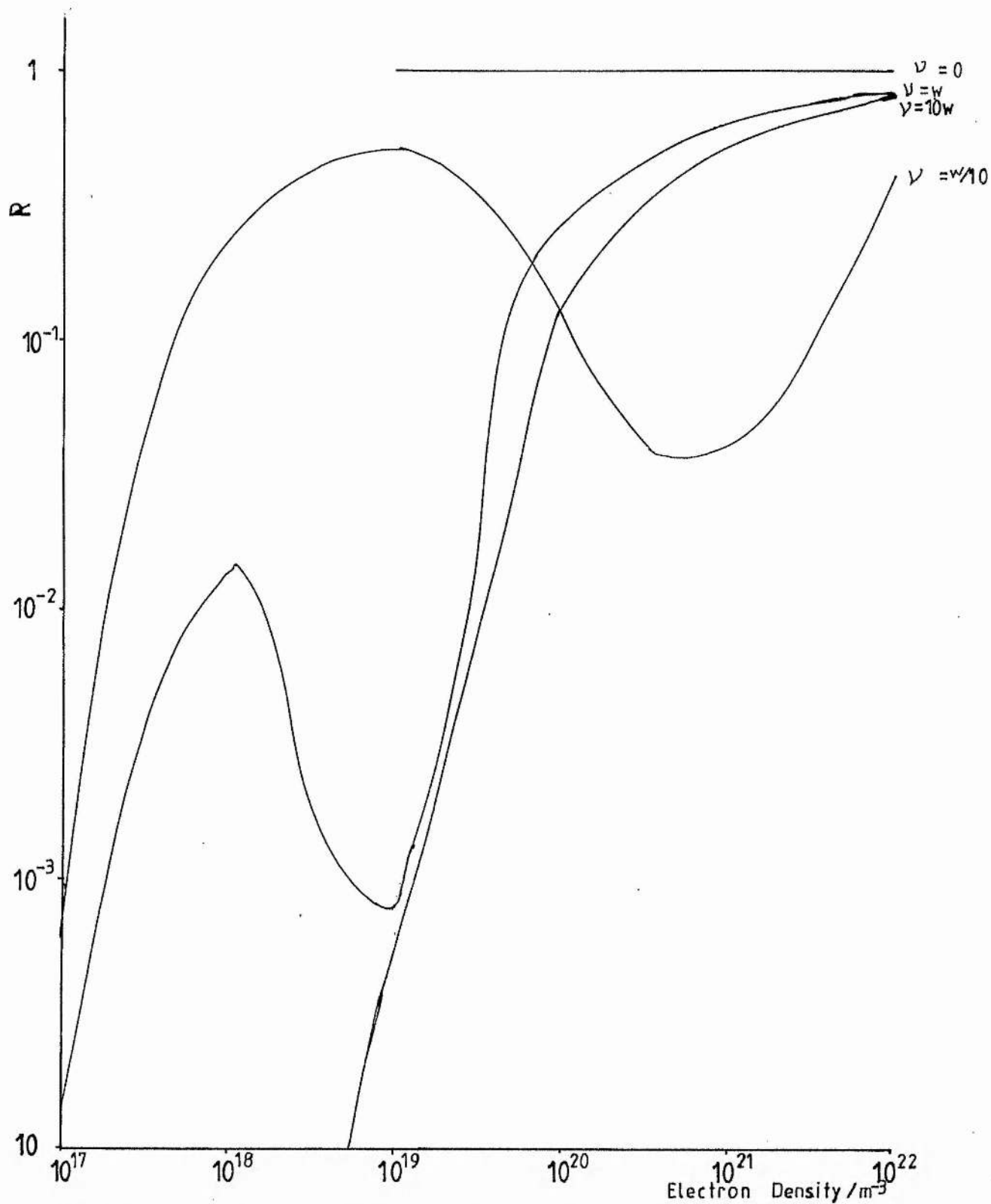


Fig 2-5 Reflection Coefficient against Electron Density.

Transmission Coefficient T against Electron Density  
in Microwave Discharge

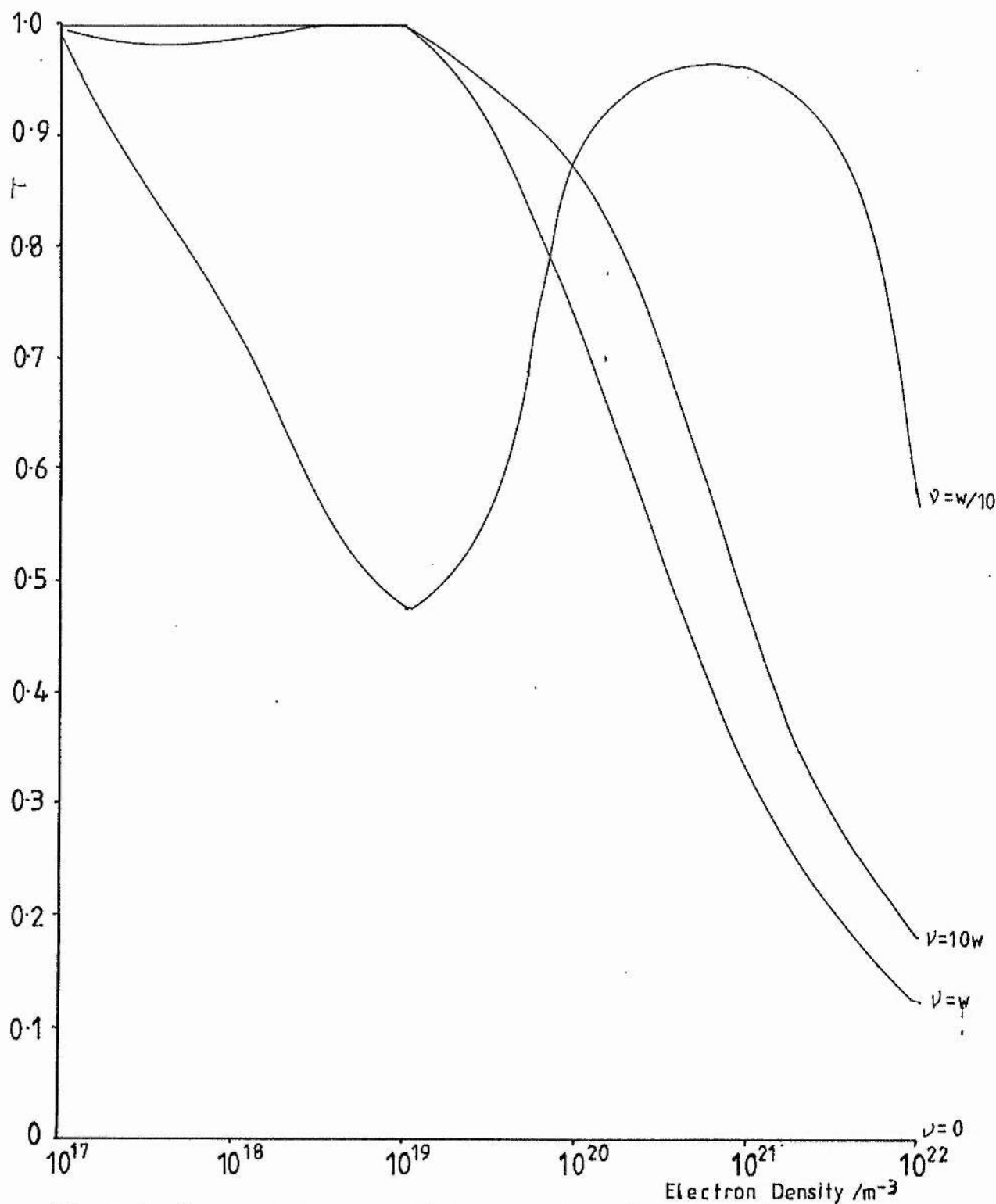


Fig 2.6 Transmission Coefficient against Electron Density

## Chapter 3 The Heat Transfer Computer Program

### 3.1 Introduction

A high power microwave pulse ionizes the gas in a TR cell, creating a discharge which then reflects the pulse and prevents it from passing through the cell to the radar receiver. The discharge, situated behind the input window of the cell, transfers heat to the window by mechanisms which will be discussed in Chapter 6, section 6.9. If the pulse contains sufficient power then sufficient heat is transferred to cause window failure either by melting or cracking.

The lower bound of the power required to cause window failure for the TR cells under consideration in this thesis is 25 W CW. The maximum acceptable arc loss (the power dissipated in the discharge) is 0.8 dB, resulting in at least 4 W CW being available for transfer from the discharge to the window. The temperature at which the window fails is not known. In this chapter a computer model of the heat transfer to the TR cell window and surround is established. The temperatures of the window, frame and flange are calculated and compared with experiment. The computer model is used in the prediction of the power handling capacity of various window materials.

### 3.2 Heat Transfer Theory

Heat is transferred by three different mechanisms, conduction, convection and radiation.

#### 3.2.1 Conduction

Heat transfer by conduction refers to kinetic and internal energy exchange between molecules of different temperatures. Energy is transferred from particles of high energy to particles of lower energy, partly through the emission and absorption of radiation by the particles and partly by direct action between them. In practice, conduction is the only mechanism of heat transfer through a solid, unless the solid is transparent to radiation.

Fourier's law for the conduction of heat relates the instantaneous rate of heat flux  $q$  through a body to  $A$ , the area through which the heat flows, the temperature gradient  $\text{grad } T$  and  $k$ , the thermal conductivity of the body by

$$q = -kA \text{grad } T \quad . \quad (3.1)$$

For steady state conduction across the boundary between two different materials 1 and 2 we have

$$k_1(dT_1/dn_1) = k_2(dT_2/dn_2) \quad , \quad (3.2)$$

where  $k_1$  and  $k_2$  are the respective thermal conductivities and  $n_1$  and  $n_2$  are the normals to the direction of heat flow. If contact resistance between the two surfaces is negligible, then  $T_1$  and  $T_2$

are equal.

### 3.2.2 Convection

Convection is the transfer of heat within a fluid due to the motion of the fluid. The motion of the fluid may be entirely the result of differences in density due to temperature differences; natural or free convection, or it may be produced by mechanical means; forced convection. Convection loss  $L$  per unit area of surface at temperature  $T$  is given by

$$L = h(T - T_o) \quad , \quad (3.3)$$

where  $h$  is  $1.42(T - T_o)^{0.25}$  for free convection from a vertical surface (Cornwell (1977)) and  $T_o$  is the ambient temperature.

### 3.2.3 Radiation

Electromagnetic radiation from a body is due to the thermal vibrations of the constituent particles. Thermodynamic limitations impose the maximum amount of thermal radiation which can be emitted by a body; black body radiation. The Stefan-Boltzmann law for  $E$ , the radiative power per unit area emitted by a body at a temperature  $T$  is

$$E = \sigma T^4 \quad , \quad (3.4)$$

where  $\sigma$  is Stefan's constant. Most materials are not perfect black bodies; they absorb and emit only a fraction  $e$  of the total radiative power, where  $e$  is the emissivity of the material, at a given temperature.

### 3.2.4 Derivation of the Heat Transfer Equation

The derivation of the governing partial differential equation for three dimensional heat transfer in the rectangular co-ordinate system is as follows. Consider a volume of dimensions  $dx$ ,  $dy$  and  $dz$ , with its centre at  $(x,y,z)$  (see fig (3.1)), to which we apply the principle of energy conservation. If this volume is located entirely within a solid then energy is transferred across its boundaries by conduction due to temperature gradients. Consider the surfaces of the volume in the planes  $x + dx/2$  and  $x - dx/2$ . For net conduction of heat across these surfaces we obtain

$$q_{(x+dx/2)} - q_{(x-dx/2)} = (q_x + dq_x/dx(dx/2)) - (q_x - dq_x/dx(dx/2)) \quad , \quad (3.5)$$

(using a Taylor's expansion of  $q_{(x+dx/2)}$  and  $q_{(x-dx/2)}$ ). Similar expression result for the net conduction in the  $y$  and  $z$  directions. The heat generated in the volume  $dx dy dz$  is  $q_g dx dy dz$ , where  $q_g$  is the heat generated per unit volume.

The first law of thermodynamics can be written

$$dU = q_i dt \quad , \quad (3.6)$$

where  $q_i$  is the heat transfer rate due to the change in the internal energy of the volume in a time  $dt$  and  $dU$  is the change in total internal energy of the volume. Also, we can write

$$c = du/dT \quad , \quad (3.7)$$

where  $c$  is the specific heat of the body and  $u$  is the internal energy per unit mass. By rearranging equation (3.6) to make  $q_i$  the subject, and substituting for  $du$  from equation (3.7) (noting that  $U$  is  $mu$  and  $m$  is  $\rho dx dy dz$ ) we obtain

$$q_1 = \rho c dx dy dz dT/dt \quad , \quad (3.8)$$

where  $\rho$  is the density of the material and  $m$  is the mass of the volume  $dx dy dz$ . Applying the principle of conservation of energy to the volume  $dx dy dz$  gives

$$q_g dx dy dz = (dq_x/dx)dx + (dq_y/dy)dy + (dq_z/dz)dz + \rho c dx dy dz dT/dt \quad . \quad (3.9)$$

So the rate of internal generation of heat equals the net rate of heat transfer across the surfaces by conduction plus the rate of change of internal energy within the system. Substituting in equation (3.9) for  $q_x$ ,  $q_y$  and  $q_z$ , using equation (3.1) gives

$$d/dx(kdT/dx) + d/dy(kdT/dy) + d/dz(kdT/dz) + q_g = \rho c dT/dt \quad . \quad (3.10)$$

If  $k$  is not a function of position then equation (3.10) becomes

$$k \Delta^2 T + q_g = \rho c dT/dt \quad . \quad (3.11)$$

By including the terms for convection and radiation loss (equations (3.3) and (3.4)), equation (3.11) becomes

$$k \Delta^2 T + q_g = 1.42(T-T_o)^{1.25} + \epsilon e(T^4 - T_o^4) + \rho c dT/dt \quad . \quad (3.12)$$

This is the partial differential equation representing heat transfer by convection, conduction and radiation, in the rectangular coordinate system.

### 3.3 Glass

#### 3.3.1 Introduction

Heat is transferred from the discharge in the TR cell to the cell window; sufficient heat may be supplied to cause window failure. The window material is a borosilicate glass whose expansion characteristics match those of the kovar window frame, to

which it is bonded, over a wide temperature range. The physical properties of the glass are listed in Appendix 1. The temperature at which the window fails is not known; it is estimated in section 3.3.2 below.

### 3.3.2 Viscosity and Temperature

When a glass is heated, it does not show a definite melting point; the viscosity of the glass simply decreases with increasing temperature. The variation of behaviour of a glass with temperature is characterised by the viscosity. A plot of the viscosity of the borosilicate glass against temperature is shown in fig (3.2). In Table 3.1 are listed the main characteristic points on a viscosity-temperature curve.

The TR cell window is subject to atmospheric pressure on one side and to a pressure of 20 torr on the other. The pressure difference of 740 torr gives a net force of  $9.83 \times 10^4$  N on the window. The window fails at its centre, where it is assumed to have reached its highest temperature. From Table 3.1 we see that the likely temperature at which the window fails is Eb, the temperature at which softening of the glass begins. At this temperature the glass begins to soften and, because of the large force on the window due to the pressure difference, the window fails. The viscosity of the glass at Eb is  $10^{12}$  poises, corresponding to a temperature of 800 K for the borosilicate glass.

### 3.4 The Computer Model

#### 3.4.1 Introduction

Heat is transferred from the discharge in the TR cell to the cell window which then loses heat to the surroundings by convection and radiation and to the frame and flange by conduction. The frame and flange also lose heat to the surroundings by convection and radiation. The window is sealed onto a kovar frame and the window and frame are then brazed into the flange of the cell using an eutectic alloy of copper and silver. The dimensions and relevant physical properties of the materials of the window, frame and flange are listed in Appendix 1. The eutectic alloy comprises silver and copper in the ratio 71.5% to 28.5%. Since both metals have a high thermal conductivity (for silver  $k$  is  $408 \text{ Wm}^{-1}\text{K}^{-1}$  and for copper  $k$  is  $387 \text{ Wm}^{-1}\text{K}^{-1}$ ), the braze does not hinder the conduction of heat from the window. The glass-to-metal seal at the window/frame boundary and the copper/silver braze at the frame/flange boundary provide negligible contact resistance between the respective surfaces so we may apply equation (3.2) to the heat conduction across these boundaries, assuming equal temperatures either side of each boundary.

The microwave power supplied to the cell is proportional to  $(E \sin(\pi x/a))^2$  at a distance  $x$  across a waveguide of width  $a$ , where  $E$  is the electric field vector of the microwave radiation. In the computer model, the power supplied to the window by the discharge

has been approximated to be decreasing linearly from the window centre (where  $x$  is  $a/2$ ).

From the window dimensions listed in Appendix 1, it can be seen that the window thickness is very much less than its length or width. Assuming that the thermal conductivity of the glass is an isotropic property, the temperature gradient across the window thickness will be equal to that across the length or width. Thus the temperature difference between the two faces of the window will be only a few percent of the temperature differences across the length or width. Hence the temperature of the window may be approximated to be uniform throughout its thickness. The conduction of heat from the discharge through the window to the frame and flange is approximately two-dimensional, therefore.

The derivation of the heat transfer equation includes the assumption that the thermal conductivity of the materials involved is constant with varying temperature. We shall also assume that the specific heat of the materials remains constant with increasing temperature. We make a further assumption that heat loss from the window, frame and flange is solely by conduction, with the losses by convection and radiation small in comparison with the heat transfer by conduction. The above assumptions and approximations will be examined in section 3.6 with the aid of results obtained using the computer program. The assumptions and approximations listed above lead to a reduced form of equation (3.12),

$$d^2T/dx^2 + d^2T/dy^2 + q_g/k = \rho c/k dT/dt \quad (3.13)$$

Equation (3.13) may be solved using a finite difference method

(Adams and Rogers (1978)).

### 3.4.2 Finite Difference Method

The window volume (the window is assumed to be a cuboid) is divided into cuboids of sides  $\Delta x$  and  $\Delta y$  and unit depth. The sum of all the finite elements forms a grid network, as shown in fig (3.3). The centre or node of each element is assigned a temperature which is considered to be the temperature of the element. In a finite difference formulation, the temperature gradient is calculated as though the temperature changes linearly between two nodes. The rows of points of temperature are labelled  $i$  and the columns are labelled  $j$ . The principle of conservation of energy is applied to each cuboid. The heat transfer between interior nodes  $(i,j)$  and  $(i,j-1)$  is, by using Fourier's Law (equation (3.1))

$$q_g/k = \Delta y(T_{i,j-1} - T_{i,j})/\Delta x \quad , \quad (3.14)$$

where  $T_{i,j-1}$  and  $T_{i,j}$  are the temperatures at the points  $(i,j-1)$  and  $(i,j)$  (see fig (3.3)). Similar equations may be obtained for the other three nodes neighbouring  $(i,j)$ . The rate of change of temperature with time,  $dT/dt$ , at a point  $(i,j)$  can be approximated by a forward difference expression

$$dT/dt \approx (T_{i,j}^{k+1} - T_{i,j}^k)/\Delta t \quad , \quad (3.15)$$

where  $T_{i,j}^{k+1}$  is the temperature at time  $k+1$ ,  $T_{i,j}^k$  is the temperature at time  $k$  and the time interval is  $\Delta t$ .

Two methods may be used to obtain the finite difference approximation for unsteady or time dependent conduction, the explicit method and the implicit method. The explicit method involves evaluating the spatial temperature derivative at a time  $k$  and evaluating the time temperature difference in a forward difference approximation. So for the simple case where  $\Delta x$  equals  $\Delta y$ , equation (3.13) can be approximated as

$$\begin{aligned} & (T_{i+1,j}^k + T_{i-1,j}^k + T_{i,j+1}^k + T_{i,j-1}^k - 4T_{i,j}^k) / (\Delta x)^2 \\ & + q_g/k = \rho c/k (T_{i,j}^{k+1} - T_{i,j}^k) / \Delta t \quad . \end{aligned} \quad (3.16)$$

An approximation associated with the above finite difference formulation is that while the temperature  $T_{i,j}^k$  changes during the time interval  $\Delta t$  to a value  $T_{i,j}^{k+1}$ , the values of  $T_{i+1,j}^k$ ,  $T_{i-1,j}^k$ ,  $T_{i,j+1}^k$  and  $T_{i,j-1}^k$  are all assumed to remain constant. This approximation assumes that the variation throughout a volume, of volume terms such as internal energy, is less than the variation in time  $\Delta t$ , and that the variation with time of surface terms such as heat flux, is negligible with respect to their spatial variation.

The implicit method, on the other hand, involves evaluating the spatial temperature derivative at a time  $k+1$  rather than at time  $k$  giving, as an approximation for equation (3.13),

$$\begin{aligned} & (T_{i+1,j}^{k+1} + T_{i-1,j}^{k+1} + T_{i,j+1}^{k+1} + T_{i,j-1}^{k+1} - 4T_{i,j}^{k+1}) / (\Delta x)^2 + q_g/k \\ & = \rho c/k (T_{i,j}^{k+1} - T_{i,j}^k) / \Delta t \quad , \end{aligned} \quad (3.17)$$

at the point  $(i,j)$ . Although the implicit method involves the simultaneous solution of a set of algebraic equations, it has the advantage that the system of equations is stable for all values of  $\alpha \Delta t / (\Delta x)^2$  (Smith (1978)) where  $\alpha$ , the thermal diffusivity, is given

by

$$\alpha = k/\rho c \quad . \quad (3.18)$$

Hence the implicit finite difference method, represented by equation (3.17), is used in the computer solution of equation (3.13), the heat transfer equation for the TR cell window.

### 3.4.3 Establishment of the Model

For the computer model the window area is divided into a grid network, with  $x$  equalling  $y$ , as shown in fig (3.4). The temperatures of the points on the grid network are calculated at one second intervals. The microwave power supplied to the cell is input to the program. The power transferred to the window is calculated in the program. It is calculated to be equal to the maximum acceptable value of the arc loss, 0.8 dB. We assume that the heating of the window is due solely to heat transfer from the discharge, direct microwave heating of the window being negligible. This has been proved in Chapter 2. To compare glass with other likely window materials, the window material is selected in the program from a choice of glass, glass ceramic, alumina or cordierite. For the physical properties of these materials see Appendix 1. The length, width and thickness of the window, assuming X-band (8-12 GHz) cells, are all variables in the program and are input to the program. The points on the window for which the temperatures are calculated lie along its centre, along its length, and have a separation of half the width of the window. The window, frame and flange are all at room temperature, 293 K, before microwave power is applied and heating commences. The solution of

The solution of equation (3.17) for each point of the grid network on the window involves the solution of a set of linear equations, one for each point. The set of linear equations is written in matrix form with the vector multiplying the matrix being the temperature at each point. The dimension of the matrix is the number of points for which the temperature is to be calculated. Greater accuracy is obtained by increasing the number of points on the grid for which the temperature is to be calculated, at the expense of increasing the computer time required.

#### 3.4.4 Calculation of the Frame and Flange Temperatures

Assuming negligible thermal contact resistance at the window/frame boundary and at the frame/flange boundary, equation (3.2) is used in the calculation of the heat conducted across the boundaries to the surroundings. In the computer model the direction of heat flow from the window to the frame is assumed to be parallel to the window surface. At the window/frame boundary we assume that the heat flows through the frame in a direction perpendicular to the length of the window, along  $\Delta x_2$ , the shortest distance through the frame to the flange (see fig (3.4)). Similarly the heat, having reached the flange, is assumed to flow straight to the flange edge, along  $\Delta x_3$ . The temperature of the surroundings at a distance  $\Delta x_4$  from the flange, where  $\Delta x_4$  is small, is 293 K. The distance  $\Delta x_4$  is adjusted to give the experimentally measured temperature of the edge of the flange when high power is applied to the cell. In the model, the window, frame and flange are all assumed to have the same thickness, that of the window.

Application of equation (3.2) to the heat transfer across the window/frame, frame/flange and flange/surroundings boundaries (with the temperatures of both materials either side of a boundary being equal) gives

$$\begin{aligned} k_1(T_W - T_{FR})/\Delta x_1 &= k_2(T_{FR} - T_{FL})/\Delta x_2 \\ &= k_3(T_{FL} - T_E)/\Delta x_3 = k_4(T_E - 293)/\Delta x_4 \quad , \end{aligned} \quad (3.19)$$

where  $k_1$ ,  $k_2$ ,  $k_3$  and  $k_4$  are the thermal conductivities of the window, frame, flange and surroundings,  $T_W$  is the temperature at the window centre,  $T_{FR}$  is the temperature at the centre of the window/frame boundary,  $T_{FL}$  is the temperature at the centre of the frame/flange boundary and  $T_E$  is the temperature at the centre of the flange edge.

The computer program to solve the heat transfer equation is given in Appendix 2. The program is written in Basic and is run on a Hewlett-Packard 9826A desk top computer.

### 3.5 Results

#### 3.5.1 Results of the Computer Program

It can be seen from Appendix 1 that of the suggested window materials, glass fails at the lowest temperature and alumina at the highest temperature, with glass ceramic and corderite intermediate. In Table 3.2 is shown the power input to the window of dimensions  $15 \times 3 \times 0.24 \text{ mm}^3$  calculated to cause window failure, for each of the four window materials. Glass, having a lower thermal conductivity, cannot dissipate the applied power as readily as the

other window materials. It also has a much lower failure temperature than the other materials, so it fails at a much lower power. The glass ceramic and corderite have similar values of thermal conductivity and failure temperature and hence fail at similar power levels. Alumina, having the highest thermal conductivity and the highest failure temperature, survives a very much higher power level than the other window materials.

In fig (3.5) is plotted the variation of temperature with position along axis AB on the TR cell (see fig (3.4)) for increasing power levels for each of the four possible window materials. The window dimensions ( $15 \times 3 \times 0.24 \text{ mm}^3$ ) and a heating time of 30 seconds are common to all the window materials. In fig (3.6) is shown a comparison of the temperatures attained by a window of dimensions  $15 \times 3 \times 0.24 \text{ mm}^3$  in each of the four materials, with 20 W applied for 30 seconds. It can be clearly seen that the temperature at the window centre is highest for glass and lowest for alumina. Glass ceramic and corderite attain similar temperatures. The temperatures at the window/frame boundary and at the frame/flange boundary are similar for all the window materials, despite the variation in the temperature at the window centre. This indicates that the temperatures of the frame and flange are more dependent on the input power than on the material of the window or on the temperature of the window centre.

In fig (3.7) are shown the plots of the variation of temperature along TR cell axis AB with window length (the other dimensions remaining constant), for 30 seconds heating with 20 W, for each of the four window materials. The graphs are plotted for window lengths 13 mm to 17 mm, at 1 mm intervals. Increasing the window length decreases the temperature of the window centre and also the temperatures at the window/frame boundary and the frame/flange boundary. Increasing the window length increases the window surface area and hence decreases the power per unit volume on the window. For a decrease in power per unit volume on the window there is a corresponding decrease in the power per unit area conducted from the window to the frame and flange. Hence the temperatures at the window-frame boundary and the frame-flange boundary decrease with increasing window length.

In fig (3.8) are shown the plots of variation of temperature along TR cell axis AB with window width (the other dimensions remaining fixed) for 30 seconds heating with 20 W, for each of the four window materials. The graphs are plotted for window widths 2 mm to 5 mm, at 1 mm intervals. Increasing the window width causes a decrease of the temperatures at the window/frame boundary and at the frame/flange boundary, but an increase of the temperature at the window centre. Increasing the window width increases the path length  $\Delta x_1$  for conduction of heat through the window material to the frame. Glass, glass ceramic or corderite have much lower thermal conductivities than the kovar of the frame. Hence, less heat is conducted to the frame and flange in a

given time interval with an increased window width. Hence the frame and flange decrease in temperature and the temperature at the window centre increases with an increase in window width. For alumina, with a similar thermal conductivity to that of the kovar frame, a minimum temperature at the window centre occurs for 4mm thickness.

Fig (3.9) shows the variation of temperature across the TR cell axis AB with thickness of the window material, the other dimensions remaining constant, for 30 seconds heating with 20 W, for the four window materials. The graphs are plotted for windows of thickness 0.2 mm, 0.24 mm, 0.3 mm, 0.4 mm and 0.5 mm. Increasing the window thickness decreases the temperatures at the window centre, window/frame boundary and frame/flange boundary. In the computer model, heat is assumed to flow in a direction perpendicular to the window surface. By increasing the window thickness the area through which heat is conducted from the window to the surroundings is increased. Hence the rate of heat conduction from the window to the frame and flange increases with increasing window thickness. The thicker the window material, the lower the temperature attained by it for a given power input.

### 3.5.2 Comparison with Experimental Results- EEV Co Data

X-band TR cells with glass windows of dimensions  $15 \times 3 \times 0.24 \text{ mm}^3$  fail at power levels of at least 25 W CW. The computer model predicts that window failure occurs at 25 W CW. So for the above-mentioned cell, the computer model successfully predicts a

lower bound for the power level required to cause window failure. The graph of position along the axis CD on the glass window of a TR cell for a fixed power input of 25 W and heating time increasing at 2 second intervals, fig (3.10), shows that the window becomes hottest at its centre and rapidly cools towards the window/frame boundary. This agrees with the experimental evidence on window failure. The windows fail by melting, producing a hole of about 1mm diameter at its centre. Isotherms at 100 degree intervals for the glass window of dimensions  $15 \times 3 \times 0.24 \text{ mm}^3$ , with 25 W applied for 30 seconds, are shown in fig (3.11). This figure clearly shows that only a very small area, at the window centre, reaches failure temperature.

Increasing amounts of power were supplied to a cell with a window of dimensions  $15 \times 3 \times 0.24 \text{ mm}^3$  and to a cell with a window of dimensions  $12 \times 2 \times 0.38 \text{ mm}^3$  in turn, at the same time measuring the temperature at the centre of the frame/flange boundary,  $T_{FL}$ . The results are displayed in fig (3.12), where it can be seen that the edge of the frame for the cell with the narrower window is much hotter than for the cell with the wider window. When window failure occurs, the temperature at the centre of the frame/flange boundary is 398 K calculated and 346 K measured for the cell with the narrower window. For the cell with the wider window, the temperature at the frame/flange boundary is calculated to be 375 K and measured to be between 323 K and 331 K. In both cases, the measured temperature is several degrees lower than the calculated temperature, indicating a more efficient heat transfer from the window than is allowed for in the model, since other processes have

been neglected. The model successfully predicts, however, that for the cell with the narrower window the temperature at the centre of the frame/flange boundary is greater than for the cell with the wider window.

The program predicts that the cell with the narrow window should fail when 40 W CW are applied, whereas the cell with the wider window is predicted to fail when 25 W are applied. Experimental observations indicate that the cells with narrow windows should fail at power levels below those containing wider windows. In the program it is assumed that of the power supplied, 0.8 dB is transferred to the window, regardless of differences in cell window dimensions and materials. The maximum acceptable arc loss is 0.8 dB; the actual arc loss may well be below this value and have different values for the two cells for the same applied power level.

Experiments carried out by EEV on a TR cell containing an alumina window having dimensions  $15 \times 3 \times 0.4 \text{ mm}^3$  showed that one cell failed at 600 W CW and one at 300 W CW. The estimated failure temperature of the alumina lies between 1400 K and 1700 K. According to the model, the above-mentioned window will fail at a power level between 280 W and 350 W. The model successfully predicts the lower bound for the failure power level for an alumina window having the above dimensions.

### 3.6 Further Consideration of the Approximations

#### 3.6.1 Radiation and Convection Losses

In section 3.4.1 it was assumed that the main mechanism of heat loss from the window, frame and flange was conduction, radiation and convection being negligible. In fig (3.11) are plotted the isotherms on the glass window of dimensions  $15 \times 3 \times 0.24 \text{ mm}^3$  at 100 degree intervals, for an input power level sufficient to cause window failure. Using equations (3.3) and (3.4) for the heat loss per unit area by convection and radiation respectively, with  $\epsilon$ , the emissivity of the glass being 0.93, the radiation and convection losses of the window are calculated as follows. The percentage of the window area between two temperature isotherms is calculated and the radiation and convection losses for each area calculated, using the temperature of the upper isotherm (see Table 3.3). The calculated total power loss from the window by radiation is 312 mW and by convection is 65 mW. Even with 25 W applied power, sufficient to cause window failure, the percentage of power supplied to the window lost by radiation and convection is 7.4% and 1.5% respectively. These losses are small in comparison with the heat loss by conduction and so may be neglected. The frame and flange are at lower temperatures than the window, so radiation and convection losses from the frame and flange are also small. Therefore the original assumption that radiation and convection losses are negligible in comparison with the conduction losses has been justified.

### 3.6.2 Variation of Specific Heat and Thermal Conductivity with Temperature

It is assumed in the computer model that the specific heat of the window materials is independent of temperature. The increase in specific heat with temperature is about 30%, going from room temperature to failure temperature for the materials used for the window. For example, considering glass and alumina, the specific heat is  $8.37 \times 10^2 \text{ Jkg}^{-1}\text{K}^{-1}$  at room temperature, rising to a value of about  $1.1 \times 10^3 \text{ Jkg}^{-1}\text{K}^{-1}$  at their respective failure temperatures (Goldsmith et al (1961)). On inserting the maximum possible values for the specific heat in the computer program, with a power input of 20 W, we obtain the results listed in Table 3.4. The results show a difference between the window temperatures for the values of specific heat at room temperature and at failure temperature of less than 1%. Thus the increase in specific heat with increasing temperature has a negligible effect on the temperature attained by the window.

In the derivation of the heat transfer equation, equation (3.12), it was assumed that the thermal conductivity of the materials was independent of temperature. If we assume a 15% variation of thermal conductivity of kovar with temperature over the range 300-800 K and a 10% variation in the thermal conductivity of steel with temperature over the range 300-600 K (Goldsmith (1961)) we obtain the results shown in Table 3.5 for the temperatures along the centre of a glass window with 20 W power

applied for 30 seconds (the maximum likely temperature attained by the frame is 800 K and by the flange is 600 K). The percentage variation of temperature of the window centre with variation of thermal conductivity of the materials of the frame and flange is of the order of 1%. This variation is small enough to be neglected. Therefore, for the frame and flange, the approximation of constant thermal conductivity is satisfactory.

We consider a typical increase in thermal conductivity with temperature for a borosilicate glass of 40% (Goldsmith et al (1961)) over the temperature range 300-800 K. At 680 K the value of the thermal conductivity is estimated to have increased by 30% from its value at room temperature. In Table 3.6 are listed the temperatures across a glass window for a power input of 20 W for 30 seconds, calculated using the values of thermal conductivity for 300 K and 680 K. The percentage difference between the temperatures calculated using the two values of thermal conductivity is about 10%. From fig (3.11), we see that 90% of the window is at a temperature below 680 K. Therefore, the increase in thermal conductivity for the greater part of the window is less than 30%. It is likely, therefore, that the percentage variation of temperature of the window centre resulting from the use of the values of thermal conductivities of the window materials at room temperature is less than 10%. This is the largest single source of error in the model.

### 3.6.3 Arc Loss

It has been assumed in the theoretical model that the power transferred to the TR cell window by the discharge is equal to the maximum acceptable arc loss, 0.8 dB. The experimental setup to measure the arc loss of a cell as a function of input power was as shown in fig (3.13). From the graphs of input power against arc loss, figs (3.14) and (3.15) it can be seen that, for the cell measured, (of window dimensions  $15 \times 3 \times 0.24 \text{ mm}^3$ ) the arc loss in dB decreased with increasing incident power, for both pulsed and CW power. For pulsed power, the arc loss is lower than the maximum acceptable value of 0.8 dB, as used in the calculation. However, for CW power the arc loss decreases from a value much higher than the limit of 0.8 dB for low incident power to about 0.8 dB at a power level likely to damage the window. So, less pulsed power is available for transfer from the discharge to the cell window than was allowed in the model. Hence, a higher pulsed power level is actually required to give the same power available to the window as is calculated in the model. For CW input power, the arc loss in the cell in dB decreases with increasing incident power. However, the arc loss power in watts increases as the incident power increases. A more accurate estimation of the power absorbed in the discharge and hence the power available for transfer to the window is required, for more accurate predictions of failure power levels of TR cell windows.

### 3.7 Conclusions

The computer model of the heat transfer from the microwave-excited discharge in a TR cell to the window of the cell successfully predicts that the glass window in an X-band cell fails at applied powers of the order of 25 W CW. It predicts that alumina windows will withstand much higher powers than glass windows; this has been proven experimentally. Of the suggested window materials, corundum has similar predicted heat transfer properties to glass ceramic, and alumina, due to its much larger thermal conductivity than those of the other materials, has the best heat transfer properties. Other factors, though, affect the choice of window material, such as ease of manufacture of the windows and of the window-to-frame seals. The window is a resonant element of a precise Q and frequency and forms part of the multi-element resonant system of the TR cell. The windows must cause minimum attenuation of the low power received signal over the required bandwidth. All the above points must be taken into account when choosing a window material.

The computer program has some limitations. The most significant one is the failure to take into account the increase of thermal conductivity with temperature of the materials of the window. Increasing thermal conductivity with increasing temperature should lead to an increase in the rate of heat conduction from the hottest parts of the system, thus slowing down the rate of increase of temperature. This would result in the system actually reaching a

lower temperature than is predicted by the model for a given power input. Thus the model gives a lower bound to the power required to cause a given temperature increase in a window material of given dimensions. The estimated error of the results produced by the program is of the order of 10%.

References

- J A Adams and D F Rogers (1978) Computer Aided Heat Transfer Analysis, McGraw Hill Book Co, London
- K Cornwell (1977) The Flow of Heat, Van Nostrand Reinhold, London
- A Goldsmith, T E Waterman and H J Hirschhorn (1961) Handbook of Thermophysical Properties of Solid Materials, Pergamon Press, New York
- G D Smith (1978) Numerical Solutions of Partial Differential Equations, Oxford University Press

Table 3.1

## Temperature and Viscosity for Glass

Temperature	Viscosity	Description of Glass
Strain Point	$10^{14.5}$	Internal stresses within the glass are decomposed within 15 hours by flow processes
Transformation Range	$10^{14} - 10^{13}$	Limiting range between brittle and viscous states
Upper annealing Temperature	$10^{13}$	Internal stresses within the glass are decomposed within 15 minutes by flow processes
Eb	$10^{12}$	Temperature at which softening begins
Softening Point	$10^{7.6}$	Temperature at which glass visibly begins to deform under its own weight
Sintering Temperature	$10^6$	Temperature at which lightly compressed glass powder will sinter to a compact piece
Working Point	$10^4$	Temperature at which glass is soft enough to be worked
Melting Point	$10^2$	Temperature at which glass is considered a fluid

Table 3.2

Power Failure Levels for Window Materials

	Temperature/K	Power/W	Thermal Conductivity/ $Wm^{-1}K^{-1}$
Glass	800	25	1.15
Glass Ceramic	1373	87	2.51
Alumina	1400	167	13.0
Corderite	1300	88	2.93

Table 3.3

Radiation and Convection Loss from a Glass Window  
at Failure Temperature

Window Area	Radiation Loss/mW	Convection Loss/mW
11% under 400 K	6.07	2.2
31% under 500 K	45.6	15.0
37% under 600 K	111.3	21.0
11% under 700 K	55.8	12.0
10% under 800 K	93.0	15.0
Total	312	65

Table 3.4

Variation of Window Temperature with Specific Heat

Temperature along Window Centre/K

Glass		Alumina	
Specific Heat $\text{Jkg}^{-1}\text{K}^{-1}$		Specific Heat $\text{Jkg}^{-1}\text{K}^{-1}$	
$8.37 \times 10^2$	$1.1 \times 10^3$	$8.37 \times 10^2$	$1.1 \times 10^3$
532.8	532.7	390.3	389.9
608.4	608.1	403.9	403.4
652.6	652.3	414.6	414.1
683.5	683.2	422.2	421.8
700.5	700.2	425.7	425.3
683.5	683.2	422.2	421.8
652.6	652.3	414.6	414.1
608.4	608.1	403.9	403.4
532.8	532.7	390.3	389.9

Table 3.5

Variation of Window Temperature with Thermal Conductivity  
of the Frame and Flange

	k Steel 54	k Steel 60	k Steel 54
	k Kovar 17	k Kovar 17	k Kovar 20
Temperature	532.8	529.0	527.0
of window	608.4	603.9	601.4
centre/K	652.6	647.5	644.7
	683.5	678.0	675.0
	700.6	694.9	691.8
	683.5	678.0	675.0
	652.6	647.5	644.7
	608.4	603.9	601.4
	532.8	529.0	527.0

Table 3.6

Variation of Window Temperatures with Thermal Conductivity of  
the Borosilicate Glass

Thermal Conductivity  $1.15 \text{ Wm}^{-1} \text{ K}^{-1}$

532.8 608.4 652.6 683.5 700.6 683.5 652.6 608.4 532.8

Thermal Conductivity  $1.5 \text{ Wm}^{-1} \text{ K}^{-1}$

489.1 549.2 584.9 609.9 623.5 609.9 584.9 549.2 489.1

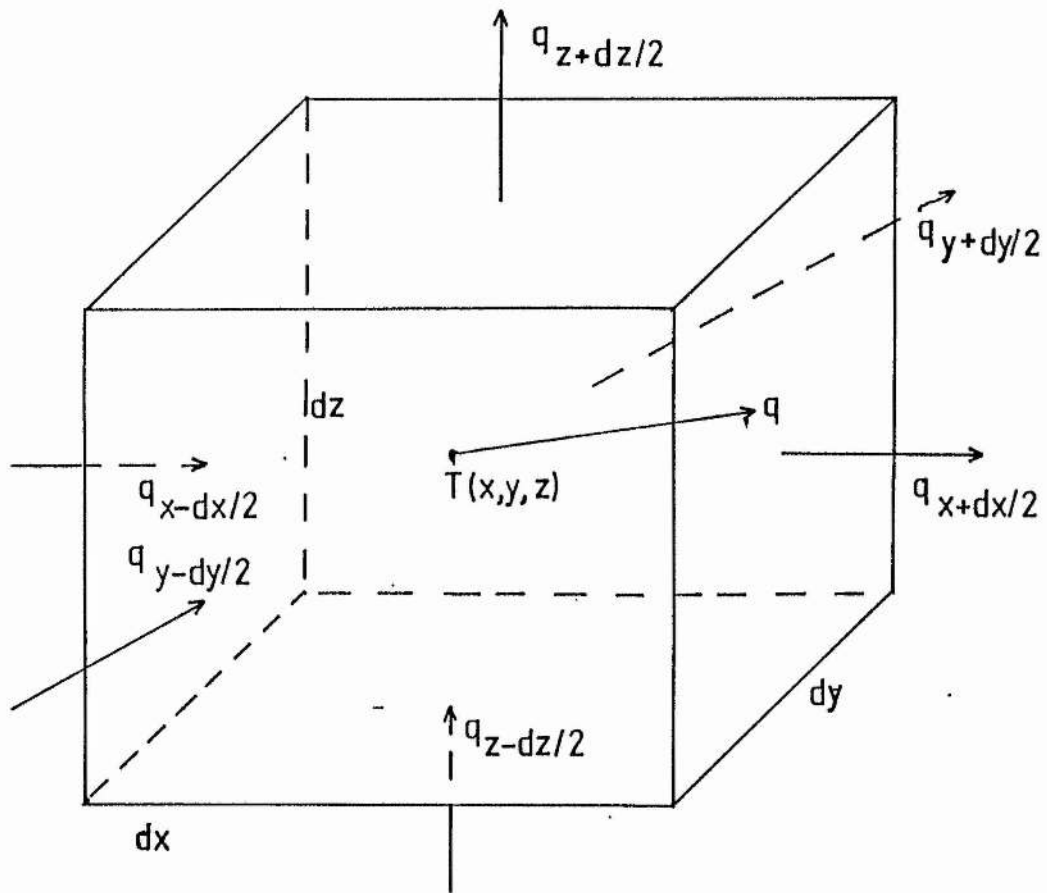


Fig 3-1 Differential Element of Volume  $dx dy dz$

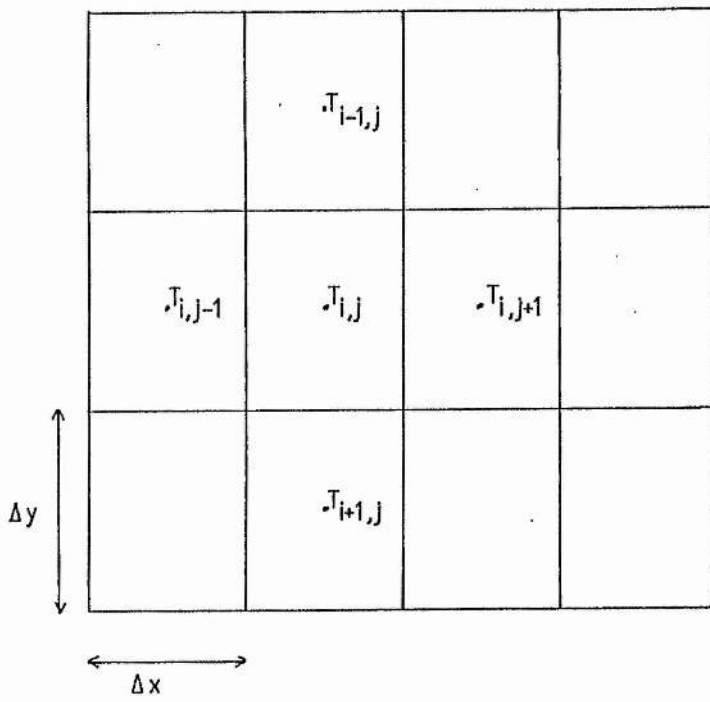


Fig 3-3. Grid Network

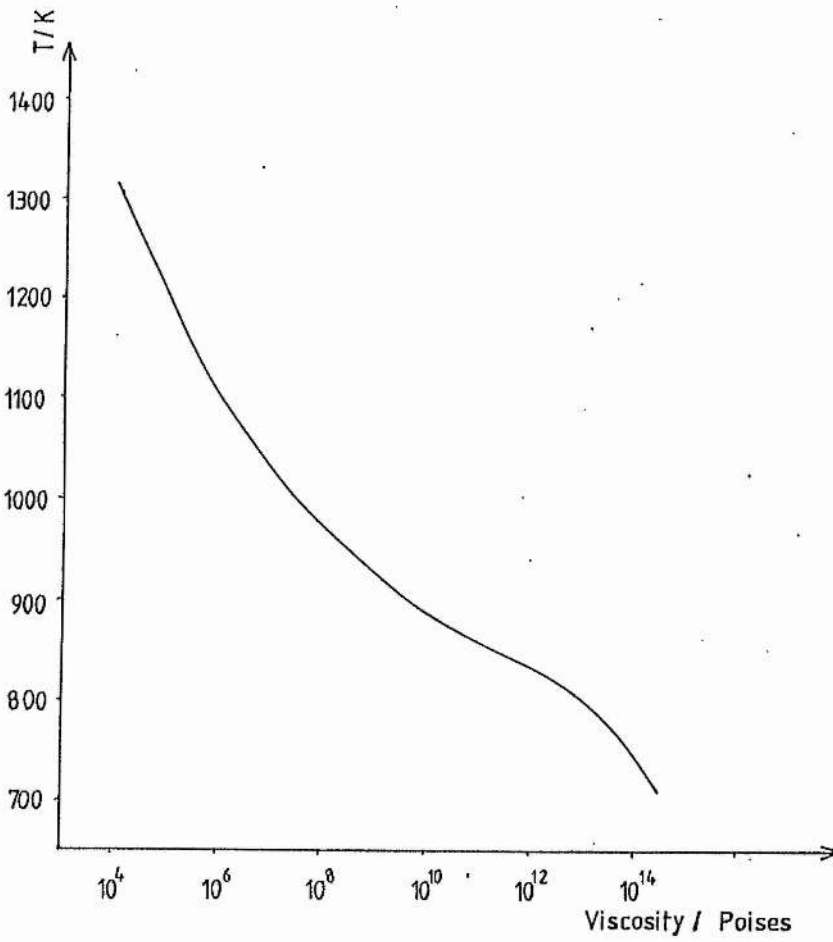


Fig 3-2 Temperature / Viscosity Curve for Borosilicate Glass



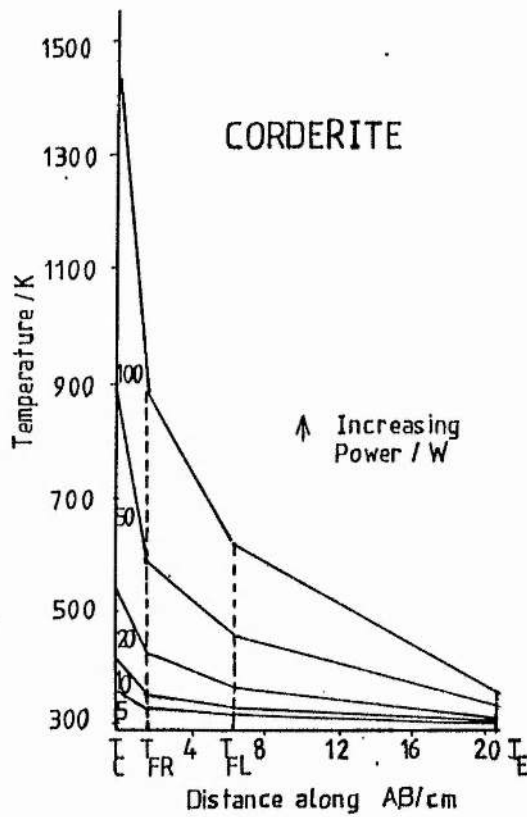
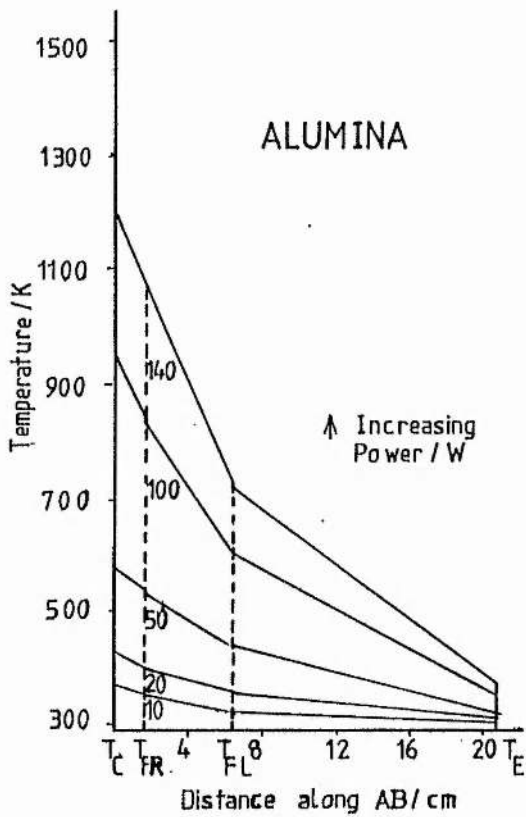
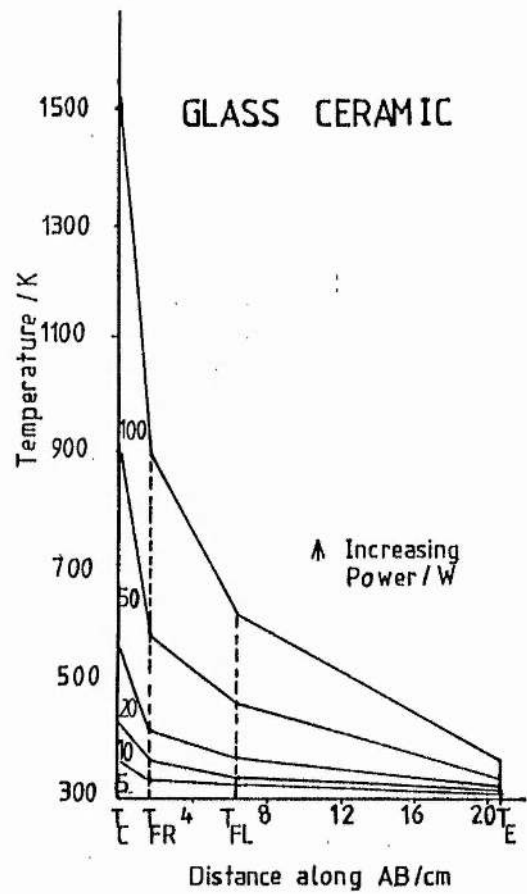
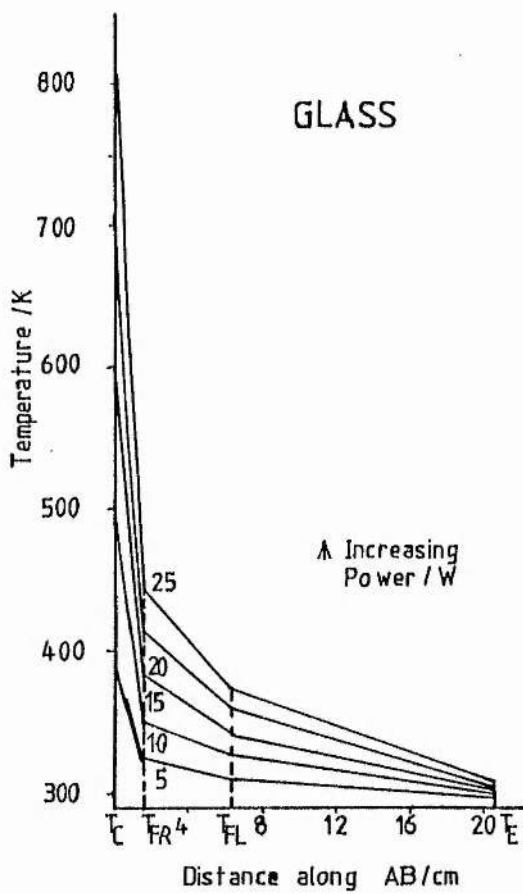


Fig 3-5 Variation of Temperature along TR Cell Axis AB with Power

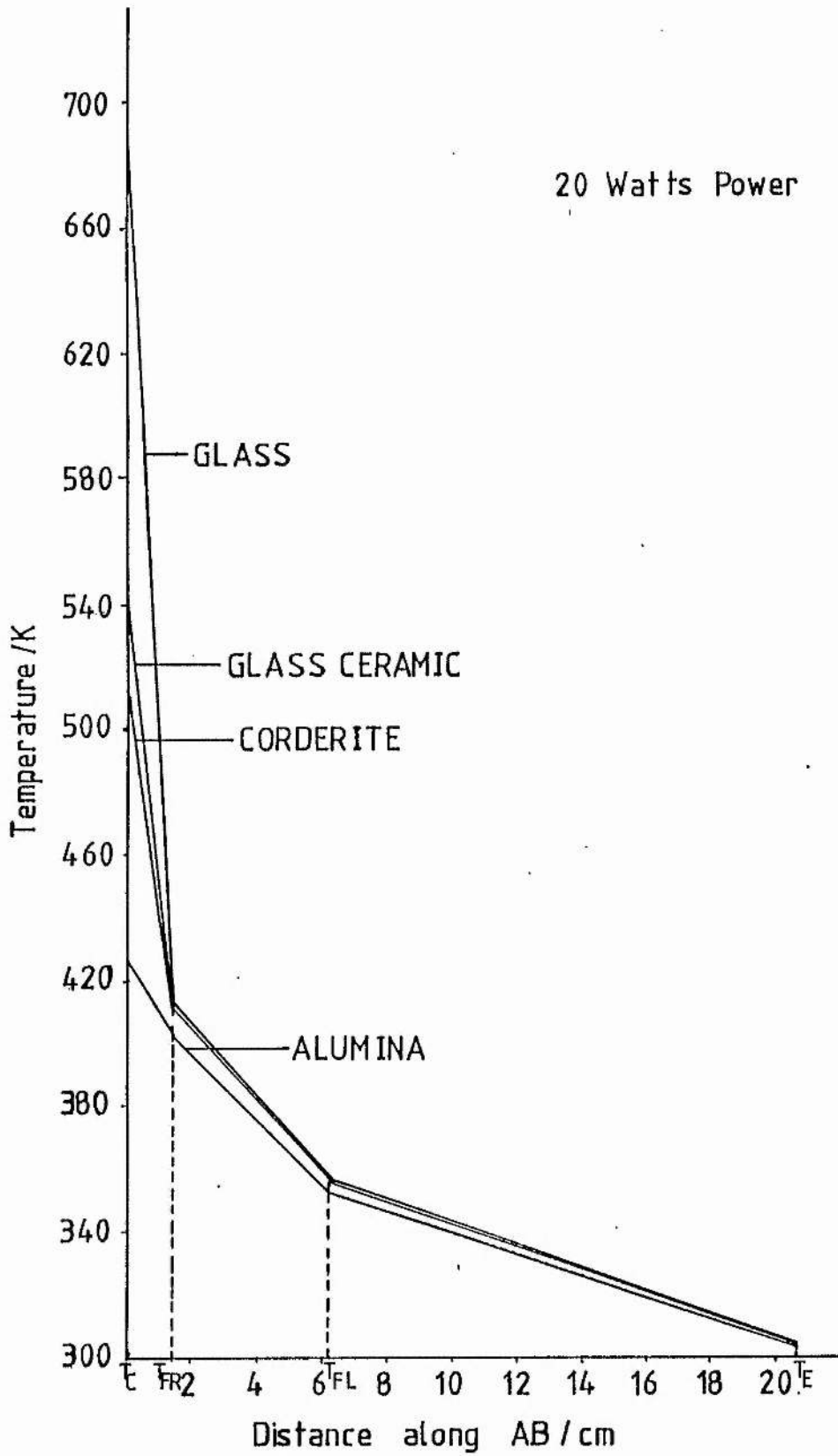


Fig 3-6 Comparison of the Temperatures along TR Cell Axis AB for the different Window Materials

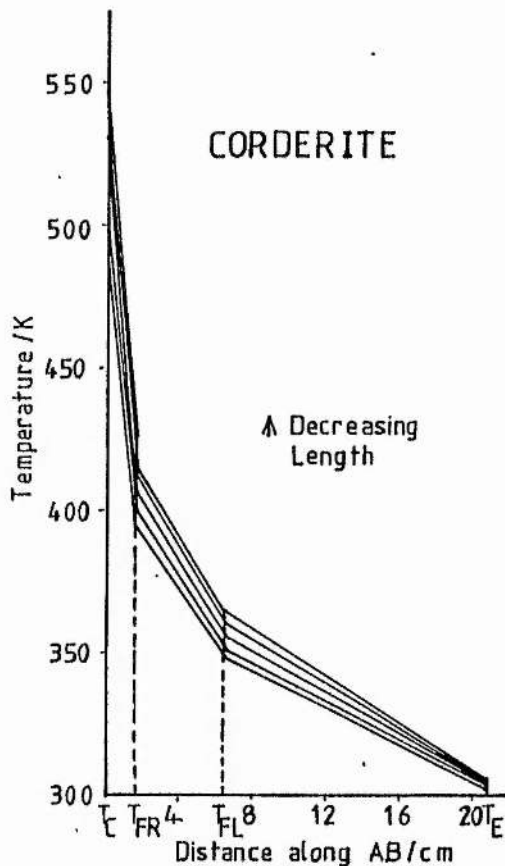
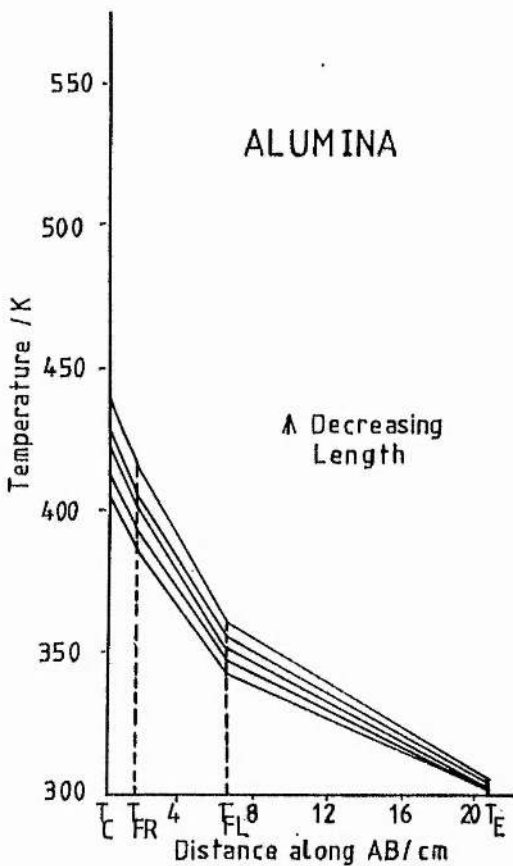
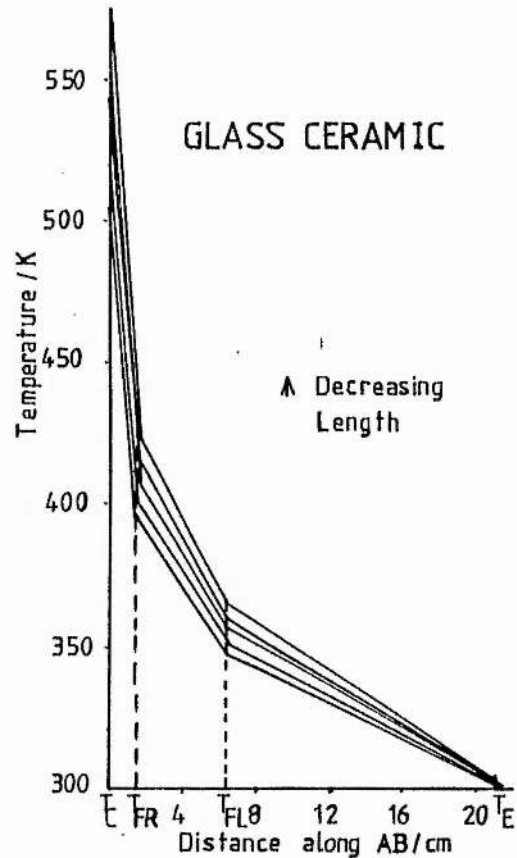
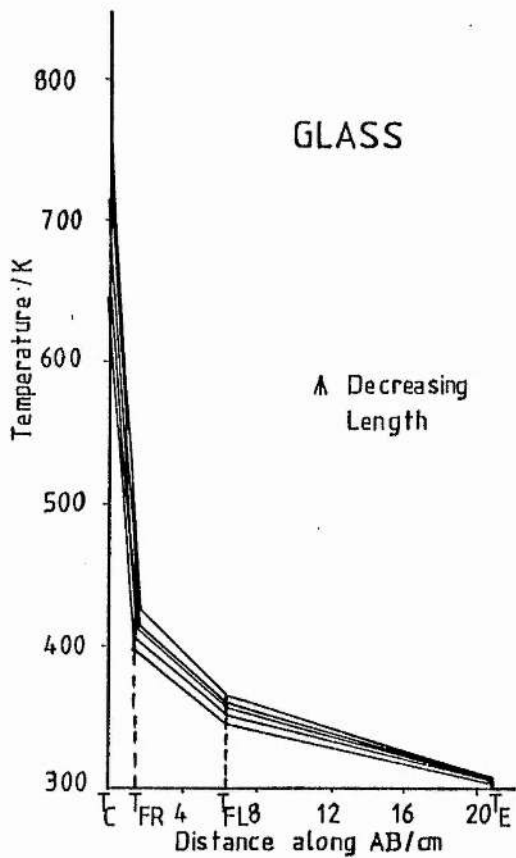


Fig 37 Variation of Temperature along TR Cell Axis AB for Varying Window Length Power Input 20 W

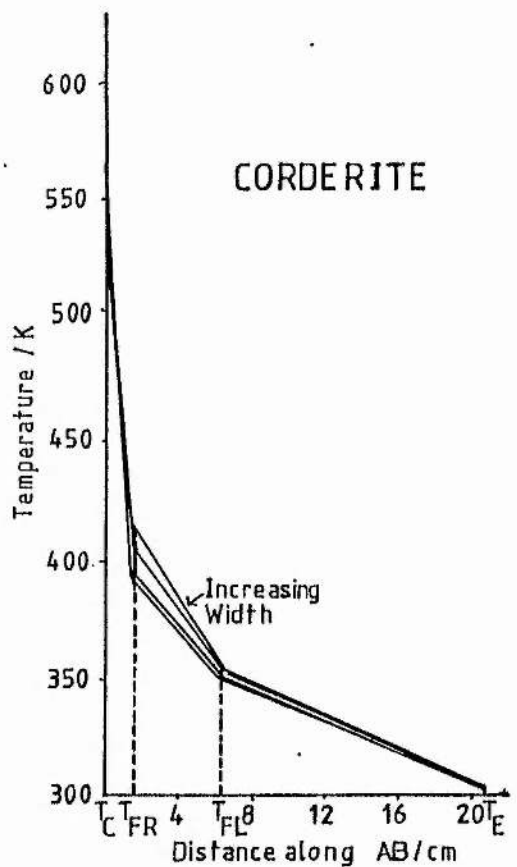
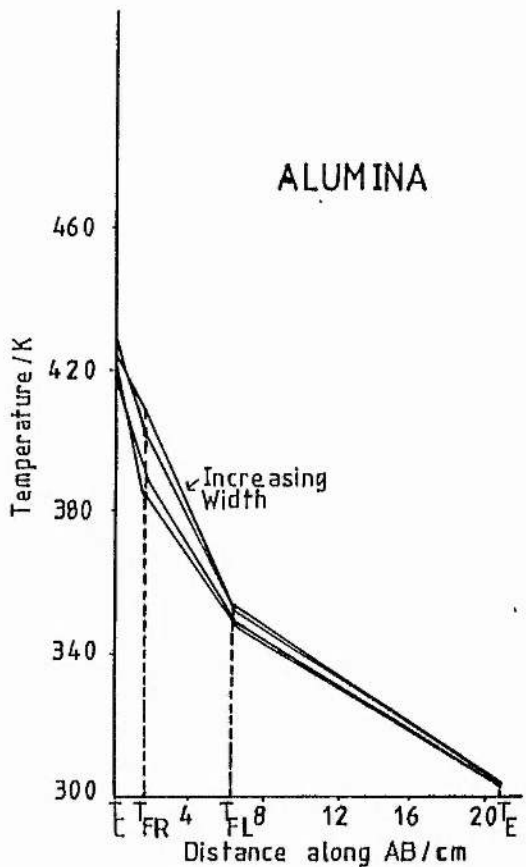
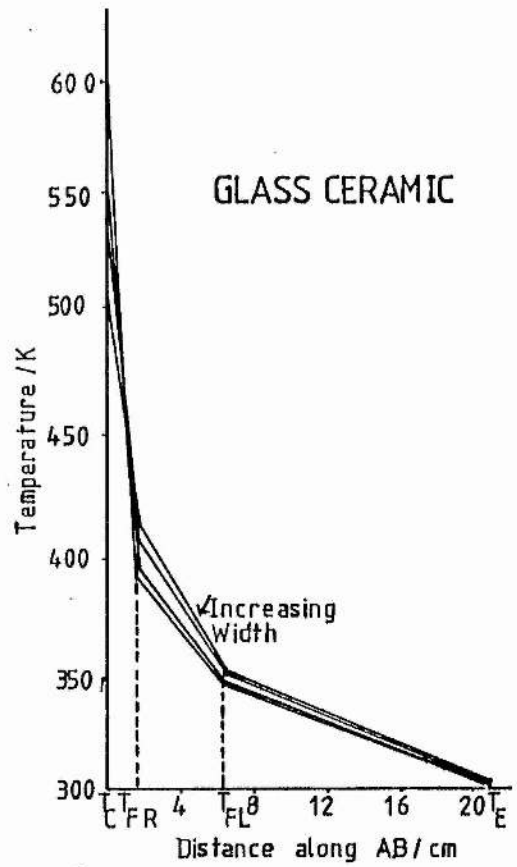
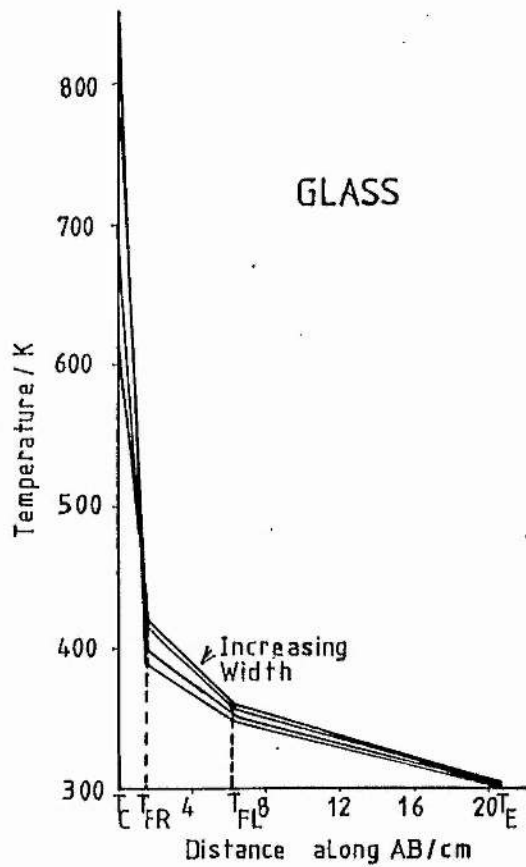


Fig 3.8 Variation of Temperature along TR Cell Axis AB for Varying Window Width Power Input 20 W

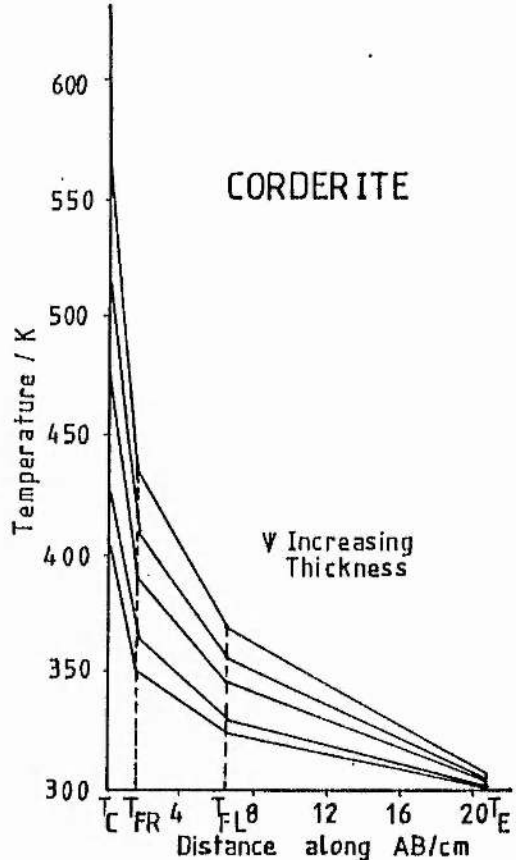
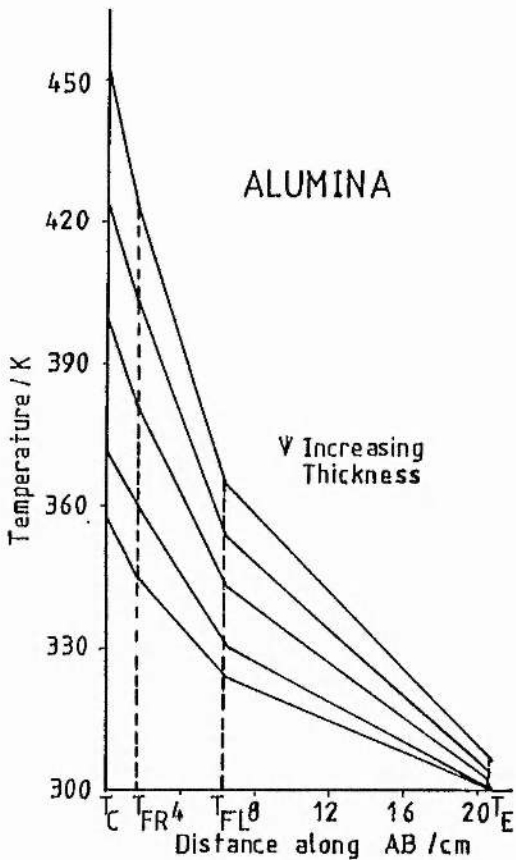
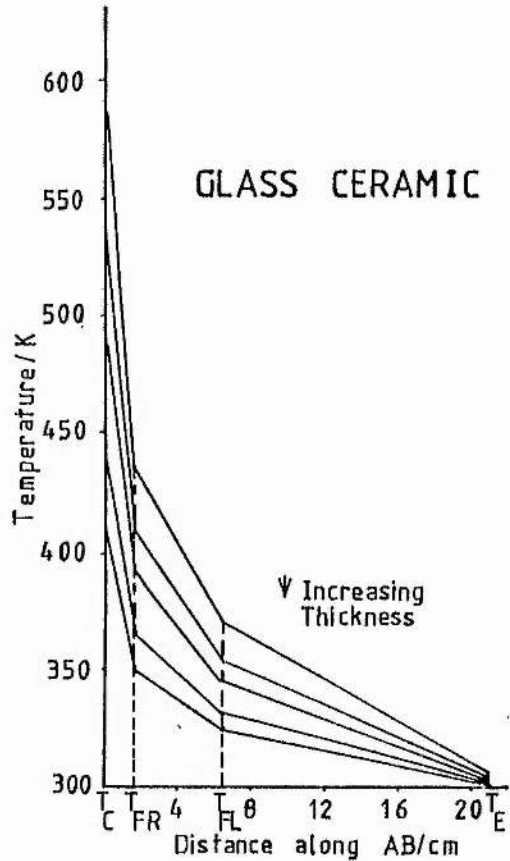
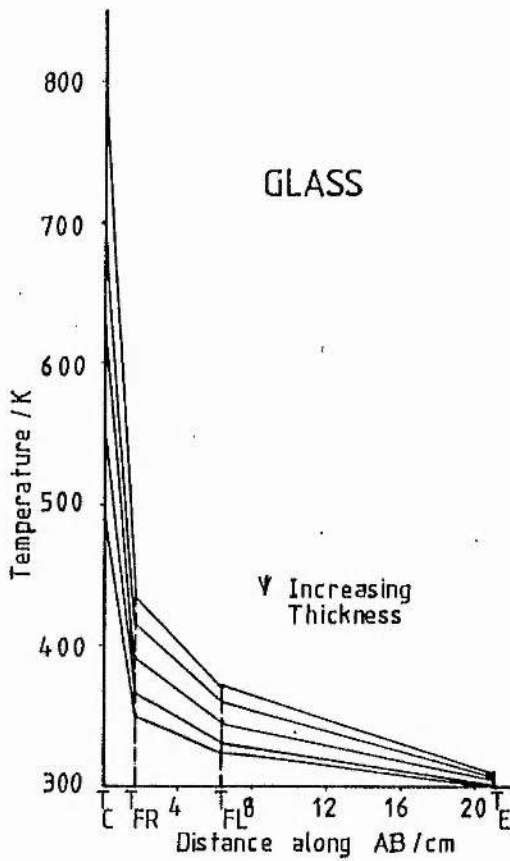


Fig 3-9 Variation of Temperature along TR Cell Axis AB for Varying Window Thickness  
Power Input 20 W

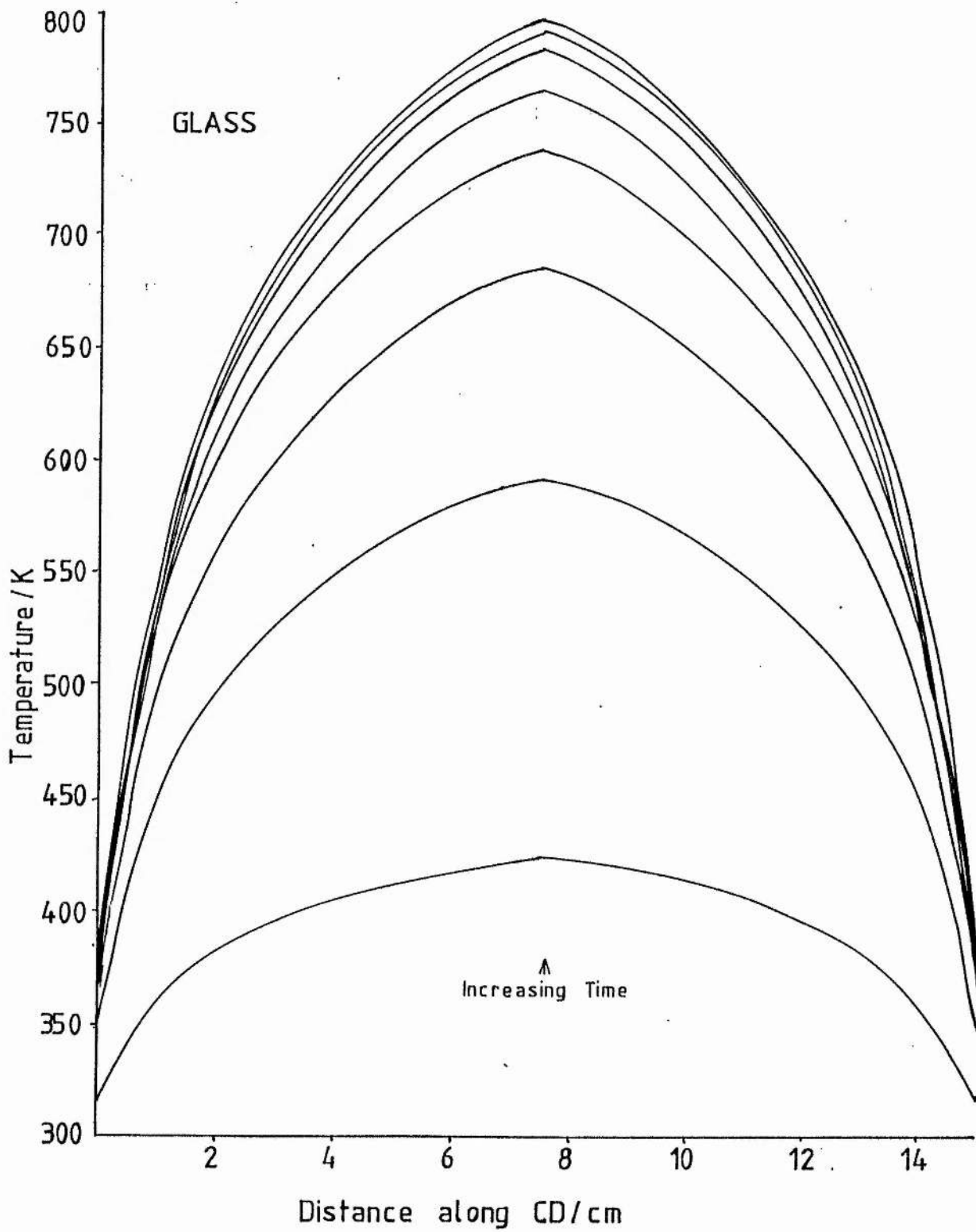


Fig 3-10 Variation of Temperature along TR Cell Axis CD with Time  
 Power Input 25 Watts      Time Interval 2 Seconds

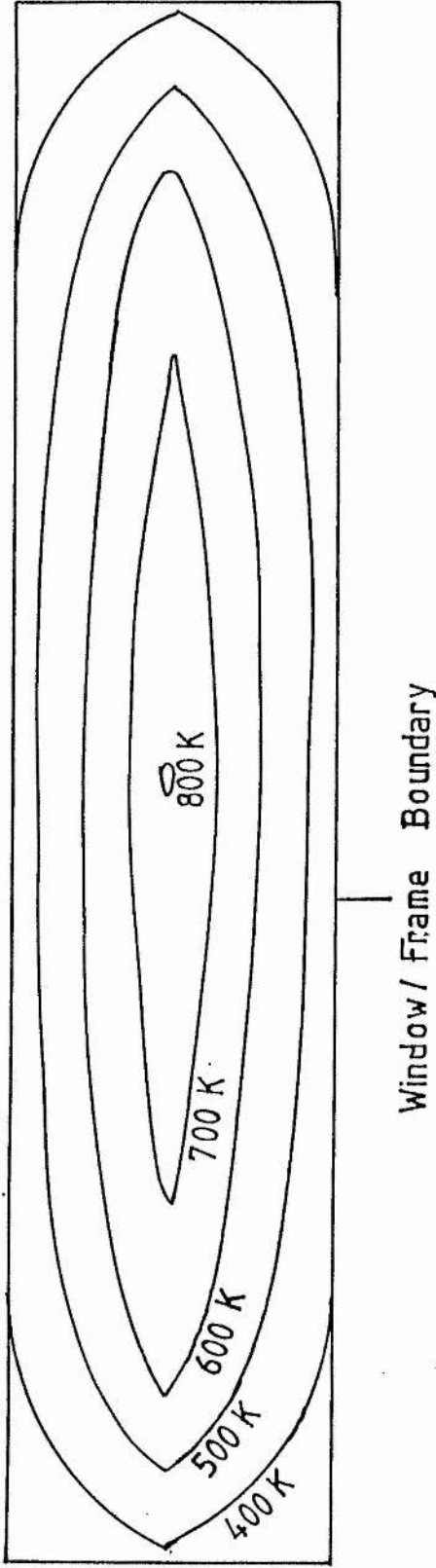


Fig 3-11 Isotherms on Glass Window for  
25 Watts Power Input

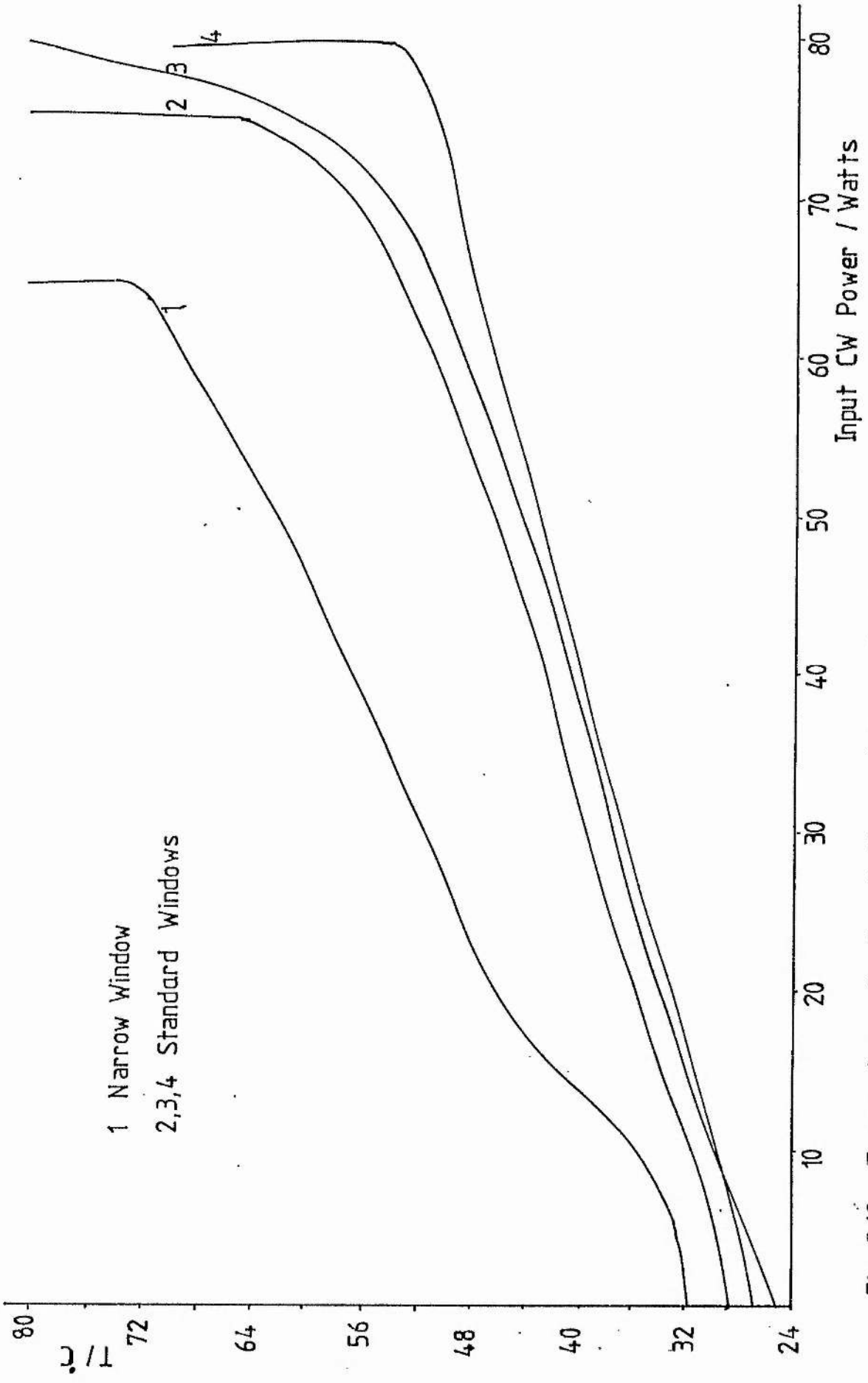


Fig 3-12 Temperature of edge of Frame / Power Input

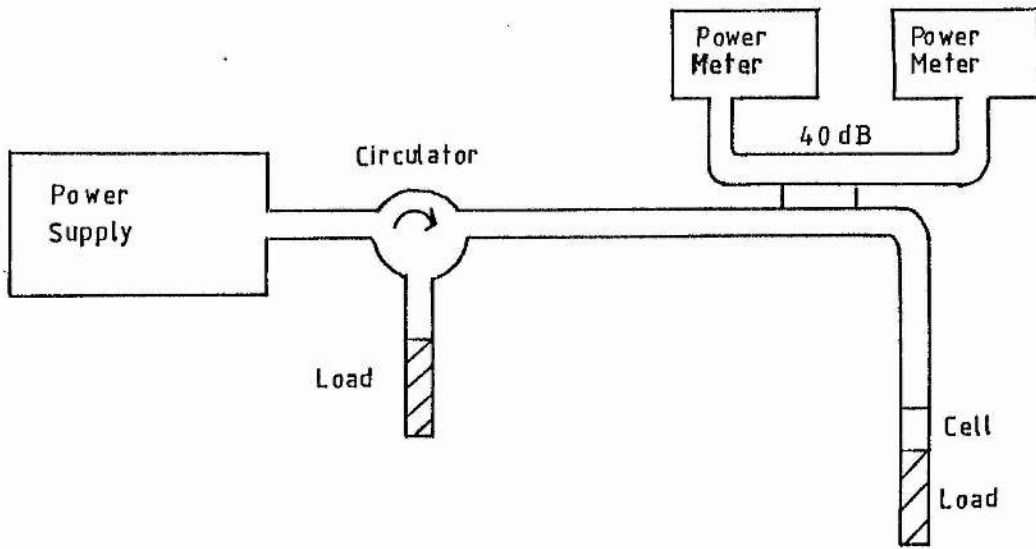


Fig 3-13 Experimental Setup used in the Measurement of the Arc Loss for a TR Cell

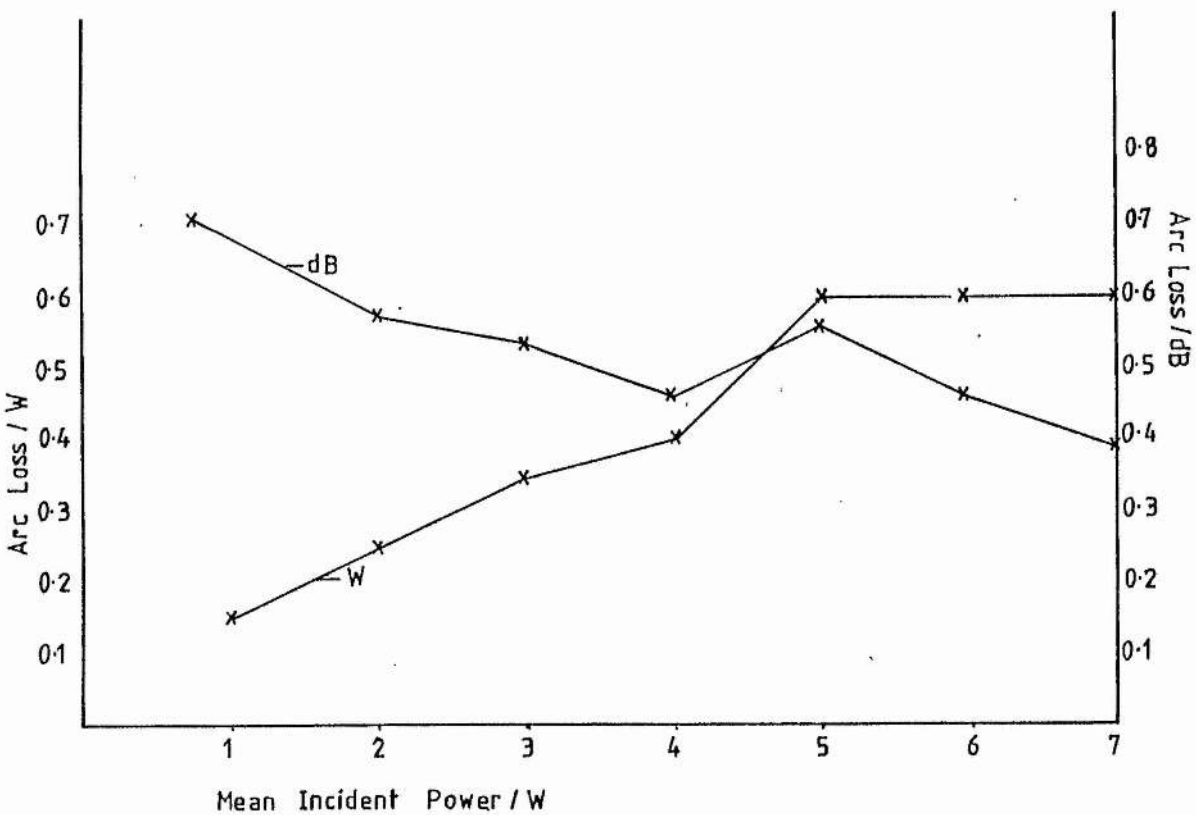


Fig 3.14 Arc Loss of TR Cell against Pulsed Incident Power

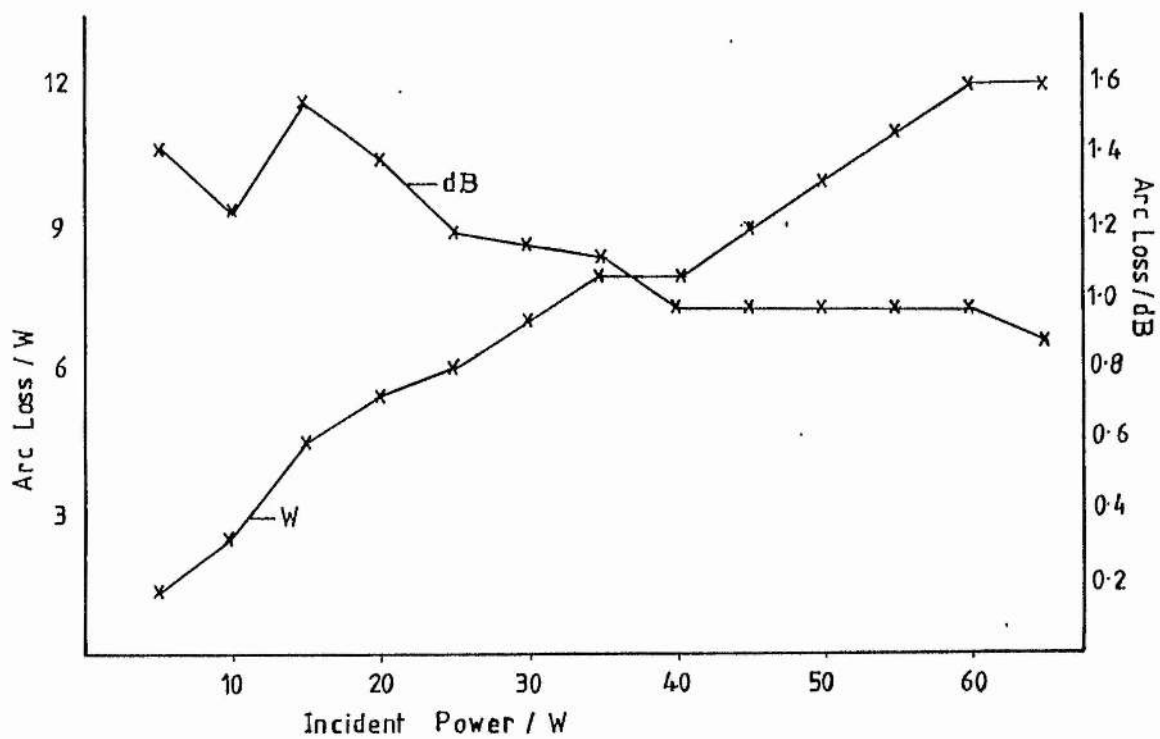


Fig 3.15 Arc Loss of TR Cell against CW Incident Power

## Chapter 4 Analysis of the TR Cell Using Emission Spectroscopy and Microwave Measurements

### 4.1 Introduction

The theory behind many of the procedures followed in the manufacture of a TR cell is not known, but we do know that these procedures improve performance and/or life. These procedures have been introduced to the manufacturing process over a period of many years. The aim of the research reported in this chapter is to discover what actually happens to the TR cell and the gas within it during the manufacturing process and at the beginning of its life. Boissiere and Romiguiere (1957) carried out a series of experiments on TR cells filled with argon and water vapour. The measurements included microwave measurements of the cell performance, examination of the emission spectrum of the discharge and mass spectroscopy of the discharge. They concluded that the water vapour in the cell is dissociated by the discharge and is absorbed by the walls of the cell, reducing the gas pressure in the cell. The high power performance of the cells was considerably modified thereby. Musson-Genon (1957) carried out a series of experiments on TR cells throughout their life. The results show that water is partly absorbed by the cell body and partly dissociated by the action of the microwave discharge. The cells studied contained windows which had been soldered in place. The solder released many gases to the cell which inhibited the efficient performance of the cell. The TR cells manufactured by EEV, however, contain windows

which are brazed into the cell, thus reducing contamination levels of the gas in the cell.

The method used in this chapter to study the TR cell is emission spectroscopy of the microwave-excited discharge in the cell. Emission spectroscopy is an important analytical tool because it provides a non-destructive measurement of a gas discharge, unlike, for example, mass spectroscopy in which a sample of gas is removed from a system for analysis. Many measurements of the emission spectrum of a system may be made without disturbing the system. On analysis, the emission spectrum shows the gases present in the discharge and an estimate of the partial pressures of the gases may be obtained from the recorded spectrum. Hence we can deduce what actually happens to the TR cell and the gas throughout its manufacture and life.

As well as taking measurements of the emission spectrum of the microwave discharge, measurements are made of the microwave transmission and reflection characteristics of the cell. It is hoped to correlate the microwave measurements and the emission spectrum measurements in order to describe the procedures involved in the manufacture of the TR cell. The theories developed will be tested using an experimental batch of cells, manufactured under non-standard conditions. Using the results obtained from the experimental batch of cells, the initial conclusions about TR cell manufacture will be examined and modified where necessary.

## 4.2 Emission Spectra

### 4.2.1 Introduction

In a microwave-excited discharge electrons gain energy from the applied microwave field and transfer it to the atoms and molecules of the gas through collisions. If sufficient energy is transferred, the atoms or molecules reach an upper excited state and, on decaying to a lower state, emit radiation in the form of light; an emission spectrum. For an atomic gas, the emission spectrum comprises a series of lines; for a molecular gas the spectrum is a series of bands. Each element or compound gives rise to a unique spectrum by which it may be identified.

### 4.2.2 Atomic Spectra

Each line in an atomic emission spectrum is the result of an electron in the atom decaying from a quantum state of higher energy to a quantum state of lower energy; the difference in energy is radiated as a quantum of light of energy  $h\nu$ . The wavenumber  $\nu$  of a spectral line is the difference between two members or terms  $T$  of a series (Rydberg-Ritz combination principle), ie

$$\nu = T_2 - T_1 = (E_{n_1} - E_{n_2})/hc = (2\pi^2\mu e^4 Z^2 / ch^3)(1/n_2^2 - 1/n_1^2) \quad , \quad (4.1)$$

where  $n_1$  and  $n_2$  are the principal quantum numbers of the upper and lower states at energies  $E_{n_1}$  and  $E_{n_2}$  respectively,  $\mu$  is the reduced mass of the atom and  $Z$  is its atomic number. The states from which a transition cannot proceed to a lower state with the emission of

radiation are called metastable.

The intensity of a line in emission is

$$I_{nm} = N_n A_{nm} h c \nu_{nm} \quad , \quad (4.2)$$

where  $N_n$  is the number of atoms in the initial state  $n$ ,  $A_{nm}$  is the fraction of atoms in  $n$  undergoing transitions to  $m$  per second and  $\nu_{nm}$  is the wavenumber of the emitted radiation. Einstein transition probabilities of spontaneous emission,  $A_{nm}$ , have been tabulated by Moore (1949) for atomic transitions. Their values are

$$A_{nm} \approx 10^8 \text{ s}^{-1} \text{ for strong dipole transitions,}$$

$$A_{nm} \approx 10^3 \text{ s}^{-1} \text{ for magnetic dipole transitions,}$$

$$A_{nm} \approx 1 \text{ s}^{-1} \text{ for electric quadrupole transitions.}$$

The latter two transition probabilities represent those for metastable states.

Initially in state  $n$ , the number density of atoms is  $N_n^0$ . After a time  $t$  we have

$$N_n = N_n^0 e^{-(\sum A_{nm})t} \quad . \quad (4.3)$$

In thermal equilibrium, the number density of atoms in state  $n$  is

$$N_n = g_n e^{-E_n/kT} \quad . \quad (4.4)$$

where  $g_n$  is the statistical weight of state  $n$  and  $E_n$  is the excitation energy of state  $n$  above the ground state. In an electric discharge, however, excitation of atoms occurs through collisions with electrons of all possible velocities. If the gas temperature is high, we have

$$e^{-E_n/kT} \approx 1 \quad (4.5)$$

$$\text{and } N_m/N_n = g_m/g_n \quad . \quad (4.6)$$

So, at high gas temperatures the number densities of atoms in

states  $m$  and  $n$  depend more on the statistical weight of each state than on the temperature of the discharge.

A transition between two states occurs at a given frequency, so we would expect the resultant spectral line to be infinitely narrow. But spectral lines are observed to have a finite width, due to collision broadening and Doppler broadening. Collisions perturb the energies of at least the outer electrons in an atom or molecule, resulting in a finite width of spectral lines (spectral lines result from the transitions of outer electrons). Doppler broadening occurs due to the motion of the particles. The motion is random, resulting in shifts to higher and lower frequencies. For a gas, the Doppler effect often determines the line width.

#### 4.2.3 Molecular Spectra

The excitation of a valence electron involves the moving of electronic charges in a molecule. The consequent change in the electric dipole of the molecule gives rise to a spectrum by its interaction with the electric field of radiation. Most molecules produce electronic spectra, when changes in the electron distribution are accompanied by a dipole change. The electronic spectra of molecules give rise to emission spectra in the optical region.

For molecules, the total energy  $E_{\text{tot}}$  can be expressed as a sum of energy terms using the Born-Oppenheimer approximation

$$E_{\text{tot}} = E_{\text{elect}} + E_{\text{vib}} + E_{\text{rot}} \quad , \quad (4.7)$$

with  $E_{\text{elect}}$  the electronic energy of the molecule,  $E_{\text{vib}}$  its vibrational energy and  $E_{\text{rot}}$  the rotational energy. Their approximate orders of magnitude are:

$$\Delta E_{\text{elect}} \approx \Delta E_{\text{vib}} \times 10^3 \approx \Delta E_{\text{rot}} \times 10^6$$

so the vibrational changes produce a coarse structure and the rotational changes a fine structure. A band system represents the totality of the transitions between two different states of a molecule, corresponding to a single line or single multiplet of an atom.

The conventional model used to consider the vibrations and rotations of a molecule in different electronic states is the vibrating rotator model, where the vibrational wavenumber  $\nu_{\text{vib}}$  is given by

$$\nu_{\text{vib}} = (v+1/2)w_e - w_e x_e (v+1/2)^2 + \dots \quad (4.8)$$

and  $w_e$  is the vibrational wavenumber and  $v$  is an integer and the rotational wavenumber  $\nu_{\text{rot}}$  is given by

$$\nu_{\text{rot}} = (h/(8\pi^2 Ic))J(J+1) - (4(h/8\pi^2 Ic)^3)/w_e^2 (J+1)^2 J^2 + \dots \quad (4.9)$$

where  $I$  is the moment of inertia of the molecule about its centre of mass. At room temperature practically all the molecules are in the lowest vibrational level of the electronic ground state. It has been observed that molecular spectra consist of a series of bands or progressions whose separation changes rather slowly. The wavenumbers of the bands can be represented approximately by the

formula

$$\nu = \nu_{00} + (a'v' - b'v'^2) - (a''v'' - b''v''^2) \quad (4.10)$$

where  $\nu_{00}$ ,  $a'$ ,  $a''$ ,  $b'$  and  $b''$  are positive constants and  $v'$  and  $v''$  are positive integers or zero. The constants are chosen such that when  $v'$  and  $v''$  are zero, then  $\nu$  is equal to  $\nu_{00}$ , the wavenumber of the first band of the first series. The wavenumbers of the bands in a band system are commonly arranged in a Deslandres table or scheme of band heads.

Each band consists of a large number of individual lines- fine structure. The lines can be represented by a formula of the type

$$\nu = c + dm + em^2, \quad (4.11)$$

where  $c$ ,  $d$  and  $e$  are constants and  $m$  is a whole number which numbers the successive lines. The series corresponding to the positive values of  $m$  is the positive or R branch; for negative  $m$  the series is the negative or P branch. For  $m$  equalling zero, there exists another series of lines, the Q branch. For rotational spectra,

$$\Delta J = 0, \pm 1$$

and the R branch corresponds to  $\Delta J = -1$ , the P branch corresponds to  $\Delta J = +1$  and the Q branch corresponds to  $\Delta J = 0$ .

The line intensities of most branches of electronic bands vary in essentially the same way as do the branches of rotation-vibration bands. In each branch there is an intensity maximum which lies at a higher  $J$  value the higher the temperature and the smaller the rotational constant. According to the Franck-Condon principle, the electron jump in a molecule takes

place so rapidly in comparison to the vibrational motion that immediately afterwards the nuclei still have very nearly the same relative positions and velocities as before the jump, and there is an intensity maximum at a  $\nu''$  value that is determined by the relative positions of the minima of the two potential curves.

It has been found experimentally (Herzberg, 1950) that the intensity distribution in emission bands occurring in an electric discharge is given by the Boltzmann distribution and the statistical weights of the levels between which the transitions occur. If a molecule is excited by electron collision, no great change in the angular momentum of the system can be produced, owing to the smallness of the electron mass. The distribution of the molecules over the different rotational levels in the upper electronic state is practically the same as in the ground state. For other modes of excitation eg by collision with metastables, chemical reactions or dissociation, large deviations from the normal thermal distribution may occur. In the TR cell discharge, dissociation of water vapour occurs and water vapour and its products react chemically with the cell walls. Hence the constituents of the TR cell discharge cannot be described by a normal thermal distribution.

### 4.3 Emission Spectra Measurements

#### 4.3.1 Introduction

In order to analyse the gas content of a TR cell at selected intervals throughout manufacture and life of the cell, the microwave-excited discharge in the cell is studied using an Optical Spectrum Analyser or OSA. The emission spectra of the gases in the discharge are separated into their constituent wavelengths using a diffraction grating. The spectral lines are detected using a vidicon and analysed in a computer. The results, in the form of intensity against wavelength for a spectral range, are displayed on the OSA screen. After calibration, the lines and bands are identified according to wavelength and the gases identified. The intensities of the lines and bands can be used to obtain an estimate of the partial pressure of each gas in the cell.

#### 4.3.2 Operation of the OSA

The OSA, supplied by B and M Spektronik, consists of an ultra-sensitive vidicon detector containing 500 channels and a memory and data-processing unit. Light is dispersed by a polychromator and focussed onto the light-sensitive matrix of the vidicon. This causes a discharge of the diodes of the detector and a signal is transmitted through a pre-amplifier to the analyser. The OSA has 30 memories and the facility for displaying many mathematical operations on the contents of the memories. The real

time display is updated every 32 mseconds.

The vidicon consists of a photodetector of dimensions  $12.5 \times 10 \text{ mm}^2$ , with a silicon base. It comprises  $500 \times 400$  photodiode detectors, which allow the measurement of not only the wavelengths but also spatial-dispersive values. Each diode has an active area of 8 microns in diameter. Illumination discharges the photodiode matrix previously placed under a negative voltage in the resistance direction. The detector electron stream recharges to the cathode potential those diodes discharged by the illumination. The current required for recharging is measured, amplified and after current/voltage conversion, gives the video signal. The scan time for one channel is 64 microseconds. The maximum scan current is 1.5 microamps. Four scans are needed to recharge the target to the cathode potential. The spectral sensitivity of the vidicon depends on the thickness of the semiconductor target and on the material used for the entry window. The SIT 500 vidicon has a spectral range of 300 to 900 nm. Maximal sensitivity lies at 430 nm at 15 photons per channel. The SIT utilises a pre-inserted electrostatically focussed image intensifier. A 190-fold increase in sensitivity can be obtained. The light travels through an optical fibre to a photocathode where the photons dislodge electrons from the cathode. The electrons are accelerated by the photocathode voltage to the target.

The polychromator is of the type BM25/25 with an Ebert mounting. Its focal length is 250 mm; the grating has 1200 lines per mm with an area of  $58 \times 58 \text{ mm}^2$ . The slit width is 0.3 mm.

At low intensities, the signal to noise ratio can be improved by multiple scanning and the electronic determination of mean values. It improves according to the square root of the number of scans. The ratio of signal  $S$  to noise  $N$  is given by

$$S/N = (N_p q T_b) / (N_r (N_{ab})^{0.5}) \quad , \quad (4.12)$$

where  $N_p$  is the number of photons per channel,  $q$  is the quantum yield,  $T_b$  is the duration of illumination,  $N_{ab}$  is the number of scans and  $N_r$  is the electron noise.

#### 4.3.3 Spectral Analysis of the TR Cell Discharge

The TR cell contains argon and water with roughly equal partial pressures. Emission lines of argon and of hydrogen and oxygen atoms are seen in the discharge in the cell over the frequency range covered by the OSA. No spectral lines from argon ions are observed, so their concentration in the microwave discharge is very small. All the argon spectral lines observed are Ar I lines due to radiation of energy from excited argon atoms. The energies of the excited levels of argon lie in the range 11.547 eV to 15.755 eV. The argon lines chosen for study are the lines at  $6965.430 \text{ \AA}$  and  $6677.282 \text{ \AA}$ . Details of all the spectral lines studied are listed in Table 4.1.

Water vapour is dissociated by the microwave discharge into many products, including hydrogen and oxygen atoms. The emission band spectrum of water is a complicated many-line system and is observed at very low intensity in the microwave-excited emission spectrum of argon and water vapour. Hence the two most intense hydrogen atom lines in the visible spectrum were studied. These are the first two members of the Balmer series,  $H_{\alpha}$  and  $H_{\beta}$  at  $6562.849 \text{ \AA}$  and  $4861.327 \text{ \AA}$  respectively. The wavenumbers  $\nu$  of the lines in the Balmer series can be written as the difference of two terms;

$$\nu = T_2 - T_1 = R_H(1/2^2 - 1/n_1^2) = 2\pi^2\mu e^4(1/2^2 - 1/n_1^2)/ch^3, \quad (4.13)$$

where  $R_H$  is the Rydberg constant for hydrogen and  $\mu$  is the reduced mass of the system. For  $n_1$  equal to 3, we have the  $H_{\alpha}$  line and  $n_1$  equalling 4 gives the  $H_{\beta}$  line. The oxygen atom spectral line measured in the study occurs at  $7771.928 \text{ \AA}$ . Further details are listed in Table 4.1.

#### 4.3.4 Experimental Technique

The experimental setup for monitoring the TR cell discharge is as shown in fig (4.1). A sample cell is inserted and the position of the cell holder adjusted slightly until the intensity of the  $H_{\alpha}$  line is  $20,000 \pm 1000$  for 20 scans of the vidicon when 1.125 kW microwave power is applied minus 20 background scans when no microwave power is applied. The grating position is adjusted until one of the spectral lines to be measured is displayed on the OSA screen. A few seconds after the discharge has been established in

the cell (to allow the discharge to stabilise) 20 scans of the vidicon target are stored in each of 5 memories of the OSA computer. The microwave power supply, a magnetron whose operating characteristics are listed in Appendix 3, is switched off and, after a few seconds (to allow the discharge to die away completely), 20 background scans of the vidicon are stored in the sixth memory. The 20 background scans are subtracted from each of the five memories in turn to give a true value for the intensity of the spectral line being measured. The above procedure is repeated for each of the spectral lines being measured, for each TR cell, at two different power levels, 0.187 kW and 0.937 kW. Twenty scans of the vidicon target, repeated five times, are taken to reduce statistical fluctuations of the intensities of the spectral lines and of the background, since from equation (4.12), the signal to noise ratio improves according to the square root of the number of scans. The contents of the OSA display or of any of the memories can be sent to a Hewlett-Packard 9826A desk top computer via an RS232 serial interface.

#### 4.4 Microwave Measurements

##### 4.4.1 Introduction

As well as measuring the TR cell discharge using the OSA, measurements are made of the performance of the cell when low and high power microwave radiation is applied. Low power measurements on a TR cell are carried out to assess the reaction of the cell to the low power signals reflected from the radar target. High power

measurements are carried out on the TR cell to assess the reaction of the cell to the high power transmitted pulses.

#### 4.4.2 Low Power Measurements

Low power measurements are made using the equipment shown in fig (4.2). The sweep oscillator operates over a range 7.0 to 12.4 GHz. The ferrite isolator allows microwave radiation to travel in one direction and absorbs all radiation travelling in the opposite direction, thus preventing possible damage to the sweep oscillator by reflected or stray microwave radiation. A fraction of the incident power travels via a 10 dB coupler to a wavemeter, to provide a marker of a known frequency on the oscilloscope screen. A fraction of the power from the wavemeter is directed back to the sweep oscillator via the Automatic Level Control (ALC) to level the signal from the oscillator as much as possible over the selected frequency range. For VSWR and insertion loss, the maximum power level is 5 mW. Using the marker provided by the wavemeter, the frequency range swept by the oscillator is adjusted to accommodate the operating range of the TR cell, 9.3 to 9.5 GHz, and is displayed by the oscilloscope.

##### (1) VSWR

A definition of VSWR is given in section 1.5.2. Initially, the cell and load are replaced by a short circuit to reflect all the incident power to the detector, giving a VSWR of 1 (see fig(4.2a)). The rotary attenuator is adjusted to give 17.8 dB

attenuation, equivalent to a VSWR of 1.3 (the maximum acceptable value) and the power level on the sweep oscillator adjusted so that the trace on the oscilloscope due to a VSWR of 1.3 is a given distance from the trace due to a VSWR of 1. The short circuit is then replaced by the cell and load, with zero attenuation on the rotary attenuator. The trace on the scope due to the cell must be below that due to a VSWR of 1.3 over the cell bandwidth, to fulfil manufacturing requirements.

## (2) Insertion Loss

The insertion loss of a TR cell is a measure of the attenuation of the device to the received signal. Measurement of the insertion loss is carried out using the apparatus shown in fig (4.2b). A section of plain waveguide first replaces the cell. For an attenuation of 0.8 dB (the maximum acceptable value) on the rotary attenuator, the trace due to the plain waveguide is drawn on the oscilloscope screen. The section of plain waveguide is replaced with the TR cell to be measured, with zero attenuation on the rotary attenuator. If the trace due to the cell is above the drawn trace at 0.8 dB over the cell bandwidth, then the insertion loss is below 0.8 dB and acceptable. The actual insertion loss may be determined by winding in sufficient calibrated attenuation to position the trace due to the cell on that due to the section of waveguide. The insertion loss is now the difference between the 0.8 dB of the drawn trace and the amount of attenuation wound on the rotary attenuator.

#### 4.4.3 High Power Measurements

The experimental setup used for the high power measurements is as shown in fig (4.3). Power from the modulator at the central frequency of the TR cell operating bandwidth is divided into two at the first 3 dB coupler. By varying the phase of one half of the power, an incident power of 40 kW with a 1 microsecond pulse length and a prf of 1 kHz is obtained. The measurements made on the TR cell are as follows.

##### (1) Keep-Alive Current

The keep-alive current is the current which flows when a voltage is applied to the keep-alive electrode. The keep-alive power supply (-1 kV) is attached to the keep-alive electrode of the TR cell and the keep-alive current measured. It should be between 100  $\mu$ A and 150  $\mu$ A after 5 seconds.

##### (2) Spike Leakage Energy

The cell is placed in cell holder 1 with the keep-alive power supply attached. A pulse length of 0.1 microsecond with a prf of 3 kHz is selected and the spike leakage energy in nanojoules per pulse is read from the power meter. The spike leakage energy is that which passes through the cell during the time (about 0.1 microsecond) before the gas has ionized sufficiently to reflect the incident microwaves, hence the choice of pulse length. To protect

the receiver, the spike leakage energy must be typically less than 15 nanojoules per pulse with a keep-alive discharge operational (primed value). The spike leakage energy with no keep-alive discharge operational (unprimed value) is also measured.

### (3) Total Leakage Power

The total leakage power is the power which leaks through the TR cell after the gas in the cell has been ionized by the microwave pulse. The cell is placed in the cell holder as above, with the keep-alive power supply attached. A pulse length of 1 microsecond with a prf of 1 kHz is selected and the leakage power read from the power meter. The maximum acceptable total leakage power is 100 mW. The unprimed total leakage power is also measured, at the same pulse length and prf.

### (4) Recovery Time

The recovery time is the time interval between the end of the high power incident pulse and the time when the low power attenuation caused by the cell decreases to 3 dB greater than the fully recovered value. The incident pulse is provided by the modulator, at 40 kW, 1 microsecond pulse length and a prf of 1 kHz. A Gunn diode provides the low power signal to be attenuated by the TR cell. The frequency of the power supplied is adjusted to the central operating frequency of the cell. The recovery time measurements are made with the keep-alive discharge in operation. With the cell in holder 1 and the power supply off, power from the

Gunn diode is directed to the oscilloscope and the level of the signal is varied to give equal displacements above and below the central line on the oscilloscope screen when the diode is switched on and off. High power is applied with the Gunn diode on and the recovery time is measured on the oscilloscope as the time taken for the trace to cross the central line (-3 dB attenuation). For normal operation, the recovery time should be under 3 microseconds.

#### (5) Low Power Breakthrough

The low power breakthrough measurement is a measure of the minimum microwave power level required to break down the gas in the cell. The TR cell is placed in holder 2 with the keep-alive discharge operational. The power incident on the cell is increased from zero to cell breakdown level. This level is indicated by a sharp decrease in the measured leakage through the cell. The low power breakthrough is therefore the maximum power passing through the cell without causing breakdown. Two breakthrough measurements were made at low power, one with 0.1 microsecond pulse length and a prf of 3 kHz and one with a prf of 1 kHz and a pulse length of 1 microsecond.

## 4.5 TR Cell Experiments

### 4.5.1 Manufacturing Procedure

The procedures followed in the filling of a TR cell and the terms employed to describe the processes involved are described below:

#### (1) Hot Exhaust

The hot exhaust process is the process whereby the cell is evacuated, baked for a specified time, then filled with the initial gas mixture. The cells are loaded onto the exhaust bench and evacuated to a pressure of  $4 \times 10^{-5}$  torr. The cells are continuously pumped and baked at  $300^{\circ}\text{C}$  for 1 1/4 hours, to drive off any gases absorbed by the cell body and in a nitrogen atmosphere to prevent external oxidation of the cell body. The cells are then filled with 7 torr of water vapour and when the pressure has reduced to 5 torr, 12 torr of oxygen is added and the cells are baked for 5 minutes at  $300^{\circ}\text{C}$ . The oven is switched off and the cells are allowed to cool to  $100^{\circ}\text{C}$ , the oxygen and water remaining in the cells. At  $100^{\circ}\text{C}$  the gas is roughly pumped out and 14 torr water vapour added. The cells are left to stand for 30 minutes. when the water vapour pressure is adjusted to 11 torr. Argon is added to 9.5 torr and the cells stand for 10 minutes before checking the keep-alive current ( $120 \mu\text{A}$  minimum) and sealing-off.

(2) Age Stand

After the hot exhaust stage, the cells, now filled with a mixture of argon and water vapour, are left to stand for one week. This stage in the manufacture is known as the age stand. The purposes of the age stand are two-fold; firstly to allow absorption of water vapour by the cell and secondly to detect possible leaks in the cells.

(3) Ageing

Following the age stand, the cells are attached to waveguide with a minimum of 2.5 kW and a maximum of 100 kW incident power and a keep-alive discharge operational and run continuously for approximately 48 hours. This operation is known as ageing.

(4) Cold Refill

Following the ageing stage, the cells are refilled with their final gas fill. This stage in the manufacture of the TR cell is referred to as the cold refill stage. The cells are evacuated to a pressure of  $10^{-4}$  torr. Water vapour is added to a pressure of 20 torr, and after 15 minutes 9.5 torr argon is added. The water pressure is adjusted to give a total pressure of 20.5 torr after 30 minutes. The keep-alive currents are checked (110-130  $\mu$ A) and the cells sealed-off.

#### 4.5.2 Experimental Procedure

A control batch of 12 cells was measured using the OSA as described in section 4.3 above and the microwave measurements listed in section 4.4 made at each stage during the manufacture and after several hours of life of the cells. The purpose of this set of experiments is to determine what actually happens to the TR cell body and the gas contained within during manufacture and for part of the life of the cell. Measurements were made at the following stages:

- (1) After hot exhaust
- (2) After 3 days age stand
- (3) After 1 week age stand
- (4) After 48 hours ageing with high power
- (5) After cold refill
- (6) After 60 hours life.

Throughout the rest of this chapter, the stages at which measurements were taken are referred to as stages 1 to 6.

At stage 6, six of the cells, chosen at random, were run with a keep-alive discharge operational; the remaining cells were not. In figs (4.4) to (4.9) are shown the results from the control batch of cells. No impurity gases were observed in the discharges of the TR cells.

## 4.6 Discharge in a Pre-TR Tube

### 4.6.1 Introduction

It is suspected that water vapour and its products, created by the action of the microwave discharge in the TR cell and the discharge at the keep-alive electrode are absorbed by the cell body. The total pressure of gas in the cell throughout the life of the cell is not known, nor are the partial pressures of the constituent gases. Maddix (1968) has measured the partial pressures of water vapour, oxygen and hydrogen, assuming that the argon partial pressure remains constant, for a TR cell containing argon and water vapour. The discharge was operational for 10 minutes, with 10 minutes recovery of the cell. The TR cells considered in this thesis have a lifetime of the order of hundreds of hours, however, and in this thesis we are considering long-term changes in the gaseous constituents of the cells. A quartz pre-TR tube is attached to a gas filling station as shown in fig (4.10) and the tube is filled with known pressures of argon and water vapour. Quartz is chosen since it is effectively impermeable to argon and water vapour and effectively chemically inert (see section 6.8 on Surface Reactions in Chapter 6). Therefore the measured pressure in the pre-TR tube should accurately represent the pressure of gas admitted to the tube. The purpose of the series of experiments is to measure the intensities of the argon, hydrogen and oxygen spectral lines measured in the TR cell discharge for varying, known pressures of argon and water vapour

and to compare these results with those taken for the TR cells, for which the pressures of argon and water vapour present are not known (except at stages 1 and 5, hot exhaust and cold refill). Because of the differing geometries of the TR cell and the pre-TR tube, the breakdown power levels differ. Hence, the intensities of the spectral lines studied are measured at a range of power levels; 1.87 kW, 2.81 kW and 3.75 kW pulsed power, using a prf of 3 kHz and a pulse length of 1 microsecond, the same as were used for the TR cell measurements.

The intensities of the spectral lines in the discharges in the TR cell and the pre-TR tube are not compared directly; we compare the ratios of two lines. The ratios of the argon line at 6965 Å to the  $H_{\alpha}$  line and to the oxygen line at 7772 Å are calculated, for the results obtained using the pre-TR tube and the TR cells; also the ratio of the  $H_{\alpha}$  line to the oxygen line above-mentioned. Graphs are plotted of the above-mentioned ratios against pressure of water vapour for varying power inputs (see fig (4.11)). The pressure of argon in the TR cell is assumed to remain constant at 9.5 torr (the pressure added at filling) since argon is known to be absorbed very slowly by the metal and glass of the cell. The two sets of results are compared by noting that the water vapour pressure in the TR cell is 11 torr after hot exhaust and after cold refill. At the various stages throughout the manufacture and life of the cells, the water vapour content may be estimated and a mechanism proposed as to the effects of each stage of manufacture and life on the TR cell and the discharge.

#### 4.6.2 Impurities in Pre-TR Tubes

Microwave-excited discharges in quartz pre-TR tubes containing a range of gases at a range of pressures have been studied. Table 4.2 gives a list of the gases studied and their pressures. Impurity gases are seen in the discharges of some of the pre-TR tubes; these gases have not been observed in the discharge in a TR cell. The impurity gases have probably been absorbed by the quartz during manufacture of the tube and subsequently released either under the action of the discharge or when the quartz is heated due to the discharge. In emission, band systems belonging to molecules that are not chemically stable, but which are formed in the discharge, often appear. Also, band systems of impurities appear frequently with a much greater relative intensity than their concentration would appear to warrant. If a tube has an air leak, then the bands of nitrogen are seen in the discharge. The impurity gases observed in the discharge are CO and also  $C_2$ , a free-radical normally only observed in electric discharges, being not chemically stable under normal conditions.

For nitrogen, the band systems observed in a microwave discharge are the First and Second Positive systems (see figs (4.12) to (4.14)). In the First Positive system, bands with values of  $v'$  (from equation (4.10)) increasing from 4 to 9 with the corresponding  $v''$  values of 1 to 6 are seen. All the bands of the Second Positive system as listed by Pearse and Gaydon (1976) are seen down to  $3943 \text{ \AA}$ . According to Pearse and Gaydon, these bands

are the most readily seen in a discharge through air, such as a leak in a discharge tube. The bands of the First and Second Positive systems are degraded to shorter wavelengths.

Carbon monoxide is one of the gases seen as an impurity in the discharge of some pre-TR tubes. Many band systems have been recorded for CO, the Angstrom and Herzberg systems being visible in the microwave discharge. The bands observed in the Angstrom system are those with  $v'$  equal to zero and  $v''$  between 0 and 3 (see equation (4.10)). The only band observed in the Herzberg system has  $v'$  equal to 0 and  $v''$  equal to 4. Other bands are not present with sufficient intensity to be observed. According to Pearse and Gaydon, the material of a new discharge tube tends to produce enough CO to give the above-mentioned bands. In both the Angstrom and Herzberg systems the bands are degraded to shorter wavelengths (see fig (4.15)). No trace of CO was observed in the tubes containing argon or tritiated argon, but it was observed in the discharges of all the other tubes. The intensity of the bands was greatly reduced in the higher pressure tubes, probably due to the reduced partial pressure of CO present.

For  $C_2$ , the Swan band system is the only one observed in the microwave discharge in a pre-TR tube. According to Pearse and Gaydon, the bands of the Swan system have been readily observed in discharge tubes containing helium and carbon monoxide. The bands are degraded to shorter wavelengths, with a single head, and the band sequences are well marked (see fig (4.16)). The bands observed in the Swan system result from the electronic transitions

(0,1) to (4,5); (0,2) to (5,7); (1,0) to (4,3) and (0,0) and (1,1), where the  $v'$  value is listed first and the  $v''$  value is listed second. Other bands are not sufficiently intense to be observed in the microwave discharge. The bands of  $C_2$  are only observed in the tubes containing argon, tritiated argon, krypton and tritiated krypton.

#### 4.7 Results of TR Cell Experiments

In figs (4.4) to (4.9) are shown the measurements on the control batch of cells. In figs (4.4) and (4.5) are shown the spread in intensities at each stage of measurement of the cells for each spectral line. at power levels of 0.187 kW and 0.937 kW peak power respectively. Figure (4.6) shows the variation of mean intensity of each spectral line at each stage, plotted as the ratio of intensity at each stage to intensity at stage 1. At the lower power level, 0.187 kW peak power, the intensities of the argon lines and the hydrogen lines increase after three days age stand but level off by the end of the week stand. The intensity increases slightly after ageing with high power for the argon lines but decreases for the hydrogen lines. At refill stage the gas in the cell is changed. so a direct comparison of the intensities of the spectral lines at this stage with the preceding results is not helpful. After 60 hours life, the intensities of the argon lines have increased from their value at the refill stage. The intensities of the two hydrogen lines decrease after 60 hours life. The intensity of the oxygen spectral line first increases after three days age stand then decreases slightly after seven days

age stand. The intensity increases after ageing and again after 60 hours life.

At the higher power level, 0.937 kW peak power, the intensities of the argon spectral lines vary in a similar way to the variation in intensity at lower power. The argon spectral lines show a net increase in intensity after one week age stand, increase again after ageing and again after 60 hours life. The hydrogen spectral lines also show a net increase after one week age stand, then decrease sharply after ageing and again after 60 hours life. The oxygen spectral line, however, decreases in intensity after standing one week and again after ageing 48 hours, but increases again after 60 hours life.

In fig (4.7) are shown the variation of the low power measurements made on the cells at stages 5 and 6, cold refill and after 60 hours life, and the low power breakthrough measurements, made at the same stages. It is unlikely that the low power measurements on the cells will contribute much information on the gas within since insufficient power is available to cause breakdown of the gas. Low power measurements provide more information on the structure and shape of the cell than on the gas within.

In fig (4.8) are shown the spread of the microwave measurements made at each stage. In fig (4.9) are plotted the ratio of the mean of each microwave measurement at each stage to the measurement at the first stage. The leakage power and the spike leakage energy both decrease after three days age stand and only the unprimed

spike leakage energy has decreased further by the end of the week stand. The recovery time decreases after age stand and increases greatly after ageing and with life. The keep-alive current remains fairly constant throughout manufacture but decreases after 60 hours life. The total leakage power, both primed and unprimed values, increases after 60 hours life. The unprimed spike leakage energy increases after 60 hours life, while the primed value remains fairly constant.

In fig (4.11) are shown the ratios of intensities of the spectral lines measured for the discharge in the pre-TR tube containing a constant partial pressure of argon and various, known partial pressures of water vapour. By comparing figs (4.11) and (4.17), the ratios of the spectral lines for the pre-TR tube and the TR cell respectively, at cold refill stage when the partial pressures of argon and water vapour in the TR cell are known, we see that the ratios of the lines in the TR cell discharge, measured at 0.937 kW peak power, correspond to a power level of about 2.81 kW peak power for the pre-TR tube discharge and that a power level of 0.187 kW peak power in the TR cell discharge corresponds to just less than 1.87 kW peak power in the pre-TR tube discharge.

The partial pressure of argon in the TR cell and in the pre-TR tube is assumed to remain constant, since argon is not absorbed by the materials of the cell or the tube. The ratios of the argon line at  $6965 \text{ \AA}$  to the  $H_{\alpha}$  line and to the oxygen line at  $7772 \text{ \AA}$  and of the  $H_{\alpha}$  line to the above-mentioned oxygen line are expected to have very similar values at hot exhaust stage and at cold refill

stage. since the same partial pressures of argon and water vapour are added at each stage. Only the ratio of the argon line at 6965 Å to the  $H_{\alpha}$  line has a similar value; the other ratios are larger at cold refill stage than at hot exhaust stage. The reason for this is not clear; perhaps the water vapour pressure falls quickly after hot exhaust, as the water vapour is quickly absorbed by the cell body.

The ratio of the argon line at 6965 Å to the  $H_{\alpha}$  line increases slightly after the age stand, indicating a decrease in the partial pressure of water vapour in the cell through absorption by the cell body. An estimate of the pressure drop during this period is 1 torr. The ratio of the argon line at 6965 Å to the oxygen line at 7772 Å at 0.937 kW peak power increases slightly, also indicating a decrease in the partial pressure of water vapour. However, at 0.187 kW peak power the above-mentioned ratio decreases after three days age stand, then increases again by the end of the week age stand. Also, after the week stand the ratio of the  $H_{\alpha}$  line to the oxygen line at 7772 Å, which should be the best monitor of the water vapour pressure, increases. The reason for these results is unclear. but they may be due to desorption of gas from the cell walls of gas which was absorbed during the hot exhaust process.

On ageing with high power, the ratio of the argon line above-mentioned to the  $H_{\alpha}$  line and the ratio of the argon line to the above-mentioned oxygen line increase again, indicating a further reduction of the water vapour partial pressure. The ratio of the  $H_{\alpha}$  line to the oxygen line decreases on ageing, also

indicating a reduction in the partial pressure of water vapour. Under the action of the microwave discharge, water vapour is dissociated, thus reducing its partial pressure in the cell. The partial pressure of water vapour in the cell is estimated to be 8 to 10 torr.

After 60 hours life the ratio of the argon line to the  $H_{\alpha}$  line increases sharply, indicating a reduction in the water vapour partial pressure, through dissociation by the discharge and cleanup at the cell walls. At low power, it is observed that the ratio of the argon line to the oxygen line increases and the ratio of the  $H_{\alpha}$  line to the oxygen line decreases. Both these observations indicate a decrease in water vapour partial pressure in the cell. However, at high power the ratio of the argon line to the oxygen line decreases, indicating either an increase in water vapour partial pressure or an increase in oxygen partial pressure. In the cell, run continuously for 60 hours, much dissociation of water vapour occurs, resulting in a reduced partial pressure of water vapour and an increased partial pressure of hydrogen and oxygen. The partial pressure of water vapour in the cell is estimated to be 8 to 10 torr.

The results from fig (4.9), showing the variation of the ratios of the mean microwave measurements at each stage to the initial measurements, indicate that the changes occurring in the TR cell after one week age stand mainly occur during the first three days. Standing the cells for a further time period does not alter the measurements significantly. A decrease of leakage power and spike

leakage energy after standing indicate a reduction of the partial pressure of water vapour in the cell and an increase in the percentage pressure of argon. A quicker. more efficient breakdown of the gas in the cell occurs when there is a greater percentage pressure of argon present; hence the leakage of power through the cell is reduced.

After ageing, all the measurements have either increased or remained stationary, with the exception of the keep-alive current. The keep-alive current decreases through running of the TR cell with high power with the keep-alive discharge in operation. through sputtering of the keep-alive electrode. The increase in the recovery time indicates a decrease of the partial pressure of water vapour present in the cell, since water vapour is added to reduce the the recovery time. Increase of the leakage power shows a decrease in the ability of the gas to break down and a reduced efficiency of breakdown. This may be due to dissociation of water vapour in the cell by the microwave discharge. with a corresponding increase in the partial pressures of oxygen and hydrogen and a decrease in the percentage pressure of argon.

After 60 hours life. the recovery time increases sharply, indicating a loss of water vapour in the cell. The leakage power and the unprimed spike leakage energy also increase, again showing the decrease of argon percentage pressure in the cell due to the increase in partial pressure of oxygen from the dissociation of water vapour. The keep-alive current decreases, probably due to build-up of deposit on the electrode, through sputtering.

To summarise the results of the measurements of the emission spectra and the microwave measurements:

(1) During the age stand of one week water vapour is absorbed by the cell body, reducing its partial pressure in the cell. The greater part of the change in the TR cell and the gas within has occurred within three days; little subsequent change occurs in the final four days of the age stand.

(2) During ageing with high power, the water vapour pressure is reduced and the pressures of oxygen and hydrogen are increased, due to dissociation of the water vapour by the microwave discharge.

(3) Throughout life, the water vapour present in the cell undergoes dissociation into hydrogen and oxygen, reducing the percentage pressures of argon and water vapour in the cell and increasing the total pressure.

(4) The pre-TR tube contains argon and water vapour, with the pressure of water vapour varying. No hydrogen or oxygen is added to the tube. Unlike the TR cell, which contains hydrogen and oxygen through the dissociation of the water vapour. The presence of the hydrogen and oxygen in the TR cell may influence the degree of excitation of the atoms in the discharge. The measurements of the intensities of the argon, hydrogen and oxygen spectral lines may be influenced by the presence of oxygen and hydrogen in the discharge, as well as by the argon and water vapour. The partial pressure of

the different gases in the cell are not known. Hence the discharge in the pre-TR tube does not accurately represent the discharge in the TR cell and it is not possible to gain accurate values for the pressures of the gases in the TR cell by comparing ratios of spectral lines for the discharges in the TR cell and pre-TR tube.

#### 4.7.1 Effect of Keep-Alive Discharge on Life

While the cells were running with high power for 60 hours, 6, chosen at random, were run without keep-alive discharges operational in the cells and 6 were run with keep-alive discharges operational. In fig (4.18) are shown the variation of mean intensities of the spectral lines at cold refill stage and after 60 hours life, for cells with and without the keep-alive discharge operational. Overall, for the cells with the keep-alive discharge operational the intensity changes are much greater than those for the cells with no keep-alive discharge operational. The change is especially marked for the oxygen spectral line, which increases greatly in intensity after 60 hours life. This is probably due to dissociation of water vapour at the keep-alive electrode and the production of free oxygen. The intensities of the argon spectral lines increase and those of the hydrogen lines decrease much more rapidly for the cells with the keep-alive discharge operational than in those without. indicating a greater decrease in the partial pressure of water vapour in the cells with the keep-alive discharge operational than in the cells without. The discharge at the keep-alive electrode causes dissociation of the water vapour, giving hydrogen and oxygen among the products and reducing the

partial pressure of water vapour in the cell. Hydrogen is readily absorbed by the walls of the cell and especially by the kovar of the window frame, leaving the dissociated oxygen.

The presence of the keep-alive discharge in the TR cell increases the dissociation of water vapour, giving oxygen, hydrogen and other products. The partial pressure of water vapour in the cell is reduced by the action of the microwave discharge and reduced further by the action of the keep-alive discharge. The use of a keep-alive discharge reduces the effective life of a cell by accelerating the loss of water vapour and by reducing the total pressure through sputtering.

#### 4.8 Results for the Experimental Batch of Cells

In an effort to confirm the conclusions reached about TR cell manufacture in section 4.7. an experimental batch of cells was studied at the same stages during manufacture and life as for the first batch of cells, and for two additional stages, 160 hours and 300 hours life. Three groups of four cells were measured; one group, group A, was a control group, manufactured normally; one group, B, was left standing for one week at 200<sup>c</sup> C instead of the normal room temperature and the third group C, were not aged with high power for 48 hours.

The two batches of cells can be compared only at hot exhaust stage. where they are filled with the same gas mixture, under the same conditions. In fig (4.19) are shown the mean values of the intensities of the spectral lines measured for each cell of each batch, at the two power levels, 0.187 kW and 0.937 kW peak power. From fig (4.19) it can be seen that the intensities of the spectral lines measured at 0.187 kW are on average only 90% of those of the second batch of cells. At 0.937 kW the intensities of the spectral lines for the first batch are 106% of those for the second batch. We compared the results for the two batches using the t-test which gives the probability that two different batches of results come from the same overall group of results (see Appendix 4 for a discussion of the t-test). From the results of the t-test, the probability is less than 95% that the batches of cells come from the same normal distribution of intensities of spectral lines of the cells. But, by using the correction factors of 90% and 106% for the low and high power measurements respectively for the second batch of cells, the probability of the intensities of the spectral lines for the cells all being from the same normal distribution is now greater than 95%.

The differences in the intensity measurements for the two batches of cells may be due to a slight variation in the partial pressures of argon and water vapour present or perhaps due to measurement error of the applied power level at which the measurements were made. Due to the variation in the intensity measurements for the two batches of cells, we will not compare the

intensity measurements directly. but compare instead the ratios of the measurements made at each stage during manufacture to those made at hot exhaust stage and the ratios of the measurements made during life to those at cold refill stage. As we have already seen, no useful information may be obtained from the comparison of the intensity measurements after the hot exhaust stage and after the cold refill stage since the cell is evacuated of the gas added at hot exhaust stage and a new gas mixture added. In figs (4.20) and (4.21) are shown the ratios of the spectral lines at each stage during manufacture to the hot exhaust stage.

At stages 2 and 3 we expect the intensities of the spectral lines from the discharges in the first batch of cells, the control group and the group not aged with high power to be similar since they have all undergone the same treatment. The intensities of the argon lines are not noticeably different for each group over the age stand of one week. The intensity of the oxygen spectral line is much greater for the first batch however; the  $H_{\alpha}$  line is much greater at high power and lower at low power and the  $H_{\alpha}$  line is lower at both low and high power, than the corresponding lines for groups A and C.

At stage 4, after 48 hours ageing with high power, there is a marked variation in the intensities of the argon lines; those for the cells of group B the largest, and the smallest from group C. The oxygen spectral line is largest for group A and smaller for the other groups. The intensities of the hydrogen lines reflect those of the argon lines at low power, but at high power group C has the

highest intensity, followed by group B then group A.

In fig (4.22) are plotted the microwave measurements made at each stage during manufacture for the first batch of cells. the control group A, the group stood at 200°C, B, and the group not aged with high power, C. The variation in the readings taken when the cells were filled initially, when each group has received the same treatment. are such that definitive conclusions about the significant variation in the spike leakage energy and total leakage power during manufacture cannot be reached. The keep-alive current is lowest after stage 4 for the cells of group B. Perhaps a chemical deposit on the keep-alive electrode of substances released during the cells' stand at 200°C has caused the reduction in the keep-alive current. The measurements of recovery time are similar for all the groups of the second batch of cells. The readings for the first batch of cells differ slightly from those of the control batch of cells. The intensities of the emission spectra from the first and second batches of cells differ slightly, so the variations in microwave measurements are to be expected. Perhaps a slight variation of the partial pressures of argon and water vapour added to each batch of cells occurs, causing the variation in the intensity and microwave measurements.

In fig (4.23) and (4.24) are shown the variation in the mean intensities of the spectral lines for each group of cells and the first batch of cells, measured at intervals throughout life, compared with the mean intensities at the cold refill stage. The intensities of the argon lines all increase similarly throughout

life. Both argon lines are largest for the cells of group B until 160 hours life, but smallest for the line at  $6965 \text{ \AA}$  at 300 hours. The argon line at  $6677 \text{ \AA}$  is largest at high power at 300 hours and comparable with those of the other groups at low power. The oxygen spectral line increases steadily with life for each group of cells. with group C having the highest intensity at 300 hours and group B having the lowest intensity. The intensities of the hydrogen lines decrease with life for the higher power measurements but at lower power the intensities first decrease in value, increase at 160 hours then decrease again. The lowest intensity lines throughout life occur for group C with the highest intensity lines for the cells of group B, except at 300 hours and low power, when the cells of group A give the highest intensities.

In fig (4.25) are shown the variation in the microwave measurements made at the various stages throughout life. The primed spike leakage energy and total leakage power values are similar for groups A and B, but lower for group C throughout life. The unprimed spike leakage energy values are very different for the control group, mainly due to a very high reading for one cell in the group. The unprimed total leakage power values diverge at 300 hours. group A being the largest and group C the smallest. The keep-alive currents increase after an initial decrease at 60 hours; the values for group C are consistently higher and for group B lower. The recovery times for each group are similar and fairly constant until 300 hours, when they increase sharply; the longest time is for group C and the shortest for group B. The low power breakthrough measurements vary greatly from cell to cell and vary

with cell structure as well as with gas fill, so few definitive conclusions can be reached from these measurements. However, the low power breakthrough measurements are greatest for group A and smallest for group C, at 160 and 300 hours.

In figs (4.26) to (4.28) are shown the ratios of the argon spectral line at  $6965 \text{ \AA}$  to the  $H_{\alpha}$  line and to the oxygen line at  $7772 \text{ \AA}$  and of the  $H_{\alpha}$  line to the above-mentioned oxygen line for each of the stages of measurement of the cells at the power levels 0.187 kW and 0.937 kW peak power. By comparing these ratios with the ratios calculated from the discharge in a pre-TR tube (fig (4.11)), we can estimate the changes occurring in the three groups of cells during manufacture and throughout life. Over the age stand of one week it is observed that water vapour is absorbed by the cell for groups A and C, thus reducing the partial pressure. A small amount of oxygen may also be desorbed, altering the proportions of gases in the cell and accounting for the values obtained for the ratio of the H line to the oxygen line at  $7772 \text{ \AA}$ . For the cells stood at  $200^{\circ} \text{ C}$ , however, some water is absorbed during the age stand of one week, but not as much as for the cells stood at room temperature. More oxygen is also desorbed. From section 6.8 on Surface Reactions in Chapter 6 we see that the amount of gas absorbed by a surface decreases with increasing temperature. The total pressure in the cells of group B is reduced by a smaller amount, therefore, and, having a different gas mix, helps to explain the differences in results for group B and those for groups A and C.

The overall change occurring during ageing with high power is the dissociation of water vapour into various products, including hydrogen and oxygen. The cells not aged with high power do not undergo this loss of water vapour, so the change in their intensity measurements is least. The cells stood at 200° C for one week show the largest change in intensity measurements since they have the largest partial pressure of water vapour before this stage.

Throughout life, the three groups of cells behave similarly, with the results of the control group measurements similar to those of the group not aged with high power, especially for the later stages of life. Water vapour is lost, by conversion to products such as oxygen and hydrogen through the action of the discharge. Hydrogen is preferentially absorbed by the metal of the cell body and especially by the kovar window frame (see section 6.8 on Surface Reactions in Chapter 6) leaving dissociated oxygen and a reduced partial pressure of water vapour in the cells. The cells which have apparently lost most water vapour in 300 hours of life are those not aged with high power for 48 hours; the cells stood at 200° C for a week lose the least amount, with the control group of cells in between.

The microwave results confirm the above conclusions about the behaviour of the cells throughout life. The recovery time at 300 hours is expected to be longest for the cells with the least amount of water vapour, those not aged with high power for 48 hours; the shortest recovery times occur for the cells stood at 200° C for a

week. The cells not aged with high power also have the lowest values of total leakage power, primed spike leakage energy and low power breakthrough, indicating that they contain the largest percentage of argon and the smallest percentage of water vapour of the three groups. The cells stood at 200° C for a week and those of the control group have much higher values of spike leakage energy, total leakage power and low power breakthrough, indicating the presence of a greater proportion of water vapour in these cells and hence a reduced breakdown of the gas within.

#### 4.9 Cells Which Fail

A cell is deemed to have failed, ie reached the end of its useful life, when one of the measured microwave parameters exceeds a defined value. Using this criterion, several of the cells fail at various stages throughout the 300 hours of the experiment. At refill stage, cell 1841 from group C had a spike leakage energy of 16 nJ/pulse, exceeding the specified maximum value of 15 nJ/pulse. The cell was allowed to proceed through life. The spike leakage energy was observed to decrease initially, then increase again.

1841	Spike Leakage Energy/nJ/pulse	16	10	12	13
	Life Time/Hours	0	60	160	300

The initial decrease in the spike leakage energy may be due to a reduction in the partial pressure of water vapour in the cell. The subsequent steady increase may be due to the increase of water

vapour products such as oxygen in the cell, or due to desorption of water vapour from the cell walls. Cell 1857 from group A had a spike leakage energy of 16 nJ/pulse at 300 hours, with the other microwave measurements remaining within their limits.

1857	Spike Leakage Energy/nJ/pulse	15	13	14	16
	Life Time/Hours	0	60	160	300

Cell 1846 from group A had an unacceptably high spike leakage energy at 160 hours, which decreased again by 300 hours.

1846	Spike Leakage Energy/nJ/pulse	15	15	16	14
	Life Time/Hours	0	60	160	300

The decrease in spike leakage energy at 300 hours may be due to a further loss of water vapour in the cell, which cannot be compensated for by the increase of water vapour products or water desorbed from the cell body.

Several of the cells fail at 300 hours with a recovery time greater than the limit of 3  $\mu$ s. Of these, one is from the control group, with a recovery time of 8  $\mu$ s, one is from the group stood at 200° C, with a recovery time of 3.2  $\mu$ s and two from the group not aged with high power, with recovery times of 7.6  $\mu$ s and 4.8  $\mu$ s respectively. In figs (4.29) to (4.31) are shown the graphs of the intensity of the argon line at 6965 Å, the oxygen line at 7772 Å

and the  $H_{\alpha}$  line for each cell for the two power levels, 0.187 kW and 0.937 kW peak power throughout the life of the cell. In fig (4.32) is shown the variation of recovery time with time for each cell. From the graphs it can be seen that for groups A and C the cells with the longest recovery times also have the largest values of intensities of the argon and oxygen spectral lines in their respective groups and the smallest values for the  $H_{\alpha}$  line. For the cells stood at 200° C, however. the intensities of the argon and hydrogen spectral lines are both the highest of the group for the cell with the longest recovery time; the oxygen line is large, but not the largest of the group. Very high values of the argon spectral line and very low values of the H line imply a reduced amount of water vapour in the cell. A large value of the oxygen spectral line indicates an increased partial pressure of oxygen in the cell, as the result of dissociation of water vapour.

The group of cells stood at 200 C behave differently throughout life to the other two groups. The intensity of the argon line for the cell with the long recovery time is large, indicating an increased partial pressure of argon in the cell and a reduced partial pressure of water vapour. The high intensity oxygen line indicates an increase in oxygen production from the dissociation of water vapour. The cell with a large recovery time has throughout life a higher intensity of the  $H_{\alpha}$  line. This cell may contain a larger proportion of hydrogen than the other cells, having absorbed more hydrogen during ageing than the other cells.

The cells which fail do so because of a decrease in the water vapour partial pressure in the cells, caused by the dissociation of the water vapour by the microwave discharge. The cells which were not aged with high power failed more rapidly since they did not receive the benefits from saturation of the walls with the dissociation products of water vapour which normally occurs during ageing. The cells which were stood at 200°C behaved differently throughout life to the control group and to the group not aged at high power; more gas was desorbed from their surface during the week stand and less water absorbed. Hence more of the dissociation products of water vapour were absorbed during the subsequent ageing. So, throughout the life of these cells, hydrogen especially was not absorbed as readily by the cell bodies. For all the cells, in each group. water vapour is dissociated by the microwave discharge and its reduced partial pressure in the cells leads to an increased recovery time.

#### 4.10 Summary and Conclusions

The object of the experimental work described in this chapter was to discover the processes occurring throughout the manufacture of the TR cell and during part of its life. The measurements carried out on the cell were of the intensities of spectral lines in the emission spectrum of the microwave-excited discharge in the cell and of the performance of the cell when subjected to high power microwave pulses. The typical spread of intensity measurements for a batch of 12 cells was 20 % at low power

percentage spread at low power is easily explained since at low power the intensities of the spectral lines are lower, resulting in greater inaccuracies in their measurement. The intensity spread may be due to the varying absorption rates for the different cells, resulting in a variation of the partial pressure of water vapour in the cells. The spread in the intensity and microwave measurements tends to increase with increasing life of the cells as the partial pressures of the gases within vary. The largest percentage spreads in the microwave measurements for a batch of cells are of the unprimed leakage values; unprimed spike leakage energy has a spread of 9 % and unprimed total leakage power has a spread of 5 % at hot exhaust stage. The corresponding primed values have spreads of 6 % and 4 % respectively. The percentage spread in the primed measurements is lower since the primed discharge provides an initial supply of electrons, giving a faster and more efficient breakdown of the gas. The percentage spread in recovery time is 9 % at hot exhaust stage, probably caused by the variation in the partial pressure of water vapour absorbed by each cell. Initially the percentage spread in the keep-alive current is under 1 %, but it increases with life as varying amounts of deposit accumulate on the keep-alive electrode through the action of its discharge. The conclusions drawn from the results of the intensity and microwave measurements must take into account the observed spread in the measurements.

A batch of 12 cells were measured at several stages throughout manufacture and life, as described earlier in this chapter. The results of the measurements show that after standing the cells for one week after the hot exhaust stage, water vapour has been absorbed by the cell body. The results also indicate that the significant changes to the cell occur after 3 days; a further 4 days stand alters only slightly the amount of water vapour absorbed. The recovery times for the cells decrease over this period, indicating an increase in water vapour pressure, which we believe to be unlikely. But the recovery time measurement is not very reliable as there is an error of up to  $0.4 \mu\text{s}$  associated with it, due to variation in the performance of the different crystal detectors used.

During ageing of the cells, water vapour is dissociated into products including hydrogen and oxygen, hence reducing the partial pressure of water vapour in the cells. The cells may also absorb some of the dissociation products at this stage.

Throughout life, water vapour in the cells is again dissociated into hydrogen and oxygen and an increasing partial pressure of oxygen is observed in the emission spectrum of the discharge throughout life. Hydrogen is readily absorbed by many metals, especially kovar, of which the cell window frame is constructed. As the running time of the cells increases, the partial pressure of water vapour gradually decreases and that of oxygen gradually increases.

Intensity measurements were carried out on the emission spectrum of the microwave excited discharge in a pre-TR tube containing argon at the same partial pressure as the TR cell and varying partial pressures of water vapour. Since quartz is very unreactive and effectively impermeable to argon and water vapour, the gas added to the tube was not absorbed, but remained in the discharge. Results of these measurements were used to model the behaviour of the discharge in a TR cell containing a constant partial pressure of argon and a varying partial pressure of water vapour. However, throughout ageing and life the TR cell also contains oxygen and hydrogen, from the dissociation of water; these gases are not present in the pre-TR tube. It has been estimated that about 1 torr of water vapour is absorbed by the cell during the week age stand and a further 1-2 torr is lost during ageing.

An experiment which was designed to show the effect of the keep-alive discharge on cell performance showed that its operation increased the rate of dissociation of the water vapour in the cell leading to a reduced lifetime.

A second batch of 12 cells was measured at several stages during manufacture and life, as described earlier. The batch was divided into three groups of four cells; one as a control, manufactured normally, one was not aged with high power and one was stood for 1 week at 200 C instead of the normal room temperature, all other processes carried out as normal. The results for the two batches of cells were compared at hot exhaust stage. The values of

the intensity measurements for each batch of cells differed, the values for the first batch being 90% of those of the second batch at 0.187 kW and 106% at 0.937 kW. This may be due to a slight difference in the power levels at which the measurements were taken, due to meter error, or a slight variation in the partial pressures of the gases in the cells for the two batches of cells. So the intensities of the lines were not compared directly, and the ratios of the lines compared instead.

The results of the measurements showed that during the age stand the cells stood at 200°C absorbed least water vapour and may also have desorbed some of the gas absorbed at lower temperatures. During ageing, these cells lost more water vapour through dissociation than the other cells. The spread in the microwave measurements within a group is such that comparison of the results between groups is not generally possible.

The cells not aged with high power gave overall the worst performance, including the longest recovery times, throughout life, indicating that they contained the lowest partial pressures of water vapour. The cells aged with high power have absorbed some hydrogen from the dissociation of water vapour, which the cells not aged have not. Later in life, the cells not aged can absorb more hydrogen than the other cells, increasing the rate of loss of water vapour from the cells.

In the following chapter, these conclusions will be investigated using the technique of mass spectroscopy to analyse the gas in the TR cell.

References

- J Boissiere and C Romiguiere (1957) Study of the Pressures and their Evolution in Gas Tubes, Vide 12, 117
- G Herzberg (1950) Molecular Spectra and Molecular Structure 1 Spectra of Diatomic Molecules, Van Nostrand Reinhold Co, New York
- H S Maddix (1968) Clean-up in TR Tubes, IEEE Trans Electron Devices ED 15, 98
- C E Moore (1949) Atomic Energy Levels, NBS Publication 467
- R Musson-Genon (1957) Physico-Chemical Problems in TR Cells, Nachrichtentechnische Fachberichte 9, 44
- R W Pearse and A G Gaydon (1976) Identification of Molecular Spectra, Chapman and Hall, London

Table 4.1

Argon Ar

Metastable Levels

11.55 eV

11.72 eV

Ionization Energy

15.759 eV

		$E_i/\text{cm}^{-1}$	$E_k/\text{cm}^{-1}$	$g_i$	$g_k$	$A/10^8 \text{s}^{-1}$	
Spectral Line	6965.430 A	93144	107496	5 <sup>i</sup>	3 <sup>k</sup>	0.067	$2P_2 \rightarrow 1S_5$
	6677.282 A	93751	108723	3	1	0.0241	$2P_1 \rightarrow 1S_4$

Hydrogen H

Ionization Energy

13.598 eV

		$E_i/\text{cm}^{-1}$	$E_k/\text{cm}^{-1}$	$g_i$	$g_k$	$A/10^8 \text{s}^{-1}$
Spectral Line	6562.849 A	82259	97492	8 <sup>i</sup>	18 <sup>k</sup>	0.4410
	4861.327 A	82259	102824	8	32	0.08419

Oxygen O

Ionization Energy

13.618 eV

		$E_i/\text{cm}^{-1}$	$E_k/\text{cm}^{-1}$	$g_i$	$g_k$	$A/10^8 \text{s}^{-1}$	
Spectral Line	7771.928	73768	86631	5 <sup>i</sup>	7 <sup>k</sup>	0.340	$5P \rightarrow 5S_0$

Table 4.2

Gas	Pressure/mb		
Argon	10	25	40
Tritiated Argon	10	25	40
5Curies/litre			
Hydrogen	10	25	40
Deuterium	10	25	40
Chlorine	10	25	40
Tritiated Argon	10	25	40
2 Curies/litre			
Water Vapour	10	25	37
Krypton	10	25	40
Tritium-Krypton	10	25	40
2 Curies/litre			

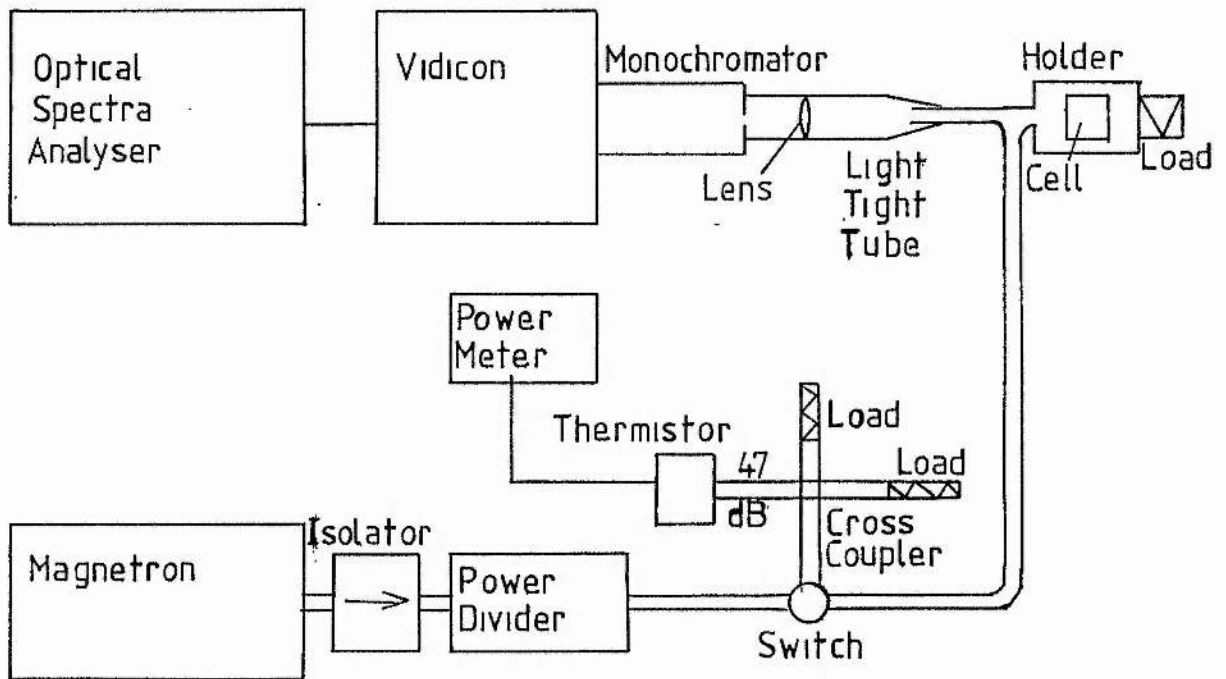


Fig 4-1 Experimental Setup to Measure the Microwave-Excited Emission Spectrum from the TR Cell

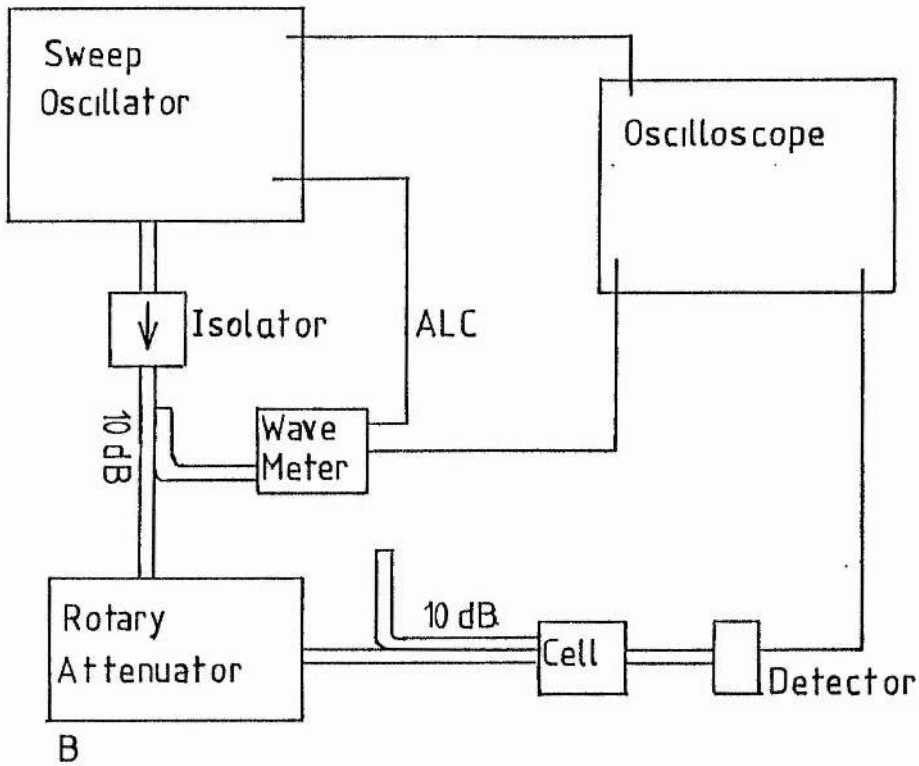
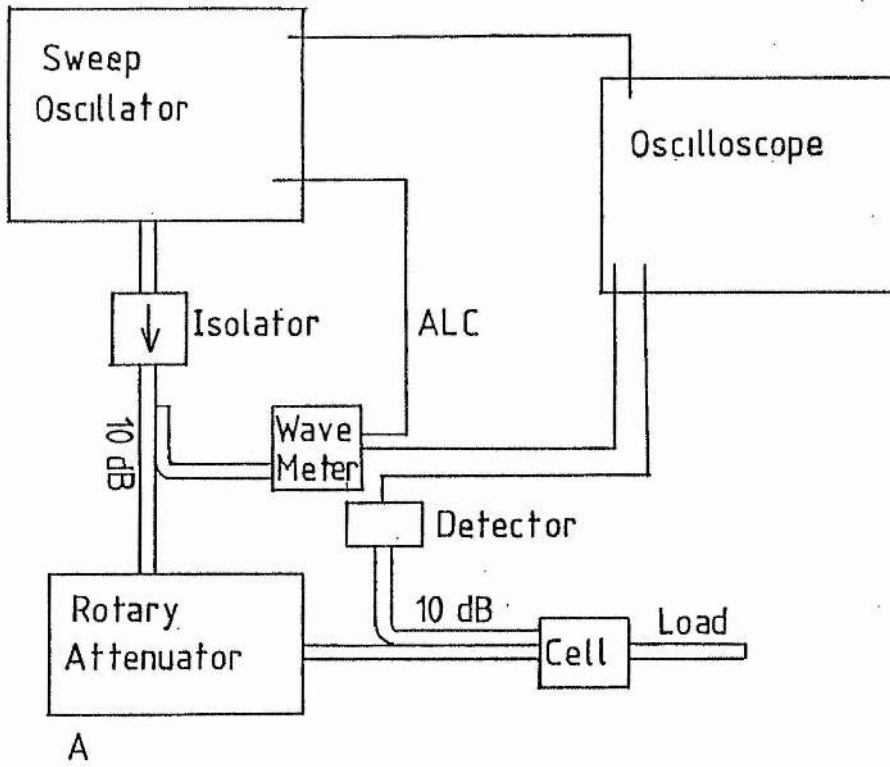


Fig 4.2 Experimental Setup to Measure - A VSWR  
 - B Insertion Loss

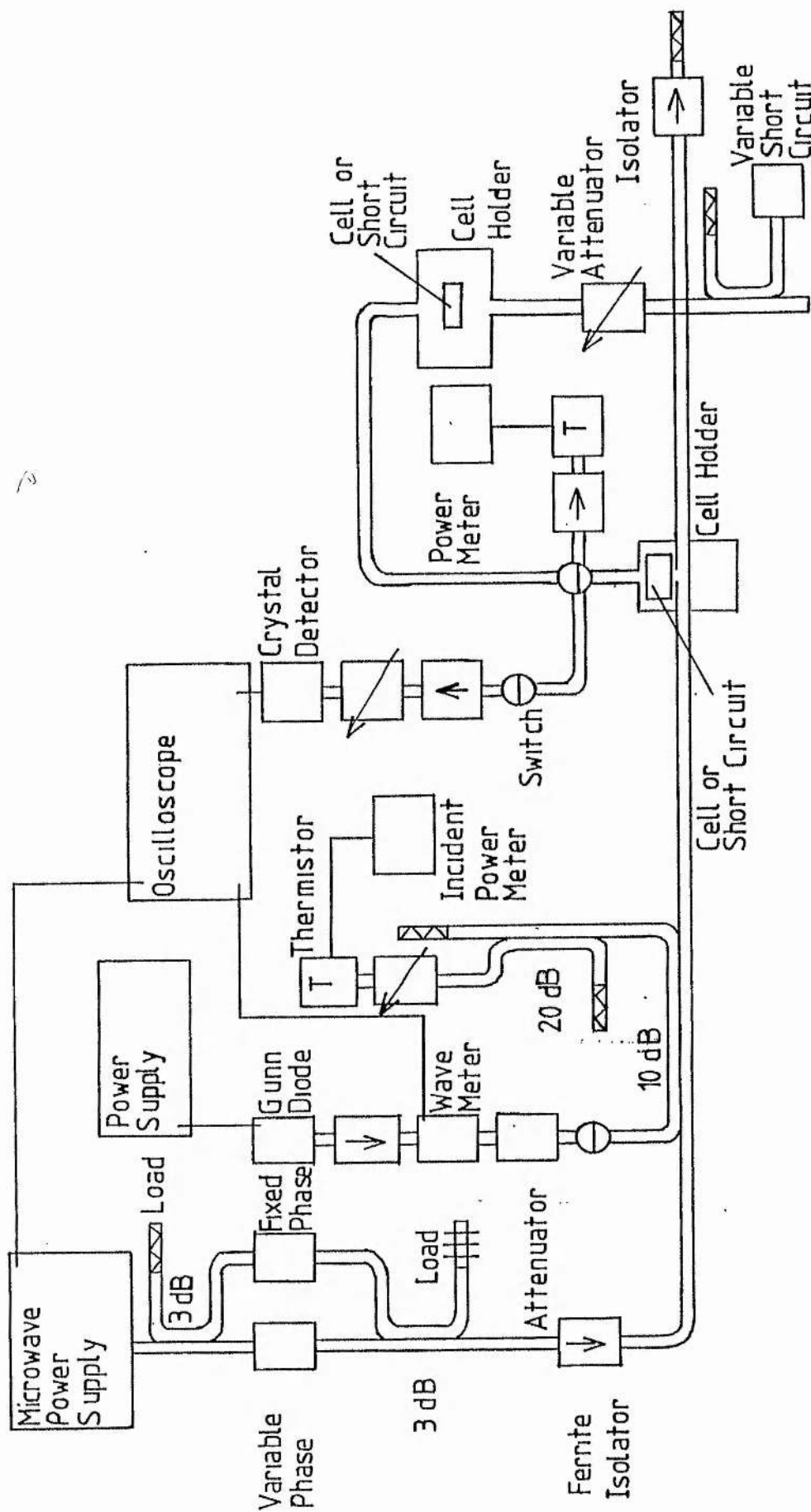


Fig 4-3 Experimental Setup for Measuring the High Power Performance of the TR Cell

Fig 4.4 Emission Spectra Measurements at 0.187 kW on the first Batch of TR Cells  
 Number of Cells against Intensity Range

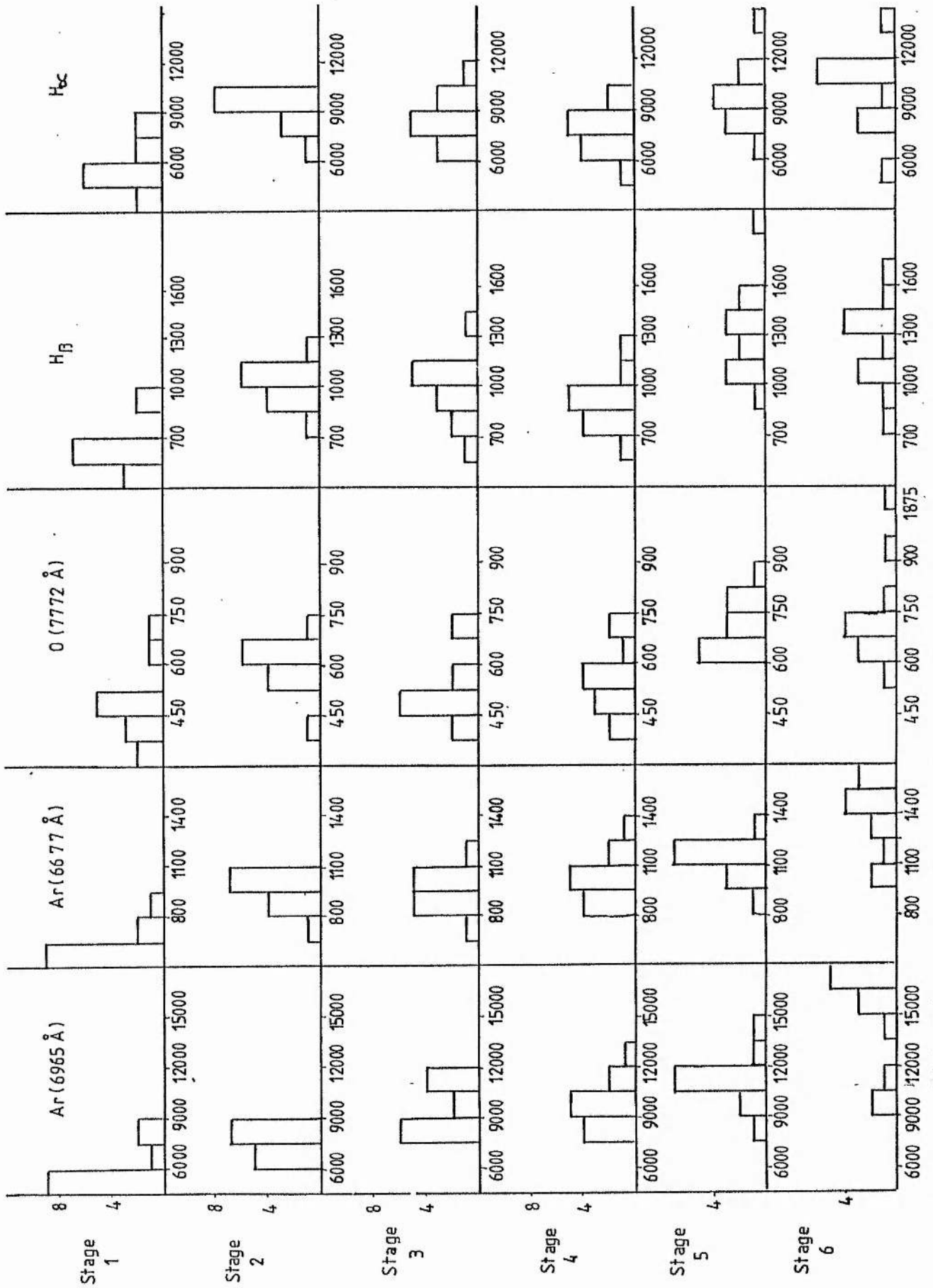


Fig 4-5 Emission Spectra Measurements at 0.937k W on the first Batch of TR Cells  
 Number of Cells against Intensity Range

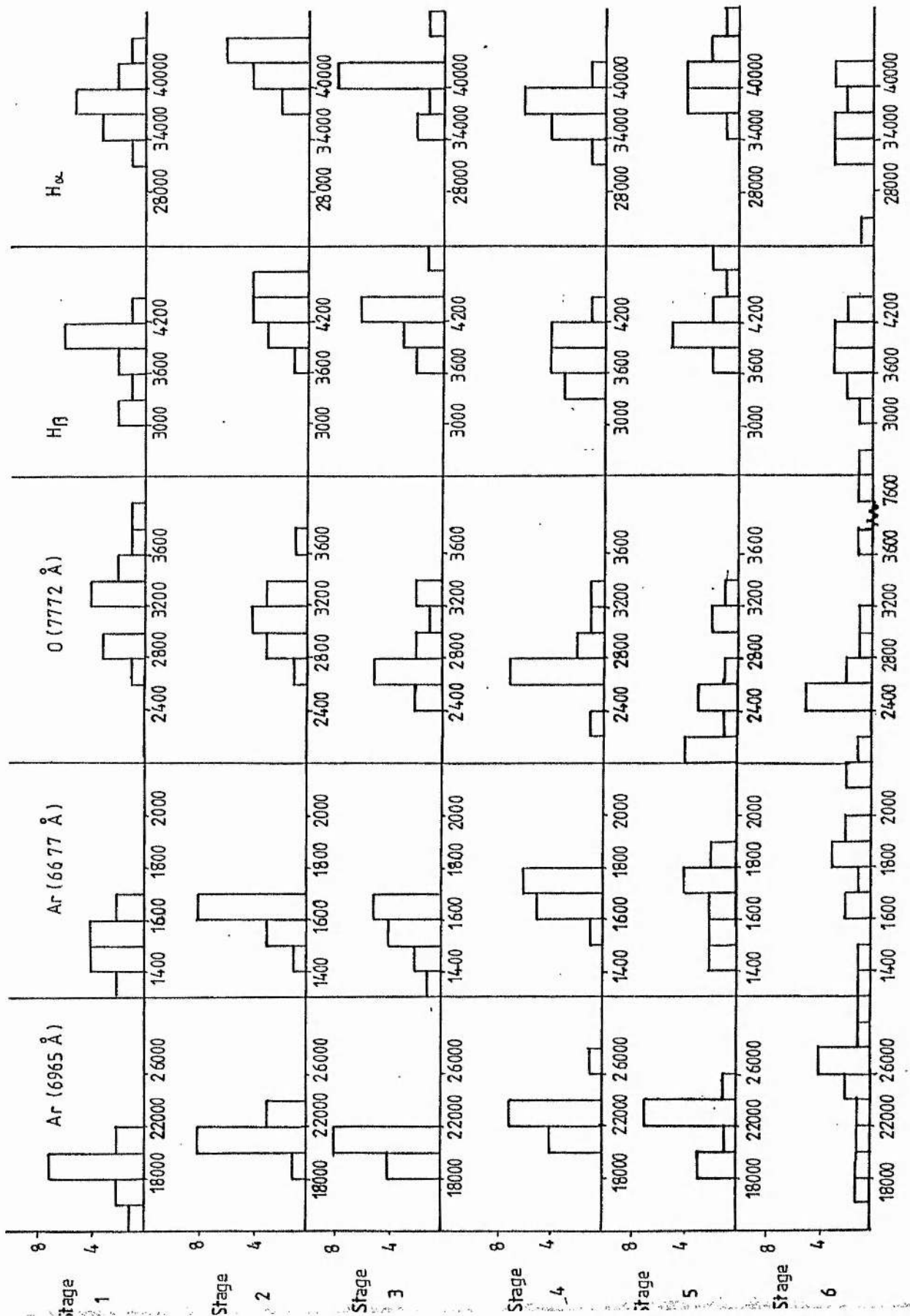


Fig 4-6 Ratio of Intensity at each Stage to Intensity at First Stage for each Spectral Line for each Stage  
First Batch of Cells

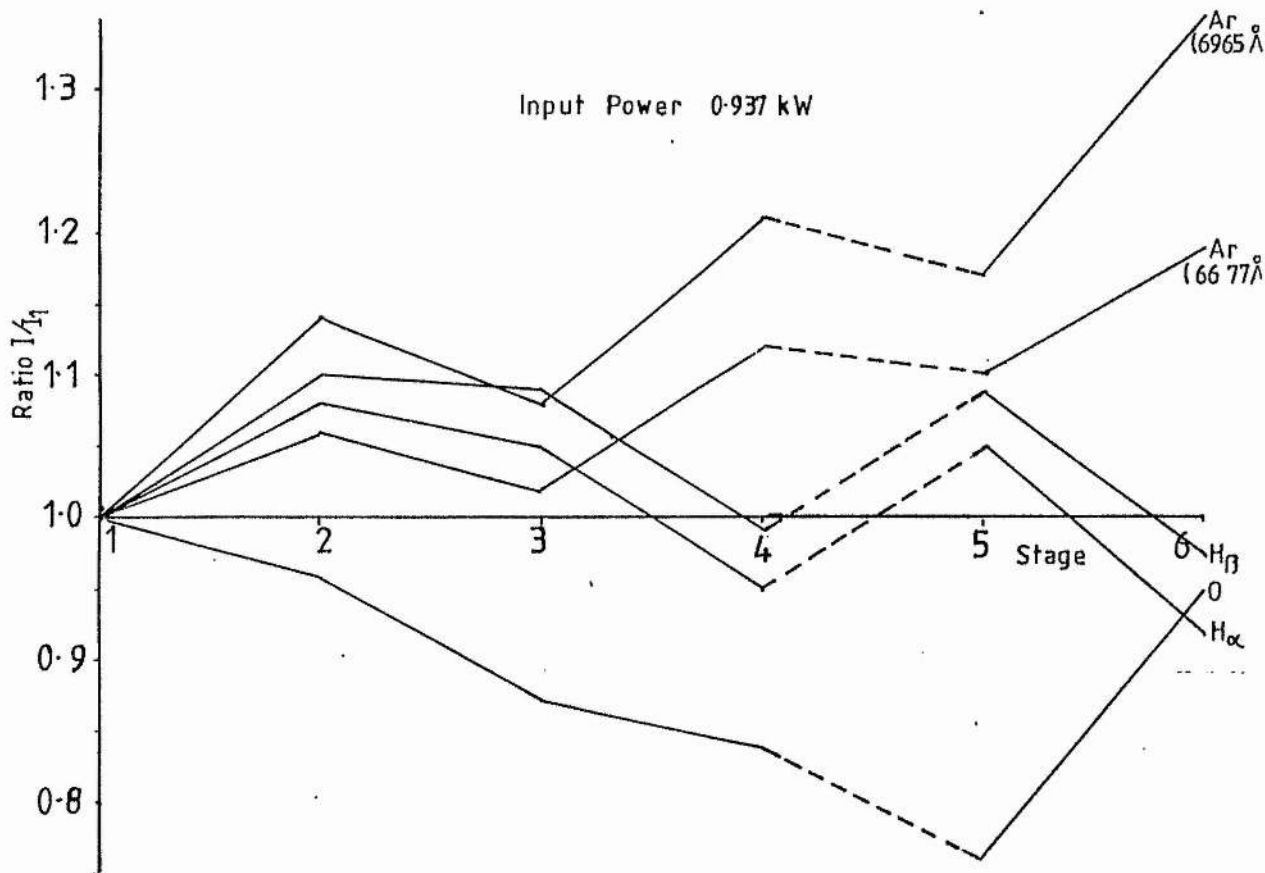
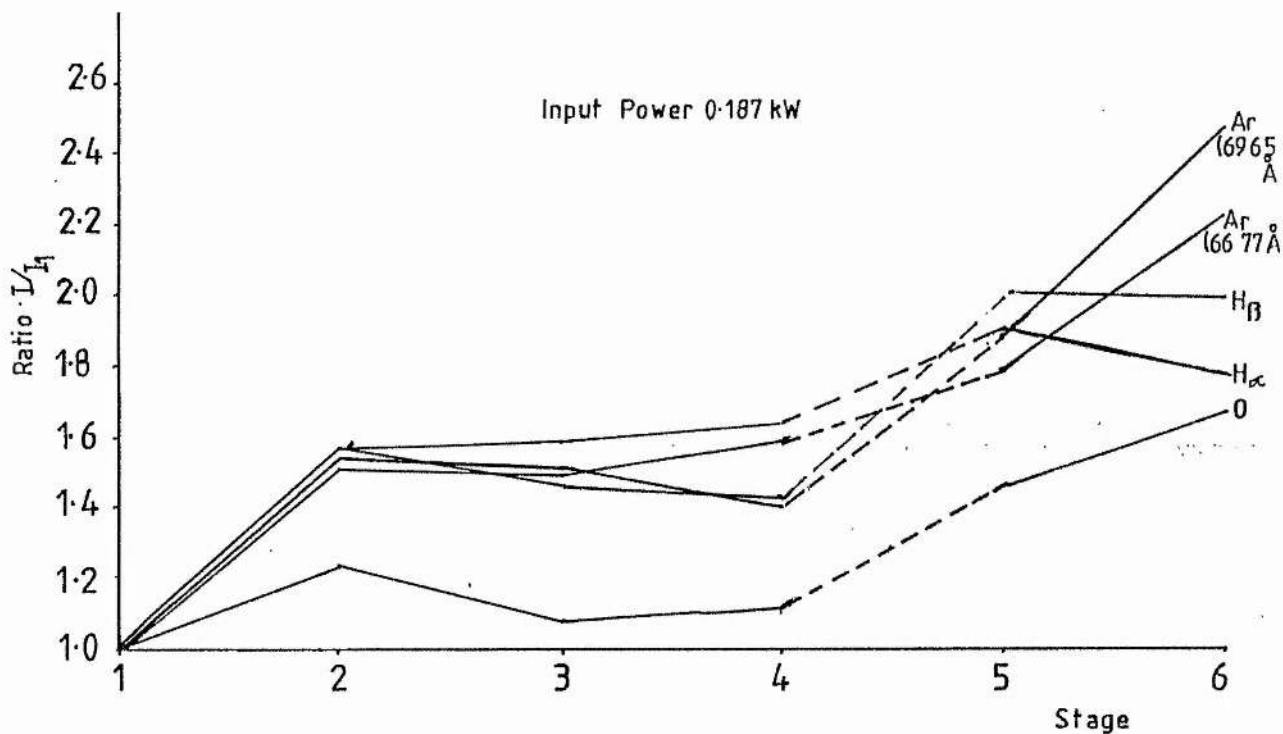


Fig 4.7 Spread in VSWR, Insertion Loss, and Low Power Breakthrough Measurements for Stages 5 and 6  
First Batch of Cells

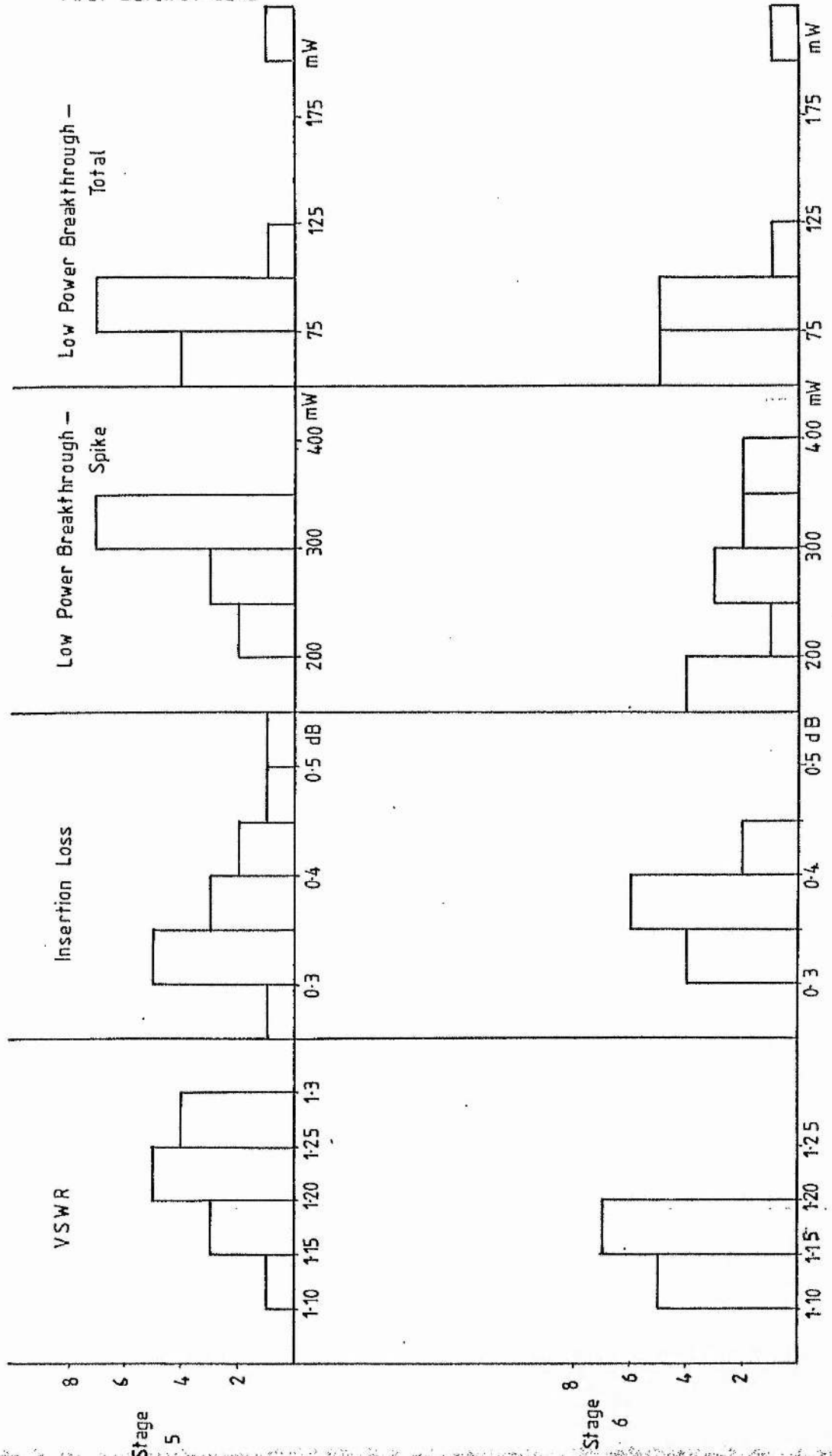


Fig 4-8 Spread of Microwave Measurements  
First Batch of Cells

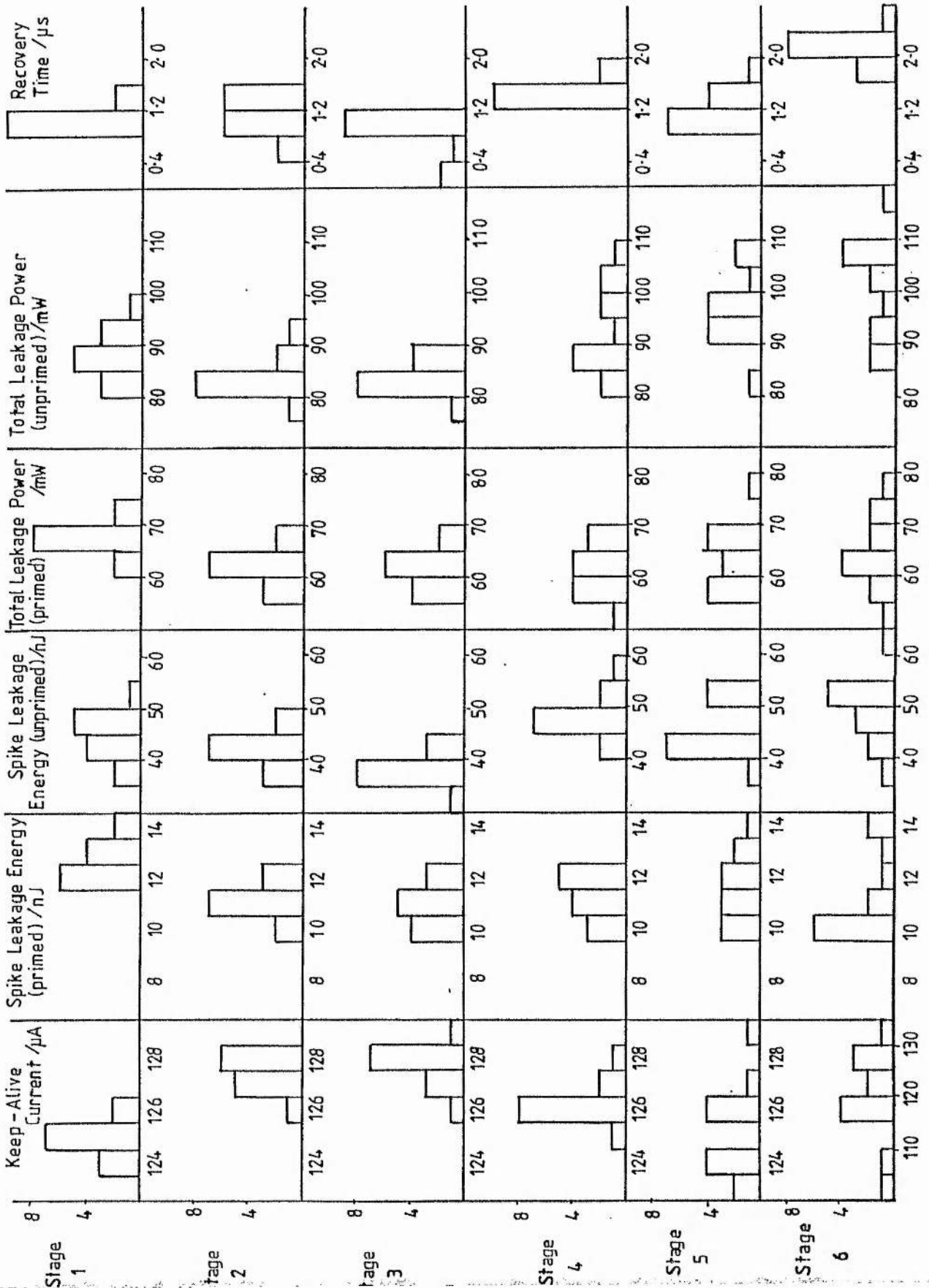
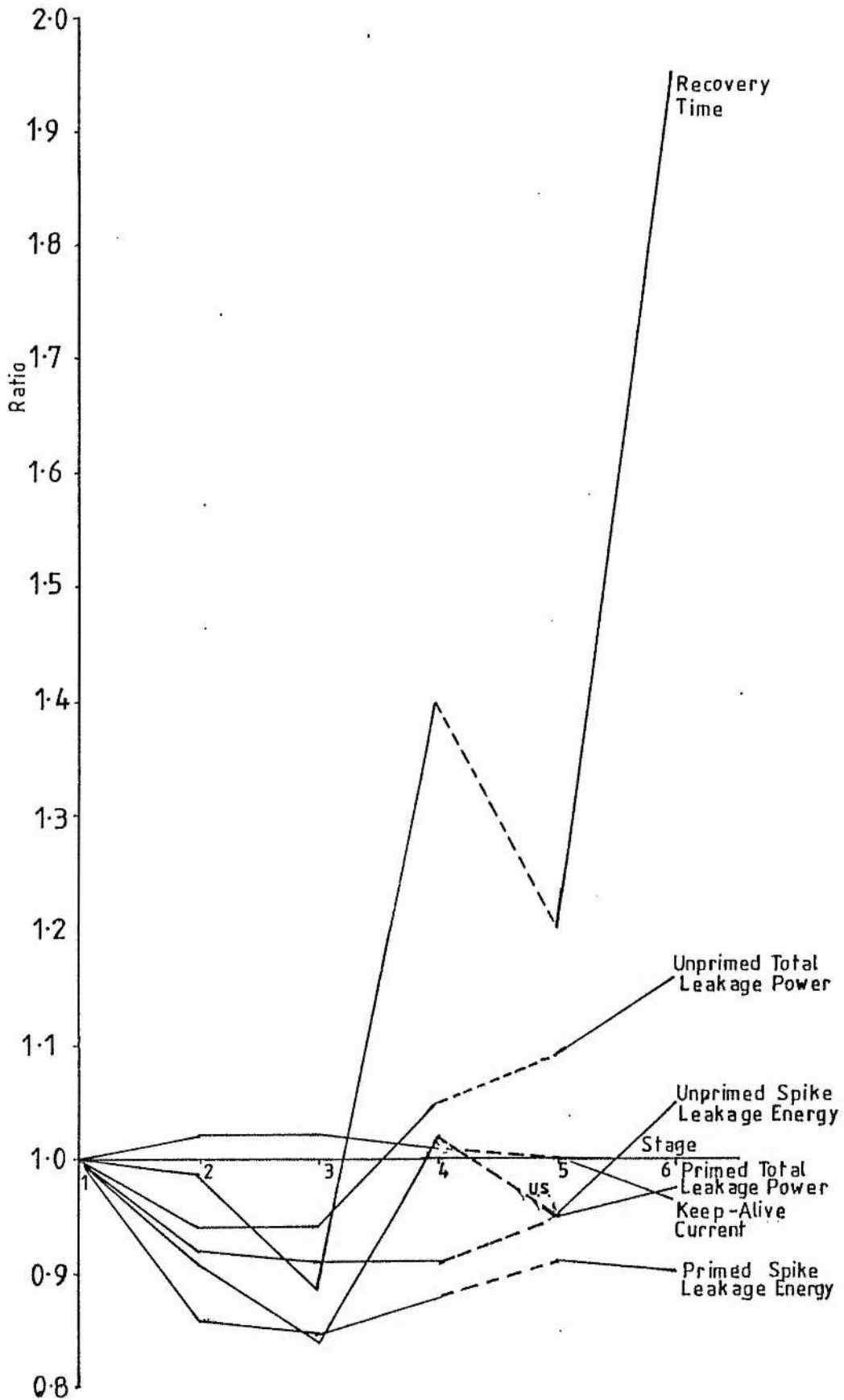


Fig 4-9 Ratio of each Microwave Measurement at each Stage to the Initial Microwave Measurement First Batch of Cells



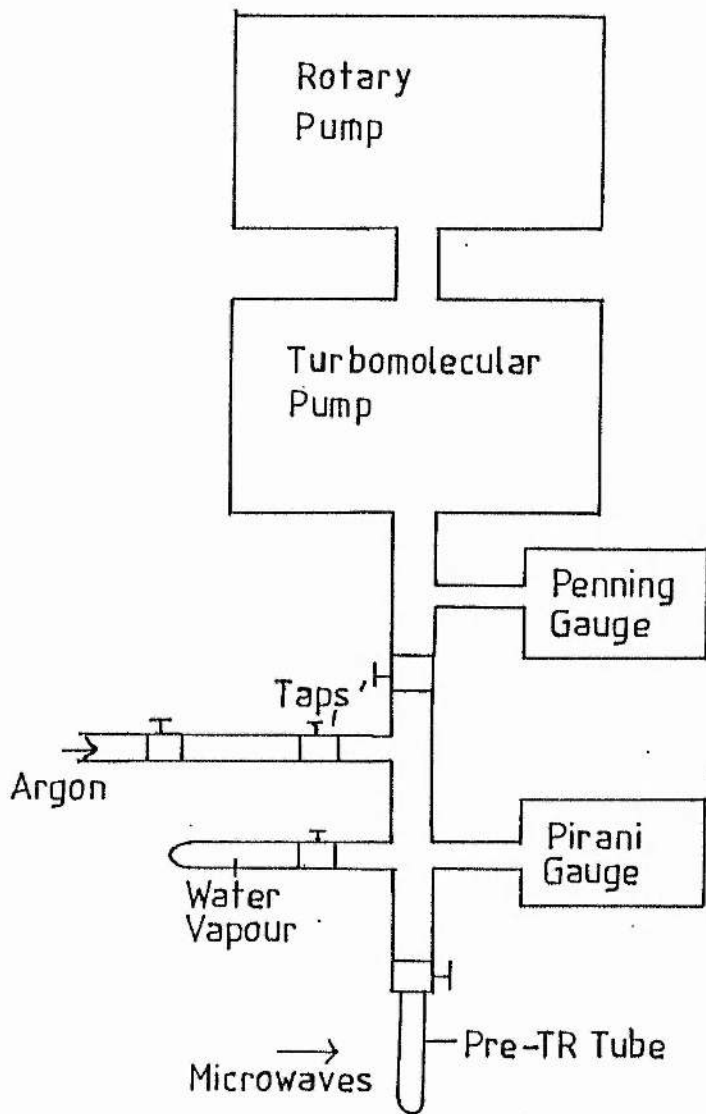
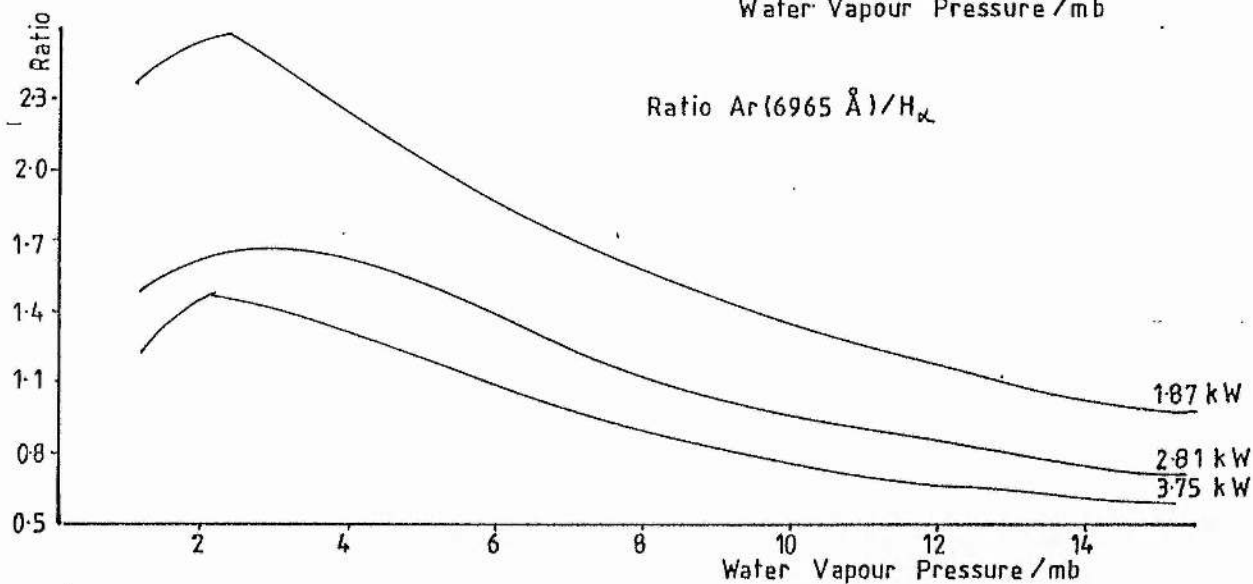
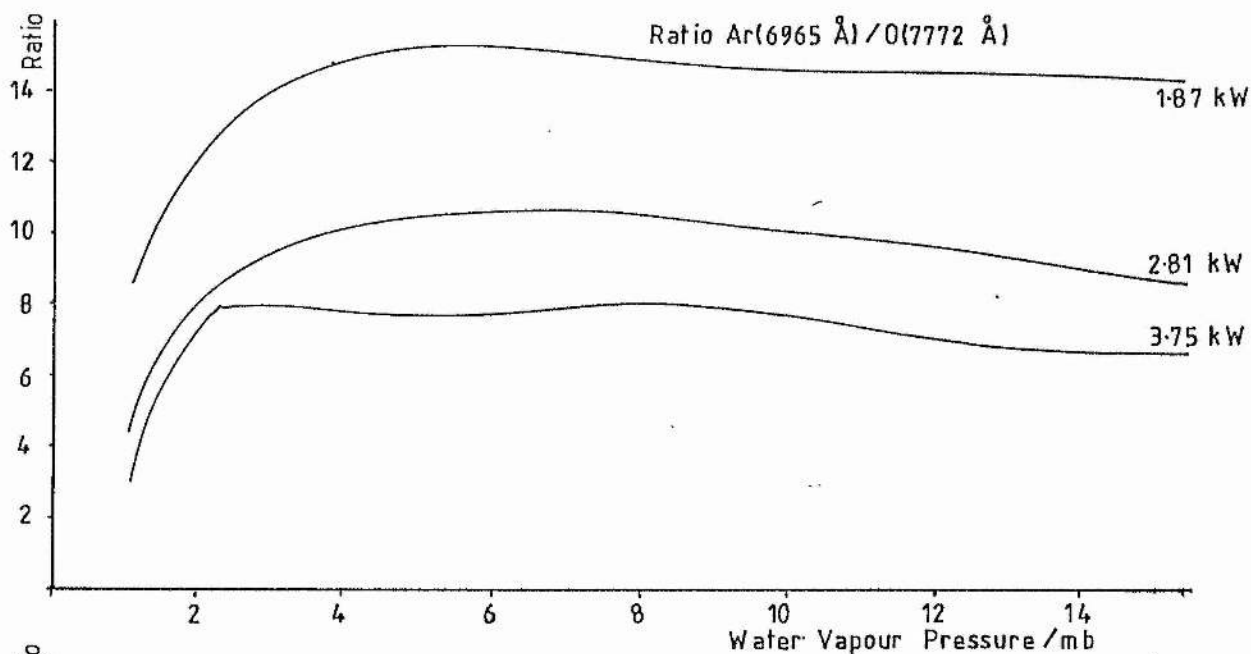
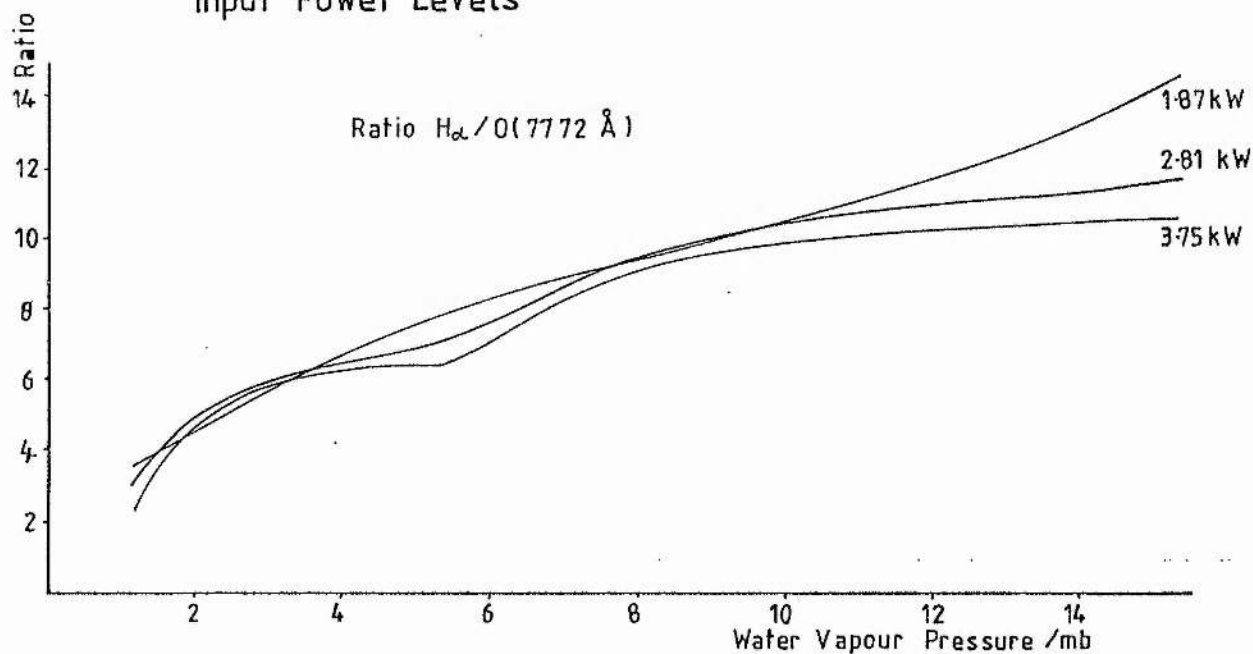


Fig 4.10 Pre-TR Tube Gas Filling Station

Fig 4-11 Ratios of Intensities of Spectral Lines from the Pre-TR Tube Microwave Discharge for Varying Input Power Levels



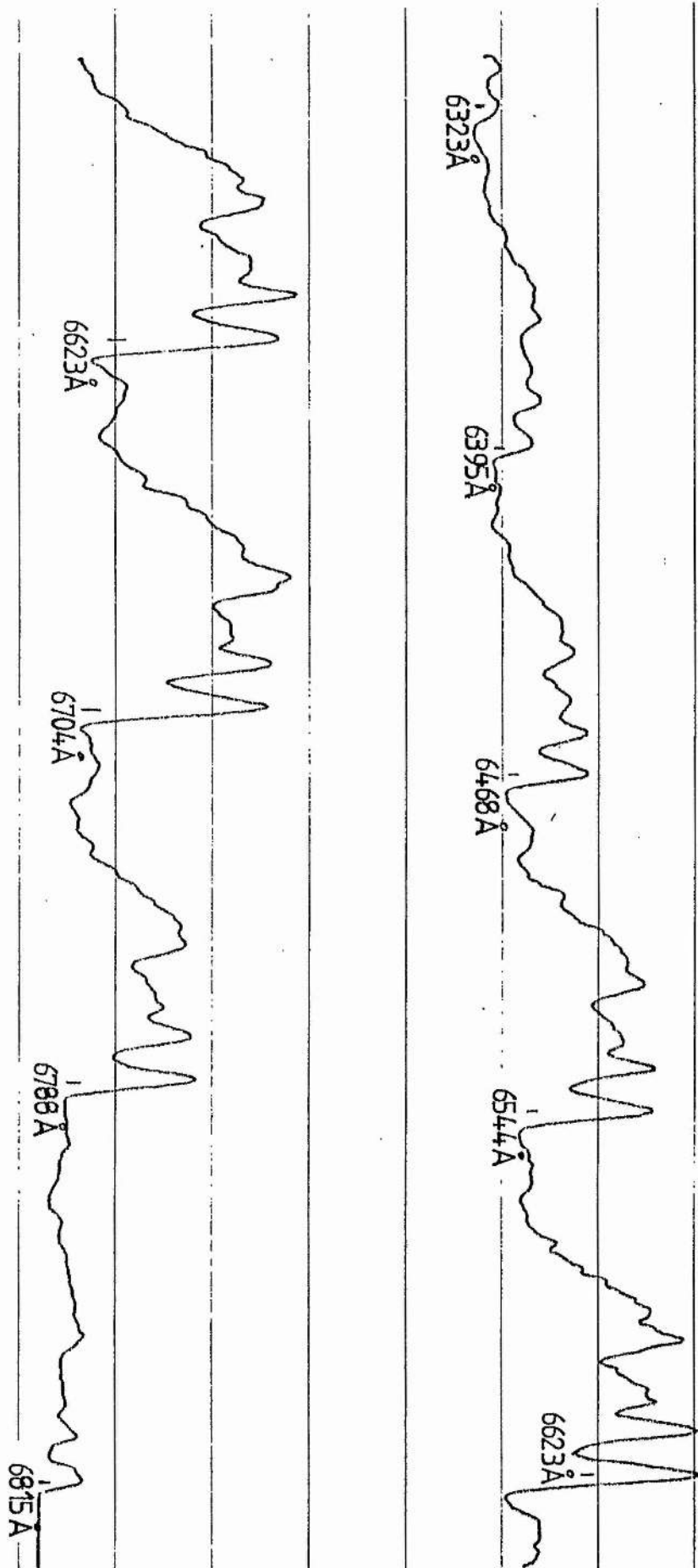


Fig 4-12 Microwave Excited Emission Spectrum of N<sub>2</sub>

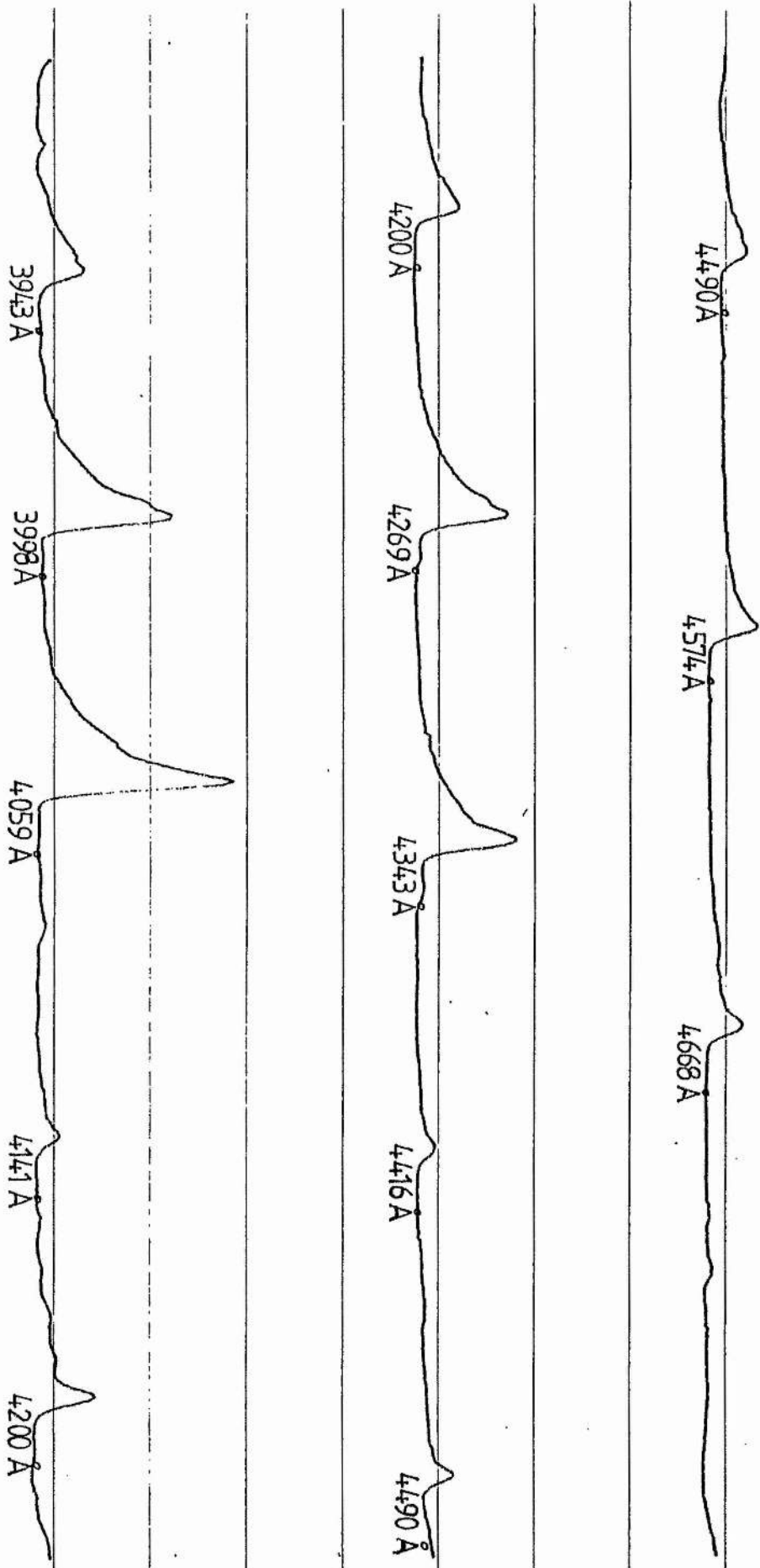


Fig 4.13 Microwave Excited Emission Spectrum of  $N_2$

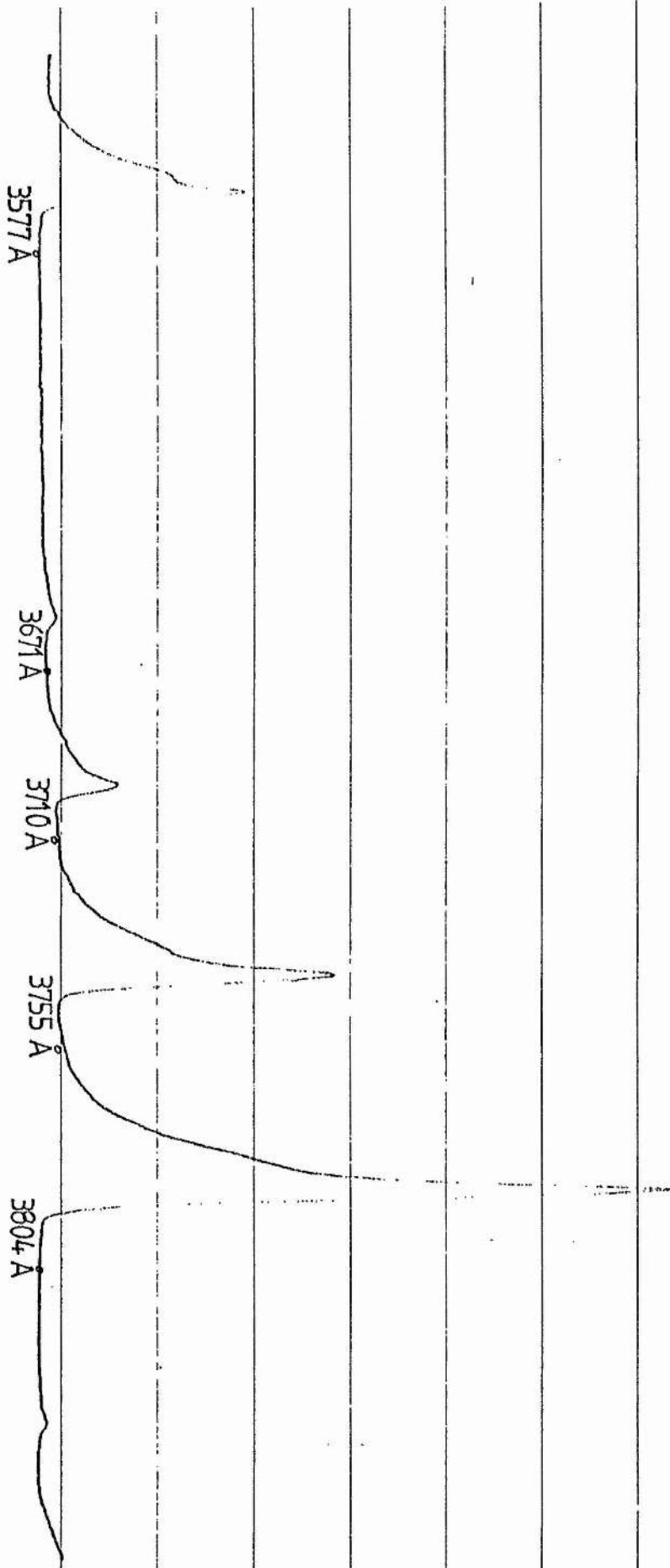


Fig 4-14 Microwave Excited Emission Spectrum of N<sub>2</sub>

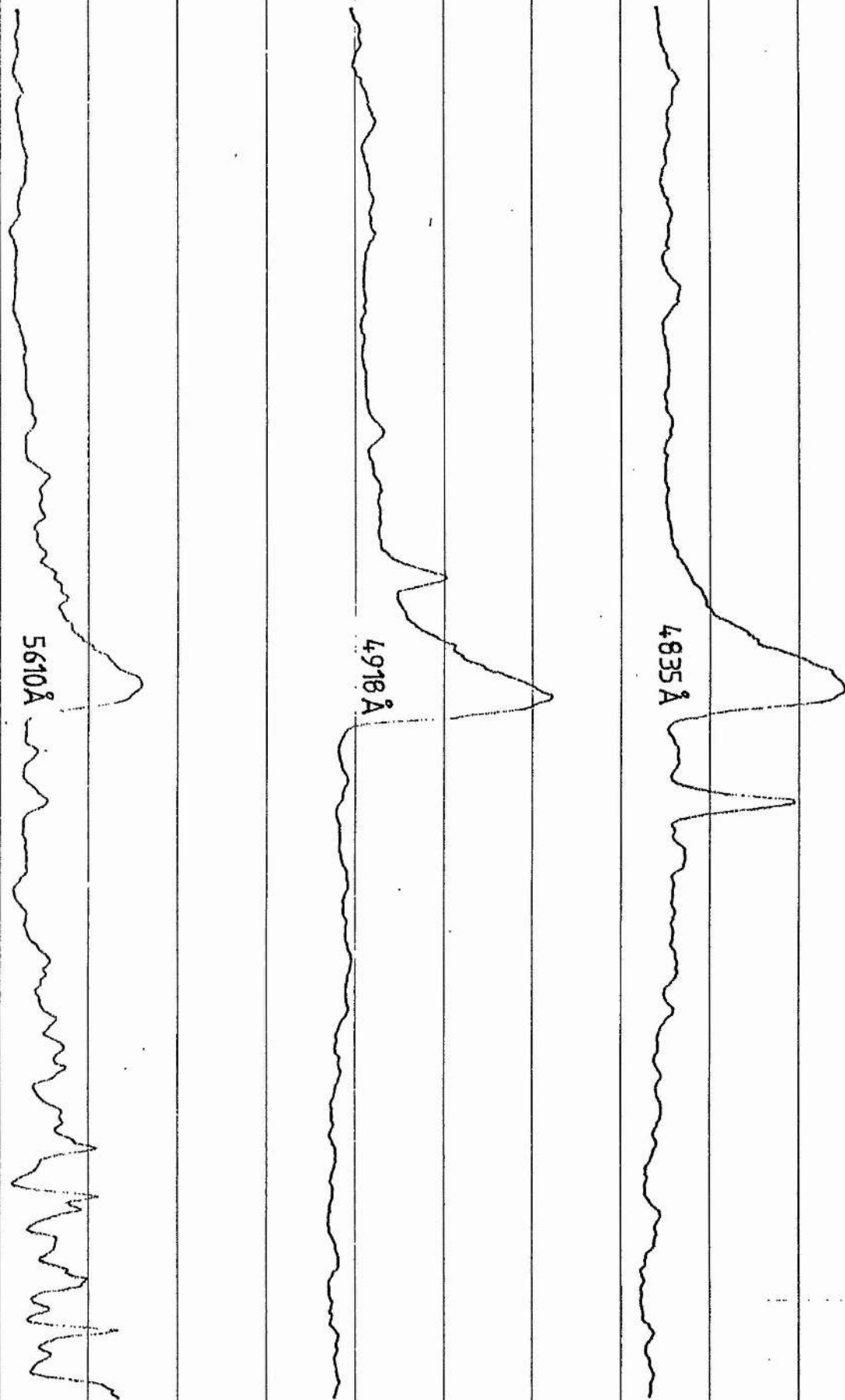


Fig 4-15 Microwave Excited Emission Spectrum of CO



Fig 4-16 Microwave Excited Emission Spectrum of C<sub>2</sub>

Fig 4-17 Ratios of Intensities of Spectral Lines for the First Batch of TR Cells for Varying Input Power Levels

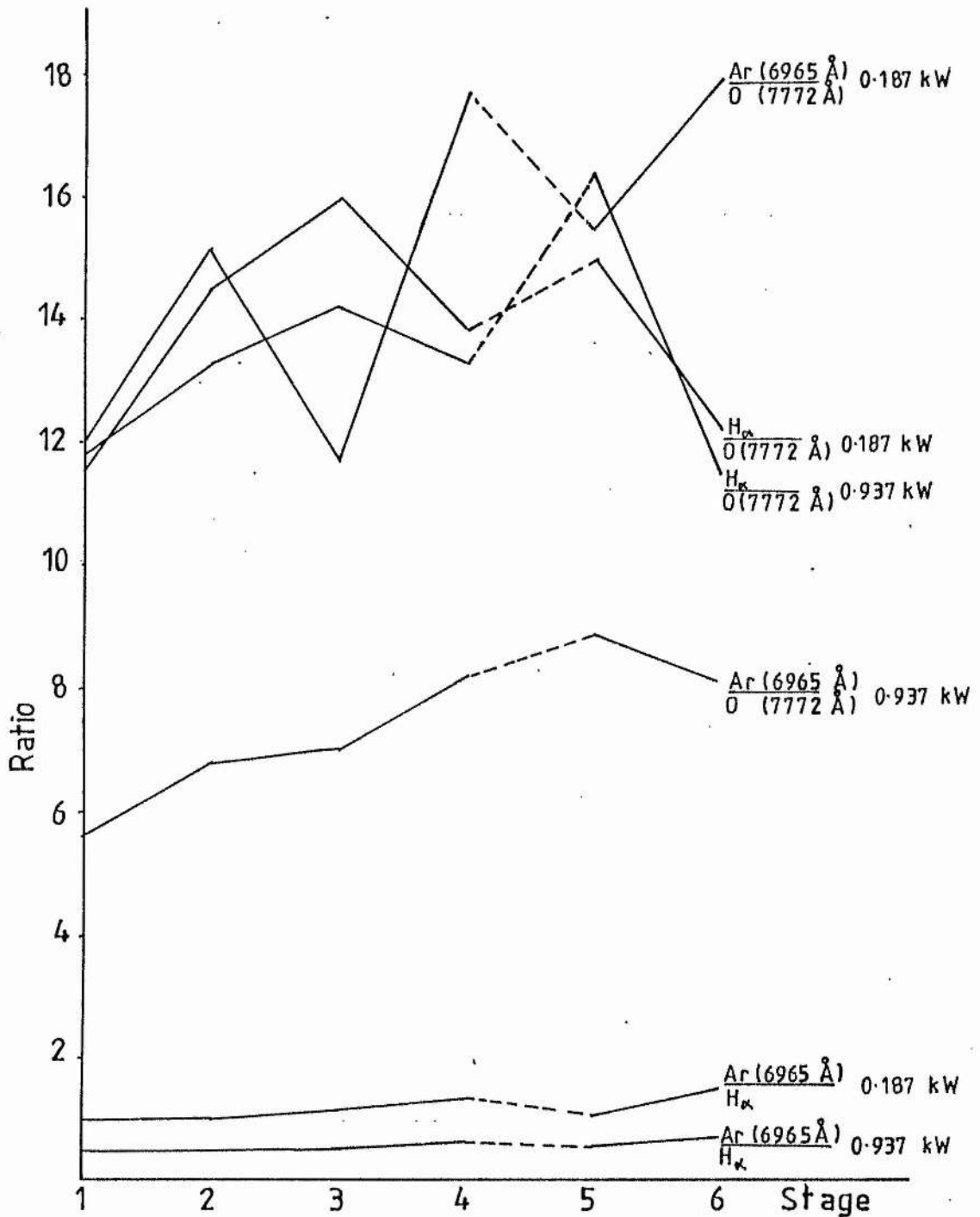
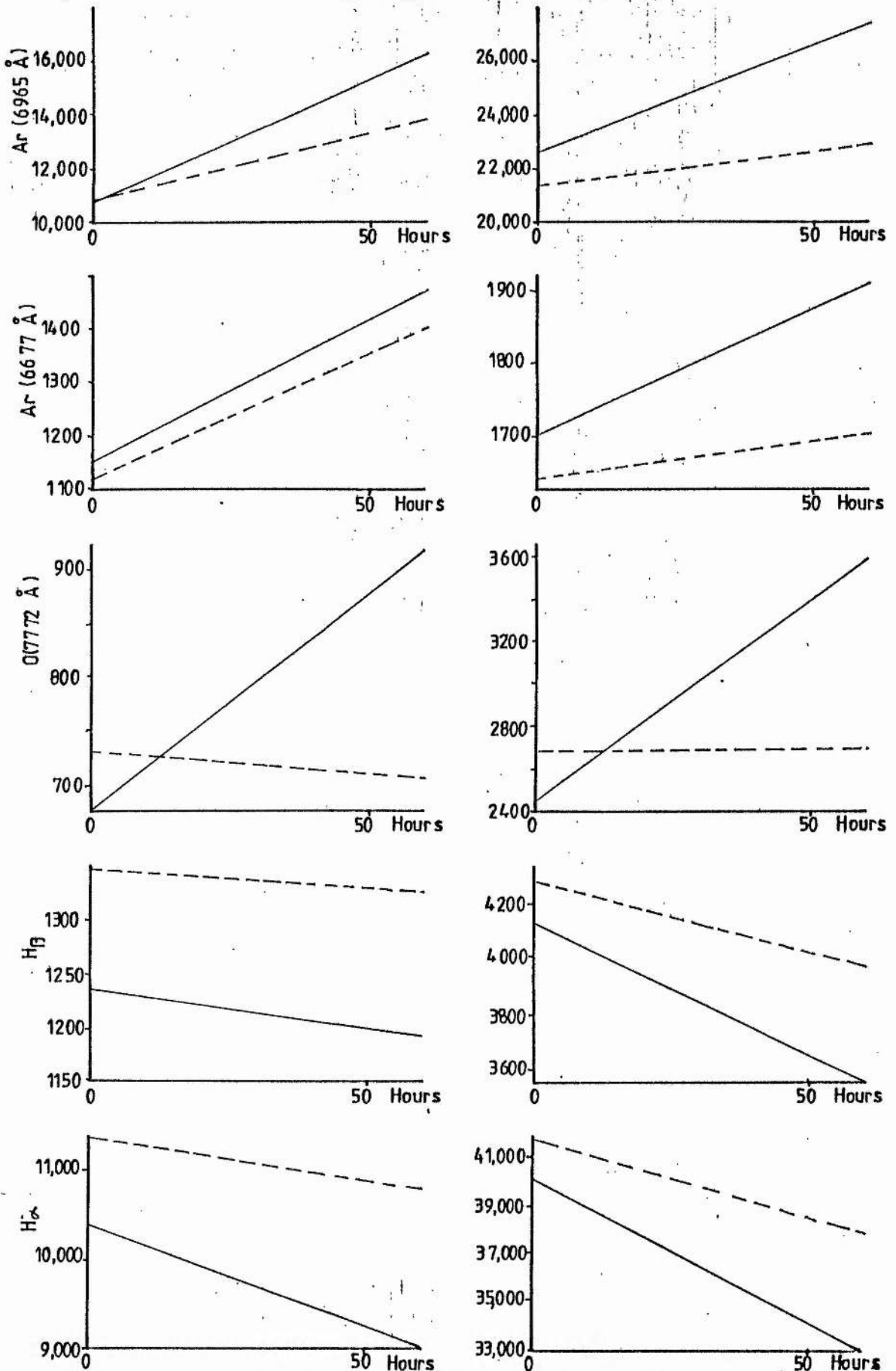
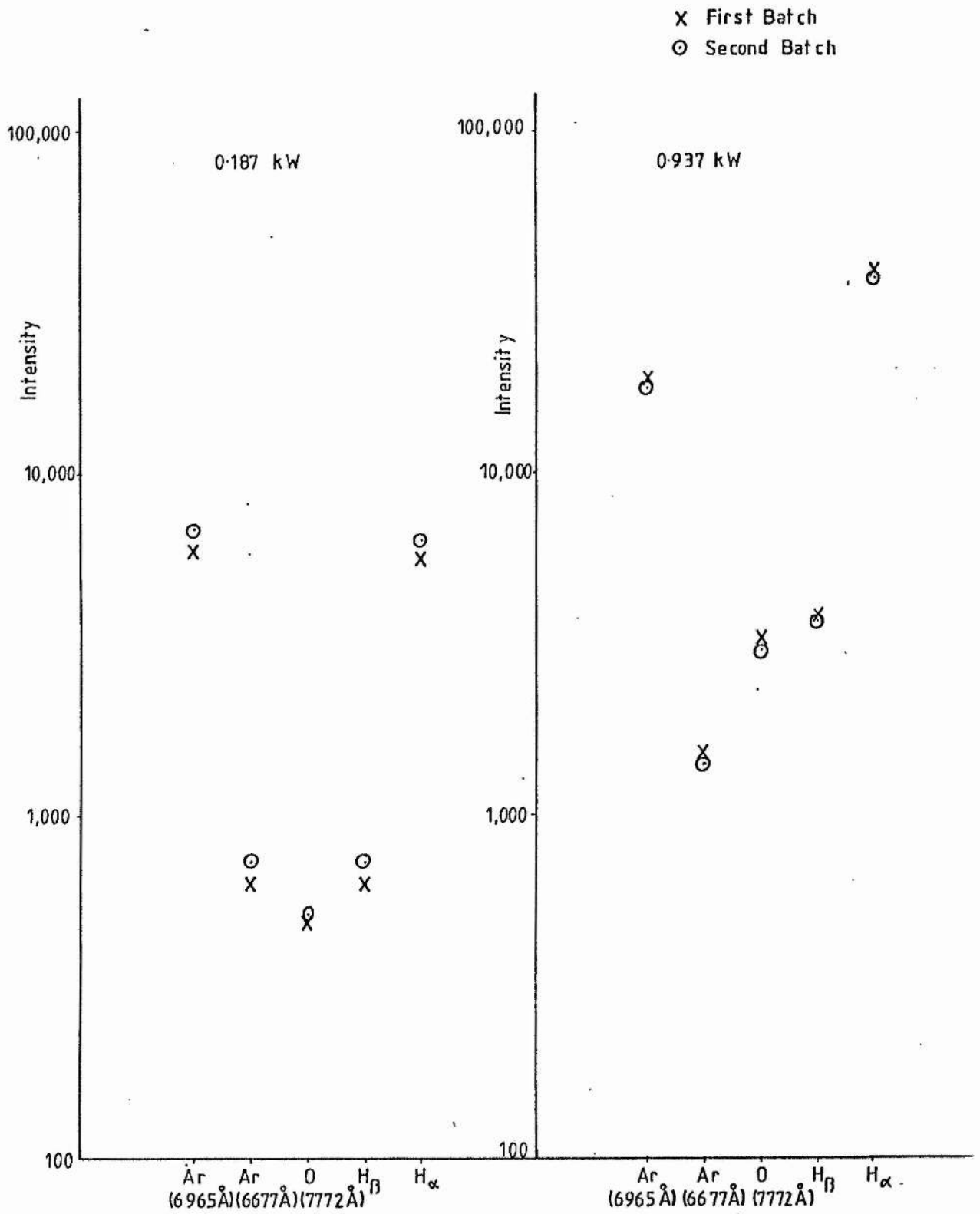


Fig 4-18 Intensity Variation of the Spectral Lines Throughout Life First Batch of Cells



— Cells with Keep-Alive Discharge Operational  
 - - - Cells without Keep-Alive Discharge

Fig 4-19 Comparison of the Intensities of the Spectral Lines for the First and Second Batches of Cells Hot Exhaust Stage



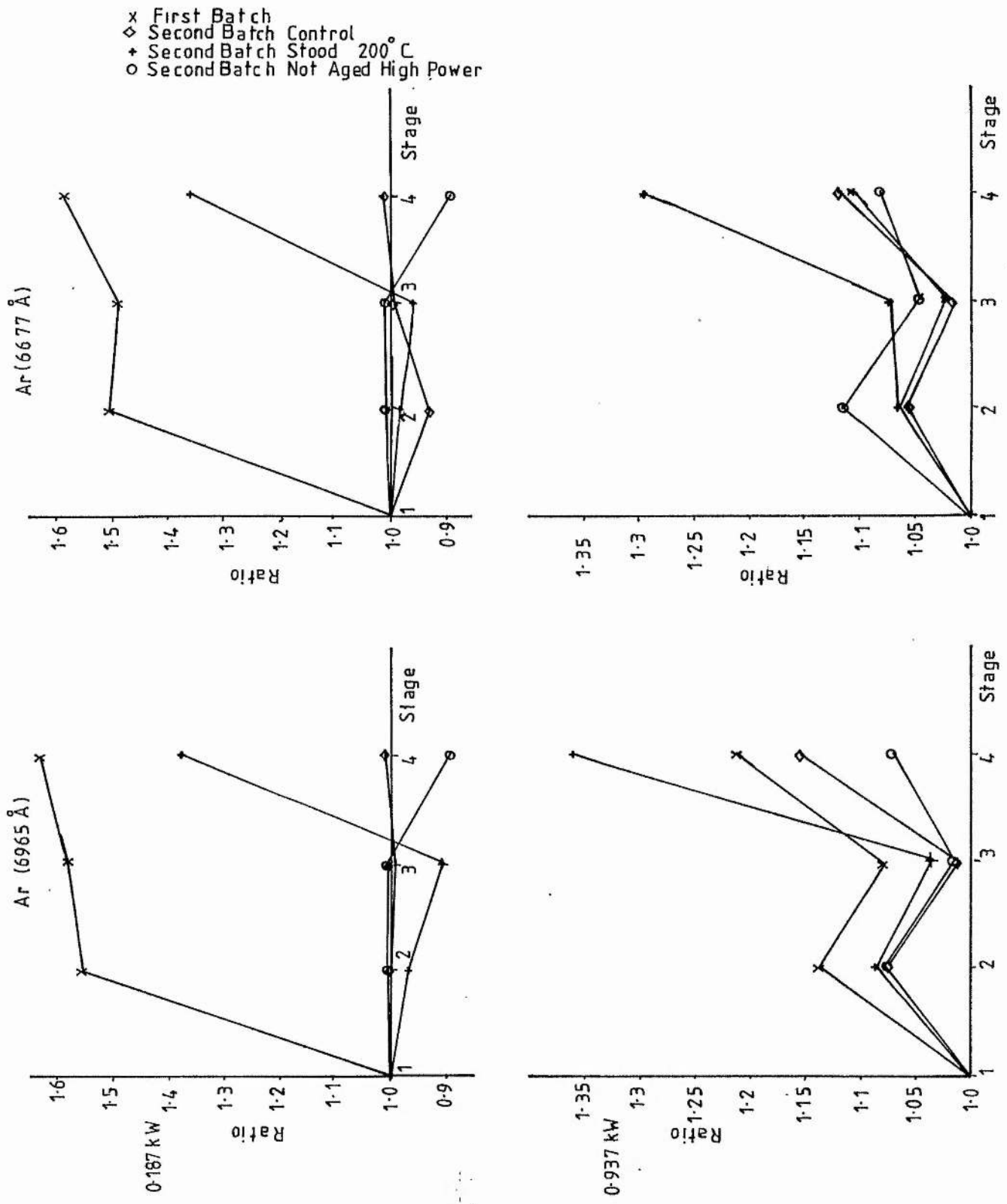


Fig 4-20 Ratio of Intensity of Spectral Lines at each Stage During Manufacture to Intensity at First Stage First and Second Batches of Cells

- x First Batch
- ◇ Second Batch Control
- + Second Batch Stood 200 °C
- Second Batch Not Aged High Power

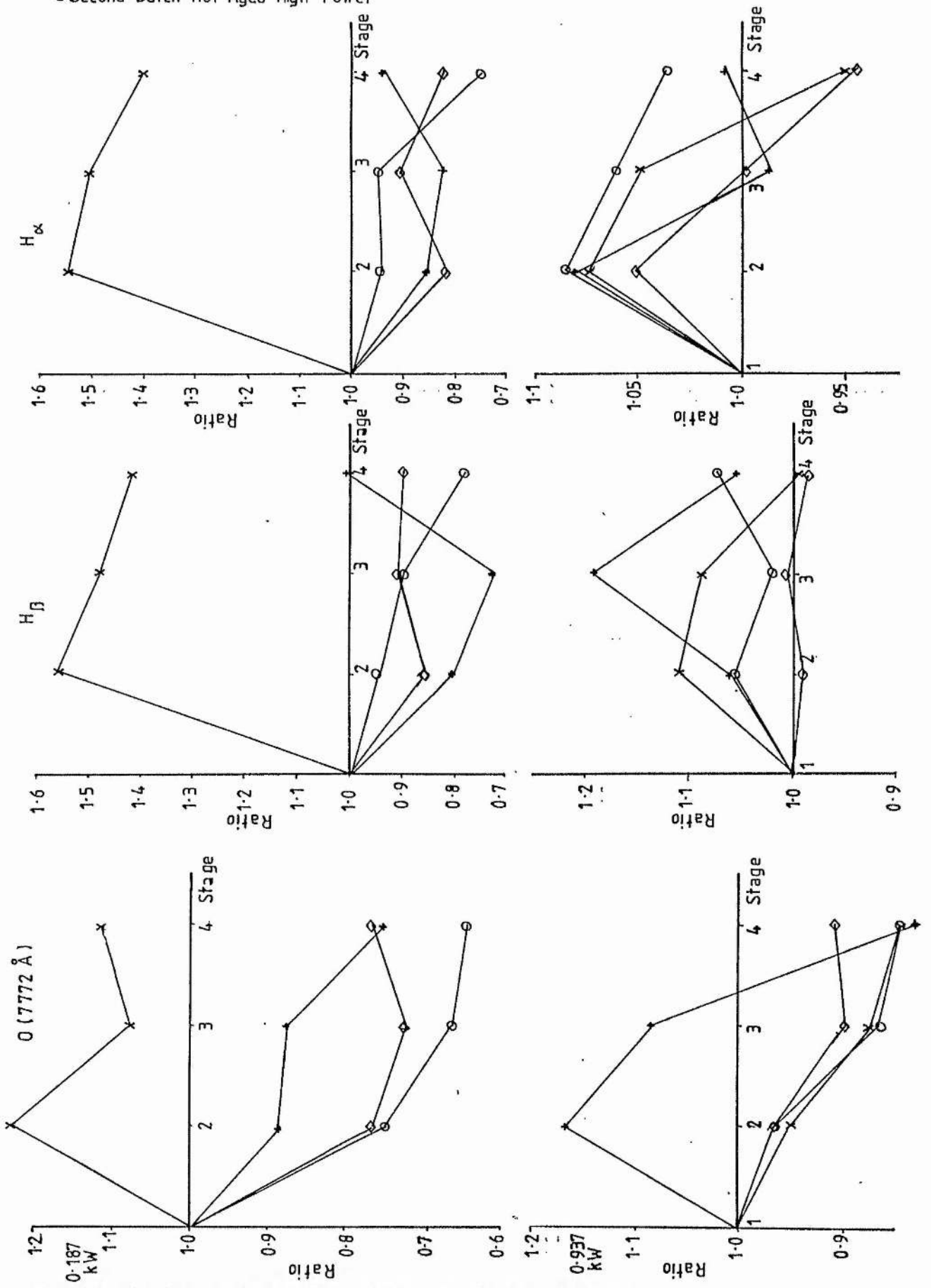


Fig 4-21 Ratio of Intensity of Spectral Lines at each Stage During Manufacture to Intensity at First Stage First and Second Batches of Cells

x First Batch  
 ◇ Second Batch Control  
 + Second Batch Stood 200°C  
 ○ Second Batch Not Aged High Power

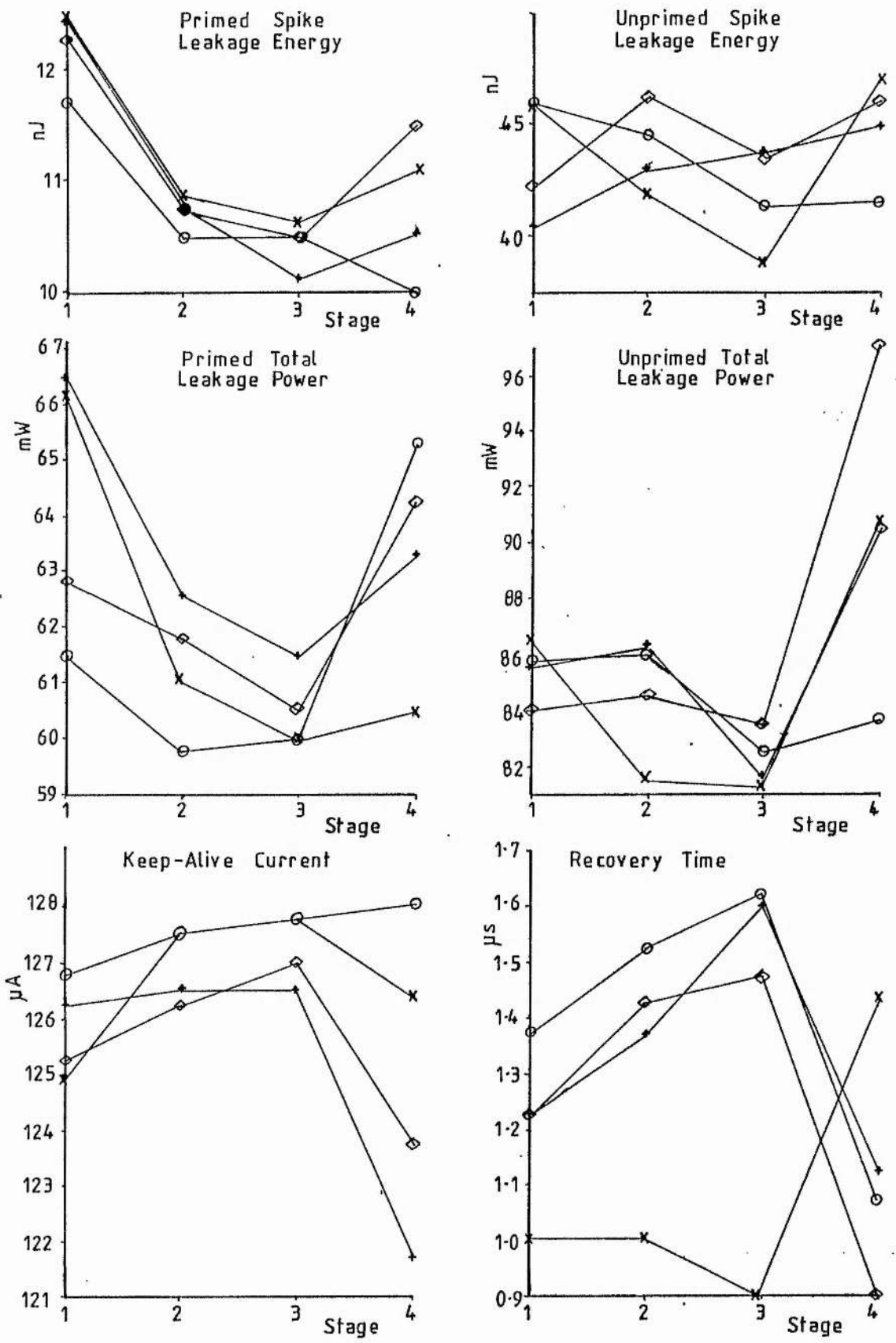


Fig 422 Microwave Measurements During Manufacture First and Second Batches of Cells

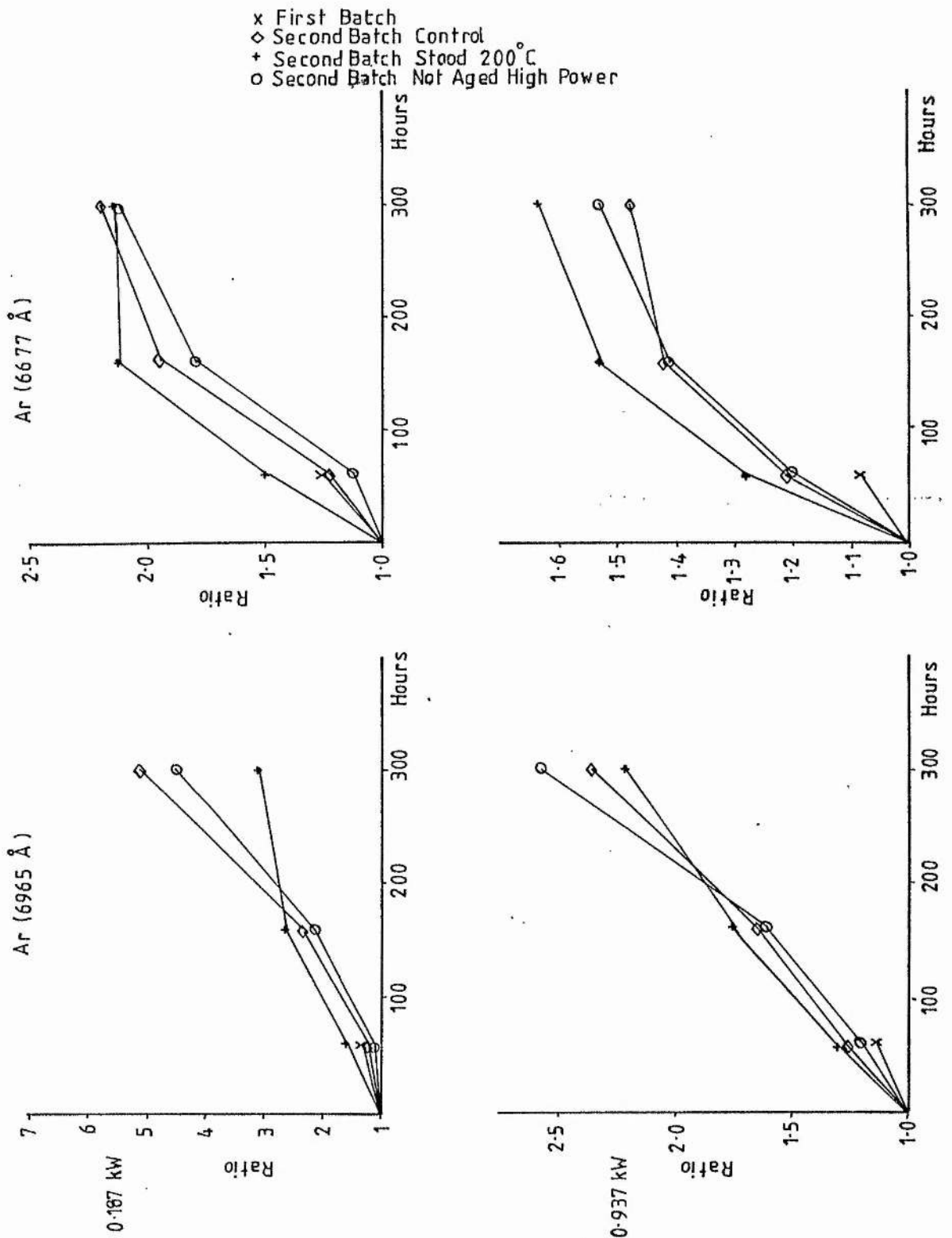


Fig 4-23 Ratio of Intensity of Spectral Lines at each Stage Throughout Life to Intensity at 0 Hours First and Second Batches of Cells

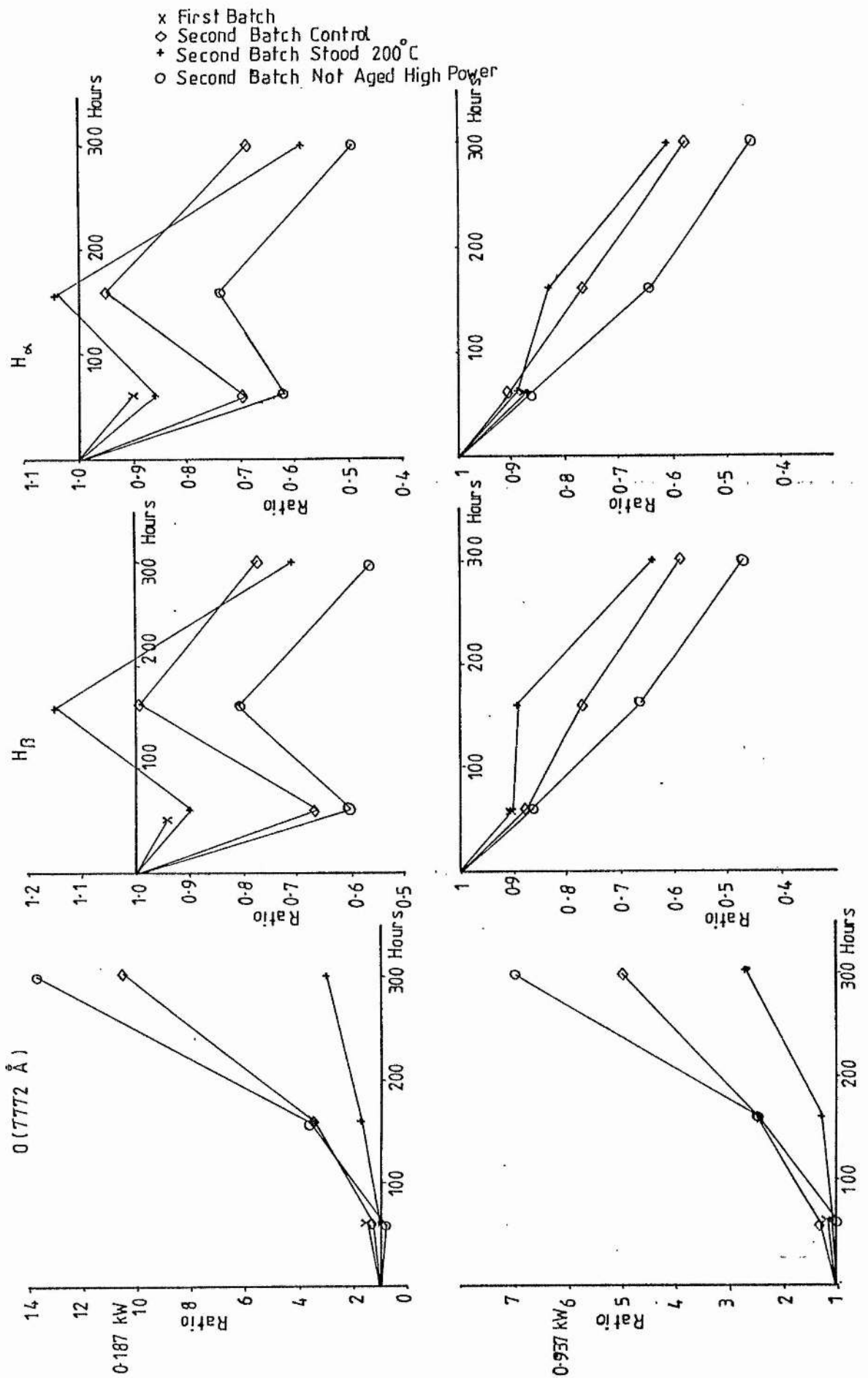


Fig 424 Ratio of Intensity of Spectral Lines at each Stage Throughout Life to Intensity at 0 Hours First and Second Batches of Cells

x First Batch  
 ◇ Second Batch Control  
 + Second Batch Stood 200°C  
 ○ Second Batch Not Aged High Power

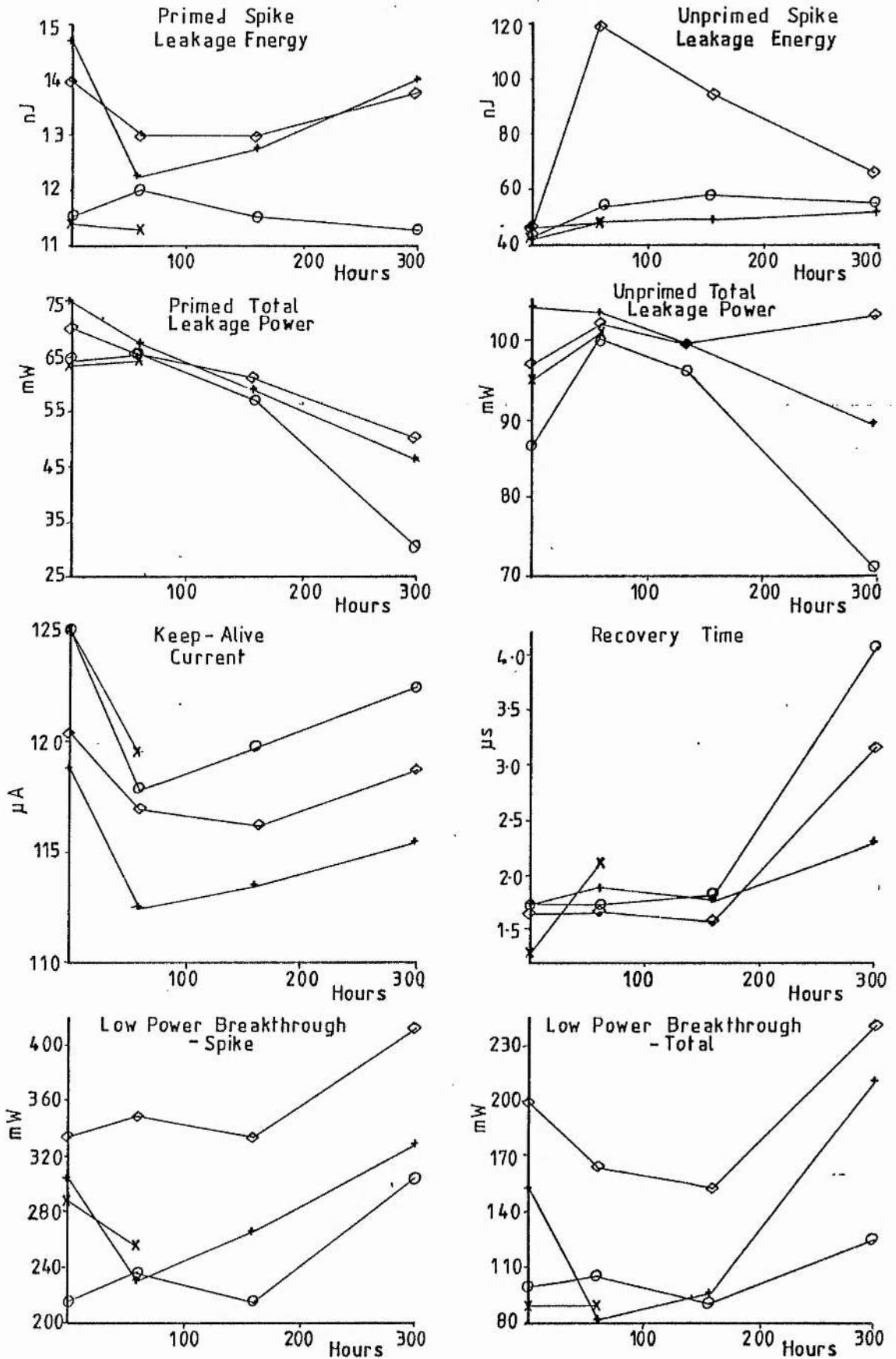


Fig 4-25 Microwave Measurements Throughout Life First and Second Batches of Cells

- x First Batch
- ◇ Second Batch Control
- + Second Batch Stood 200°C
- Second Batch Not Aged High Power

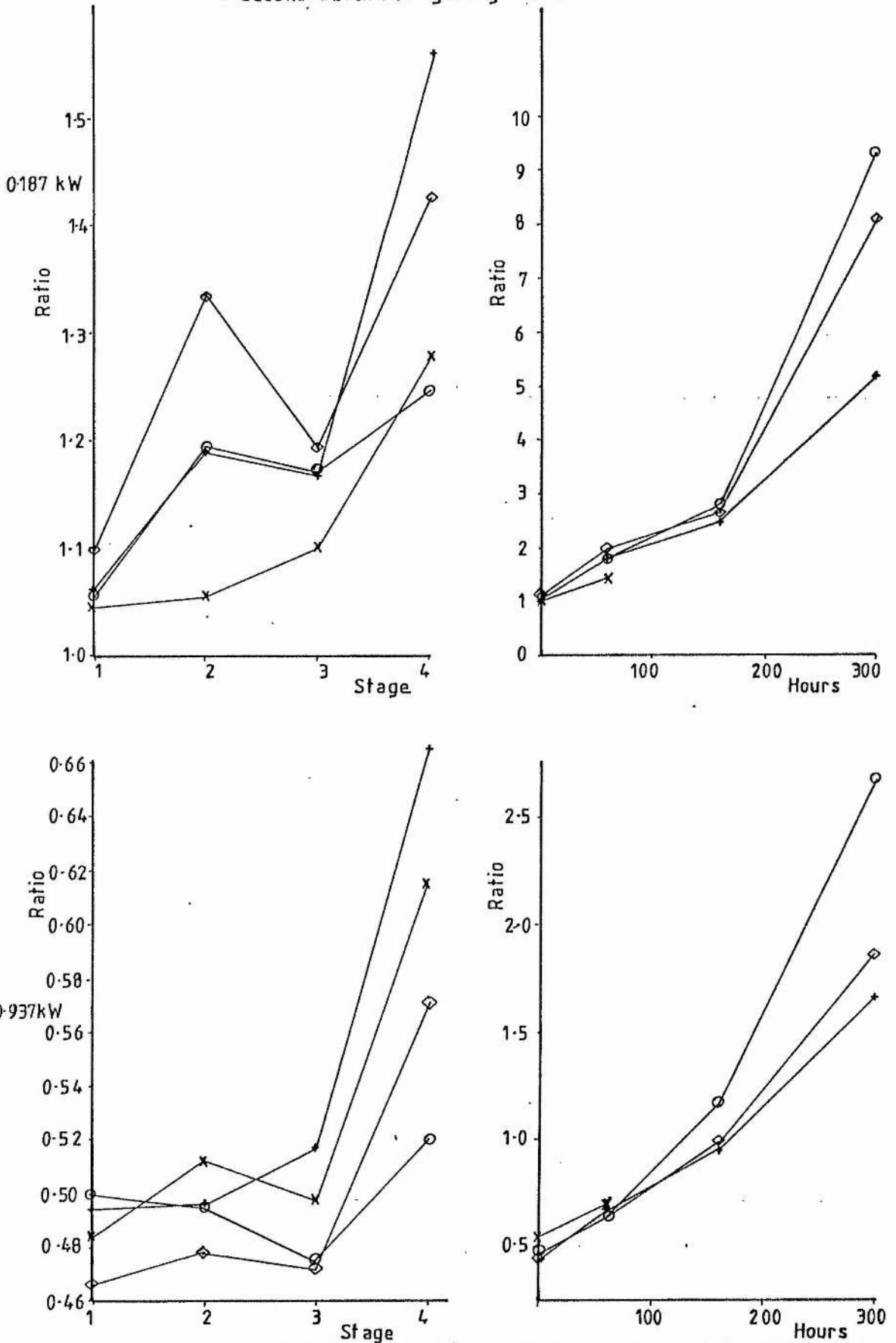


Fig 4.26 Ratio of the Intensity of the Ar Spectral Line at 6965 Å to the H<sub>α</sub> Line During Manufacture and Life First and Second Batches of Cells

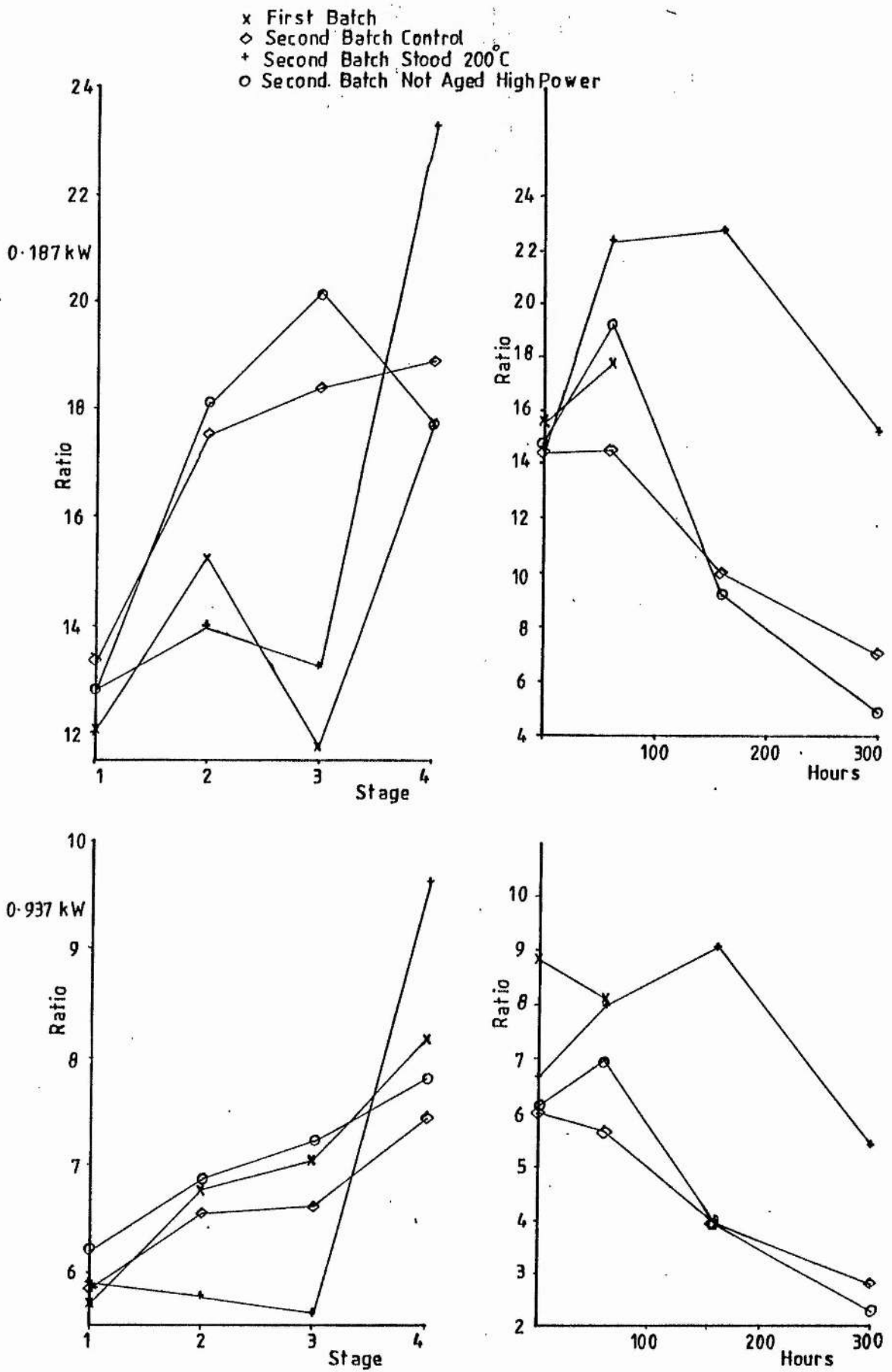


Fig 4-27 Ratio of the Intensity of the Ar Spectral Line at 6965 Å to the O Line at 7772 Å During Manufacture and Life First and Second Batches of Cells

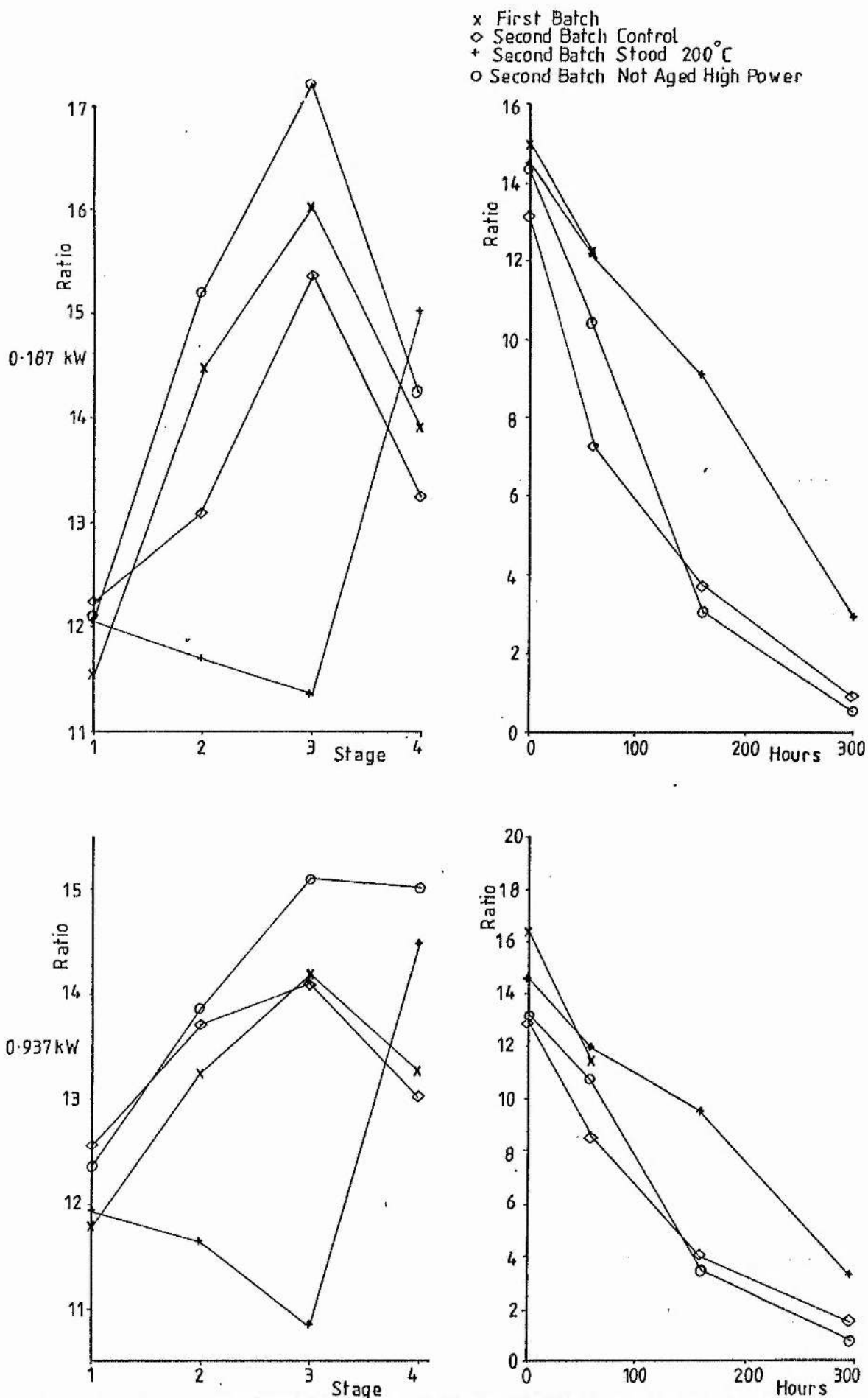


Fig 4-28 Ratio of the Intensity of the  $H_{\alpha}$  Spectral Line to the O Line at  $7772 \text{ \AA}$  During Manufacture and Life First and Second Batches of Cells

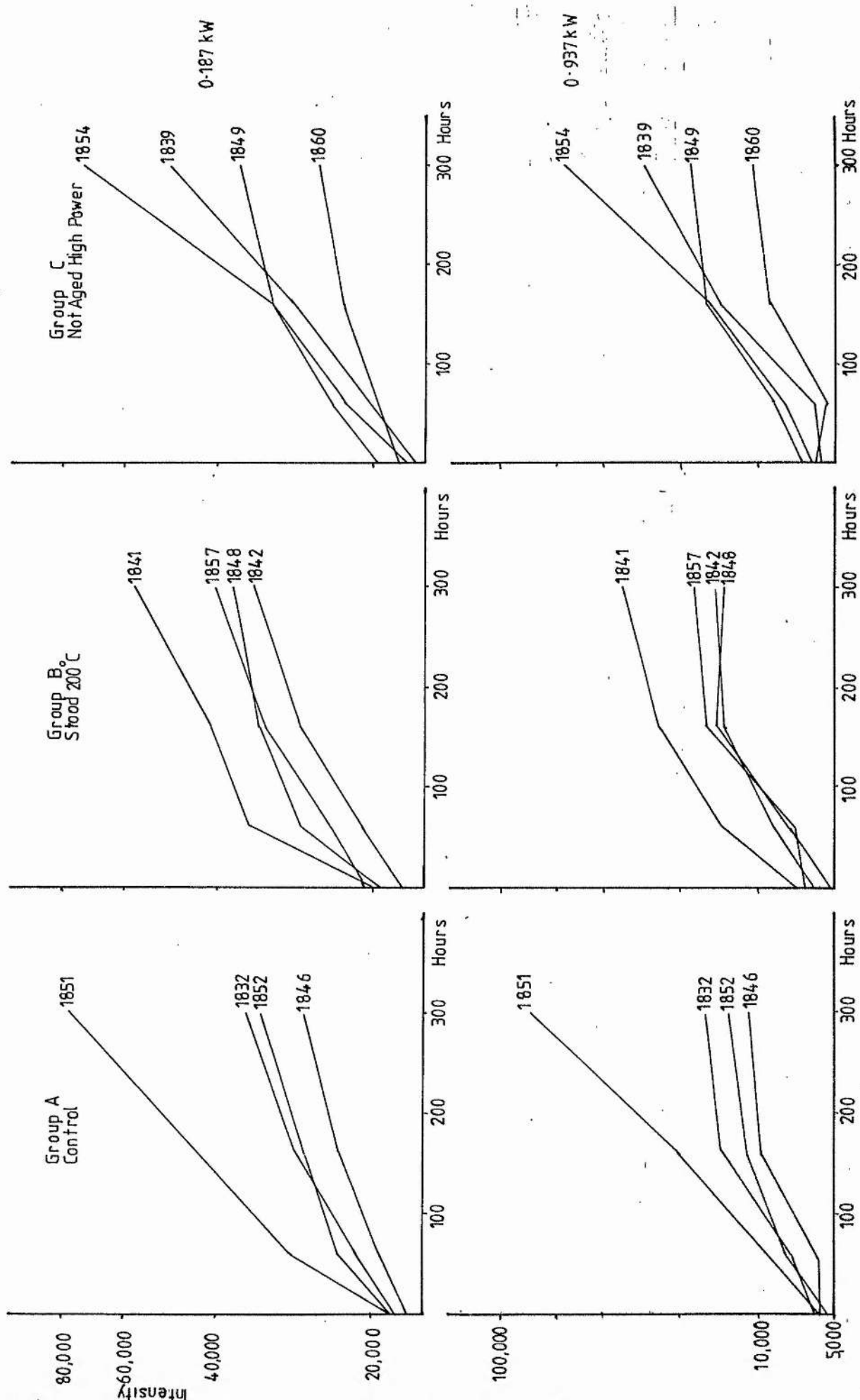


Fig 4-29 Intensity of the Ar Spectral Line at 6965 Å against Life Time Individual Cells of Second Batch

Fig 4.30 Intensity of the O Spectral Line at 7772 Å against Life Time Individual Cells of Second Batch

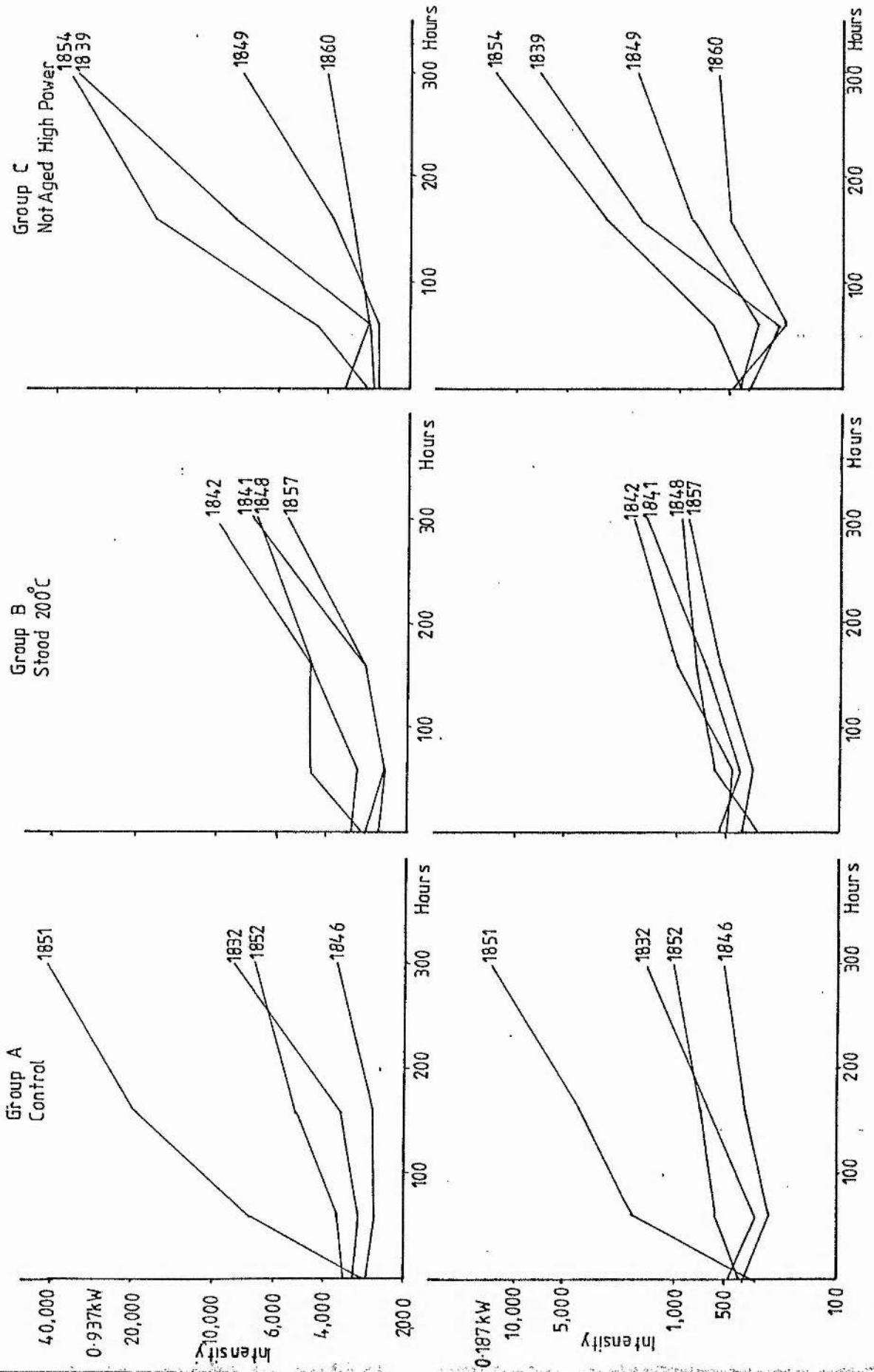


Fig 4-31 Intensity of the  $H_{\alpha}$  Spectral Line against Life Time  
Individual Cells of Second Batch

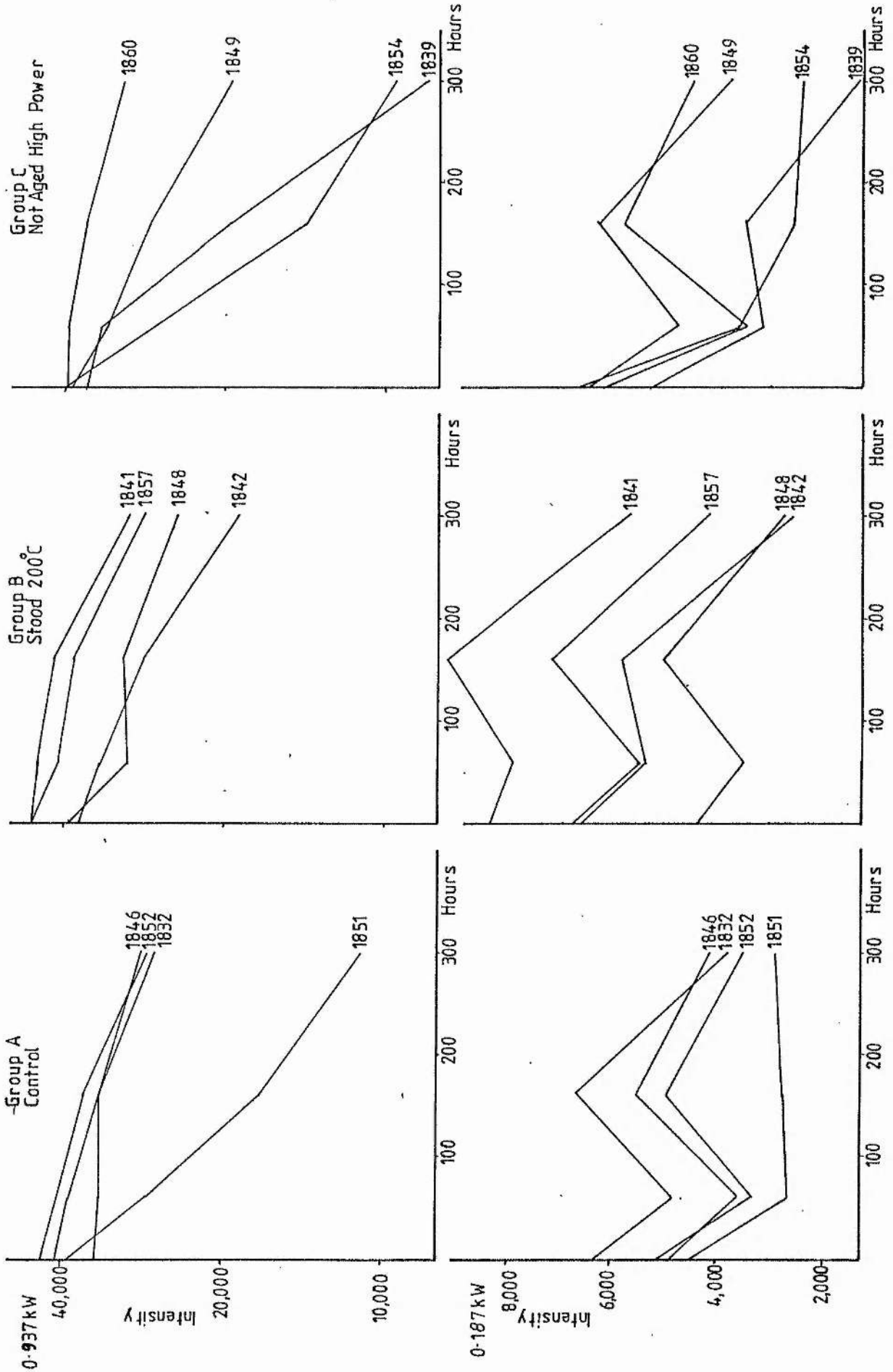
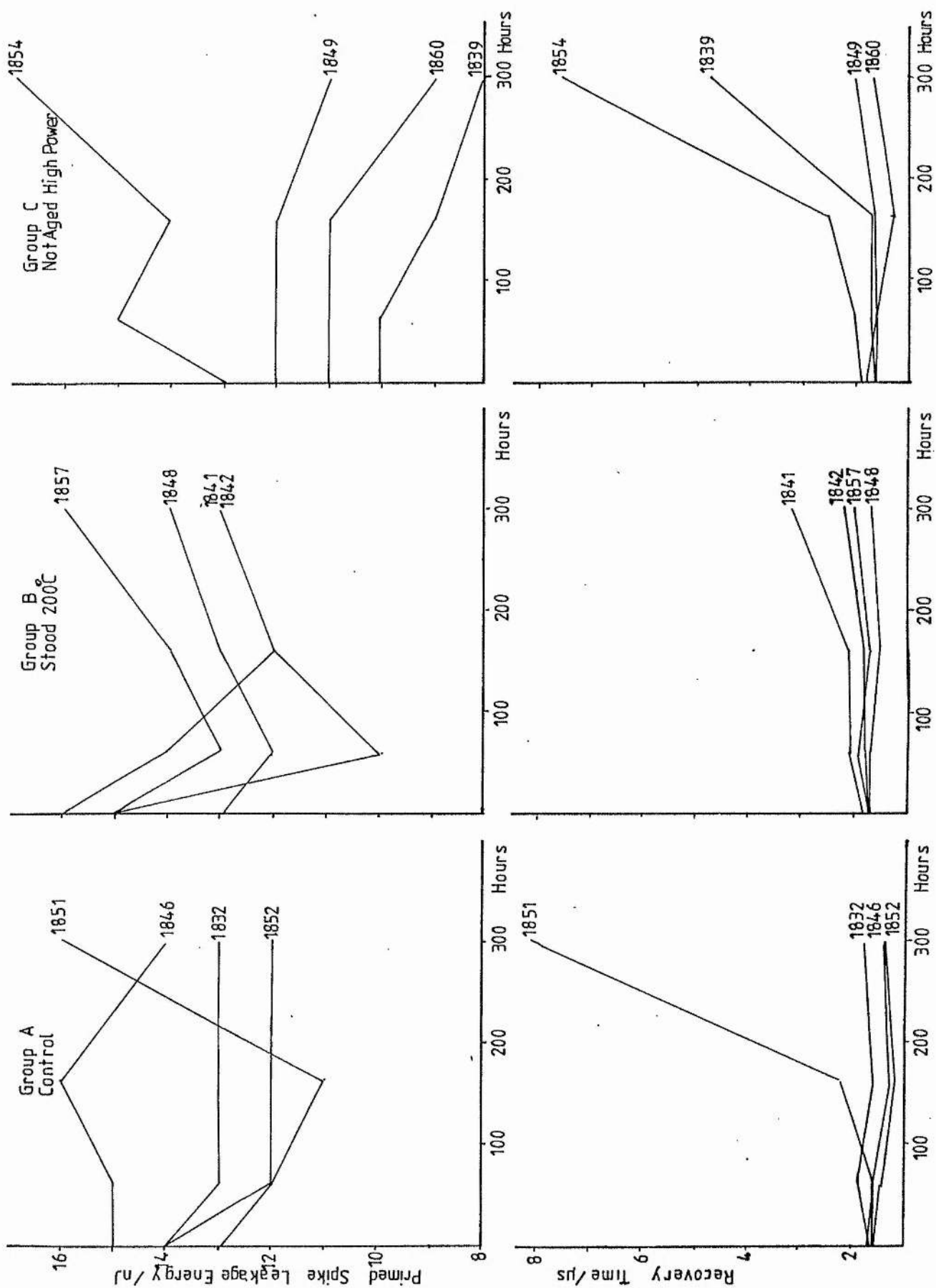


Fig 4-32 Primed Spike Leakage Energy and Recovery Time against Life Time  
Individual Cells of Second Batch



## Chapter 5 Mass Spectrometric Analysis of the Gas in the TR Cell

### 5.1 Introduction

Examination by mass spectrometry of a gaseous system can give information on the types and partial pressures of the gases in it, through analysis of a sample of the gas removed from it. In this chapter are described the results of a series of experiments conducted on the TR cell. Measurements are made of the microwave-excited emission spectra of several TR cells, at several stages throughout their life. microwave measurements are made on the cells at the same stages and finally the gas in the cells is analysed using a quadrupole mass spectrometer. The aim of this chapter is to provide more evidence for the ideas produced in Chapter 4 on the likely processes occurring throughout the life of the TR cell.

### 5.2 Quadrupole Mass Spectrometer

The quadrupole mass spectrometer was developed by Paul and Steinwedel (1953). In this instrument. ions are injected along the axis of a quadrupole electric field. produced between four parallel rods of hyperbolic section when a rf and a superimposed dc voltage are applied. This system acts as a mass filter. Only ions within a certain mass range perform oscillations of constant amplitude and are collected at the far end of the filter. All ions outside this range perform oscillations of increasing amplitude, collide with

the metal rods and fail to reach the collector.

The gas to be ionized is introduced to the ionizer at low pressure, less than  $10^{-4}$  torr, since the ions must travel some considerable distance without collision. A small percentage of the gas is ionized by electron bombardment and the ions formed are accelerated and focussed into the quadrupole section. The quadrupole assembly comprises four stainless steel rods, held in the four corners of a square array of ceramic insulators. Opposite pairs of rods are electrically connected, with the phase and sign of the voltages opposite for the two pairs of rods. The rf and superimposed dc voltages are applied to the rods. The potential  $\phi$  of the electrostatic field created is

$$\phi = (V_1 + V_2 \cos wt)(x^2 - y^2)/r_0^2, \quad (5.1)$$

where  $V_1$  is the dc voltage and  $V_2$  is the rf voltage of frequency  $w/2\pi$  and  $r_0$  is the distance between the centre of the array and a rod. The force on a singly charged ion is

$$m\ddot{x} = -e \partial\phi/\partial x = -e(V_1 + V_2 \cos wt) 2x/r_0^2 \quad (5.2)$$

$$m\ddot{y} = -e \partial\phi/\partial y = +e(V_1 + V_2 \cos wt) 2y/r_0^2 \quad (5.3)$$

$$m\ddot{z} = -e \partial\phi/\partial z = 0 \quad (5.4)$$

Equations (5.2) and (5.3) are of a type known as Mathieu's differential equations and describe the oscillations of an ion under the influence of a periodic force. From equation (5.4) we see that the axial velocity of ion is its value at the entrance to the quadrupole filter; this velocity is constant and independent of the voltages applied to the rods of the filter. The ions with a given range of  $m/e$ , determined by the values of the rf and dc voltages applied to the rods of the quadrupole, pass through the

quadrupole and are collected by the ion detector. Varying the ratio of the rf voltage to the dc voltage, increases or decreases the range of values over which Mathieu's equations are stable and the ion trajectory is stable. If the ratio of  $V_1/V_2$  remains constant at approximately 0.168, the range of m/e ratios producing ions with stable trajectories is small. Ions outside this range have trajectories which result in collisions with the rods. In scanning a mass spectrum the values of  $V_1$  and  $V_2$  are varied, keeping the ratio  $V_1/V_2$  constant. The mass of the ions which reach the detector is

$$m = 0.136V_2/(r_0^2 \times f^2) \quad . \quad (5.5)$$

where  $V_2$  is in volts,  $r_0$  in cm and  $f$  in MHz. Cylindrical rods of radius  $R$ , where  $R/r_0$  is equal to 1.16, produce fields nearly equivalent to hyperbolic rods and are much cheaper and easier to manufacture.

A quadrupole mass spectrum is characterised by equal peak widths. Resolution is affected by the ratio of the rf to dc voltages and the ion energy. Increasing the ion energy decreases the time spent by the ions in the quadrupole field and hence the peak separation. Decreasing the ion energy improves resolution at the expense of sensitivity.

The output of the mass spectrometer is in the form of peaks at different m/e ratios. Each gas present in the system can be identified from its unique cracking pattern, which gives the relative heights of all the peaks due to that gas. Cracking pattern reproducibility is governed by many variables such as gas

temperature and ionizing electron energy. Gas temperature is controlled by the filament power, which governs the temperature of the ionization chamber walls, so a change in the filament resistance changes the gas temperature and hence alters the degree of dissociation of the gas. Electron energy is kept constant to ensure a constant degree of ionization or dissociation of a molecule by electron impact. Cracking pattern data has been tabulated by the Mass Spectrometry Data Centre (1970) and by Cornu and Massot (1966).

The mass spectrometer used in these experiments is the Supavac, manufactured by Vacuum Generators. It has a high sensitivity and a good resolution over the mass range 1-135 amu. On most ranges, it is sensitive enough to give an oscilloscope display without the use of an electron multiplier tube. It has 10% valley resolution over the whole mass range. The ion source is an electron impact, radially symmetric source. The quadrupole rods are 125 mm long and 6.3 mm in diameter. The electron source is a tungsten filament wire, heated by passing a current of about 4 A through it. The electrons are accelerated through a potential difference of 62 V, giving the optimum electron energy for ionizing most molecules likely to be present in a vacuum system. Normally one, but sometimes two electrons are removed from the atoms/molecules through collision with an electron. The ions formed are at a -57 V potential with respect to the focus plate and are focussed to the quadrupole mass filter. The detection system is a fast-scanning positive ion Faraday plate collector with an earth shield and electron suppressor. The minimum detectable partial pressure is

$2 \times 10^{-11}$  mb.

### 5.3 Experimental Apparatus

The experimental arrangement used for sampling the gas in the TR cell is as shown in fig (5.1). The mass spectrometer pumping system comprises an air-cooled diffusion pump, backed by a rotary pump. The cold trap is filled with liquid nitrogen, to encourage the condensation of residual gases in the system and oil from the diffusion pump, thereby reducing further the system pressure. The system pressure is monitored by the ionization gauge. Gas is leaked into the mass spectrometer system via a fine needle valve and the system is sealed off using tap (1). The seals attaching the mass spectrometer head, the ionization gauge and the needle valve to the diffusion pump are of the copper gasket type, bakeable to 400 C, to ensure a good working vacuum in the system.

The TR cell is sealed off via a 'Speedivac' tap, drilled out to the diameter of a glass tube, which has been sealed to a short length of kovar pipe situated above the cone in the cell not containing the keep-alive electrode. The cell is attached to the mass spectrometer system via copper piping connecting taps (1) and (2) and sealed using a neoprene o-ring seal. Beyond tap (2) is a second pumping system. the purpose of which is to evacuate the piping between the TR cell and the mass spectrometer inlet tap, tap (1). The second system comprises a turbomolecular pump, backed by a rotary pump. The seals are of the neoprene o-ring type.

The analogue output (in volts) from the mass spectrometer control unit goes via the chart output (scanning speed 1 amu/sec) to a 5180A Hewlett-Packard waveform recorder where it is converted into digital form via a 10-bit A-D converter and displayed on a fast sampling oscilloscope. A completed scan (0-50 amu) can be transferred to a Hewlett-Packard 9826A desk top computer and stored on disc. The internal timebase of the waveform recorder required a signal output at a faster rate than the chart output of the mass spectrometer was capable of producing, so the waveform recorder was externally triggered using a PG102 Farnell pulse generator. Pulses with a period of 5  $\mu$ s, having a delay of 0.5  $\mu$ s, a width of 5  $\mu$ s and an output level of 5 V were found to trigger the waveform recorder satisfactorily and allowed storage of the mass spectrometer output.

#### 5.4 Experimental Procedure

The measurements carried out on the TR cells were of selected lines from the optical emission spectra of the microwave excited discharge at 0.187 kW and 0.937 kW peak power at 9.4 GHz, using a prf of 3 kHz and a pulse length of 1  $\mu$ s. Also, the spike leakage energy and total leakage power (both primed and unprimed values), the keep-alive current and the recovery time were measured. The equipment used and the procedure followed in making these measurements has been described in Chapter 4.

After having measured the emission spectrum and the microwave performance of a cell, its gas content was analysed using the mass spectrometer, by following the general procedure outlined below.

Firstly, the cold trap was filled with liquid nitrogen at least two hours before each gas analysis and the tap on the TR cell was sealed to the pumping system at A using an o-ring seal (see fig (5.1)). The system was then evacuated up to tap (1) to a pressure of typically  $4-5 \times 10^{-5}$  mb (typically 1 hour), using the turbomolecular pump backed by a rotary pump.

After about 2 hours the mass spectrometer system pressure, as measured on the ionization gauge, had reached about  $10^{-7}$  torr. The mass spectrometer filament was switched on. The system pressure increased both when the ionization gauge and the mass spectrometer filament were first switched on. due to degassing of the filaments. The system pressure was monitored until it reached a steady, low, level of less than  $2 \times 10^{-7}$  torr (about 30 minutes). Tap (1) was then opened and 3 separate scans of the residual gases in the system were stored on disc, using the  $10^{-8}$  mb scale. (No change in the system pressure was observed on opening tap (1)). Taps (1) and (2) were closed and the tap sealing the TR cell was opened fully, allowing the gas inside to occupy the total volume between taps (1) and (2) as well as the cell volume. Tap (1) was opened, allowing gas to flow through the needle valve, opened to a predetermined level, into the mass spectrometer. The mass spectrometer output (over a range 0-50 amu) was stored on disc at

regular intervals (timed using a stopclock) using the  $10^{-7}$  mb scale. along with the system pressure. Since the gas was quite quickly pumped away, the gas content of each cell was monitored for less than 30 minutes. At the end of the experiment, the remaining gas is pumped away via the turbomolecular pump when tap (2) was opened. Finally, tap (1) was closed and any gas remaining in the mass spectrometer system was pumped away via the diffusion pump.

One problem encountered in the analysis of the gas mixture in the TR cell is that the cell contains water vapour. Water vapour is always present as one of the background gases in the mass spectrometer system. but it can be removed from a system by baking it at a temperature greater than  $150^{\circ}\text{C}$ . Water vapour is introduced to the system each time a cell is analysed. It was not practical to bake the system after each gas analysis. so some water vapour remains. However, its presence may be allowed for by taking a background scan of the gas in the system before introducing the gas from the cell and subtracting the quantity of water vapour already in the system from that in the system and cell.

The tungsten filaments in the mass spectrometer and in the ionization gauge react with carbon originating from the cracking of hydrocarbons (eg from the diffusion pump oil), producing tungsten carbide,  $\text{W}_2\text{C}$ . When hot, tungsten carbide reacts with water vapour, producing large quantities of CO and  $\text{CO}_2$ . So when water vapour is allowed into the mass spectrometer, during analysis of the gas in the TR cell, CO and  $\text{CO}_2$  are produced and detected along with the gases from the TR cell. So the observed concentrations of CO and

CO<sub>2</sub> will be higher than their actual concentrations in the cell. The mass spectrometer and ionization gauge filaments are switched on at least 30 minutes before analysis takes place, to allow degassing to occur and the gases produced to be pumped away, so avoiding contamination of the gas from the TR cell.

The TR cell contains approximately 7 cm<sup>3</sup> of argon and water vapour with a total pressure of 20 torr. With the tap on the cell open and taps (1) and (2) closed, the total volume of gas is now 13.5 cm<sup>3</sup> at a pressure of 10.4 torr. The needle valve was opened to a level giving an initial pressure of about 10<sup>-6</sup> torr on the ionization gauge. But the pressure falls steadily throughout a period of 20 to 30 minutes by about 25%, because the gas is continually pumped away via the diffusion pump. Hence, it was not possible to sample the gas in the TR cell over a long period of time. So gas was sampled at regular intervals after opening the cell, timed using a stopclock.

The chart output of the mass spectrometer control unit, used for the collection of mass spectral data, operates at 1 amu/sec; so a scan over the range 0-50 amu takes almost 1 minute. Consequently, relatively few scans could be recorded before the loss of gas from a cell became significant. Scans were recorded using a 10 V maximum output scale to accurately determine the height of the argon peak at mass 40 and a 2 V scale to determine the heights of the smaller peaks to greater accuracy. The height of the peak at mass 40 was calculated for the 2 V scan assuming a linear change in peak height with time.

## 5.5 Effect of Keep-Alive Discharge on Cell Life

### 5.5.1 Introduction

A batch of 5 cells were manufactured normally, as described in Chapter 4, until the cold refill stage. The cells were then refilled as follows:

- (1) The cells were evacuated to  $7 \times 10^{-5}$  mb.
- (2) 11.5 torr water vapour was added and the cells stood for 15 minutes. The water pressure was then adjusted to 11 torr and 9 torr argon added.
- (3) After a further 15 minutes, the taps were closed to seal the cells.

Two cells, 4639 and 4641, were life tested for 384.8 hours (at 9.4 GHz, 10 kW peak power, prf 1 kHz and pulse length 1  $\mu$ s) with keep-alive discharges operational, two cells, 4622 and 4648, were life tested without keep-alive discharges operational and one cell, 4631, was simply stood throughout the period of the experiment. Microwave measurements and emission spectra measurements were carried out at intervals throughout the life of the cells. After 384.4 hours the gas in each cell was analysed in turn, using the mass spectrometer.

### 5.5.2 Results of Microwave and Emission Spectra Measurements

In figs (5.2) to (5.4) are plotted the ratios of the intensities of each spectral line at each measurement stage to its intensity at stage 1, 0 hours life. We can compare these results with those obtained earlier, and described in Chapter 4. Previously, the intensities of the argon spectral lines were found to increase throughout life; in these experiments the intensities increase initially, then decrease, and finally increase again after about 150 hours. The intensity ratio is lowest for the cells life tested with no keep-alive discharge operational. Previously, the intensity of the oxygen spectral line was observed to increase with increasing life of a cell; this trend is not observed with this batch of cells when measured at 0.187 kW, where the intensity increases initially, then decreases. Here, using 0.937 kW, the intensity increases, after an initial decrease. Previously, the hydrogen spectral lines decreased in intensity, after an increase at 100 hours, when measured at the lower power level. This trend is not observed here, where the intensity of the hydrogen lines increases initially, then starts to decrease after about 250 hours. On average, the cell which stood for the period of the experiment showed the smallest change in the intensities of the spectral lines.

The microwave measurements, plotted in fig (5.5), follow the trend of the previous results, with the exception of the keep-alive current, which steadily decreased for all the cells of the present batch. The cell stood throughout the period of the experiment gave unexpectedly high readings for all the measurements, except keep-alive current, which was unexpectedly low.

Emission bands of nitrogen (as shown in figs (4.12) to (4.14)) were observed in the microwave excited discharge in cell 4631, the cell stood for the period of the experiment, indicating that either the cell leaked slightly, or that some air had been trapped in it during refilling. The primed spike leakage energy and total leakage power of this cell increased steadily throughout the experiment, indicating a decreasing ability of the gas to break down quickly and a decreasing efficiency of the discharge. A likely cause is the presence of an electron attaching gas, such as nitrogen or oxygen from air. A trace of CO (as shown in fig (4.15)) was observed in the emission spectrum of cell 4639, one of the cells life tested with the keep-alive discharge operational. Larger quantities of CO were observed in cells 4648 and 4622, cells with no keep-alive discharge operational. No CO was observed in the emission spectrum of the other two cells. Cell 4641, with a keep-alive discharge operational, had consistently the lowest values of spike leakage energy and total leakage power, both primed and unprimed values. Both cells in which no CO was observed, 4631 and 4641, gave consistently higher values for the intensities of the argon spectral lines. The unexpected results of the microwave

measurements made on cell 4631 are therefore likely to be due to the presence of a small quantity of air. Normally, cells are sealed off by sealing the glass tube through which they are filled. Here, however, a tap is sealed to the glass tube, using a neoprene o-ring seal, and closing the tap seals the cell. This arrangement does not provide such an excellent seal. especially over the time period of the experiment of nearly 400 hours. The leakage of a TR cell is greater if a cell contains CO; CO apparently inhibits the breakdown of the gas in the cell. Recovery time is unaffected by the presence of CO; it depends mainly on the amount of water vapour present. So the presence of CO and nitrogen has almost certainly caused the difference between the results obtained here and those obtained previously.

The larger intensities of the argon spectral lines and smaller intensities of the hydrogen lines and the larger ratio of the spectral lines of argon ( $6965 \text{ \AA}$ ) to  $H_{\alpha}$  for the cells with the keep-alive discharge operational show that these cells lose more water than the cells life tested with no keep-alive discharge operational, through dissociation of water at the keep-alive electrode. The spike leakage energy and total leakage power are lower for the cells with the keep-alive discharge operational; this is a likely result of their containing a trace of CO. Recovery times for the cells life tested with and without a keep-alive discharge operational are not significantly different over the period of the experiment.

### 5.5.3 Mass Spectra Results

The TR cells were all filled to the same pressure of gas, and contained equal volumes of gas. However, on opening the cells under identical conditions, the initial total pressure of gas in each cell as measured by the ionization gauge was as listed in Table 5.1.

Table 5.1

Cell	Keep-Alive Discharge	Pressure/torr
4631	NO	$1.9 \times 10^{-6}$
4622	NO	$2.1 \times 10^{-6}$
4648	NO	$2.0 \times 10^{-6}$
4641	YES	$1.6 \times 10^{-6}$
4639	YES	$1.7 \times 10^{-6}$

So, assuming equal detection rates of the gases in the cells, the cells with the keep-alive discharge operational contained a lower total pressure of gas. The pressure difference between the cells with and without a keep-alive discharge operational is between 15% and 25%. Cleanup of the gas in a TR cell with a keep-alive discharge operational occurs through sputtering at the keep-alive electrode. The sputtered metal is deposited on the walls of the cell, burying gas molecules. So the cells with the keep-alive discharge operational are likely to contain a lower overall pressure of gas.

The typical sensitivity of an ionization gauge to various gases is as follows:

H <sub>2</sub>	N <sub>2</sub>	CO	CO <sub>2</sub>	H <sub>2</sub> O	Ar
0.46	1.0	1.04	1.45	1.18	1.22

A greater degree of dissociation of water vapour into products such as hydrogen and oxygen occurs for the cells with the keep-alive discharge operational. For equal partial pressures of water vapour and hydrogen, the gauge detects a greater partial pressure of water vapour. So the cells containing more hydrogen and oxygen and less water vapour apparently register a lower overall pressure. Also, the cells with no keep-alive discharge operational contain more CO, which increases their total pressure.

The mass spectrometric analysis of the gas in each cell was carried out as described above. The mean background scan for each cell is tabulated in Table 5.2. The background scan is subtracted from each scan and the partial pressures of each gas in the cell calculated with the aid of a computer program. The computer program was originally written by T Govindanunny (private communication) and adapted for the present gas system. The computer program is listed in Appendix 5. In the computer program a series of simultaneous equations is solved, one for each gas present, using the tabulated cracking pattern data for the gases and the heights of the peaks at each mass in the range scanned. Negative partial pressures of gases as calculated in the computer program are neglected as having no physical meaning. The quantities of gas involved are usually very small, less than 1%.

In figs (5.6) to (5.8) are plotted the amounts of each gas present, calculated as a fraction of the amount of argon present. From the graphs it can be seen that the cells with the keep-alive discharge operational contained less hydrogen, CO, CO<sub>2</sub> and CH<sub>4</sub>. The amount of nitrogen present in a cell depended on its individual leak rate; nitrogen was observed in all cells. however. In fig (5.9) is shown the variation in intensity of argon and water vapour for each cell throughout the period of the experiment. The partial pressure of argon detected decreases with time and that of water vapour increases, due partly to their different flow rates from the TR cell and partly to differences in detection rates for the gases.

#### 5.5.4 Conclusions

The results for this batch of cells indicate that the keep-alive discharge causes dissociation of water vapour in addition to that caused during the microwave discharge, reducing the partial pressure of water vapour still further. The results from this batch of cells have been influenced by nitrogen leaking into the cells throughout the period of the experiment. The pressure of nitrogen present in each cell is estimated to be at most a few percent of the argon total pressure in all but the cell stood throughout the period of the experiment; it contained a substantially higher percentage. Emission bands of nitrogen were observed in the microwave excited discharge in the cell stood throughout the period of the experiment but not for any of the other cells. Trace amounts of CO were also observed in the discharges of some of the cells in this batch; CO was not seen in

any cell in previous experiments.

## 5.6 Cells Tested at Intervals Throughout Life

### 5.6.1 Introduction

A batch of seven cells were manufactured normally, as described in Chapter 4, until the cold refill stage. The cells were then refilled as follows:

- (1) The cells were evacuated to  $7 \times 10^{-5}$  torr.
- (2) 12 torr of water vapour was added, and after 10 minutes water vapour was added to give a total pressure of 9.5 torr. 10.5 torr of argon was added.
- (3) After 15 minutes, the cells were sealed off, 6 by closing the taps attached to the glass tubes and 1 cell- 4644 by sealing the glass tube.

Six cells were put on life test at an operating power level typical for the device (9.4 GHz, 10 kW peak power, 1 kHz prf and pulse length  $1 \mu s$ ) without a keep-alive discharge operational. Cell 4644 was stood throughout the period of the experiment, as a control. At intervals throughout the life of the cells, measurements are made on the emission spectra of the cells and of their microwave performance. At each stage of measurement, the gas from one cell was analysed using the mass spectrometer. The time at which the gas in each cell was analysed is listed below.

Time/Hours	0	19.5	38.1	87.9	132.15	170.2
Cell	4628	4642	4621	4650	4653	4618

No gas analysis of cell 4642 was possible, due to an accident.

#### 5.6.2 Results of Microwave and Emission Spectra Measurements

From the graphs of the ratios of the intensities of each spectral line at each stage to the intensity at the initial stage, figs (5.10) and (5.11), we see that the intensities of the argon lines initially decrease then increase again. This trend was also observed in the results described in section 5.5. The intensity of the oxygen spectral line decreases overall throughout the period of the experiment, whereas that for the cells measured and described in section 5.5 decreased initially, then increased. At low power, the hydrogen spectral lines decrease; at high power they increase with life. The cell which had stood throughout the period of the experiment showed little change in the intensity of the spectral lines, so few changes are occurring to the gas in the cell.

The ratios of the spectral lines, the argon line at  $6965 \text{ \AA}$  to the  $H_{\alpha}$  line and to the oxygen line at  $7772 \text{ \AA}$  and the ratio of the  $H_{\alpha}$  line to the oxygen line are plotted in fig (5.12). We can compare these results with those taken previously and displayed in figs (4.26) to (4.28). Here, the ratio of the argon line to the  $H_{\alpha}$  line increases slightly over the period of the experiment for the cell stood throughout the period of the experiment, due to absorption of water vapour by the cell walls. The same ratio for the cells on life test decreases initially, then increases. Water vapour is initially released from the cell walls and then dissociated through the action of the microwave discharge. The

ratio of the argon line to the oxygen line remains fairly constant for the cell stood throughout the experiment; it first decreases then increases for the cells on life test. The initial decrease may be due to the production of oxygen from the dissociation of water vapour. The subsequent increase may be due to the reaction of the oxygen, producing oxides of nitrogen and carbon. The ratio of the  $H_{\alpha}$  line to the oxygen line remains fairly constant for the cell stood throughout the period of the experiment, indicating little dissociation of water vapour; for the cells on life test it increases fairly steadily, perhaps due to the creation of hydrogen in the microwave discharge. The oxygen produced reacts with carbon and nitrogen, giving several oxides. Traces of CO have been observed in some of the cells.

The microwave measurements made on this batch of cells and displayed in fig (5.13) show that the cell not life tested has changed little throughout the period of the experiment. The recovery time measurement is an exception; this measurement is the most inaccurate of those performed and the one most dependent on the experimental equipment used. For this batch of cells the primed spike leakage energy increases throughout life. The total leakage power increases initially, then decreases. The recovery time increases then decreases then finally increases again. The general trends shown here agree with the earlier results described in Chapter 4 (see fig (4.25)), and show the gradual loss of water vapour and increase of oxygen. The increase in spike leakage energy and total leakage power indicates an increase in the partial pressure of an attaching gas, such as water vapour, or perhaps

oxides of carbon and nitrogen, produced throughout the cell life. The subsequent decrease of the total leakage power is probably due to the loss of water vapour, which has reached a significant level by about 100 hours. The keep-alive current also starts to increase at about 100 hours, also due to the loss of water vapour (these cells have not been life tested with the keep-alive discharge operational, so no sputtering at the keep-alive electrode has occurred). The recovery time also increases after 100 hours, again showing a significant loss of water vapour.

### 5.6.3 Mass Spectra Results

Each cell was opened in turn, at intervals throughout the period of the experiment and the gas analysed in the mass spectrometer. The mean background scan for each cell is tabulated in Table 5.3. The background scan is subtracted from each scan. The results are displayed in figs (5.14) to (5.16). The partial pressure of argon is fairly constant throughout the batch of cells, indicating that it has not been absorbed by or reacted with the cell body or the gas in the cell. The partial pressure of water vapour first increases then decreases again. The initial increase is due to desorption of water vapour from the cell walls. After about 100 hours the water vapour pressure starts to decrease, through dissociation via the microwave discharge. The concentration of hydrogen steadily increases throughout life, created through the dissociation of water vapour. The quantity of CO present increases initially, then decreases again, while the quantity of oxygen decreases at first, then increases. If a cell

contains more carbon initially, oxygen can react with it, creating CO and CO<sub>2</sub>. So cells containing more oxygen contain fewer oxides of carbon. The amount of oxygen finally increases, so much having been created through the dissociation of water vapour that all the carbon present has already been oxidized. Small quantities of NO, NO<sub>2</sub> and N<sub>2</sub>O are also present in the cells, created through the oxidation of nitrogen, which has leaked into the cells.

#### 5.6.4 Conclusions

The results from the measurements show that throughout the life of a cell, water vapour is dissociated into products, such as oxygen and hydrogen, increasing their partial pressures in the cell and decreasing its own partial pressure. Water vapour absorbed in the cell walls is released, which increases the partial pressure of water vapour and helps to prolong the life of the cell. The mass spectra results show a steady increase in the partial pressure of hydrogen with cell life. Oxygen is also created; it oxidizes any carbon or nitrogen present and is seen in the form of these oxides. Oxygen is seen itself in greater quantities in the cell towards the end of the experiment when all possible oxidation has already occurred. The presence of oxides of carbon and nitrogen adversely affect the cell performance. Differences between these results and those described in Chapter 4 are likely to be due to their presence. The cell which has stood throughout the period of the experiment changes little, which is what we expect, so indicating good control.

## 5.7 Summary and Conclusions

In this chapter are described two series of experiments on batches of TR cells. Each series of experiments comprises measurements of the microwave performance of the cells, measurements of the microwave excited emission spectra and, finally, analysis of the gas in the cells. Microwave performance and emission spectra measurements have already been carried out on previous batches of cells. The results are described in Chapter 4. The results have been compared for these experiments and those in Chapter 4. The overall trends of the results are the same, showing the increasing loss of water vapour throughout the life of the cell through the action of the microwave discharge. The results for both these series of experiments differ from the previous results in several ways. These cells were not sealed off using a glass seal; instead a tap was attached and the tap closed to seal the cells. This arrangement was found to leak slightly, allowing nitrogen to enter the cells. Nitrogen was seen in the microwave excited spectrum of one cell and in the mass spectra of each cell. Nitrogen inhibits the breakdown and maintenance of a discharge, affecting the spike leakage energy, total leakage power and keep-alive current measurements. The oxygen created in the microwave discharge oxidized the nitrogen, producing species which also adversely affect the performance of the cell. Traces of CO were observed in the microwave excited discharge of many cells, and detected by the mass spectrometer. It was not observed in previous experiments. Its source is as yet uncertain. It affects the

discharge and performance of the cell in a similar way to that of the oxides of nitrogen. The presence of these gaseous oxides at first influence the emission spectra results but after about 100 hours life, changes in the water vapour content of the cells outweigh the influence of these impurity gases.

The mass spectra results confirmed the presence of the oxides of nitrogen and carbon; where the partial pressure of oxygen in a cell was high, the partial pressures of the oxides were low. Previously, cells were assumed to contain oxygen after lifetime experiments. In these series of experiments, oxides of nitrogen and carbon were seen, and not the oxygen itself, until after at least 100 hours running of the cells. The concentration of hydrogen was seen to increase steadily throughout the period of the experiment, showing that it is one of the products created during a microwave discharge in water vapour.

The experiment to discover the effect of the keep-alive discharge on cell life showed that a greater degree of dissociation of water vapour occurs in the cells with the keep-alive discharge operational.

The numbers of cells tested in each batch were small. We saw in Chapter 4 that there is a spread of microwave and emission spectra measurements within a batch of cells. For these series of experiments every attempt was made to ensure that the results obtained were due to differences in the treatment of the cells and not in the cells themselves.

References

A Cornu and R Massot (1966) Compilation of Mass Spectral Data,  
Heyden and Son Ltd, London

T Govindanunny, Private Communication

W Paul and H Steinwedel (1953) A New Mass Spectrometer without a Magnetic  
Field, Z Naturforsch 8a, 448

Eight Peak Index of Mass Spectra (1970) Mass Spectrometry Data  
Centre, AWRE, Reading

Table 5.2 Background Spectra

Effect of Keep-Alive Discharge on Life

Cell	4639	4641	4648	4622	4631
Mass	Peak Heights				
2	.121	.641	.089	.163	.137
12	.072	.097	.037	.076	.033
13	.009	.035	.009	.021	.004
14	.028	.093	.016	.039	.010
15	.029	.175	.016	.049	.019
16	.066	.128	.031	.075	.028
17	.211	.515	.108	.229	.095
18	.694	1.873	.367	.770	.335
20		.023			
25		.028	.004	.008	
26	.033	.156	.012	.051	.018
27	.051	.349	.031	.097	.029
28	.541	1.116	.282	.741	.237
29	.042	.249	.024	.079	.018
30	.008	.055	.006	.018	
31		.027			
32		.033		.024	
36		.068		.016	
37		.048	.010	.027	
38	.023	.100	.015	.053	
39	.093	.327	.055	.151	.034
40	.007	.085	.025	.047	
41		.251	.013	.067	.008
42		.132		.044	.001
43		.168		.057	.005
44	.129	.236	.031	.144	.021
45	.005	.103		.017	.007

Table 5.3 Background Spectra

Cells Opened at Intervals Throughout Life

Cell	4628	4621	4650	4653	4618
Hours	0	38.1	87.9	132.15	170.2
Mass	Peak Heights				
2	.218	.125	.158	.198	.187
12	.073	.058	.065	.065	.051
13	.029	.025	.025	.025	.025
14	.057	.039	.052	.044	.037
15	.114	.076	.105	.095	.071
16	.062	.046	.053	.051	.047
17	.173	.129	.178	.157	.129
18	.631	.441	.611	.564	.444
20					
25	.019	.013	.026	.019	.012
26	.107	.055	.087	.088	.051
27	.221	.126	.213	.180	.105
28	.546	.373	.450	.550	.342
29	.142	.085	.141	.112	.070
30	.051	.052	.107	.028	.023
31	.008	.017	.007	.011	.005
32		.005			
36		.003		.012	
37	.016	.009	.015	.021	.020
38	.044	.032	.039	.043	.038
39	.147	.086	.165	.149	.097
40	.040	.028	.038	.037	.034
41	.113	.066	.125	.101	.060
42	.073	.031	.073	.061	.036
43	.060	.040	.070	.060	.039
44	.089	.053	.081	.072	.050
45	.045	.033	.039	.039	.015

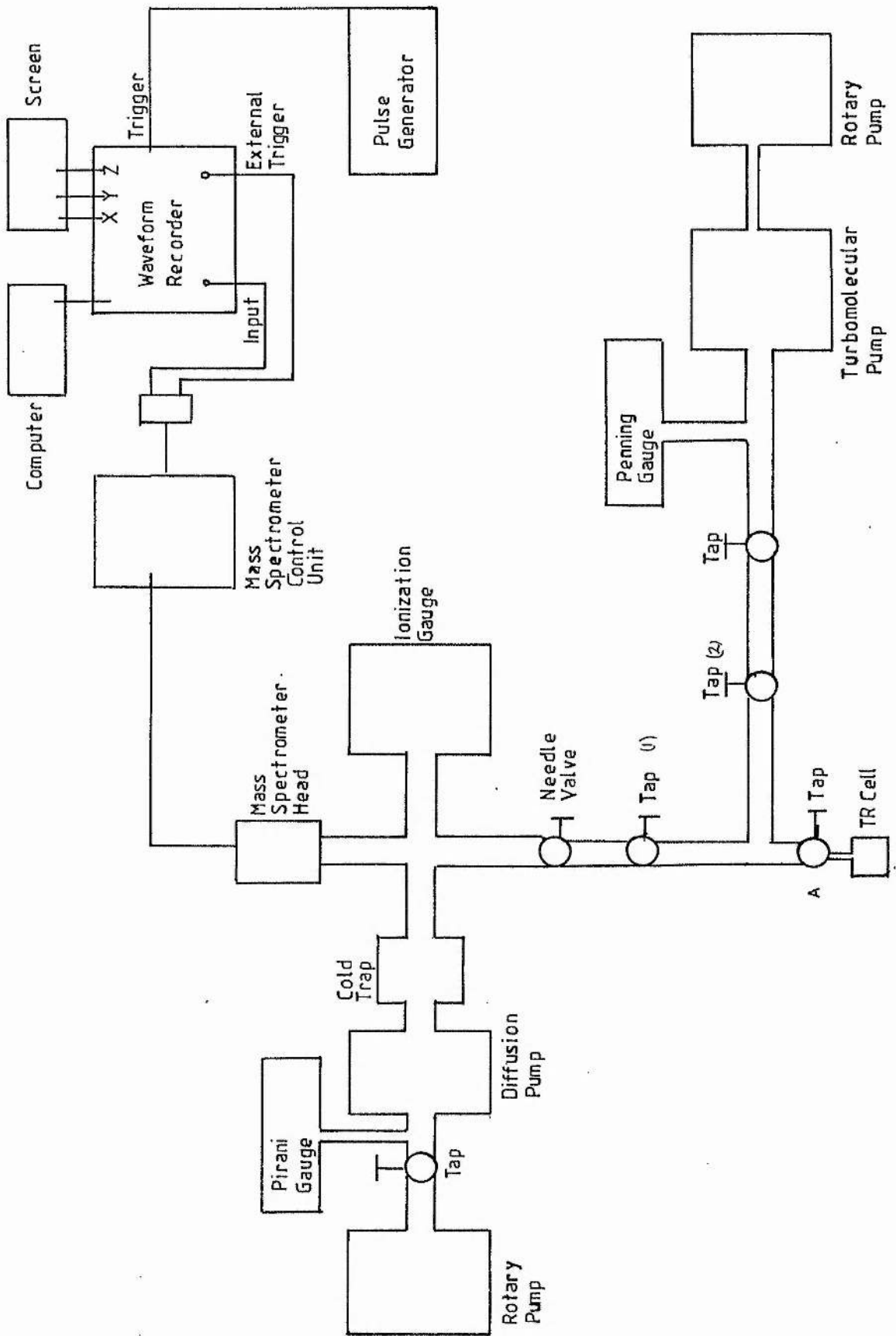


Fig 5-1 Schematic of the Mass Spectrometer Gas Analysis Equipment

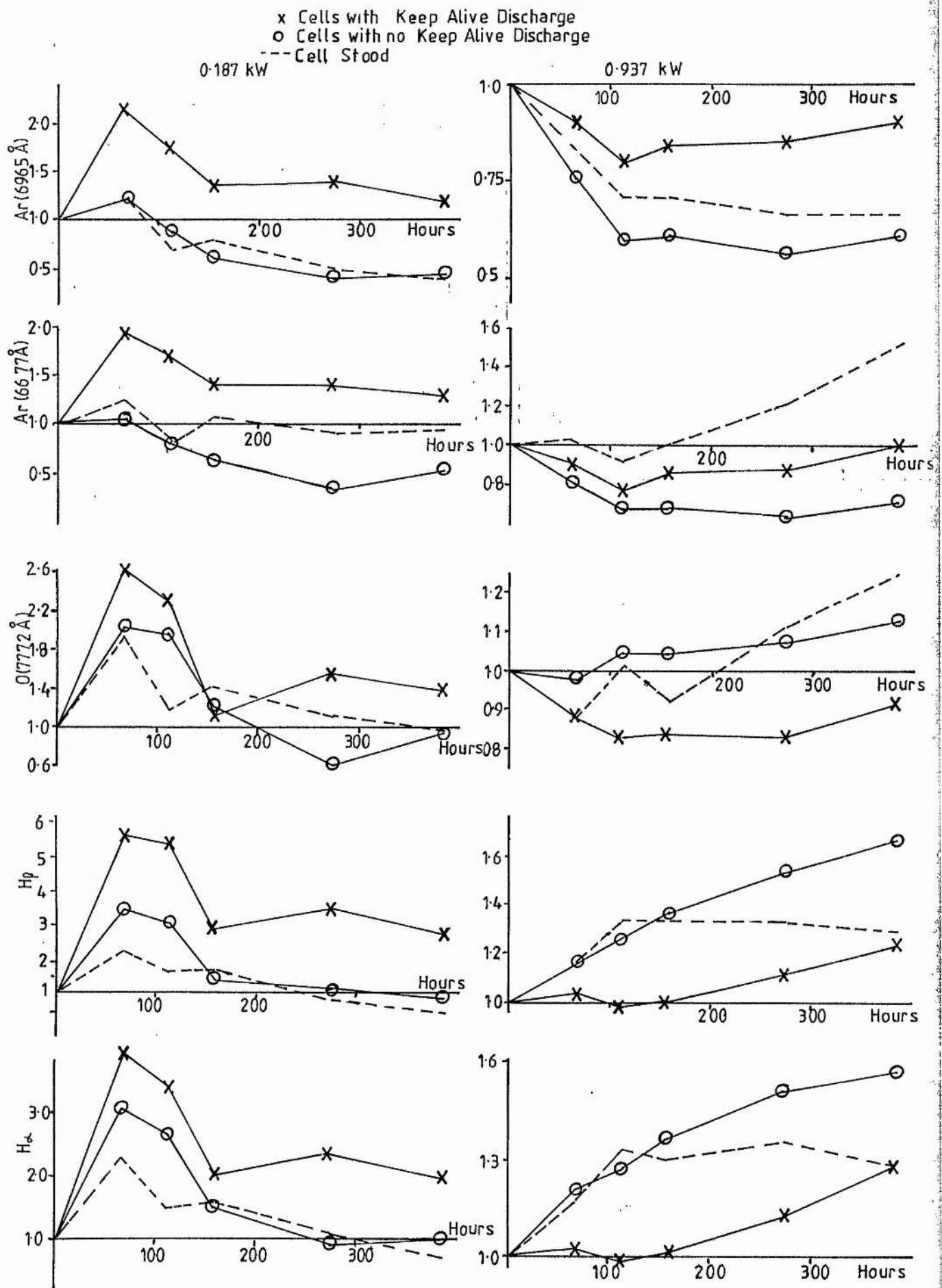


Fig 5-2 Emission Spectra Measurements  
Ratio  $I/I(\text{time } 0)$  against time

$Ar_1 = Ar(6965 \text{ \AA})$   
 $Ar_2 = Ar(6677 \text{ \AA})$

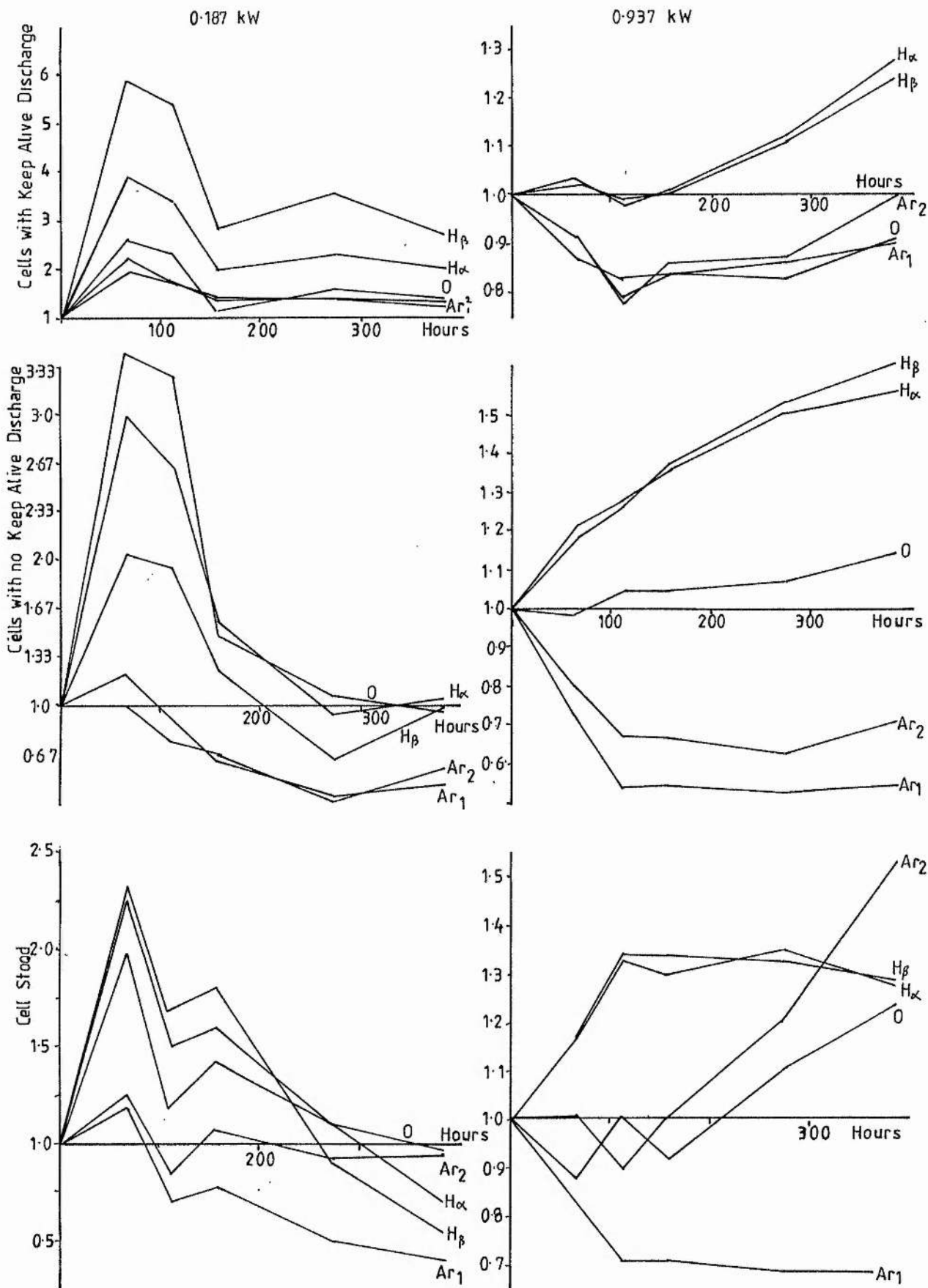


Fig 5.3 Emission Spectra Measurements  
 Ratio of Intensity/Intensity (time 0) against time

x Cells with Keep Alive Discharge  
 o Cells with no Keep Alive Discharge  
 --- Cell Stood

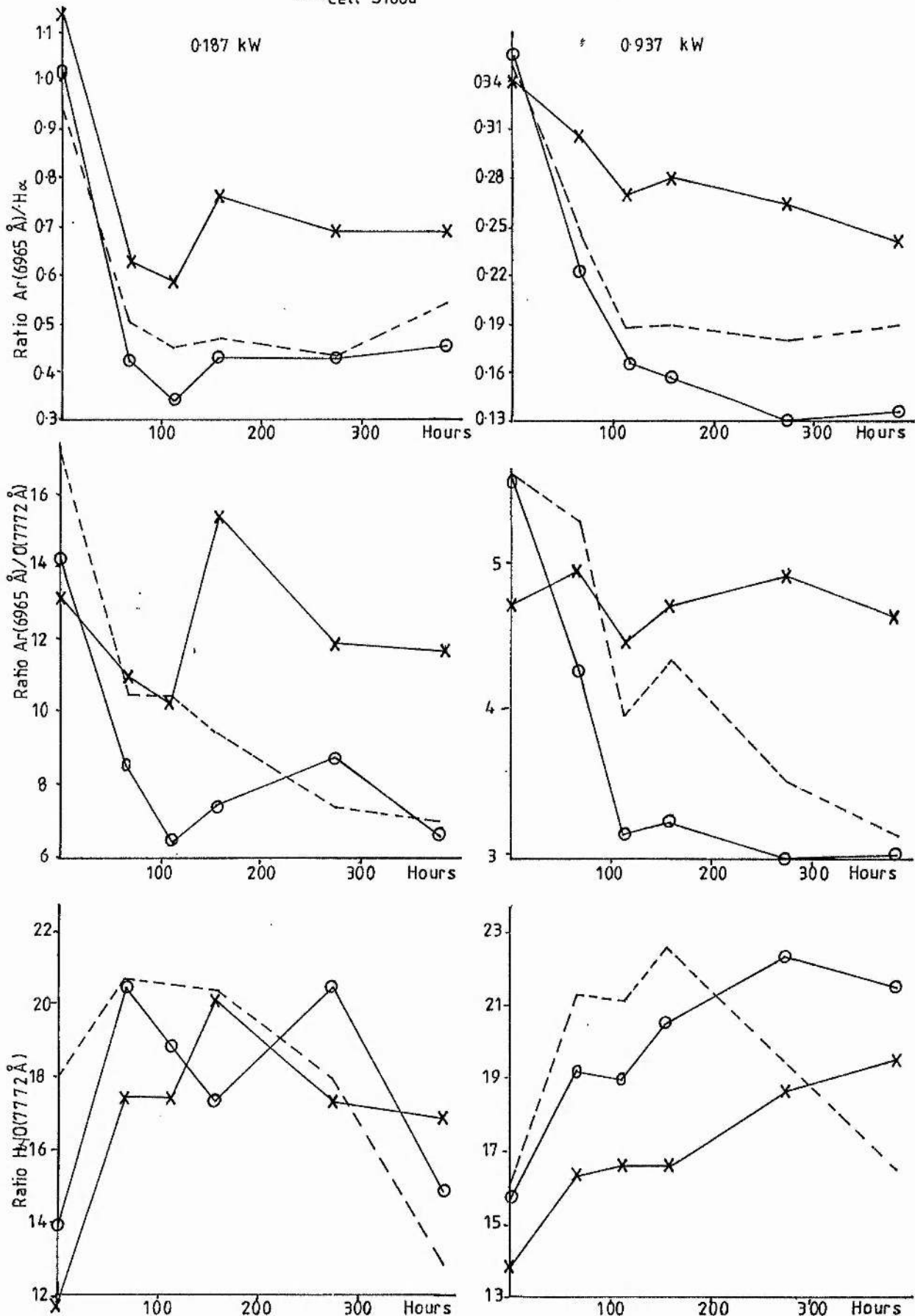


Fig 5-4 Emission Spectra Measurements Ratios of Spectral Lines against time

x Cells with Keep Alive Discharge  
 o Cells with no Keep Alive Discharge  
 --- Cell Stood

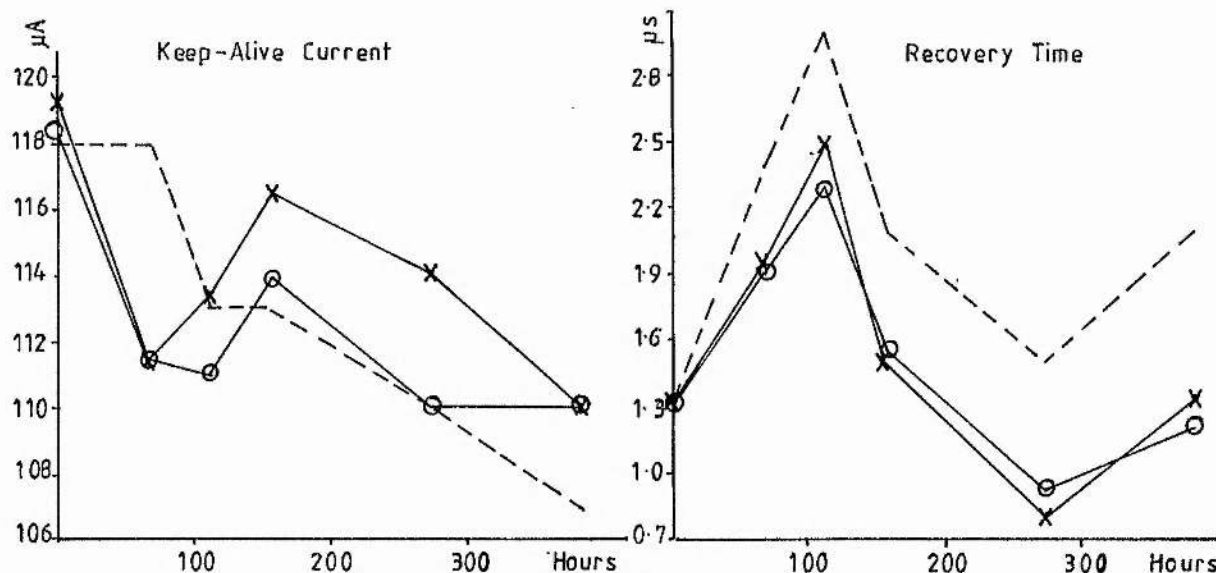
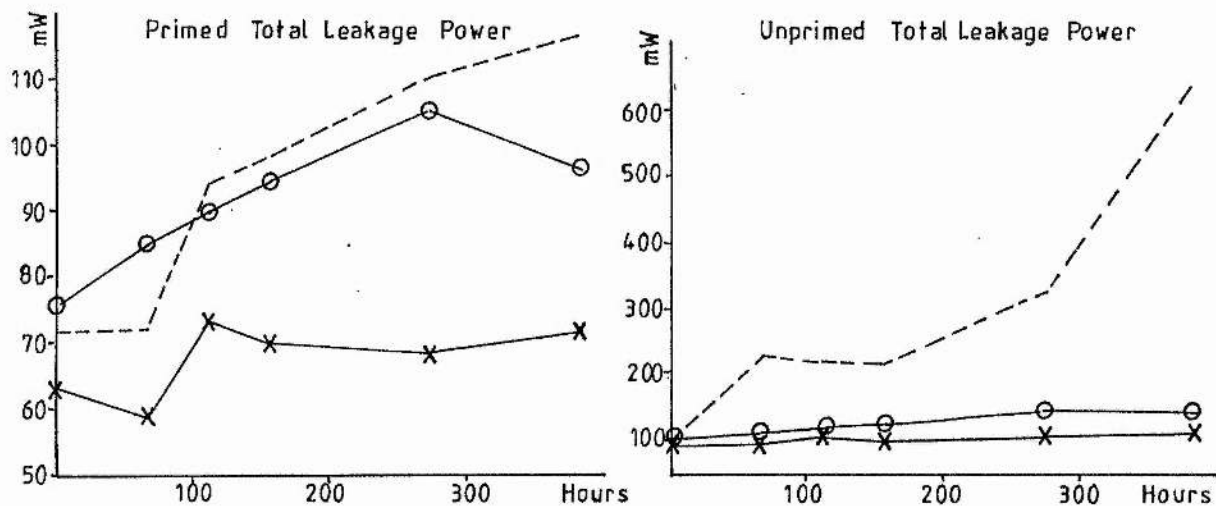
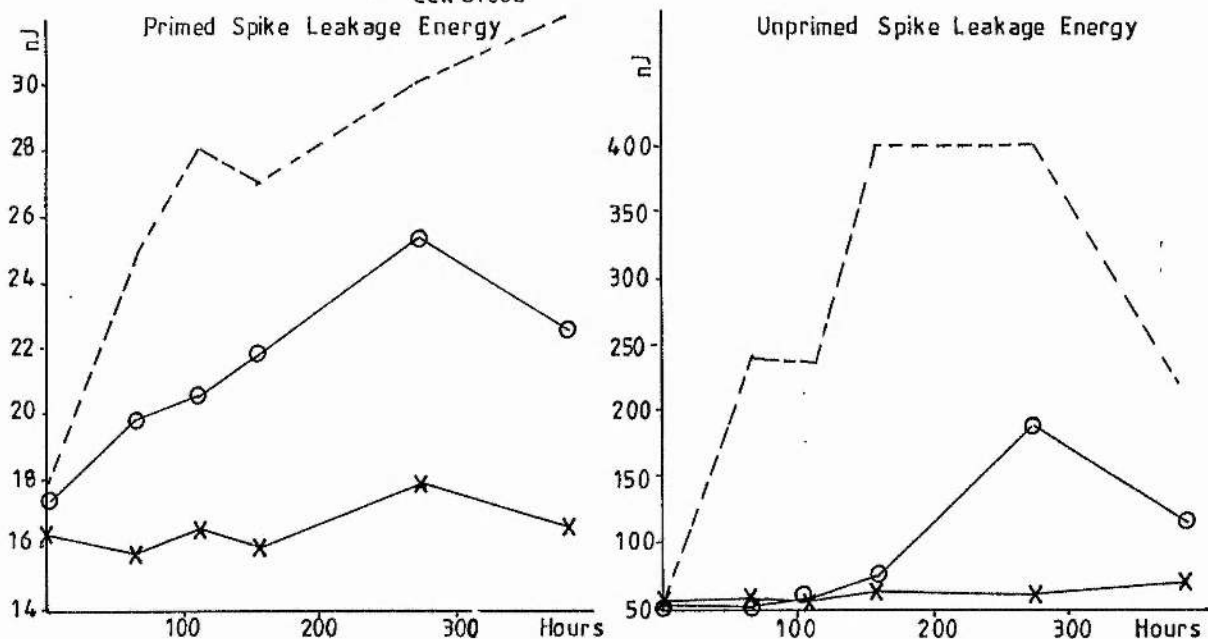
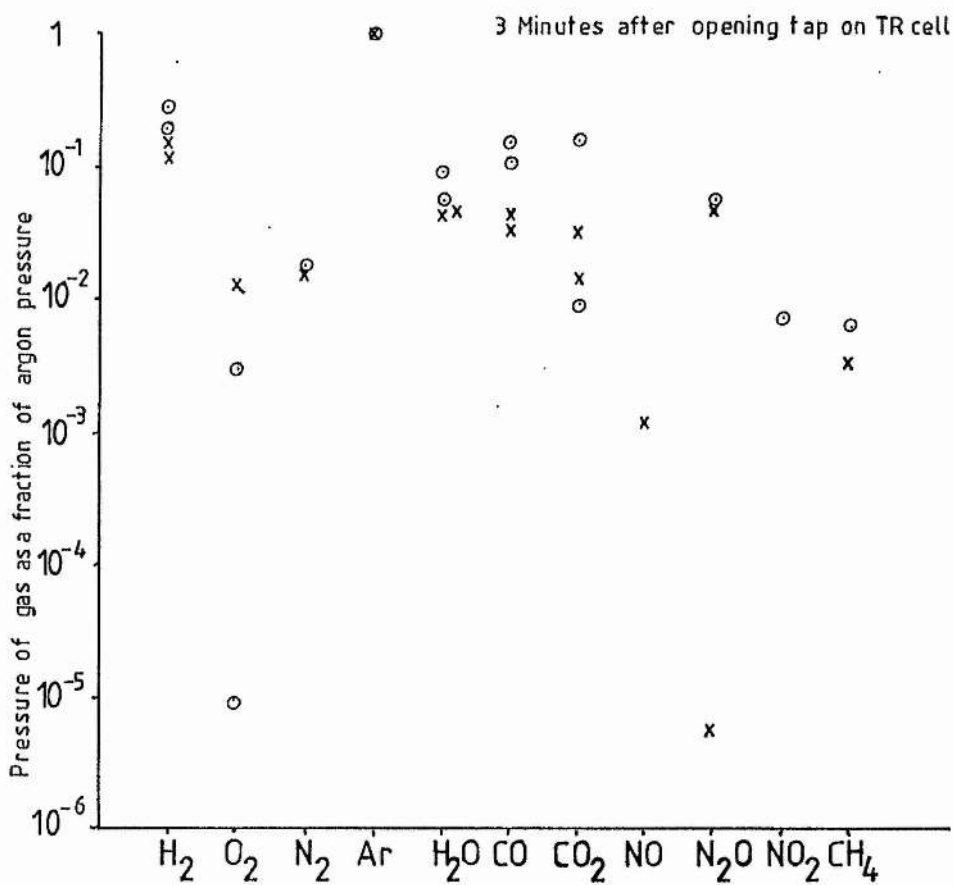
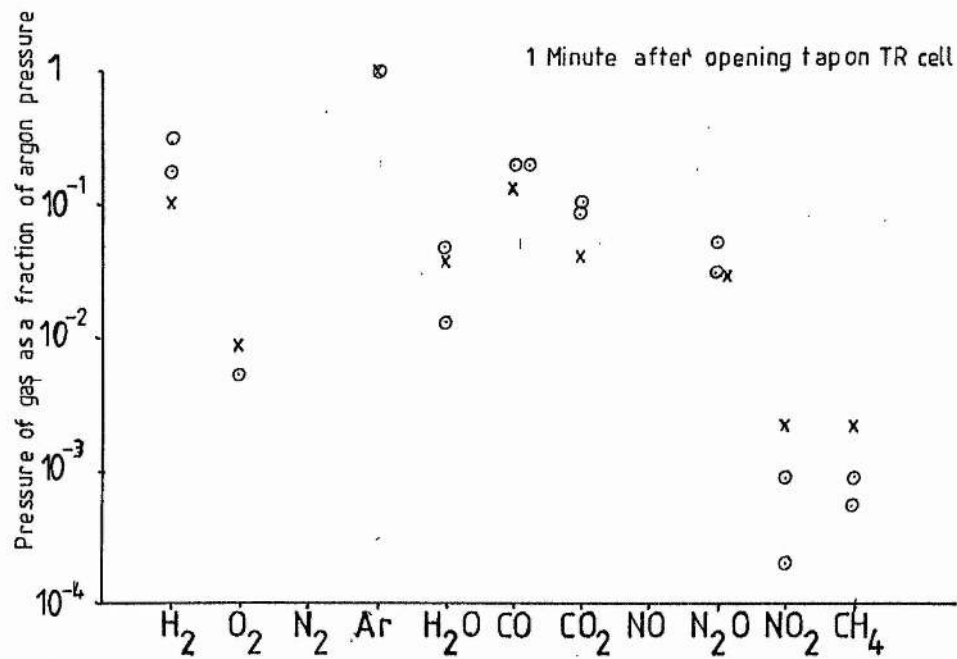


Fig 55 Microwave Measurements against time



x Cells with Keep-Alive Discharge on  
 o Cells with no Keep-Alive Discharge

Fig 5.6 Mass Spectra Results

x Cells with Keep Alive Discharge  
 o Cells with no Keep Alive Discharge  
 ◇ Cell Stood

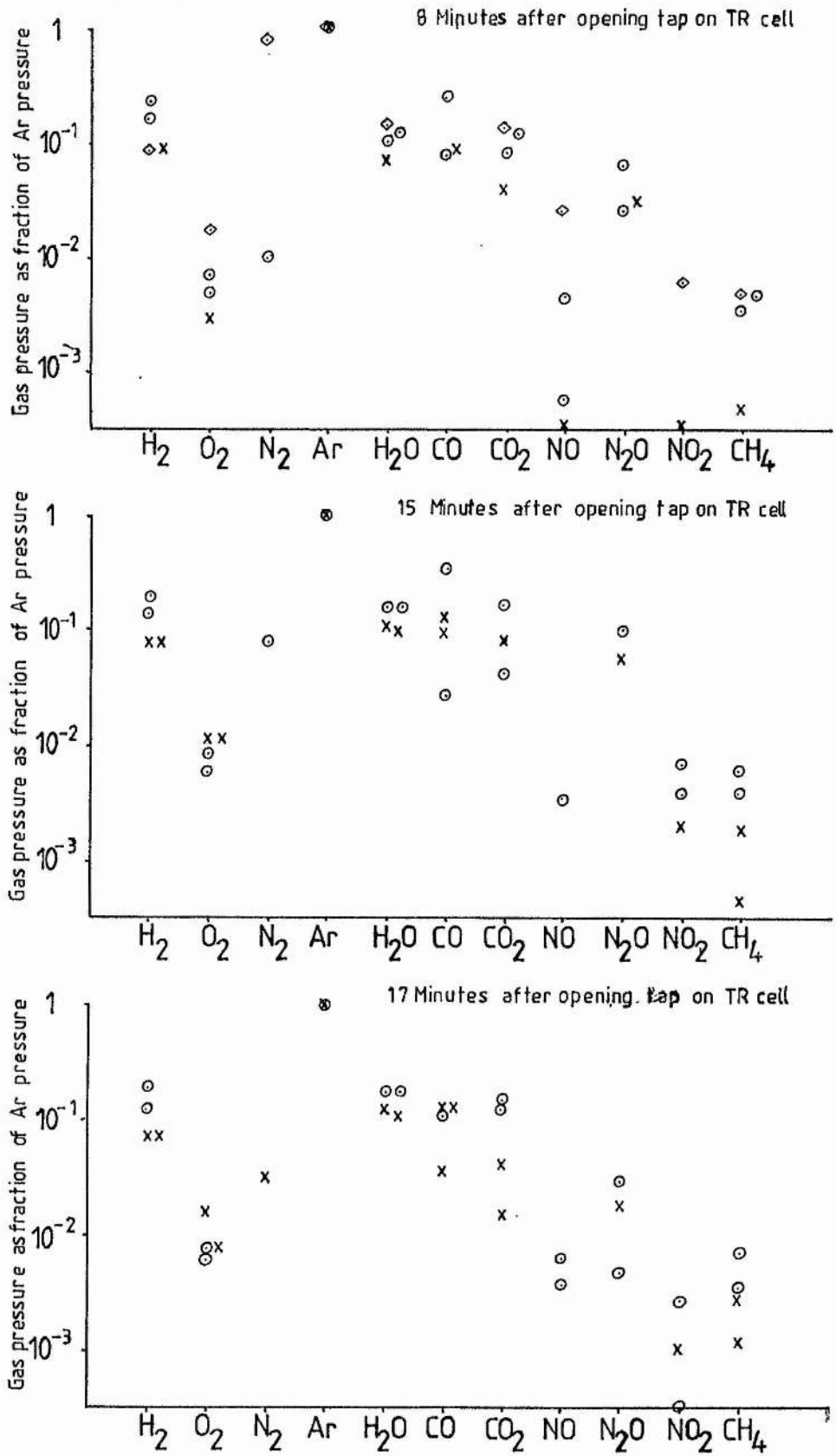


Fig 5.7 Mass Spectra Results

- x Cells with Keep Alive Discharge on
- o Cells with no Keep Alive Discharge
- ◇ Cell Stood

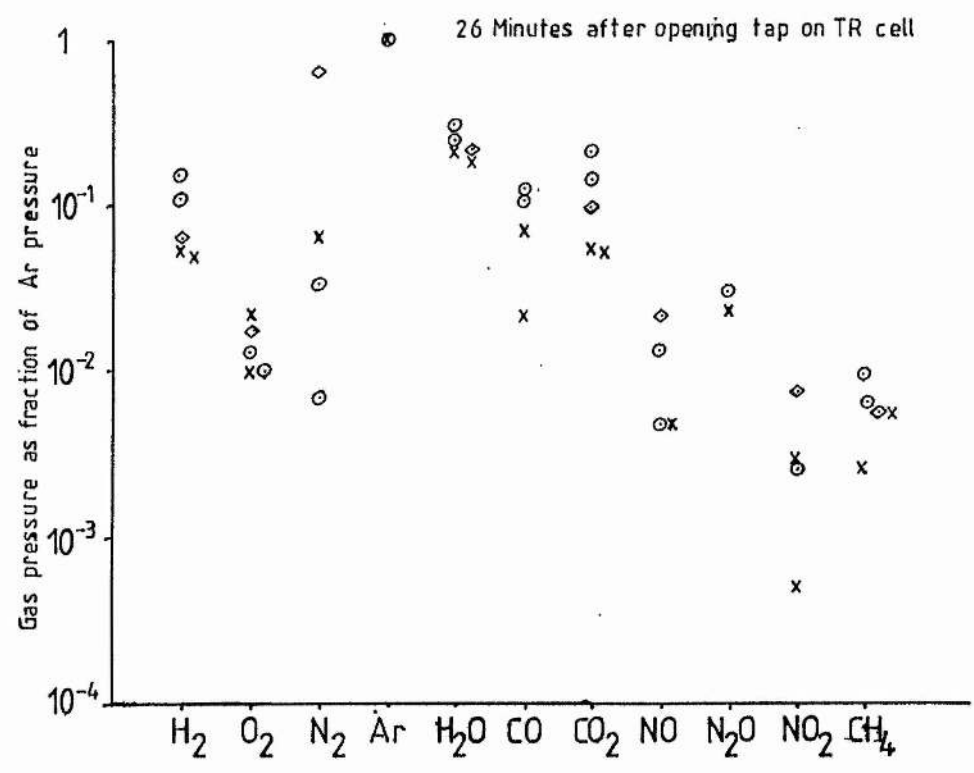
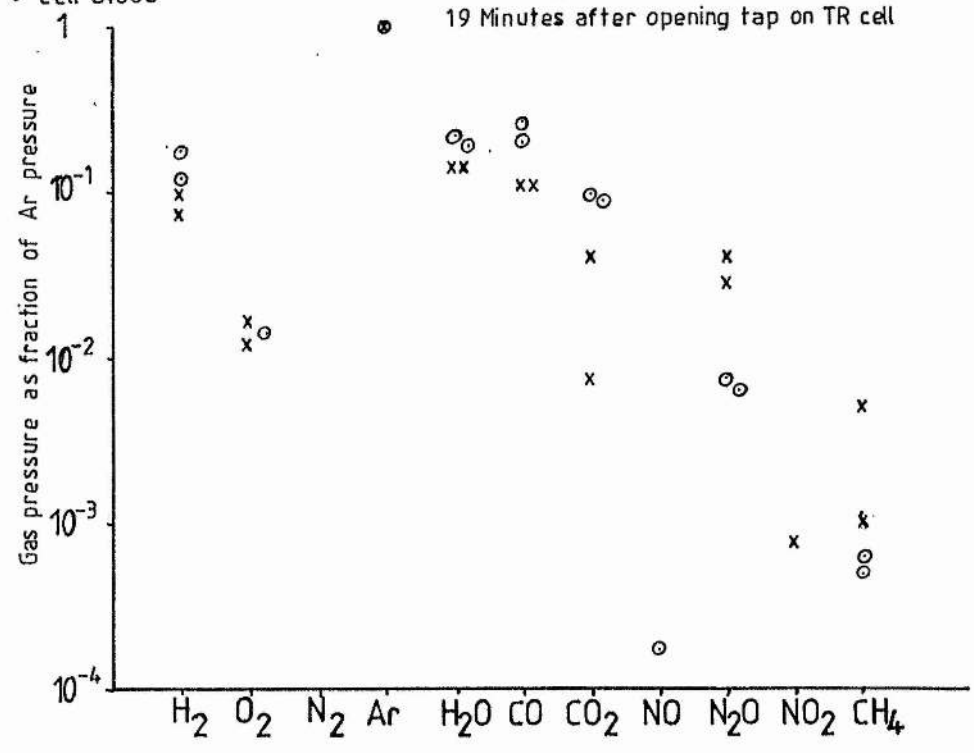


Fig 5-8 Mass Spectra Results

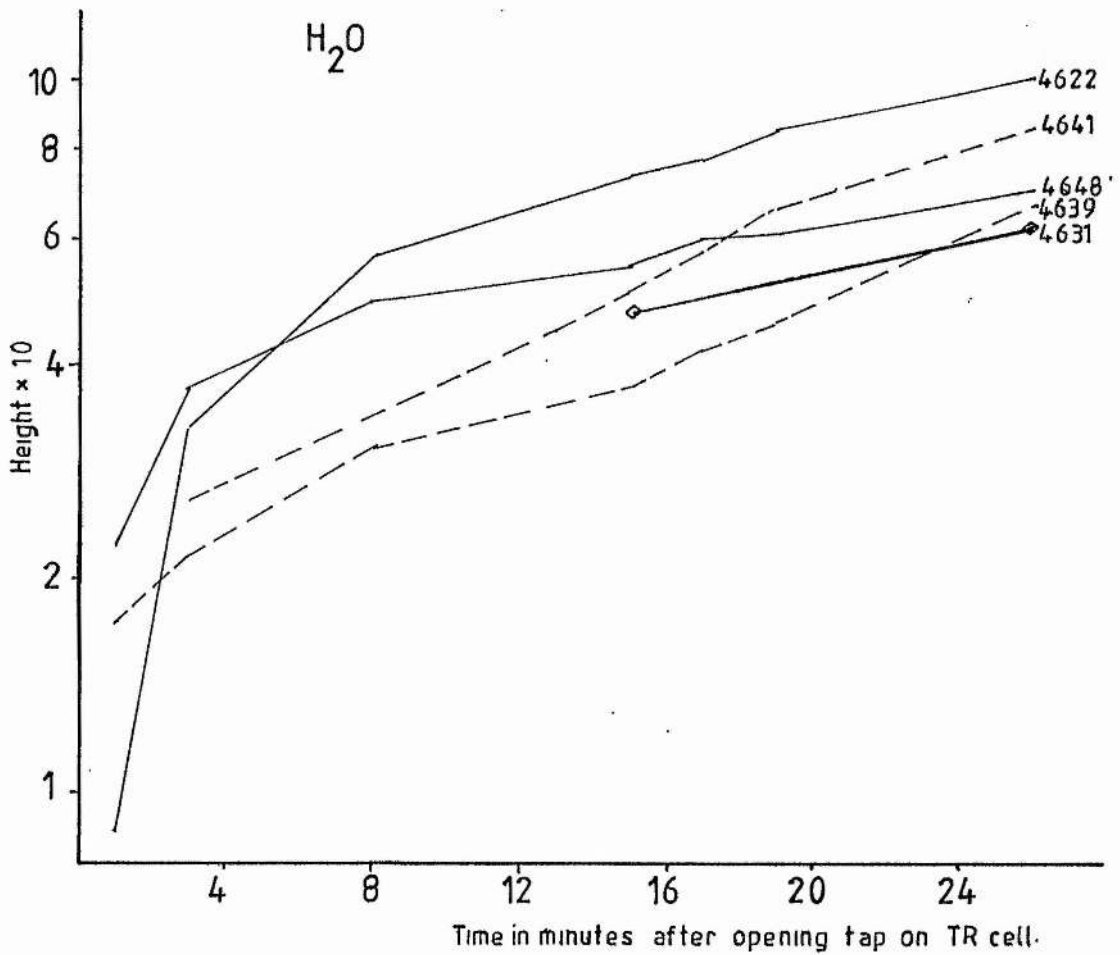
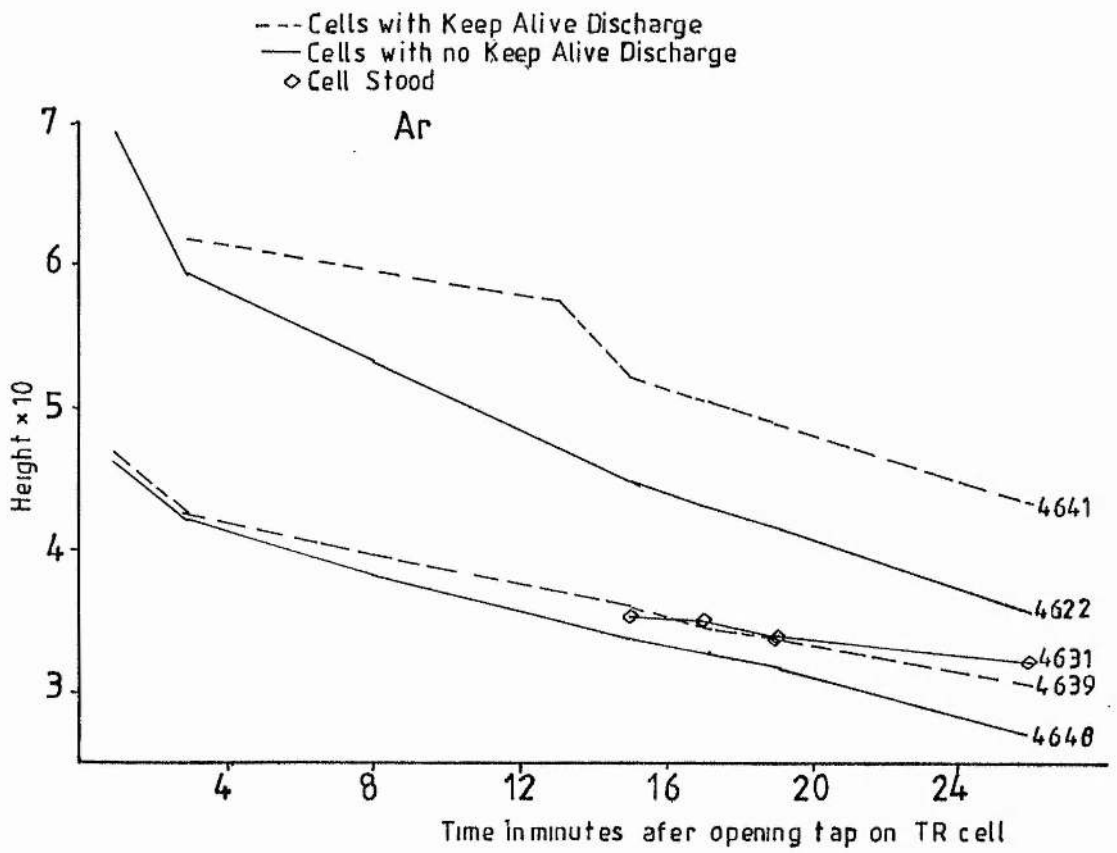


Fig 5.9 Variation of Partial Pressures of Ar and H<sub>2</sub>O During the Mass Spectral analysis of the gas in the TR Cell

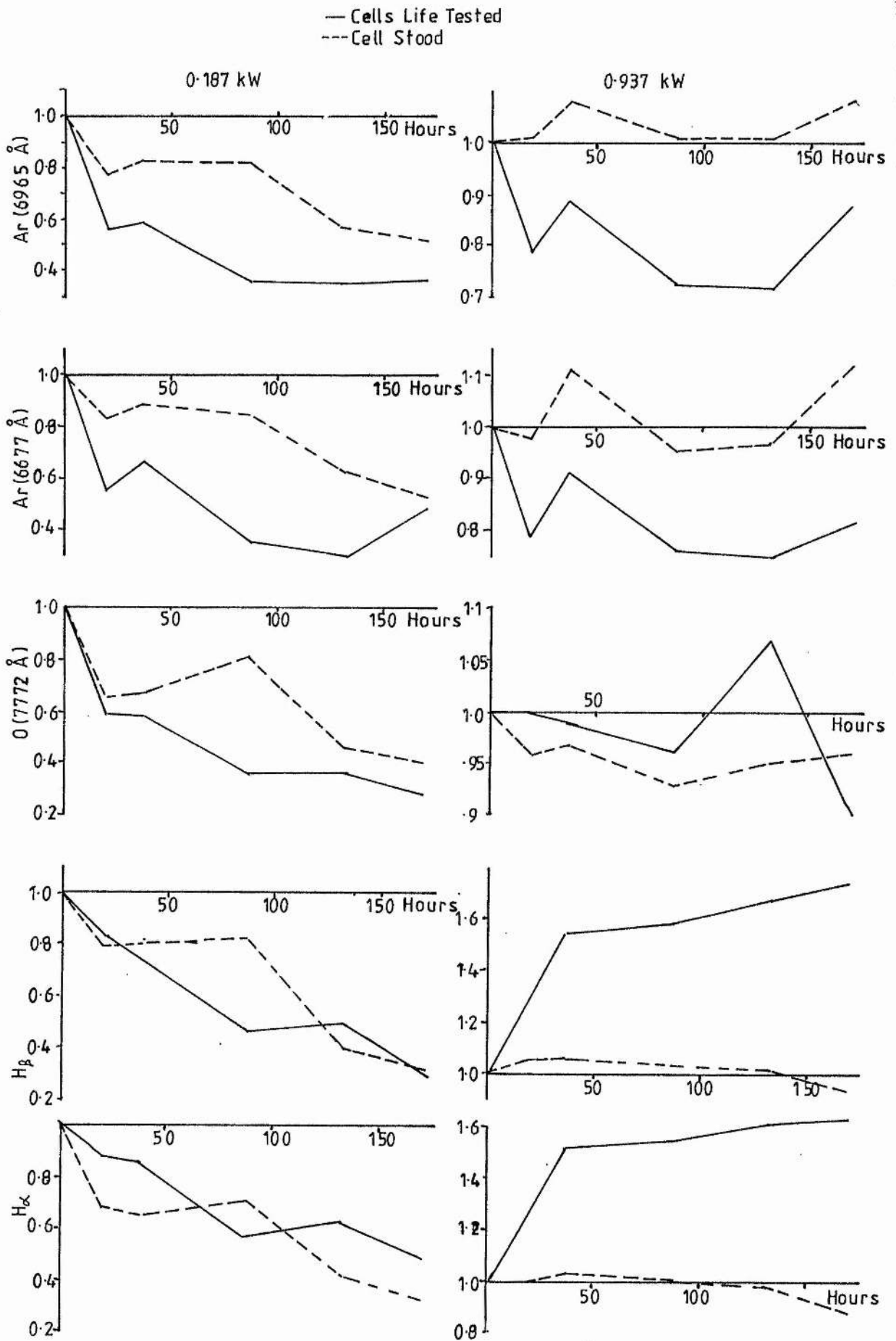


Fig 5.10 Emission Spectra Measurements  
Ratios of Intensity/Intensity(time 0) against time

Ar<sub>1</sub> = Ar (6965 Å)  
 Ar<sub>2</sub> = Ar (6677 Å)

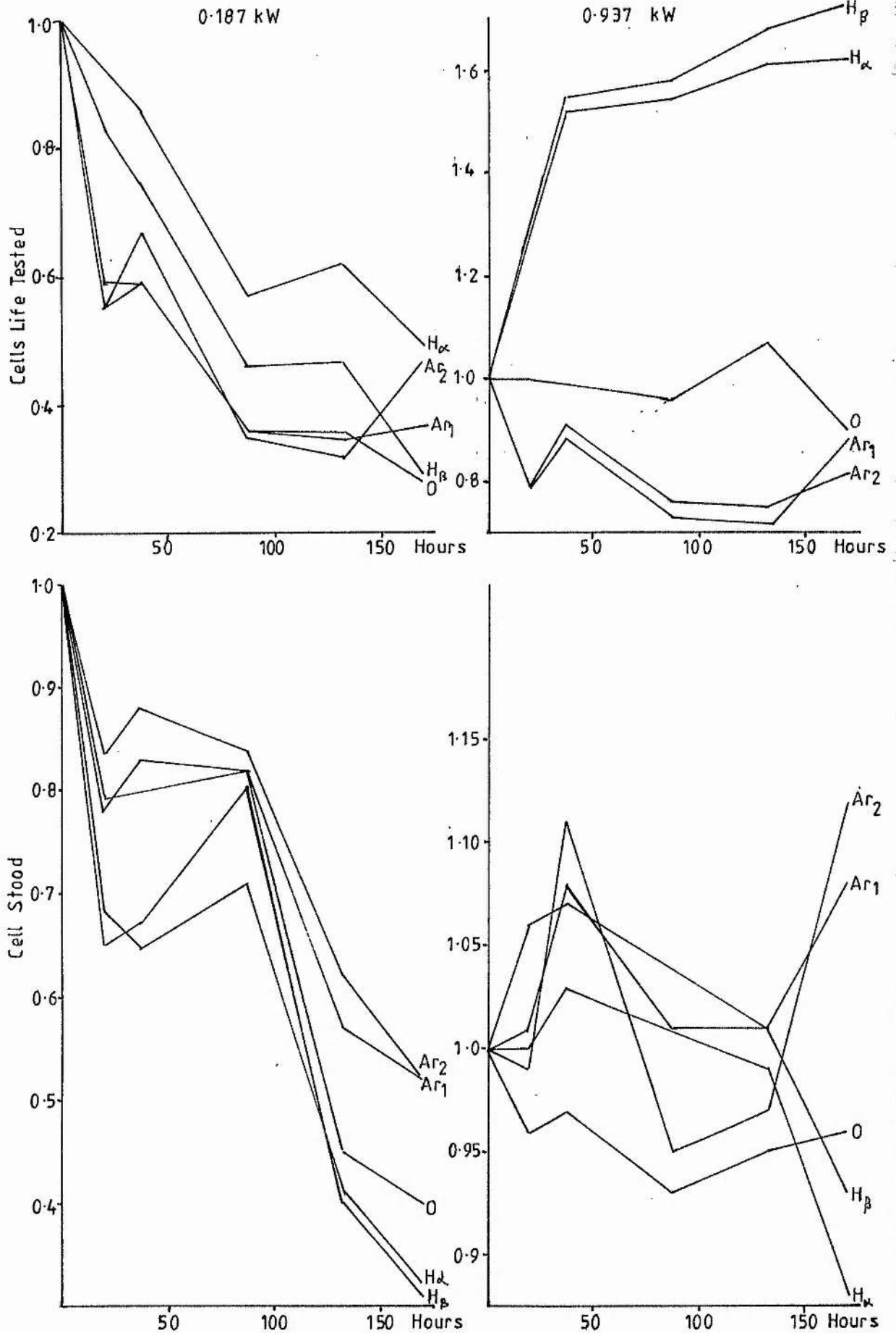


Fig 511 Emission Spectra Measurements  
 Ratios of Intensity/Intensity(time 0) against time

—Cells Life Tested  
 ---Cell Stood

0.187 kW

0.937 kW

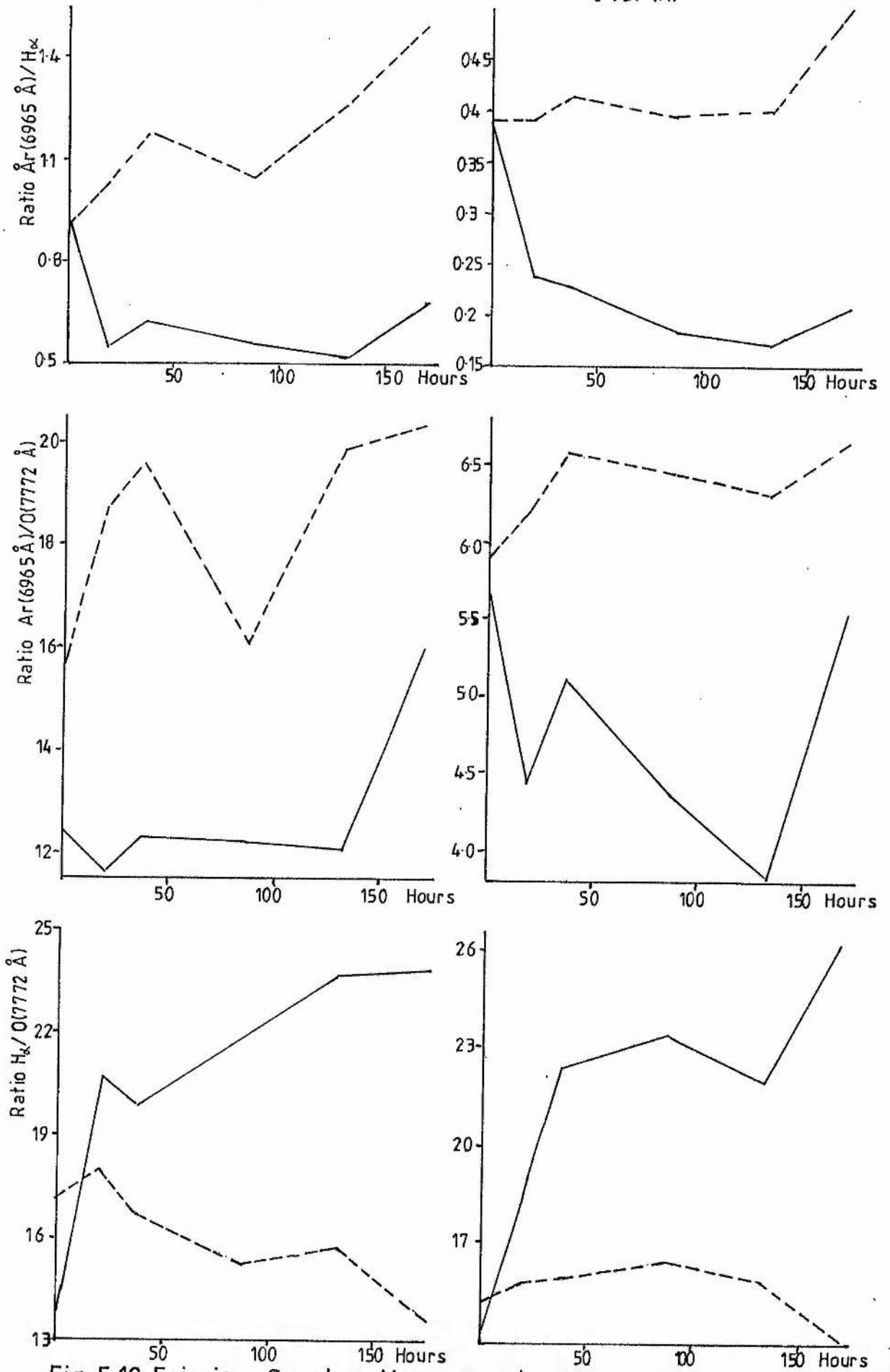


Fig 5.12 Emission Spectra Measurements  
 Ratios of Spectral Lines against time

— Cells Life Tested  
 --- Cell Stood

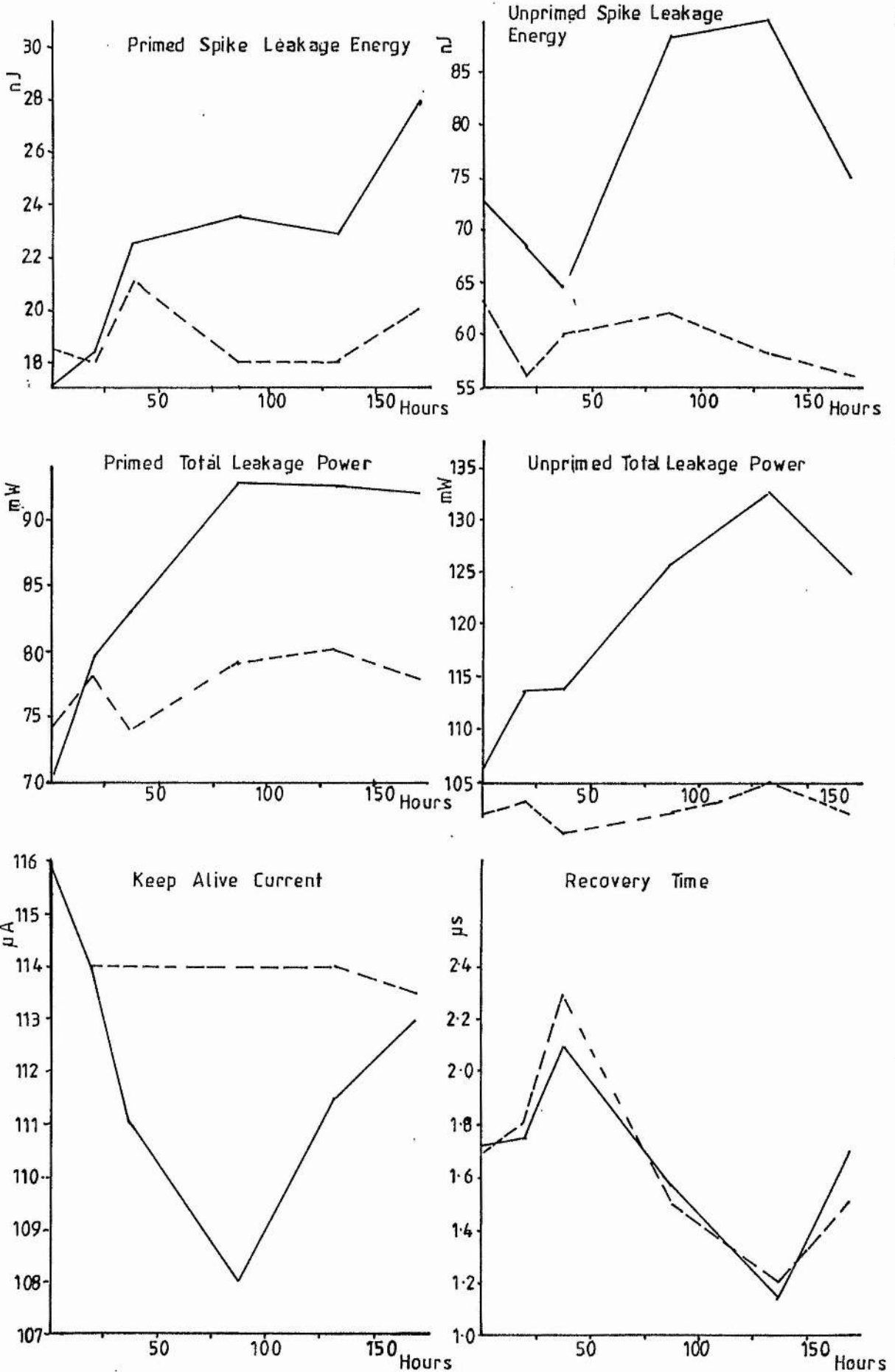


Fig 5-13 Microwave Measurements against time

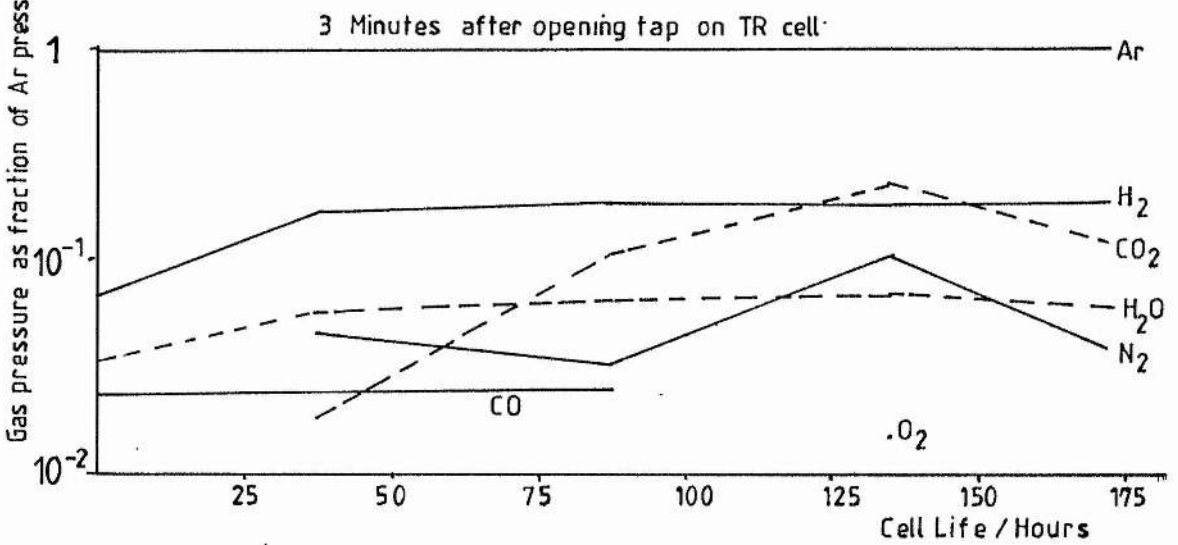
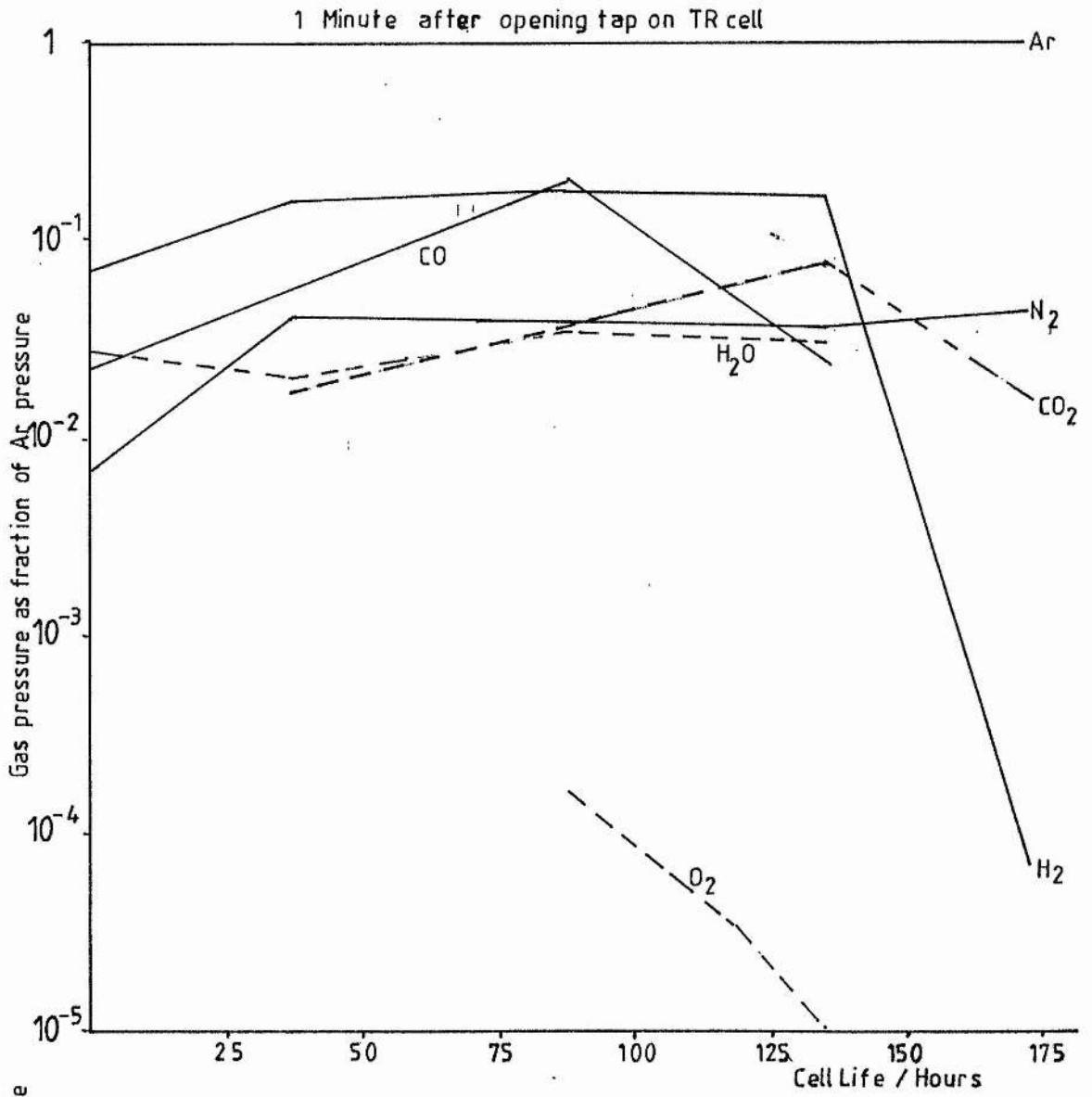


Fig 5.14 Mass Spectra Results

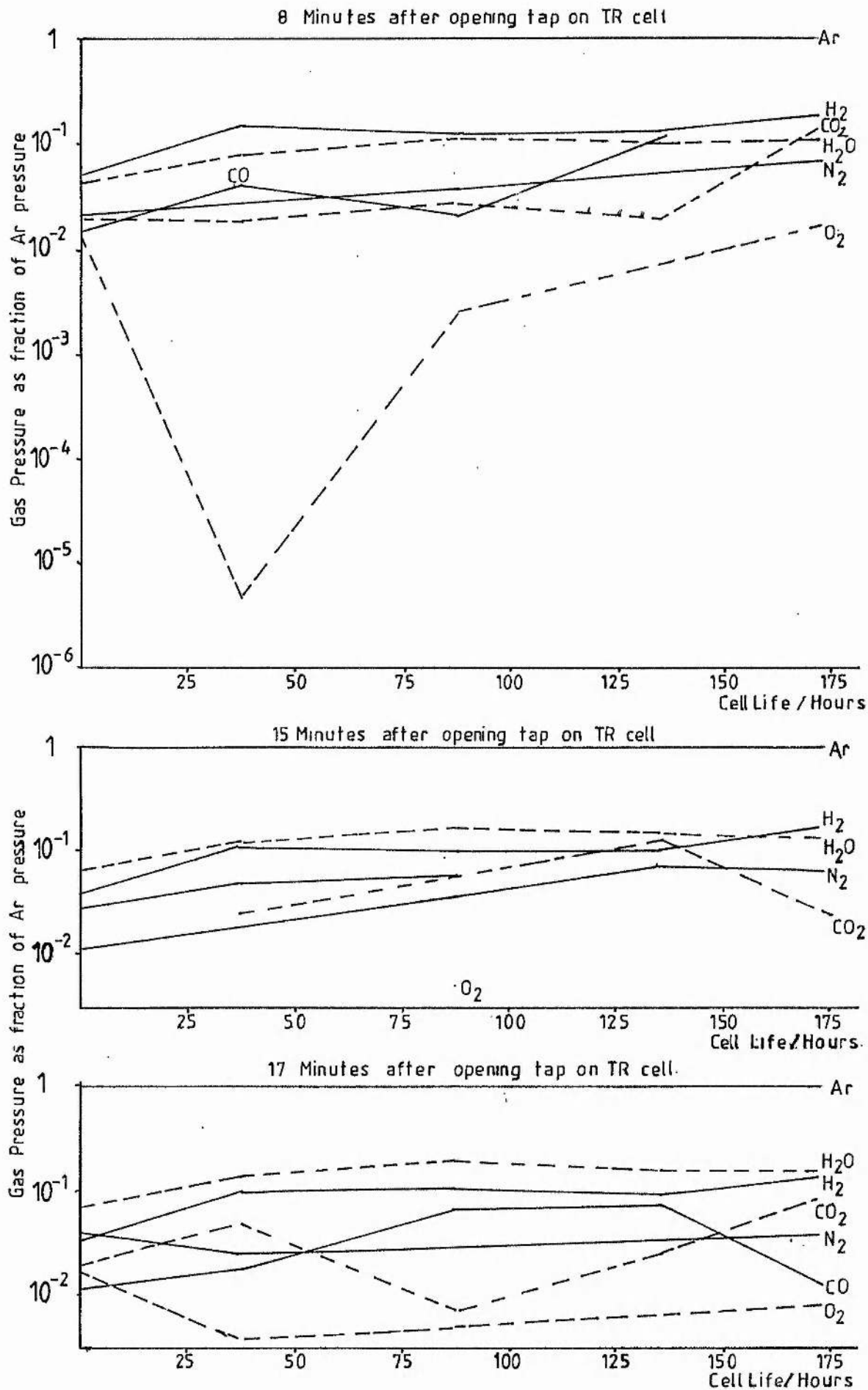


Fig 5.15 Mass Spectra Results

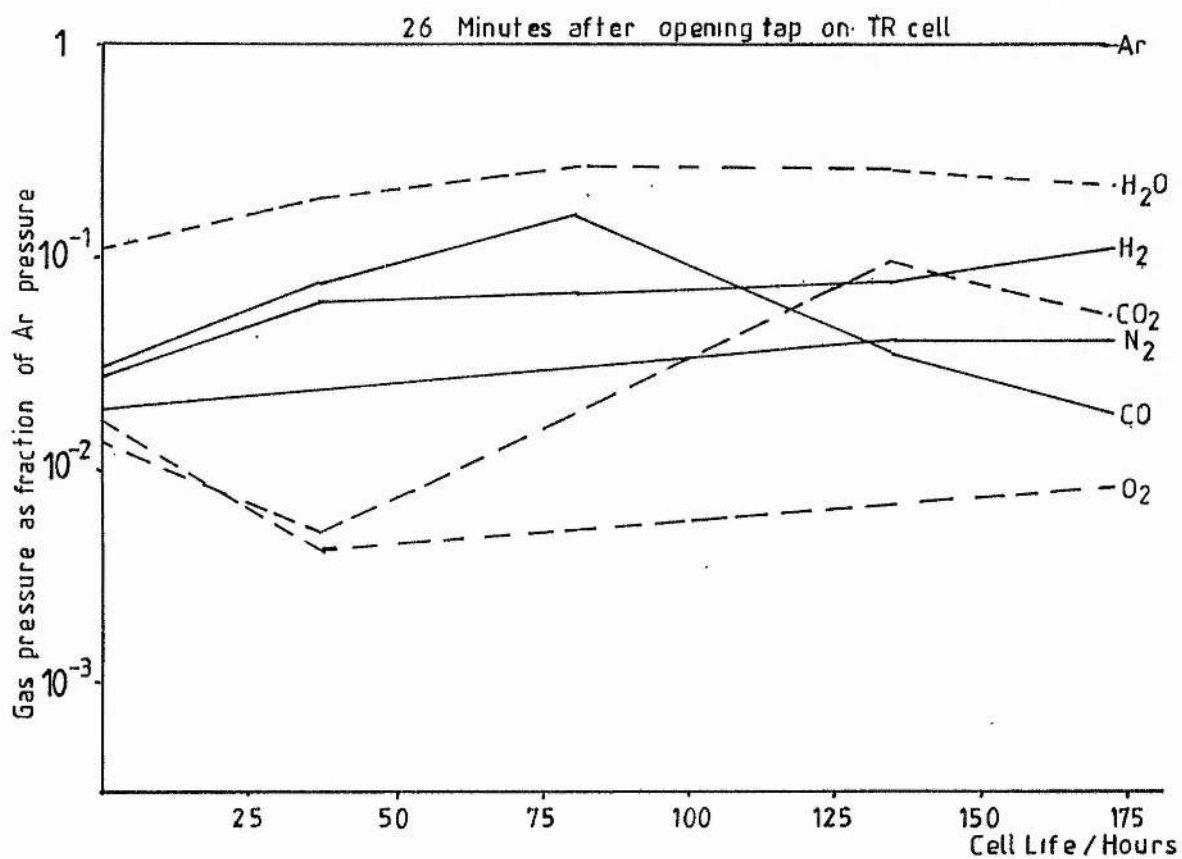
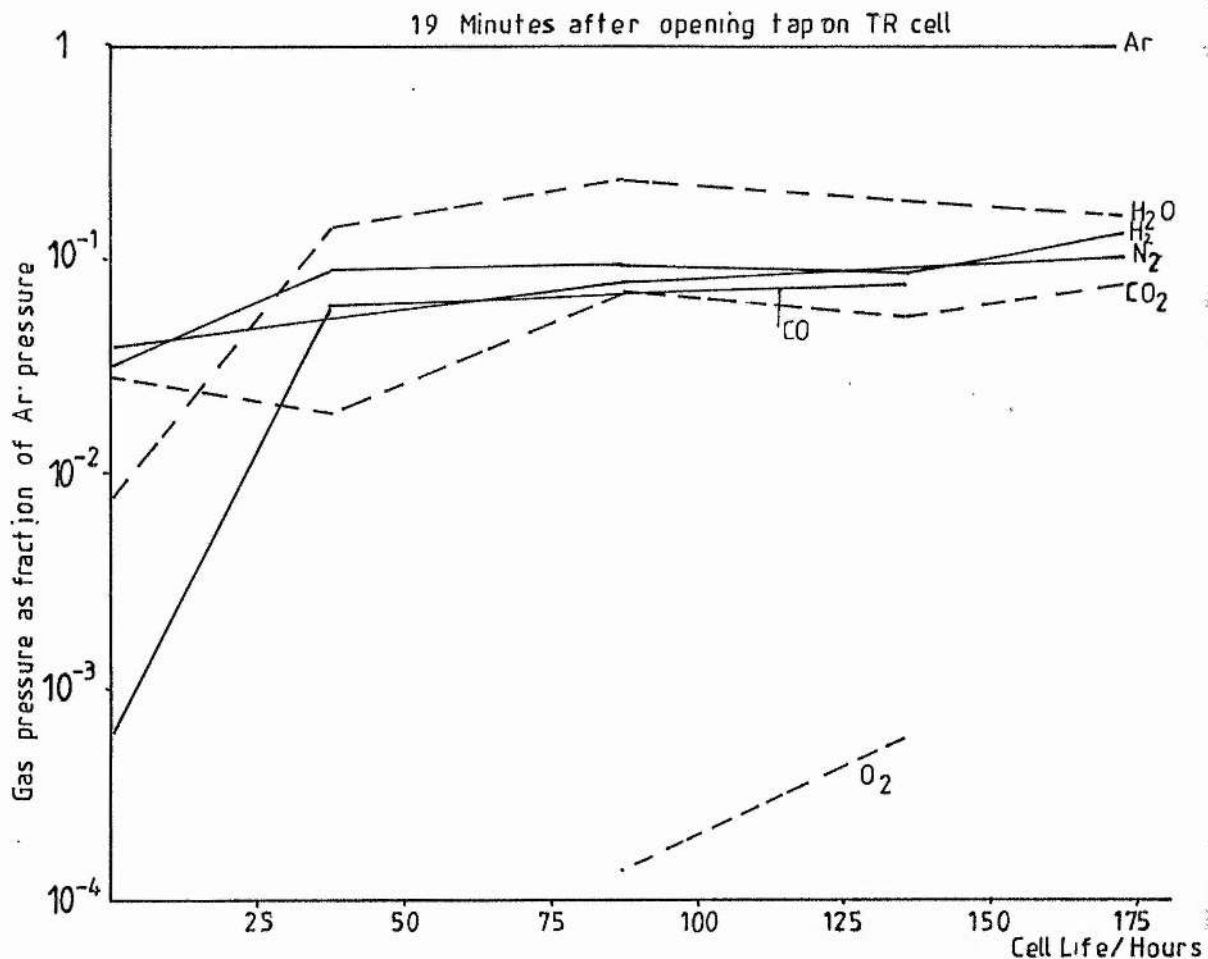


Fig 5-16 Mass Spectra Results

## Chapter 6 Computer Model of the TR Cell Discharge

### 6.1 Introduction

The TR cell has a finite lifetime, due to a continual modification of the gas in the cell through the action of the discharge. The cell is filled with a mixture of two gases; argon to promote breakdown of the gas and water vapour to decrease the time required for the gas to deionize. The object of this chapter is to model the effect of microwaves on the gas in the TR cell using the available data on the reaction rates of the species likely to be in the cell and the electric field incident on the gas and the resultant electron density, as calculated in Chapter 2. The model will be used to predict the useful lifetime of a typical TR cell.

### 6.2 Reactions of Argon

Electrons accelerated by the incident microwave field collide with argon atoms and raise them to an excited or ionized state by transferring energy (inelastic collisions), ie



The argon atom in an excited state,  $\text{Ar}^*$ , rapidly decays via an electric dipole transition, often to a metastable state and emits radiation of frequency  $\nu$ , ie



Cross-sections for momentum transfer, excitation and ionization have been measured as a function of incident electron energy, using a monoenergetic beam of electrons, or as a function of  $E/N$ , where  $N$  is the gas number density, for an electron swarm.

Attempts have been made to produce a self-consistent set of electron impact cross-sections and of excitation and ionization rates for argon, through the numerical solution of the Boltzmann equation with the use of the available experimental data (Ferreira and Loureiro (1983), Jacob and Mangano (1976)). The ionization cross-section of argon as a function of electron energy as measured by Rapp and Englander-Golden (1965) were used in these models. The model of Jacob and Mangano produced a total excitation cross section as a function of electron energy over the range 11.5-17 eV, which was smaller than that calculated by Eggarter (1975), using existing data, and larger than that measured by Schaper and Scheibner (1969). The model of Ferreira and Loureiro, over the range 10-100 Td (1 Td is  $10^{-17}$  Vcm<sup>2</sup>), included the momentum transfer cross sections of Frost and Phelps (1964), obtained by comparing the theoretical and experimental values of electron swarm data, and the excitation cross sections of Peterson and Allen (1972), Eggarter and Chutjian and Cartwright (1981).

Specht et al (1980) measured electron ionization coefficients of argon in the low  $E/N$  region, between 5 and 40 Td, and calculated a set of inelastic cross-sections based on their results, using the transport equation. The total electron impact cross sections for argon as a function of electron energy as obtained by the above

authors are shown in fig (6.1).

The percentage electron energy losses in argon over the range 10-100 Td are shown in fig (6.2). In fig (6.3) are shown the cross sections for momentum transfer, total excitation and ionization of argon by electrons.

Kucukarpaci and Lucas (1981) have measured electron swarm parameters in argon and compared measured and calculated values over the range 5.6-5657 Td. Their calculated values of the cross sections for collision, ionization and excitation as a function of electron energy are displayed in fig (6.3). Their calculations of electron energy losses in an argon discharge as a function of  $E/N$  are displayed in fig (6.2), to compare with those of Ferreira and Loureiro. Their calculation of the mean electron energy in argon before and after a collision as a function of  $E/N$  is shown in fig (6.4).

### 6.3 Water Vapour

To date, there is relatively little information available on the products of the interaction of microwaves with water vapour. Considerable data exists on the interactions of electrons of a known energy with water vapour, but the properties of electron swarms in pure water vapour have not been extensively studied.

Some of the earliest work on the products from the interaction of 100 eV electrons with water vapour was carried out by Mann et al (1940). Their work was later repeated by Schutten et al (1965) and by Melton (1970), amongst others. Schutten et al measured the ionization cross section of water vapour as a function of electron energy over the range 0.1-20 keV. Melton measured the cross section for ion production on collision with electrons for 100 eV electrons and lists the possible reaction mechanisms.

Buchel'nikova (1959) measured the electron capture cross section of water vapour as a function of electron energy. Melton (1972) measured the dissociative attachment cross sections for the following reactions:



as a function of incident electron energy. Melton and Neece (1971) have measured the rate constants and cross sections for the reactions of the principal negative ions formed in water vapour with water vapour. Compton and Christophorou (1967) have studied electron attachment in water vapour using the swarm technique. In a recent review article on electron swarm data in electronegative gases Gallagher et al (1983) discuss the available data on electron transport properties and electron swarm coefficients for water vapour and give recommendations on its reliability.

Reactions of neutral radicals and molecules present in a water vapour discharge have been tabulated eg by Venugopalan and Jones (1966) and collected by Baulch et al (1976), who also give recommendations for reaction rates over specified temperature ranges. Warman et al (1979) have measured the rate constant for the recombination of electrons and positive ions in water vapour as a function of pressure.

Shukla et al (1970) investigated the interaction of microwaves with water vapour and observed the partial dissociation of water vapour into H and OH. Kaufman and Del Greco (1961) studied OH production and decay in a microwave excited discharge in a mixture of argon and water vapour. They observed that such a discharge is an efficient source of H, not OH; any OH produced was created in a secondary reaction



Howgate (1962) measured the concentrations of neutral radicals produced in an rf discharge in water vapour over the pressure range 0.05-0.2 torr. Rutscher and Wagner (1983) have modelled the dissociation of water vapour in a hollow cathode glow discharge.

#### 6.4 The Microwave Discharge in Argon and Water Vapour

Pahl et al (1972) and Lindinger (1973) have observed products of reactions between argon and water vapour in a steady state hollow cathode discharge and have measured rate constants for the principal reactions. Hurst et al (1961) added small amounts of

water vapour to pure argon and measured the electron capture cross section in an electrical discharge. By extrapolating their results to zero water vapour concentration, a value may be obtained for the cross section for electron capture in water vapour, averaged over the energy distribution characteristic of argon at a given value of  $E/p$ . Their results showed the dependency of the attachment coefficient for electrons on the ratio of the partial pressures of argon and water vapour present, since an increase of water vapour partial pressure implies a decrease in the number of electrons in the energy range where dissociative attachment takes place. However, Crompton et al (1965) say that the experimental method of Hurst et al does not enable the attachment coefficient for electrons in water vapour to be determined as a function of  $E/p$ .

Wang and Lee (1985) have measured the attachment rate of water vapour in argon buffer gas as a function of  $E/N$  in the range 2-15 Td. The measured attachment rate constants of water vapour in argon increase with  $E/N$  over the above range. Wang and Lee say that for electron attachment to occur in water vapour  $E/N$  must exceed 40 Td; if argon is added,  $E/N$  is reduced, because for the same  $E/N$ , the electron energy in argon is higher than in water vapour.

Now, we must adapt the available data on reaction rates and cross sections in argon and water vapour discharges, discussed above, to the case of the microwave discharge in the TR cell, which contains equal partial pressures of argon and water vapour. We have calculated the electric field incident on the gas and the

electron density in the discharge in Chapter 2; now we need information on the electron energy distribution and the mean electron energy in the gas mixture in the TR cell. Gallagher et al (1983) state that the electron energy distribution in a gas mixture may vary considerably from those of the individual mixture components under the same experimental conditions. The mixture distribution cannot be determined directly from the distributions of the pure gas components; it is necessary to solve the Boltzmann equation using as input the component collision cross sections.

However, we do not know the extent of the interaction of argon and water vapour in a microwave discharge. So, as a first approximation, we neglect the interaction between argon and water vapour and assume that the electric field acts equally on argon and water vapour. We calculate the electric field  $E_i$  acting on each gas as being proportional to the partial pressure of each gas present, giving

$$E/N = \sum_i x_i E_i / N_i, \quad (6.8)$$

where

$$x_i = N_i / \sum_i N_i, \quad (6.9)$$

and  $E$  is the total incident electric field vector,  $N$  is the total molecule number density and  $N_i$  is the number density of molecules of type  $i$ . Without solving the Boltzmann equation, we calculate the mean electron energy in the discharge as the average of the electron energies in each gas separately, at the value of the electric field calculated using equation (6.8). Hence we obtain a value for the mean electron energy in the microwave discharge in argon and water vapour throughout the pulse. Using this value of the mean electron energy we obtain values for the mean reaction

rates in the TR cell during the discharge period.

## 6.5 The Model

### 6.5.1 Introduction

The TR cell contains approximately equal partial pressures of argon and water vapour. When a high power microwave pulse is applied, argon is ionized; the plasma then reflects the incident microwaves. At the end of the pulse, electrons are removed from the discharge through capture by water vapour. The operation of the TR cell is divided into cycles, lasting 1 ms, each comprising

- (1) the pulse, lasting 1  $\mu$ s
- (2) the recovery period, lasting 3  $\mu$ s
- (3) the period between pulses, lasting 996  $\mu$ s.

Initially, the number densities of argon and water vapour in the TR cell, for partial pressures of 10 torr, are  $3.3 \times 10^{17} \text{ cm}^{-3}$ . The electric field incident on the cell is  $4.268 \times 10^5 \text{ Vm}^{-1}$ , from Chapter 2. From equation (6.8) the electric field acting on each gas is  $2.134 \times 10^5 \text{ Vm}^{-1}$ . Using fig (6.4) we obtain a value of 13.6 eV for the mean electron energy in argon for the calculated value of E/N of 647 Td. The mean electron energy in water vapour has not been extensively studied to date. The mean electron energy in water vapour for E/N of 647 Td is calculated to be 11.5 eV (Gallagher et al (1983)). So, the mean electron energy in the mixture of argon and water vapour is taken to be 12.5 eV, which corresponds to an electron velocity of  $2.1 \times 10^6 \text{ ms}^{-1}$ . We use this

value for the mean electron energy in the discharge to obtain the appropriate rates of reaction for the species likely to be present in the discharge.

#### 6.5.2 The Microwave Pulse

A microwave pulse is applied for  $1 \mu\text{s}$ ; about  $0.01 \mu\text{s}$  after the start of the pulse, the gas in the cell is sufficiently ionized to reflect the microwaves. So we assume that the level of the discharge is constant throughout the pulse period. We also assume that the discharge is situated inside the input window of the cell throughout the pulse duration, although breakdown of the gas occurs initially at the keep-alive electrode. However, the discharge at the keep-alive electrode very rapidly transfers to the input window of the cell.

The reactions included in the computer model of the microwave pulse are those of electrons with argon atoms, producing metastables and ions (equations (6.1) and (6.2)) and the reactions of the argon ions with water vapour; the rates of which have been determined by Lindinger (1973) for a steady state negative glow of a hollow cathode discharge in argon with 0.15% water vapour. Reactions of neutral radicals also take place throughout this period. From fig (6.5) we see that the cross section for electron capture by water vapour is very small for the calculated mean electron energy in the pulse, so this reaction is not included here. Lindinger observed that the  $\text{H}_2\text{O}^+$  ion is formed mainly through secondary reactions, not by direct electron impact. The

ionization rate of water vapour in a microwave discharge is unknown. But we know that the energy required to ionize water vapour is 12.6 eV. The dissociation rate of water vapour by electrons in a microwave discharge is estimated to be  $2 \times 10^{-9} \text{ cm}^3 \text{ s}^{-1}$  (see Table 6.1). The energy required to produce argon metastables through electron collision is 11.55 and 11.72 eV respectively, below that for the ionization of water vapour. The rate of production of argon metastables is  $2 \times 10^{-13} \text{ cm}^3 \text{ s}^{-1}$  (see Table 6.1). It is likely, therefore that the ionization rate of water vapour is less than  $2 \times 10^{-13} \text{ cm}^3 \text{ s}^{-1}$ , and since the dissociation rate of water vapour is  $2 \times 10^{-9} \text{ cm}^3 \text{ s}^{-1}$ , dissociation is likely to be the main electron-water vapour reaction. So we do not consider electron impact ionization of water vapour.

The rates of reaction considered in the pulse period and their sources are listed in Table 6.1.

### 6.5.3 The Recovery Period

A few microseconds after the end of the microwave pulse the gas in the TR cell has sufficiently deionized to allow a low power microwave pulse to pass through the cell. In Chapter 2 we saw that an ionized gas with an electron density below the critical electron density (calculated to be  $1.09 \times 10^{18} \text{ m}^{-3}$  for this system) is transparent to microwaves. So, in a few microseconds the electron density falls from about  $5 \times 10^{21} \text{ m}^{-3}$  during the pulse (calculated in Chapter 2) to less than  $10^{18} \text{ m}^{-3}$ . Following the analysis of the recovery period, given in Chapter 2, we assume that the initial

fall in electron density occurs via capture of the fast, though rapidly slowing down, electrons by water vapour.

From the Kinetic Theory an electron loses on average  $2m/M$  of its energy per collision, where  $m$  is the mass of the electron and  $M$  the mass of the colliding particle. When an electron collides with an argon atom the electrons lose  $2.7 \times 10^{-5}$  of its energy per collision. The collision frequency for momentum transfer  $\nu_m$  is

$$\nu_m = N\sigma\bar{v} \quad , \quad (6.10)$$

where  $N$  is the atom number density,  $\sigma$  the collision cross section and  $\bar{v}$  the mean electron velocity. Using an average electron energy in the recovery period of 6.4 eV (approximately midway between the mean energy at the beginning and end of the recovery period, when the electrons have slowed down to room temperature) and the corresponding electron-argon collision cross section (Kaye and Laby (1975)) we calculate the collision frequency to be  $6.5 \times 10^{10} \text{ s}^{-1}$ . So we estimate that in  $0.5 \mu\text{s}$ , an electron loses all its energy through collisions. Allowing for the decrease in electron-argon collision cross section with electron energy, we consider that the recovery period lasts  $3 \mu\text{s}$ .

The mean electron energy in the recovery period corresponds to the electron energy for which the electron capture cross section for water vapour (see fig (6.5)) is a maximum. The reaction which occurs, leading to the production of  $\text{H}^-$  ions, is given in equation (6.4). The electron capture reactions leading to the production of  $\text{O}^-$  ions and  $\text{OH}^-$  ions have much lower cross sections at this electron energy, so they are not included in the model. But we

include the main reactions of the negative ions produced in equation (6.4) in the model. We assume that now the only reactions of the positive ions created during the microwave pulse are electron-ion recombination reactions, and that the argon metastable number density is reduced through collisions with electrons. Also included in the model of the recovery period are the reactions of the neutral radicals present.

The rates of the reactions considered in the recovery period and their sources are listed in Table 6.2.

#### 6.5.4 The Period Between Pulses

By now the electron density has fallen sufficiently for the TR cell to become transparent to microwaves. The electron temperature is now in thermal equilibrium with the atoms at room temperature. Following Chapter 2, we assume that in this period the main electron loss mechanism is electron-positive ion recombination. The cross section for electron capture by water vapour is negligible for low temperature electrons. In this period, reactions of the neutral radicals take place, through two and three body recombination in the gas volume or recombination on the TR cell window, which is adjacent to the discharge region.

The rates of the reactions considered in the period between pulses and their sources are listed in Table 6.3.

## 6.6 The Computer Program

The net rate of change of a species  $n$  in a system is expressed as the sum of the products of the rate constants for each reaction producing species  $n$  and the number densities of the reacting species minus the sum of the products of the rate constants for each reaction destroying  $n$  and the number densities of the reacting species. The resulting set of simultaneous first order differential equations, one for each species present in the cell, is integrated over the appropriate time interval, using a computer, to give the number densities of the species present at the end of the time interval. The number density of argon and of water vapour present initially in the cell is  $3.3 \times 10^{17} \text{ cm}^{-3}$ . The electron density at the beginning of each pulse is input to the program. It has the same value at the beginning of each pulse, since the dc discharge at the keep-alive electrode supplies a constant degree of ionization to the gas. The initial number densities of the other species present in the cell is input to the program. Their subsequent number densities are calculated in the program.

The sequence of operation of the computer program is as follows:

- (1) Input initial number densities of the species present
- (2) Calculate number densities of species present after the  
microwave pulse
- (3) Input number densities of species present after the microwave  
pulse

- (4) Calculate number densities of species after recovery period
- (5) Input number densities of species after the recovery period
- (6) Calculate number densities of species before the start of the next pulse
- (7) Input number densities of species before the start of the next pulse.

Stages 2-7, covering one cycle of  $10^{-3}$  seconds in the life of a TR cell, are repeated according to the number of pulses applied to the cell.

The computer program is listed in Appendix 6.

## 6.7 Results of the Computer Program

### 6.7.1 Number Densities of the Species Created Throughout a Cycle

The variables, which are input at the start of the program, are species number density, electron number density, ionization rate of argon and recombination rate of O, H and OH. First we consider the initial values of the variables in the program, which are listed in Appendix 6 and we examine the variation throughout a cycle of the number densities of species created. We see that the percentage changes in number densities between the end of the pulse and the end of the recovery period are less than 0.1% for most species. However, the number densities of  $H^-$  and  $OH^-$  increase by 36%, since they are created during the recovery period. The species lost through recombination are  $H_2O^+$ ,  $H_3O^+$  and e, which decrease by 0.2%, 0.8% and 8% respectively.

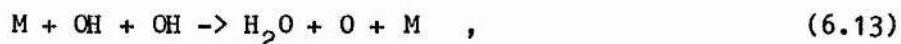
The number densities of most species change between the end of the recovery period and the start of the next pulse. The species which increase, by 0.05%, are  $H_2$  and  $O_2$ , created through radical recombination. The species which decrease significantly are  $H^-$ ,  $OH^-$ ,  $H$ ,  $OH$ ,  $ArH^+$ ,  $H_2O^+$  and  $H_3O^+$ , which decrease by 36%, 36%, 19%, 22%, 36%, 50% and 75% respectively. The number density of  $O$  decreases by 0.3% and that of  $e$  by 1.5%. The other species are unchanged throughout this period.

#### 6.7.2 Variation of the Ionization Rate of Argon

Data was unavailable for the rate of ionization of argon (equation (6.2)) in a microwave discharge. The rate of this reaction is important for the stability of the program. No solution is obtained when the rate exceeds  $7 \times 10^{-13} \text{ cm}^3 \text{ s}^{-1}$ , the other variables being at their initial values. For a 10-fold decrease in the ionization rate of argon, from  $10^{-14}$  to  $10^{-15} \text{ cm}^3 \text{ s}^{-1}$ , the number densities of  $OH^-$  and  $e$  increase, by 0.2% and 0.02% respectively. The decrease in number density is greatest for  $Ar^+$ ,  $ArH^+$ ,  $H_2O^+$  and  $H_3O^+$ , which all decrease by about 20%. The number densities of the other species decrease by between 0.1% and 0.3%. A further 10-fold decrease in the ionization rate has a less significant effect on the number densities of the species produced, with most of the species changing by less than 0.1%. However,  $Ar^+$ ,  $Ar^*$ ,  $ArH^+$ ,  $H_2O^+$  and  $H_3O^+$  all decrease by about 3%, being the species most directly affected by the change in the ionization rate of argon.

### 6.7.3 Variation of the Recombination Rate of O, H and OH Radicals

The recombination rates of H, OH and O radicals in this system are not accurately known, so we assume that they are equal for the recombination reactions



where M is the surface on which they recombine. For a recombination rate of  $1.8 \times 10^{-10} \text{ cm}^3 \text{ s}^{-1}$  or less, the computer program is stable. For a 10-fold decrease in the recombination rate from  $10^{-10}$  to  $10^{-11} \text{ cm}^3 \text{ s}^{-1}$ , the species which increase significantly are  $H^-$ , H, OH, O,  $OH^-$ ,  $H_2$  and  $ArH^+$ , which increase by between 20% and 71%. The electron number density increases by 1% for this decrease in recombination rate. The other species all decrease by between 0.1% and 3%. When the recombination rate is reduced by a further factor of 10, similar, but smaller, changes in the number densities of the species produced occur. This is due to the decreased significance of the recombination reactions. The decrease in the number density of O is greater than expected, due to a change in the dominant O reaction from recombination to reaction with OH.

#### 6.7.4 Variation of Input Electron Density

Next, we study the effect of varying the input electron density. The model is unstable for electron densities greater than  $10^9 \text{ cm}^{-3}$ . When the number density of electrons is increased from  $10^7$  to  $10^8$  to  $10^9 \text{ cm}^{-3}$ , the number densities of  $e$ ,  $\text{H}^-$ ,  $\text{O}_2$ ,  $\text{Ar}^+$ ,  $\text{H}_2$  and  $\text{H}_3\text{O}^+$  increase by about a factor of 10 also. Several species increase by a factor of about 3;  $\text{O}$ ,  $\text{OH}$  and  $\text{H}$ ; showing their dependence on electron density. The number density of  $\text{Ar}^+$  increases by factors of 15 and 28,  $\text{ArH}^+$  by 15 and 18 respectively and  $\text{H}_2\text{O}^+$  by 1.5 and 3 respectively. The number density of  $\text{H}_2\text{O}$  decreases slightly, to compensate for the increase in number densities of the other species. One species decreases with increasing electron number density,  $\text{OH}^-$ , by factors of 2/3 and 1/3 respectively.

#### 6.7.5 Variation of the Initial Number Density of the Species

It was observed that the number densities of the species produced was independent of initial number density (to the accuracy produced in the computer program), up to a number density of  $10^4 \text{ cm}^{-3}$ .

### 6.7.6 Comment on the Results

From the results of varying the various input parameters, we choose the values which model the operation of the TR cell most closely. We choose the largest input electron density for which the computer model is stable,  $10^9 \text{ cm}^{-3}$ , since this value corresponds most closely to that calculated in Chapter 2. We choose the initial species number density to be  $10^4 \text{ cm}^{-3}$ , which is the largest value which can be input without influencing the output number densities. The recombination rate of the O, H and OH radicals is chosen to be  $1.8 \times 10^{-10} \text{ cm}^3 \text{ s}^{-1}$  and the ionization rate of argon is chosen to be  $10^{-15} \text{ cm}^{-3} \text{ s}^{-1}$ , since they give results which most closely model the TR cell performance. The optimum rates and number densities are listed in Appendix 6. In figs (6.6) to (6.9) are shown the graphs of species number density at the beginning of each pulse, as a function of number of pulses.

From the results of the measurements on the TR cell described in Chapters 4 and 5, we expect to see the production of oxygen and hydrogen and the loss of water vapour throughout the operating time of the cell. We observed that after a few hundred hours of operation, a cell has lost a substantial partial pressure of water vapour, of the order of a few torr. If we assume that a loss of 5 torr of water vapour leads to cell failure, we find that the cell has an expected lifetime of 39.3 minutes (by extrapolating from the number densities of water vapour calculated at 500 pulse intervals, up to 2500 pulses (see fig (6.6))). This lifetime is about two

orders of magnitude shorter than expected. One reason for this result may be the inclusion of dissociation rates of  $H_2O$ ,  $O_2$  and  $H_2$  appropriate to a hollow cathode glow discharge, which may be significantly different to the equivalent rates in a microwave discharge. The model also makes no allowance for the release of water vapour from the cell surface, prolonging the cell life.

In Chapter 2 we calculated the electron density at the end of the pulse to be about  $5 \times 10^{15} \text{ cm}^{-3}$ . Here, for an input electron density of  $10^9 \text{ cm}^{-3}$ , we obtain electron densities of  $1.0114 \times 10^9 \text{ cm}^{-3}$  at the end of the pulse, falling to  $9.314 \times 10^8 \text{ cm}^{-3}$  at the end of the recovery period and  $9.2 \times 10^8 \text{ cm}^{-3}$  by the beginning of the next pulse. So, in the model insufficient electrons are created in a pulse and insufficient numbers recombine when the pulse stops. Number densities of argon ions present are about six orders of magnitude less than those of argon metastables, which agrees with observations made of the microwave excited emission spectrum from argon. There, only transitions due to excited argon atoms and not from excited argon ions were seen. Number densities of all the ions are several orders of magnitude lower than those of the radicals, which agrees with their much higher reaction rates and the greater amount of energy required for their production. Also, during the pulse  $Ar^+$  may be formed in a two-step reaction involving collisions between excited argon atoms. The pulse duration is 1 s; hence insufficient time may be available for the reaction.

## 6.8 Surface Reactions

### 6.8.1 Chemisorption

Chemisorption involves the transfer of electrons between a solid and a gas, so a monolayer of gas is formed on the surface of the solid. Chemisorption readily occurs during adsorption at a heated surface. Inert gases are not chemisorbed.

### 6.8.2 Absorption

Absorption occurs when a gas molecule diffuses into a solid. Gases diffuse through a solid according to Fick's law, discussed in Chapter 2 and given in equation (2.7). Rare gases and polyatomic molecules do not diffuse noticeably through metals.

### 6.8.3 Adsorption

The surface of a solid exerts forces of attraction normal to the surface, Van der Waals forces, on polar molecules which are adsorbed on collision with it. One or more layers of gas may be formed on the surface of the solid. Physical adsorption is instantaneous and reversible and decreases with increasing temperature. Gases adsorbed as a result of thermal activation, however, cannot be removed at that temperature but only at higher temperatures. The adsorption of a given component of a

multicomponent gas mixture increases with increasing partial pressure. Hydrogen, due to its small size, is strongly adsorbed while noble gases are not, due to their chemical inactivity. Very little gas can remain adsorbed at room temperature in a high vacuum.

#### 6.8.4 Outgassing

Heating a surface accelerates the rate of outgassing or desorption. It may also cause activated chemisorption of physically adsorbed gas, in particular water vapour. Water vapour can then be desorbed only by prolonged heating at much higher temperatures than those at which chemisorption occurred.

#### 6.8.5 Cleanup in TR Cells

Cleanup of the gas in a TR cell is defined as the active absorption of the gas by the cell, through the action of the discharge. The cleanup rate varies with discharge intensity, ambient temperature, wall materials and gas type. Several mechanisms may be in operation during cleanup;

- (1) Chemical action between the gas and wall
- (2) Mechanical action between the gas and wall
- (3) Chemical action due to active species
- (4) Mechanical occlusion of the gas in the wall
- (5) Mechanical occlusion of the gas in the sputtered deposit.

If sputtering occurs, cleanup proceeds at a rate greater than if sputtering is absent. Gas may be captured by chemical reaction

with the metal or mechanically buried beneath the relatively enormous masses of high velocity metal striking the wall, due to sputtering.

According to Blodgett and Vanderslice (1960), cleanup of rare gases in a cell in which metal is being sputtered is governed largely by the rate at which metal is sputtered. The cleanup rate increases with increasing discharge intensity. Cleanup due to an electrodeless discharge in a glass tube proceeds by ion penetration of the walls of the tube. The probability of cleanup of a given ion is higher the higher its kinetic energy, since a faster moving ion penetrates further into the surface and spends a longer time in the vicinity of the surface where it can be buried by the sputtered metal.

Maddix (1968) carried out a series of investigations into cleanup in TR cells. The cleanup rate of hydrogen was measured for quartz, 7070 glass, copper, nickel, molybdenum and kovar by monitoring the changes in partial pressures of the gases in the cell. Maddix describes the process of cleanup in terms of a physical model, where the container surface is bombarded with energetic ions from the plasma. The ions penetrate a short distance into the surface where they are trapped and neutralised. The lifetime of the trapped ions is of the order of  $1 \mu\text{s}$ . The majority of these molecules are then desorbed. However, some are absorbed and diffuse into the surface, causing cleanup.

Maddix observed that cleanup of argon in a TR cell is negligible in comparison with cleanup of the other gases contained within, since it is sputter buried only. He observed that, in the TR cell, cleanup on the glass window and at the cones is negligible in comparison with cleanup at the kovar window frame and that hydrogen is very rapidly cleaned up by the kovar.

Paik et al (1970) have investigated the microwave discharge in a TR cell, to discover the active discharge area and the critical regions of gas sorption in the cell. From the work of Maddix described above, the major source of cleanup in a TR cell was found to be of hydrogen on the kovar window frame. His cells were filled with a mixture of gases; argon, water vapour, hydrogen and tritium as a radioactive tracer. One cell was operated with a discharge for six hours, one was not. A comparison of the amount of radioactive gas absorbed by each cell showed that cleanup occurred only in the cell containing the discharge, and that it took place almost exclusively at the input window frame. Paik et al suggest that a reasonable estimate of the cleanup area is the exposed area of kovar window frame.

#### 6.8.6 Discussion of our TR Cell Manufacturing Procedures

During the initial filling procedure (hot exhaust stage) the TR cell is evacuated to a pressure of  $4 \times 10^{-5}$  torr and baked at  $300^{\circ} \text{C}$  for 75 minutes. Heating the cell under vacuum accelerates the desorption of gas from its surface so, by the end of 75 minutes

under vacuum at 300°C, the cell is relatively free of gas adsorbed or adsorbed. The cell is then allowed to cool to 100°C and then 7 torr water vapour and 12 torr oxygen are added. The cell is left to stand for 5 minutes, during which time water vapour and oxygen are adsorbed by the cell body (adsorption is effectively instantaneous). The cell is roughly pumped out and 14 torr water vapour and 9.5 torr argon are added. Water vapour is adsorbed by the surface of the cell and absorbed by the body. It can then be released later in the life of the cell, to replace water vapour lost through dissociation in the microwave discharge.

#### 6.9 Surface Recombination

In Chapter 3, we saw that if sufficient incident power was applied to the TR cell, its input window failed, either by melting or cracking. The mechanism by which the window fails is not known. In Chapter 2 we calculated that the amount of power absorbed by the window when a microwave pulse was applied did not exceed 0.24% of the incident power, at an incident power level sufficient to cause window failure. When the gas in the TR cell has broken down, the discharge is situated just inside its input window. The arc loss, the power dissipated in the discharge, contains sufficient power to damage the window. So, it is likely that the power which damages the window comes directly from the discharge.

There are several mechanisms whereby an ionized gas may transfer heat to the surrounding walls:

- (1) Recombination of ions and electrons which diffuse to the walls
- (2) Excited atoms give up their excitation energy at the walls
- (3) Dissociated atoms reassociate at the walls and give up their dissociation energy

The probability of recombination per collision of H, OH and O radicals on glass surfaces,  $\gamma$ , has been investigated (Mandl and Salop (1973), Smith and Austin (1974), Wood and Wise (1962), Greaves and Linnett (1958) and Smith (1943)). The values of  $\gamma$  obtained by the above authors are tabulated below:

Table 6.4

Value of $\gamma$	Radical	Surface	Source
$8 \times 10^{-5}$	OH	pyrex	Smith
$1.2 \times 10^{-4}$	O	pyrex	Greaves and Linnett
$5.8 \times 10^{-3}$	H	pyrex	Wood and Wise
$2.6 \times 10^{-4}$ to $5.2 \times 10^{-4}$	O	pyrex	Smith and Austin
$5.5 \times 10^{-4}$ to $1.9 \times 10^{-3}$	H	borosilicate	Mandl and Salop

Smith gives the energy liberated on recombination of H as 4.3 eV and of H and OH as 5.5 eV. Wood and Wise observed that  $\gamma$  increased with increasing surface temperature. If we assume an average lower bound for  $\gamma$  of  $10^{-4}$  for OH, H and O and an average energy liberated per recombination of 5 eV, we can calculate a lower bound for the energy transfer to the TR cell window via surface recombination. In the computer model, the rates of dissociation of  $H_2O$ ,  $H_2$  and  $O_2$

by electrons are assumed to be  $2 \times 10^{-9} \text{ cm}^3 \text{ s}^{-1}$ . The pulse duration is  $1 \mu\text{s}$ , the water vapour number density is  $3.3 \times 10^{23} \text{ m}^{-3}$  and the electron number density in the discharge is  $5 \times 10^{21} \text{ m}^{-3}$  (calculated in Chapter 2), so we calculate the total number density of OH and H created to be  $3.3 \times 10^{24} \text{ m}^{-3}$ . The collision frequency  $f$  per unit area on a surface is

$$f = N\bar{c}/4 \quad , \quad (6.14)$$

where  $N$  is the particle number density and  $\bar{c}$  the mean velocity, given by

$$\bar{c} = (8kT/\pi m)^{1/2} \quad , \quad (6.15)$$

and  $T$  and  $m$  are the particle mass and velocity. For OH radicals at room temperature,  $\bar{c}$  is  $602 \text{ ms}^{-1}$ . The window area is  $15 \times 3 \text{ mm}^2$ . Hence, for  $\gamma$  equalling  $10^{-4}$  and for 5 eV liberated per collision, we calculate the energy transferred to the window per second to be at least 1.8 W. This value is a lower bound for the energy transferred through surface recombination;  $\gamma$  increases with surface temperature, so the hotter the window becomes, the more likely a recombination reaction becomes. This is one reason for the centre of the window failing; heat is not conducted quickly away, due to the low thermal conductivity of the glass, so the recombination rate increases, adding more heat to the centre. Eventually, its temperature reaches failure temperature. Also, with higher input powers, the molecules are raised to temperatures greater than room temperature, increasing the recombination rate still further.

## 6.10 Conclusions

The computer model of the microwave discharge in the TR cell predicts a lifetime for the cell which is about two orders of magnitude smaller than expected, but predicts the production of oxygen and hydrogen, which has been observed in Chapters 4 and 5. However, the model does not produce the expected electron number densities throughout a cycle; the calculated rates of production and loss are lower than expected. Number densities of the other species produced compare well with experimental evidence, as far as it exists. Calculations have shown that radical recombination on the TR cell window can produce sufficient heat to cause window failure.

Rates of reaction were adapted from the available literature to model this particular discharge. They may not be accurate. Only the fastest reactions were incorporated in this model. It is likely that some reactions of importance have not been included in the model, such as the cleanup of hydrogen at the kovar window frame in the cell, the reduction of gas pressure through sputtering and reactions of the species in the cell with the cell itself. More information is required on reactions and their rates in the microwave discharge in order to successfully model such a complicated system as the microwave discharge in the TR cell. Such a model would enable predictions to be made of the expected lifetimes of TR cells containing gases with different partial pressures than the one modelled here, thus reducing life test

trials. Information on the number densities of species produced throughout the lifetime of the cell may be used to improve performance and/or life. A successful model of the TR cell discharge would reduce development times for new devices and help to improve their performance.

## References

- D L Baulch, D D Drysdale, D G Horne and A C Lloyd (1976)  
Evaluated Kinetic Data for High Temperature Reactions Vol 1  
Butterworths, London
- M A Biondi (1963) Studies of the Mechanism of Electron-Ion Recombination  
I, Phys Rev 129, 1181
- A B Blagoev and Te Popov (1979) Investigation of the Electron Energy  
Distribution Function in an Argon Afterglow Plasma, Phys Lett 70A, 416
- K B Blodgett and T A Vanderslice (1960) Mechanism of Inert Gas  
Cleanup in a Gaseous Discharge, J App Phys 31, 1017
- I S Buchel'nikova (1959) Cross Sections for the Capture of Slow Electrons  
by O<sub>2</sub> and H<sub>2</sub>O Molecules and Molecules of Halogen Compounds,  
Sov Phys JETP 35(8), 783
- A Chutjian and D C Cartwright (1981) Electron Impact Excitation of  
Electronic States in Argon at Incident Energies Between 16 and 100 eV,  
Phys Rev A 23, 2178
- R N Compton and L G Christophorou (1967) Negative Ion Formation in  
H<sub>2</sub>O and D<sub>2</sub>O, Phys Rev 154, 110
- R W Crompton, J A Rees and R L Jory (1965) The Diffusion and Attachment  
of Electrons in Water Vapour, Aust J Phys 18, 541
- E Eggarter (1975) Comprehensive Optical and Collision Data for  
Radiation Action II Argon, J Chem Phys 62, 833
- C M Ferreira and J Loureiro (1983) Electron Transport Parameters  
and Excitation Rates in Argon, J Phys D 16, 1611
- L S Frost and A V Phelps (1964) Momentum Transfer Cross Sections for  
Slow Electrons in He, Ar, Kr and Xe from Transport Coefficients  
Phys Rev A 136, 1538

- J W Gallagher, E C Beaty, J Dutton and L C Pitchford (1983), An Annotated Compilation and Appraisal of Electron Swarm Data in Electronegative Gases, J Phys Chem Ref Data 12, 109
- J C Greaves and J W Linnett (1958) Recombination of Oxygen Atoms at Surfaces, Trans Faraday Soc 54, 1323
- F P Del Greco and F Kaufman (1962) Lifetime and Reactions of OH Radicals in Discharge Flow Systems, Disc Faraday Soc 33, 128
- D W Howgate (1962) Dissociation of the Hydroxyl Radical in an rf Discharge, J Chem Phys 36, 239
- G S Hurst, L B O'Kelly and T E Bortner (1961) Dissociative Electron Capture in Water Vapour, Phys Rev 123, 1715
- J H Jacob and J A Mangano (1976) Total Electron Impact Excitation Cross Sections of Ar and Kr, App Phys Lett 29, 467
- F Kaufman and F P Del Greco (1961) Formation, Lifetime and Decay of OH Radicals in Discharge-Flow Systems, J Chem Phys 35, 1895
- G W C Kaye and T H Laby (1975) Tables of Physical and Chemical Constants and Some Mathematical Functions, Longman, London
- H N Kucukarpaci and J Lucas (1981) Electron Swarm Parameters in Argon and Krypton, J Phys D 14, 2001
- W Lindinger (1973) Reaction Rate Constants in Steady-State Hollow Cathode Discharges: Ar+H<sub>2</sub>O Reactions, Phys Rev A 7, 328
- H S Maddix (1968) Clean-Up in TR Tubes, IEEE Trans Electron Dev E D 15, 98
- A Mandl and A Salop (1973) Magnetic Resonance Spectrometer Measurements of Atomic Hydrogen Surface Recombination, J App Phys 44, 4702
- M M Mann, A Hustrulid and J T Tate (1940) The Ionization and Dissociation of Water Vapour and Ammonia by Electron Impact, Phys Rev 58, 340
- C E Melton (1970) Radiolysis of Water Vapour in a Wide Range Radiolysis

- Source of a Mass Spectrometer I Individual and Total Cross Sections for the Production of Positive Ions, Negative Ions and Free Radicals by Electrons, J Phys Chem 74, 582
- C E Melton (1972) Cross Sections and Interpretation of Dissociative Attachment Reactions Producing  $\text{OH}^-$ ,  $\text{O}^-$  and  $\text{H}^-$  in  $\text{H}_2\text{O}$ , J Chem Phys 57, 4218
- C E Melton and G A Neece (1971) Rate Constants and Cross Sections for the Production of  $\text{OH}^-$  from  $\text{O}^-$  and  $\text{H}^-$  in Water, J Am Chem Soc 93, 6757
- M Pahl, W Lindinger and F Howorka (1972) Mass Spectrometric Studies of the Negative Glow of a Cylindrical Hollow Cathode Discharge, Z Naturforsch A 27a, 678
- S F Paik, H S Maddix, J D Keith and W R Ghen (1970) Radioactive Tracer Study of Gas Cleanup in Duplexer Discharges, IEEE Trans Electron Dev E D , 378
- L R Peterson and J E Allen (1972) Electron Impact Cross Sections for Argon, J Chem Phys 56, 6068
- D Rapp and P Englander-Golden (1965) Total Cross Sections for Ionization and Attachment in Gases by Electron Impact, J Chem Phys 43, 1464
- A Rutscher and H E Wagner (1983) Modelling of Water Vapour Dissociation in Hollow Cathode Glow Discharges, 16th International Conference in Ionized Gases, Proceedings, Dusseldorf, Germany
- M Shaper and H Scheibner (1969) Absolute Determination of the Total Excitation Cross Sections of Inert Gases by Electron Collision, Beitr Plasmaphys 9, 45
- J Schutten, F J De Heer, H R Moustafa, A J H Boerboom and J Kistemaker (1966) Gross- and Partial-Ionization Cross Sections for Electrons on Water Vapour in the Energy Range 0.1-20 keV, J Chem Phys 44, 3924
- R V Shukla, S K Jain, S K Gupta and A N Srivastava (1970) Experimental Study of the Deactivation of Excited H Atoms by

- Atmospheric Gases, J Chem Phys 52, 2744
- W V Smith (1943) The Surface Recombination of H Atoms and OH Radicals,  
J Chem Phys 11, 110
- A L S Smith and J M Austin (1974) Atomic Oxygen Recombination in  
Carbon Dioxide Laser Gases, J Phys B 7, L191
- K Smith and R M Thomson (1978) Computer Modelling of Gas Lasers,  
Plenum, New York
- L T Specht, S A Lawton and T A De Temple (1980) Electron Ionization  
and Excitation Coefficients for Ar, Kr and Xe in the Low E/N  
Region, J App Phys 51, 166
- M Venugopalan and R A Jones (1966) Chemistry of Dissociated Water  
Vapour and Related Systems, Chemical Reviews 66, 133
- W C Wang and L C Lee (1985) Electron Attachment to Water Vapour in  
Ar, N<sub>2</sub> and CH<sub>4</sub> in Electric Field, J App Phys 57, 4360
- J M Warman E S Sennhauser and D A Armstrong (1979) Three-Body Electron  
Ion Recombination in Molecular Gases, J Chem Phys 70, 995
- B J Wood and H Wise (1962) The Kinetics of Hydrogen Atom Recombination  
on Pyrex Glass and Fused Quartz, J Phys Chem 66, 1049

Table 6.1 Reactions Which Occur During the Microwave Pulse

Reaction	Rate /cm <sup>-3</sup> s <sup>-1</sup>	Reference
Ar + e → Ar <sup>+</sup> + 2e		
Ar + e → Ar* + e	2.1x10 <sup>-13</sup>	Kucuparci and Lucas (1981)
Ar* + Ar* → Ar <sup>+</sup> + Ar + e	1.2x10 <sup>-9</sup>	Blagoev and Popov (1979)
Ar <sup>+</sup> + H <sub>2</sub> O → ArH <sup>+</sup> + OH	1.2x10 <sup>-9</sup>	Lindinger (1973)
Ar <sup>+</sup> + H <sub>2</sub> O → Ar + H <sub>2</sub> O <sup>+</sup>	1.5x10 <sup>-10</sup>	"
H <sub>2</sub> O <sup>+</sup> + H <sub>2</sub> O → H <sub>3</sub> O <sup>+</sup> + OH	1.3x10 <sup>-9</sup>	"
ArH <sup>+</sup> + H <sub>2</sub> O → H <sub>3</sub> O <sup>+</sup> + Ar	4.5x10 <sup>-9</sup>	"
H <sub>2</sub> O + e → H + OH + e	2x10 <sup>-9</sup>	Rutscher and Wagner (1983)
H <sub>2</sub> + e → H + H + e	2x10 <sup>-9</sup>	"
O <sub>2</sub> + e → O + O + e	2x10 <sup>-9</sup>	"
O + O → O <sub>2</sub>		
H + H → H <sub>2</sub>		
OH + OH → H <sub>2</sub> O + O		
OH + OH → H <sub>2</sub> O + O	2.5x10 <sup>-12</sup>	Del Greco and Kaufman (1962)
OH + O → O <sub>2</sub> + H	2x10 <sup>-11</sup>	"

Table 6.2 Reactions Taking Place During the Recovery Time

Reaction	Rate / cm <sup>-3</sup> s <sup>-1</sup>	Reference
Ar <sup>#</sup> + e → Ar + e	2.8x10 <sup>-10</sup>	Blagoev and Popov (1979)
Ar <sup>+</sup> + e → Ar	6x10 <sup>-10</sup>	Biondi (1963)
H <sub>2</sub> O <sup>+</sup> + e → H <sub>2</sub> O	4.1x10 <sup>-6</sup>	Warman, Sennhauser and Armstrong (1979)
H <sub>3</sub> O <sup>+</sup> + e → H <sub>2</sub> O + H	1.1x10 <sup>-6</sup>	Lindinger (1973)
e + H <sub>2</sub> O → H <sup>-</sup> + OH	1.3x10 <sup>-13</sup>	Melton (1972)
H <sup>-</sup> + H <sub>2</sub> O → OH <sup>-</sup> + 2H	3.8x10 <sup>-9</sup>	Melton and Neece (1971)
OH <sup>-</sup> + H → H <sub>2</sub> O + e	1.0x10 <sup>-9</sup>	Smith and Thomson (1978)
O + O → O <sub>2</sub>		
H + H → H <sub>2</sub>		
OH + OH → H <sub>2</sub> O + O		
OH + OH → H <sub>2</sub> O + O	2.5x10 <sup>-12</sup>	Del Greco and Kaufman (1962)
OH + O → O <sub>2</sub> + H	2x10 <sup>-11</sup>	"

Table 6.3 Reactions Taking Place Before the Next Pulse

Reaction	Rate / cm <sup>-3</sup> s <sup>-1</sup>	Reference
Ar <sup>#</sup> + e → Ar + e	2.8x10 <sup>-10</sup>	Blagoev and Popov (1979)
Ar <sup>+</sup> + e → Ar	6x10 <sup>-10</sup>	Biondi (1963)
H <sub>3</sub> O <sup>+</sup> + e → H <sub>2</sub> O + H	1.1x10 <sup>-6</sup>	Lindinger (1973)
H <sub>2</sub> O <sup>+</sup> + e → H <sub>2</sub> O	4.1x10 <sup>-6</sup>	Warman, Sennhauser and Armstrong (1979)
O + O → O <sub>2</sub>		
H + H → H <sub>2</sub>		
OH + OH → H <sub>2</sub> O + O		
OH + OH → H <sub>2</sub> O + O	2.5x10 <sup>-12</sup>	Del Greco and Kaufman (1962)
OH + O → O <sub>2</sub> + H	2x10 <sup>-11</sup>	"

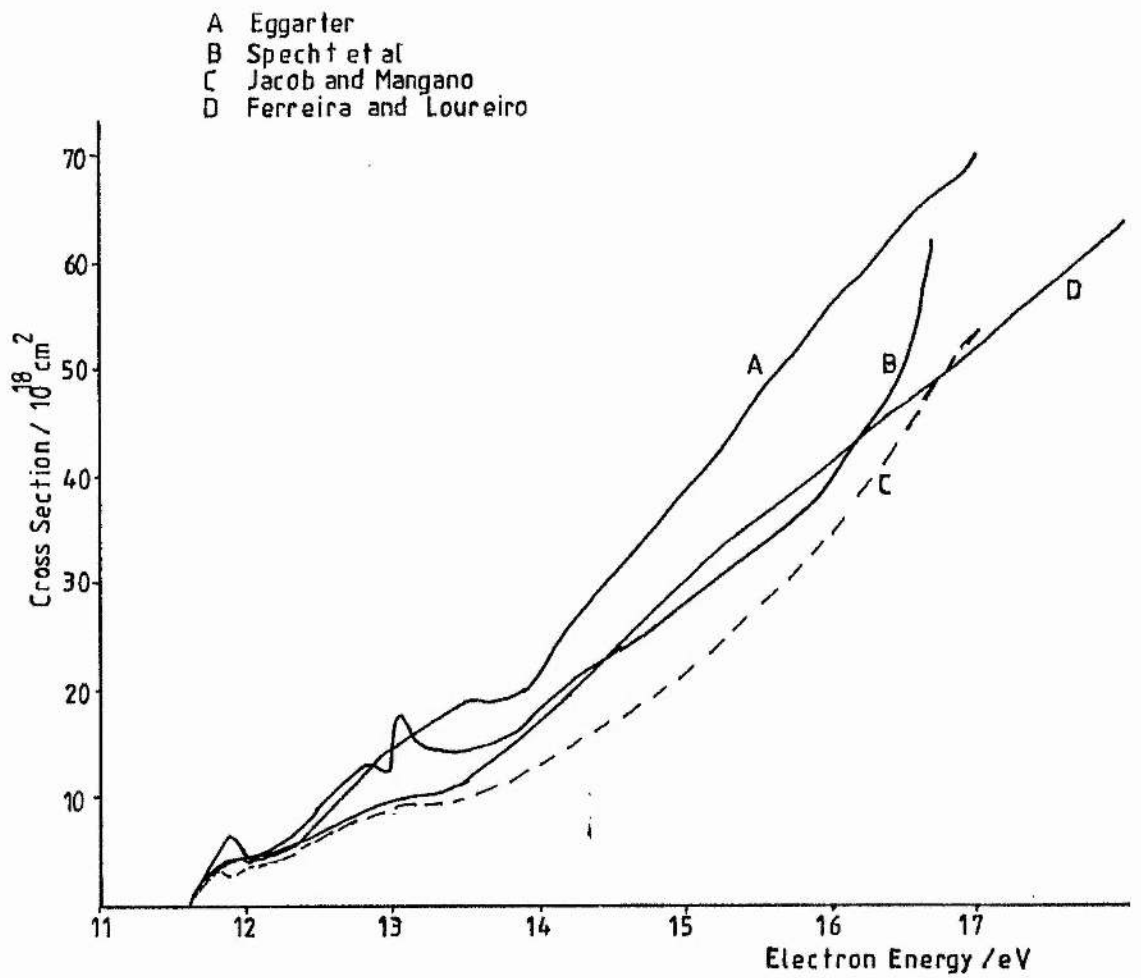


Fig 6-1 Total Excitation Cross Section for Argon

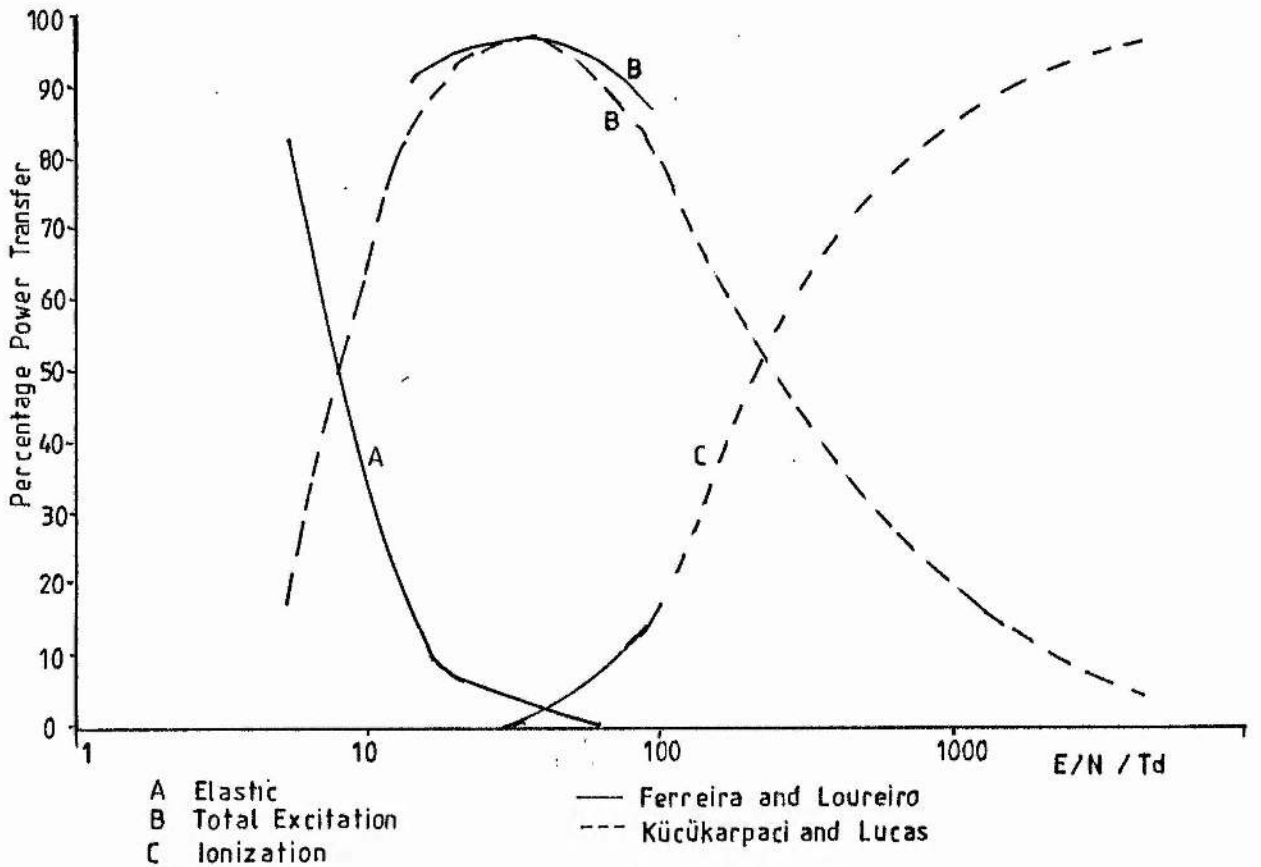


Fig 6-2 Percentage Electron Energy Losses in Argon

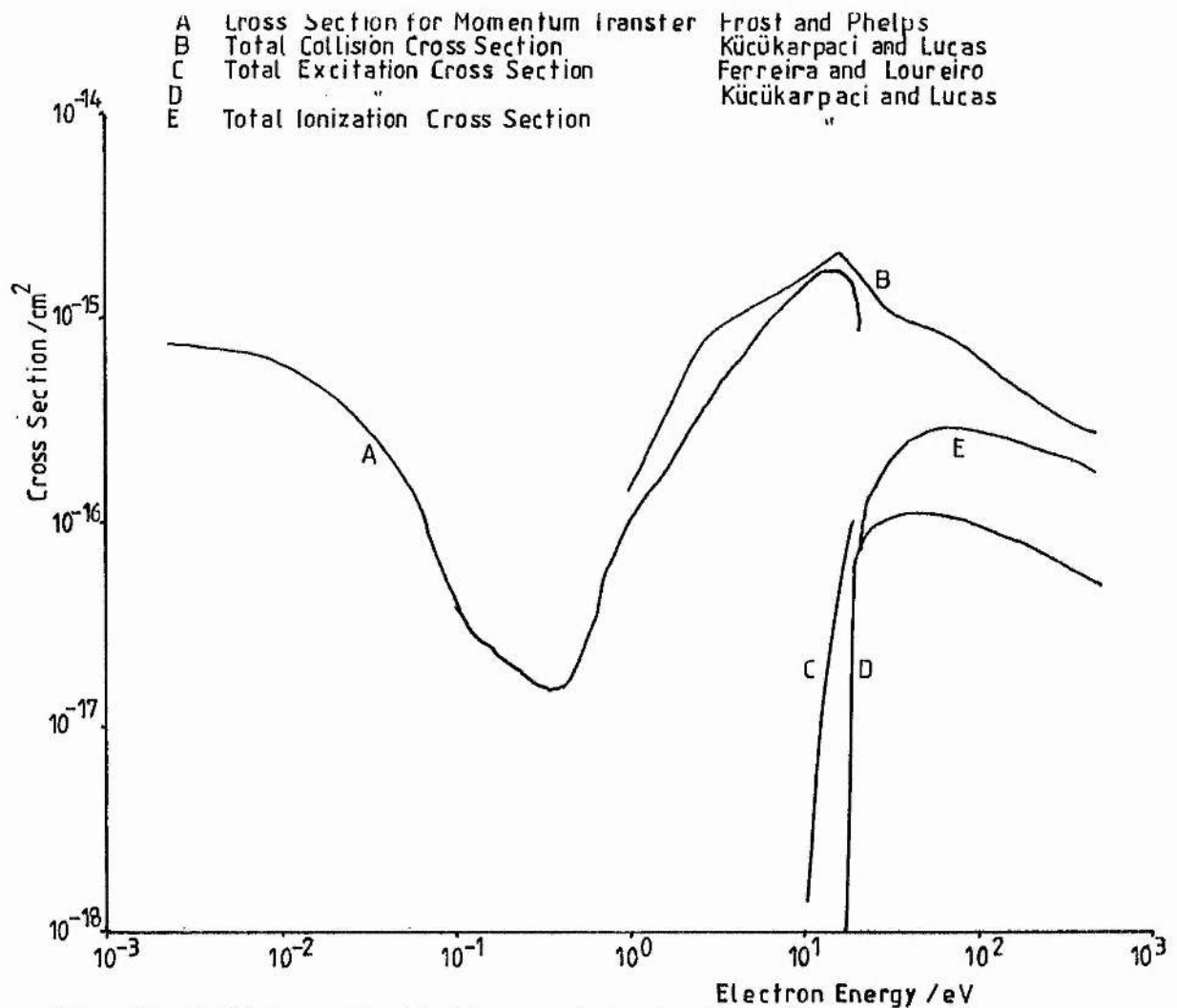


Fig 6.3 Collision, Excitation and Ionization Cross Sections in Argon as a function of Electron Energy

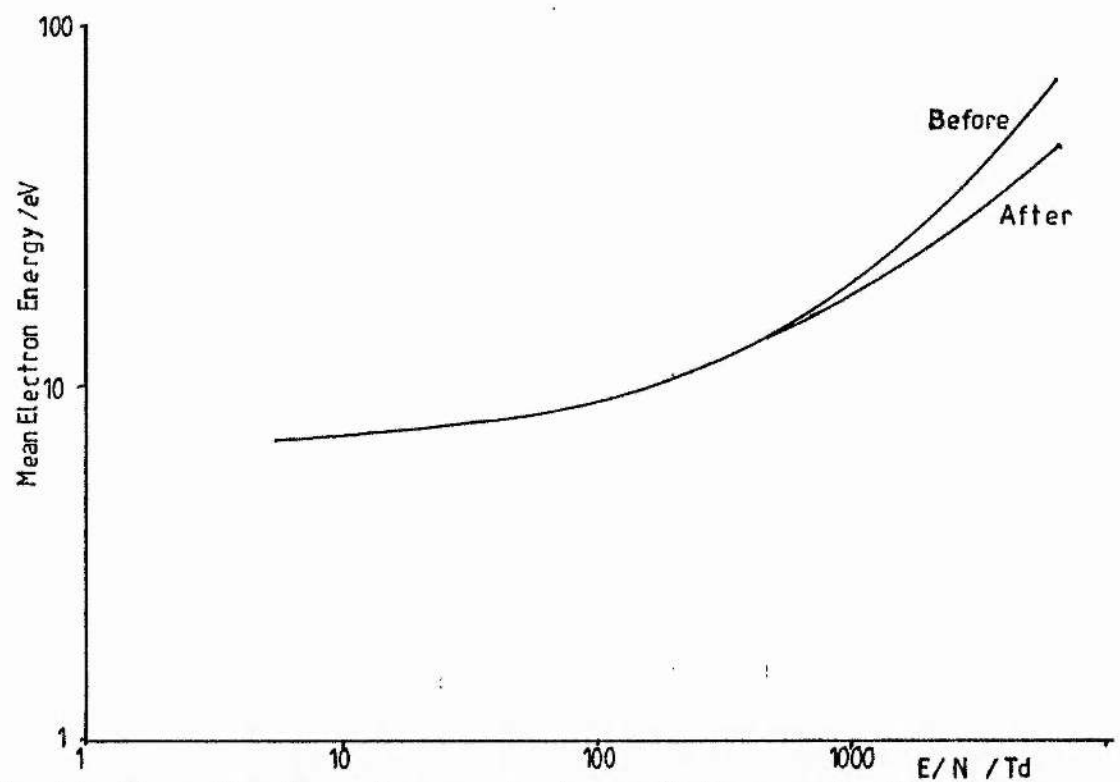


Fig 6.4 Mean Electron Energy in Argon Before and After a Collision

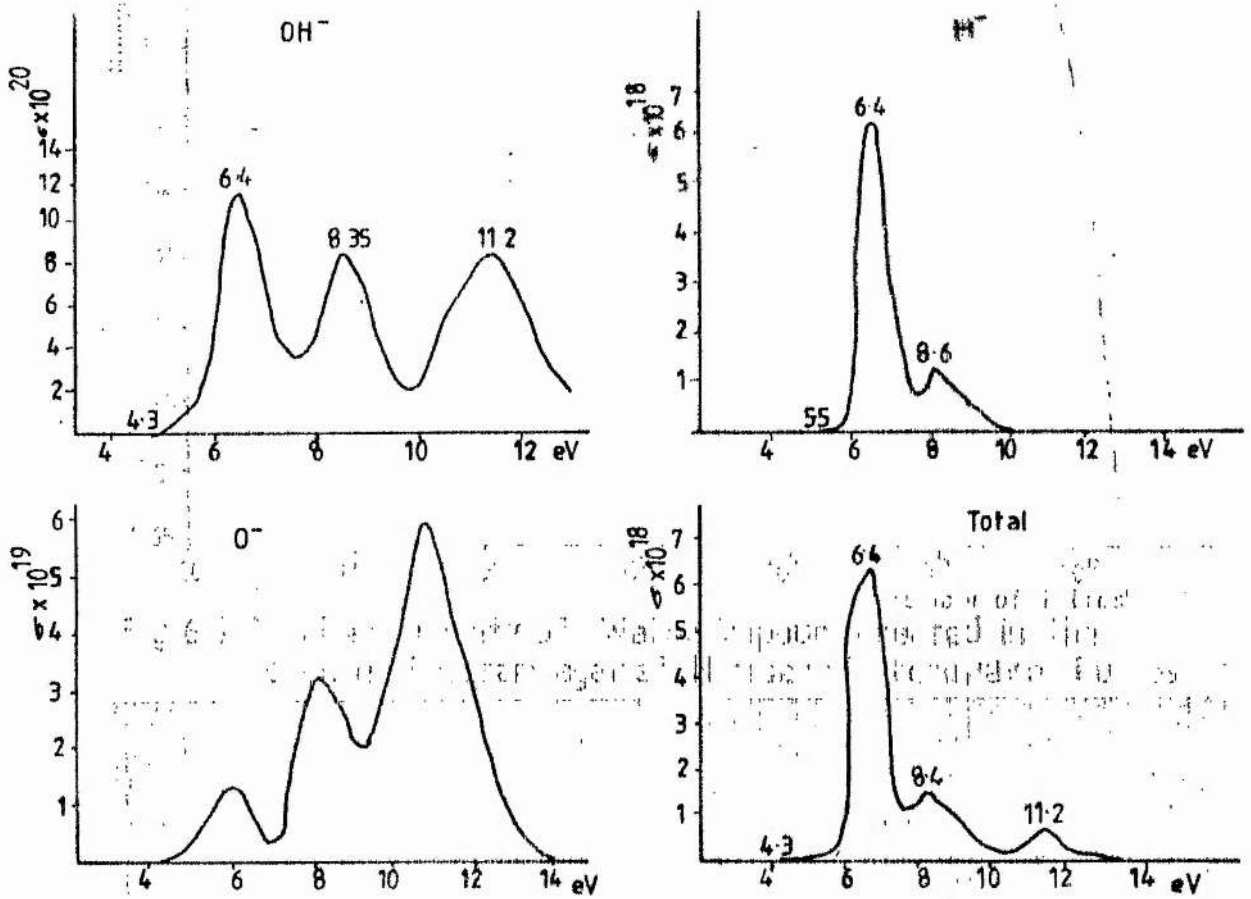


Fig 65 Dissociative Attachment Cross Sections  $\sigma$  for Water Vapour as a Function of Electron Energy

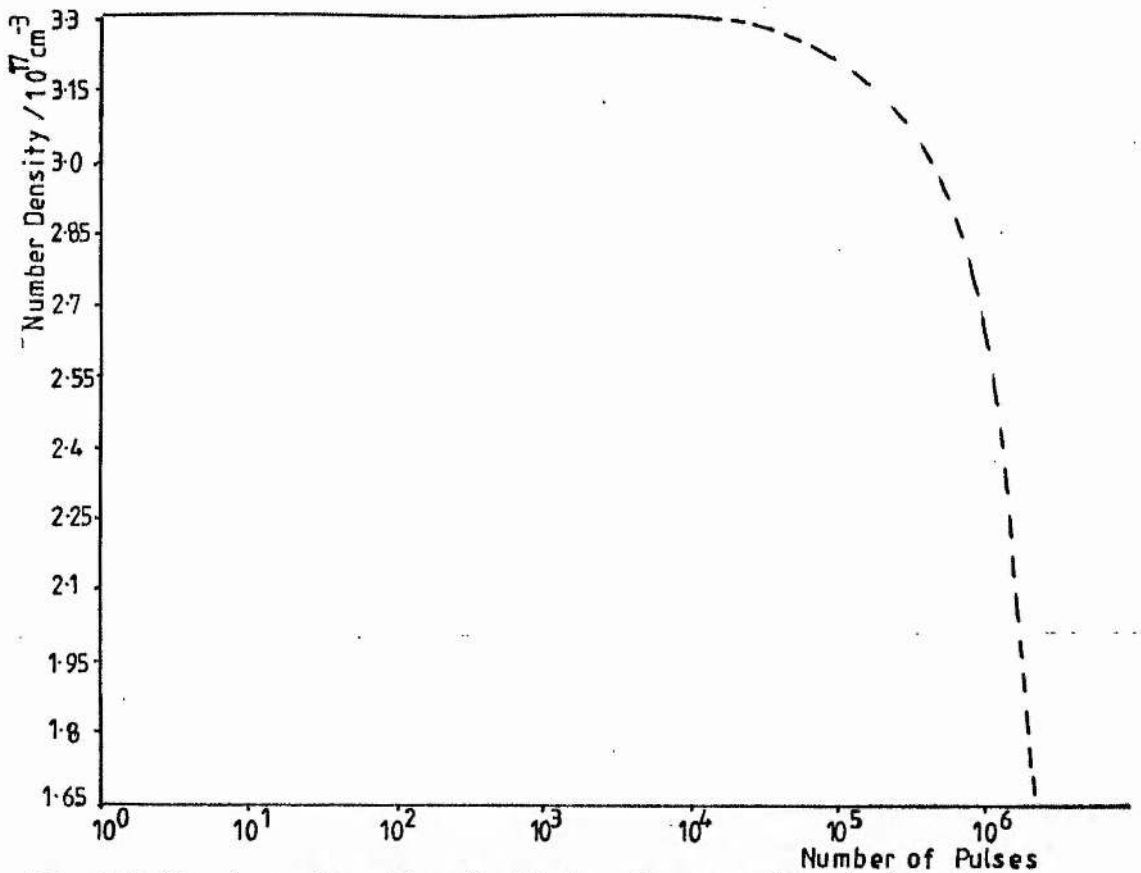


Fig 6.6 Number Density of Water Vapour Created in the Computer Program against Number of Microwave Pulses

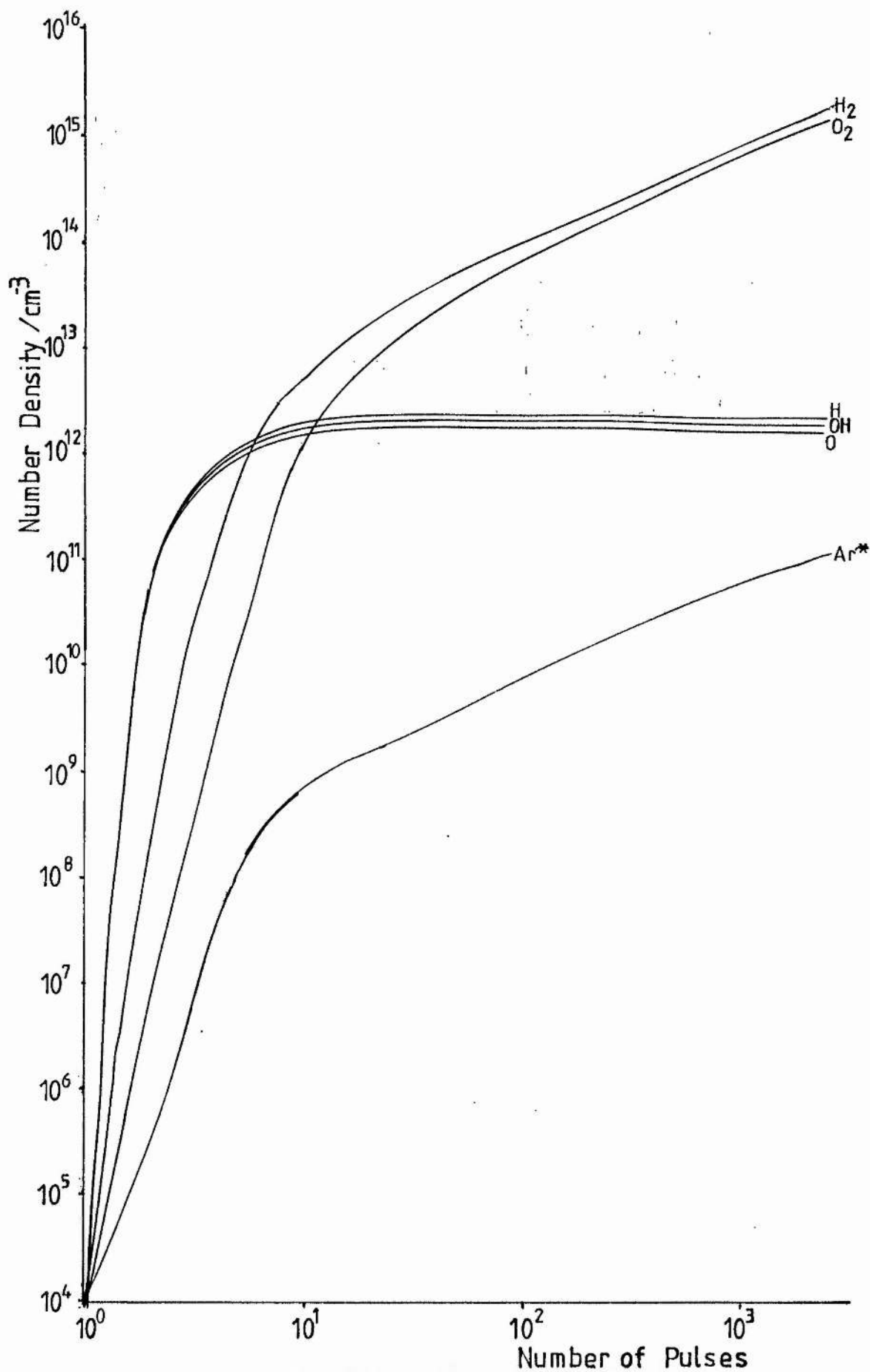


Fig 6-7 Number Densities of Species Created in the Computer Program against Number of Microwave Pulses

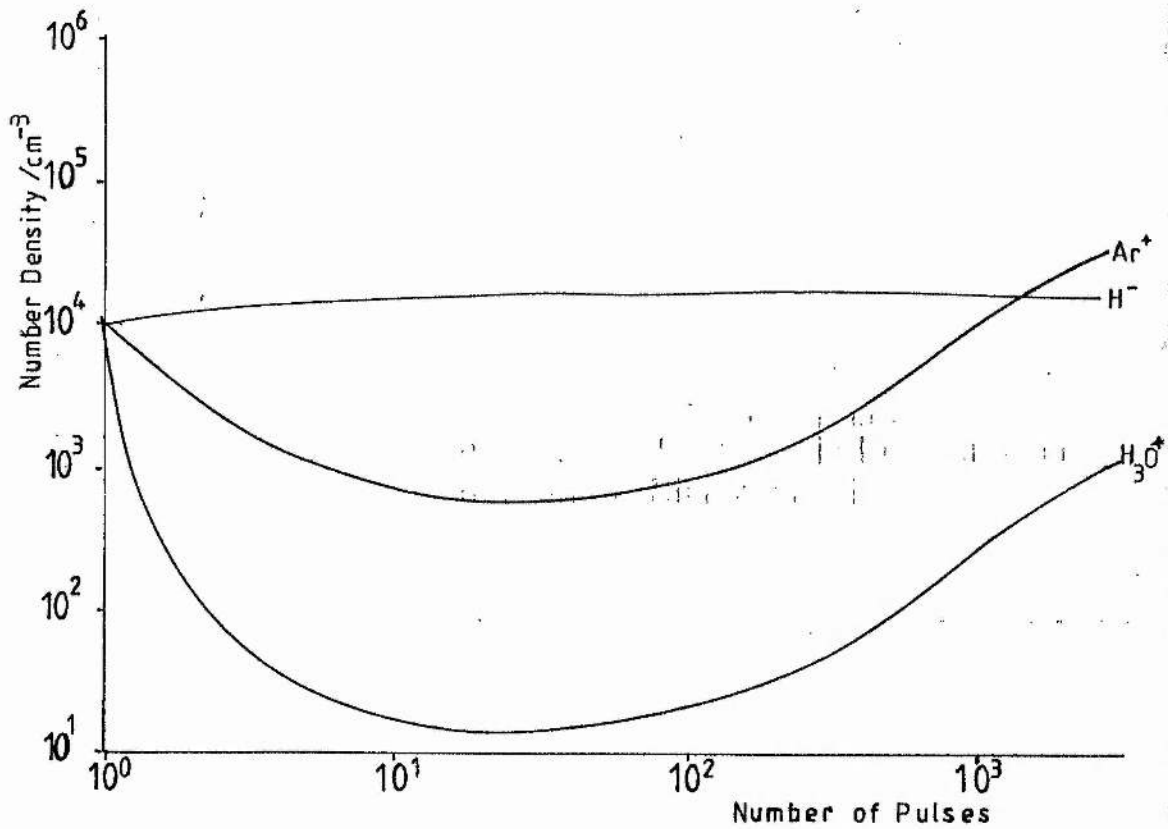


Fig 6-8 Number Densities of Species Created in the Computer Program against Number of Microwave Pulses

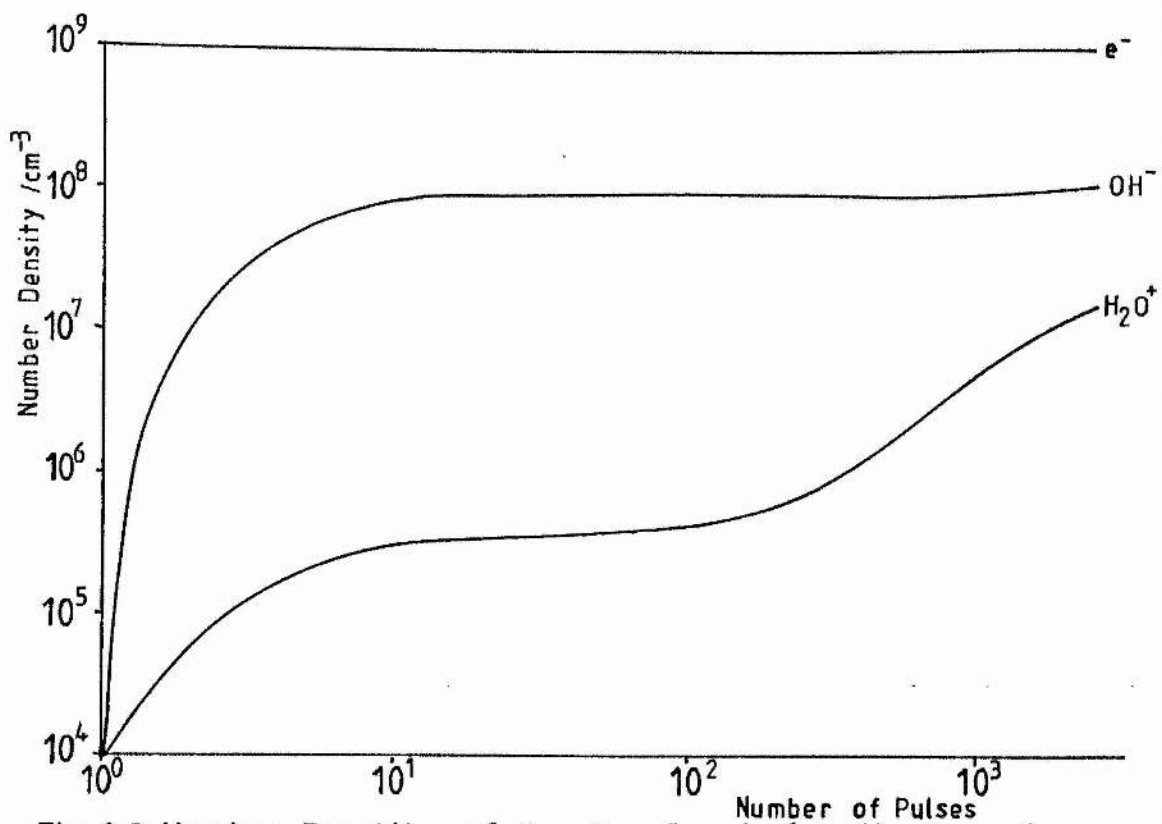


Fig 6-9 Number Densities of Species Created in the Computer Program against Number of Microwave Pulses

### Conclusions

This thesis has been concerned with the study of the performance of the TR cell throughout manufacture and life. In Chapter 2, theory of the microwave discharge and microwave transmission in a waveguide are discussed. Calculations of the refractive index, attenuation index and reflection and transmission coefficients of the microwave discharge lead to values of the electron density in the discharge as a function of input power. A discussion of the recovery period leads to the conclusion that electron capture by water vapour is the initial mechanism whereby electrons are removed from the discharge area after the microwave pulse. After a few microseconds, however, electron positive ion recombination in water vapour becomes the dominant mechanism.

In Chapter 3 a computer model was established, in which was calculated the temperature of the input window of the TR cell when varying microwave power levels were applied. In the program the dimensions and materials of the window were selected and the applied power entered. The mechanism of heat transfer was by conduction; radiation and convection losses were shown to be small in comparison. The output was in the form of temperatures at selected points across the TR cell window, frame and flange. Results produced in the computer program gave good agreement with experimental results obtained by EEV for several devices. The model may be used in the prediction of the power handling capacity of different window materials with varying dimensions, to

facilitate the design of TR cells with different operating requirements to those already in existence. The maximum error in the results produced by the program is estimated to be 10%, due mainly to the variation in thermal conductivity of the materials with temperature.

In Chapter 4 the manufacturing procedure of the TR cell was studied, through analysis of the microwave discharge in the cell and measurements made of the performance of the cell when subjected to high power microwave pulses. Observations on the manufacturing procedure were as follows. When the cell is baked at 300°C under vacuum for 1 1/4 hours, all the gases previously absorbed by it are desorbed, so minimising the presence of impurity gases. Oxygen and water vapour are then added; they are absorbed by the cell and may be released to the cell at a later stage. The cells are then filled with a mixture of argon and water vapour and stood for one week, to allow water vapour to be absorbed by the cell. No significant increase in the amount of water vapour absorbed occurs after three days. However, the week stand has a second purpose, that of the detection of leaks in the cell. Microwave power is then applied to the cell for 48 hours. The purpose of this operation is to allow the walls to absorb as much as possible of the hydrogen and oxygen, produced through the dissociation of water vapour by the discharge. Later in life, the cell absorbs less hydrogen and oxygen, which helps to slow down the loss rate of water vapour and hence to prolong life. It has been shown that the cells not subjected to microwave power for 48 hours during manufacture have a shorter lifetime, due to a more rapid loss of

water vapour, than other cells.

Some cells were allowed to stand for one week at 200° C instead of the normal room temperature. This had the effect of reducing the amount of water vapour absorbed by the cell at this stage. However, when microwave power was applied for 48 hours, greater amounts of hydrogen and oxygen were absorbed by the cell body. This had little overall effect on the cell performance or life. The decrease in water vapour absorbed by the cell during the week age stand to be released later in the life of the cell was offset by the greater degree of saturation of the cell with hydrogen and oxygen created through the dissociation of water vapour in the microwave discharge.

The effect of the keep-alive discharge on TR cell life was also studied. It was observed that the discharge at the keep-alive electrode caused dissociation of water vapour in the cell, resulting in a reduced partial pressure of water vapour and hence a reduced lifetime for the cell.

Measurements of the emission spectrum of the microwave excited discharge in the TR cell, measurements of its performance when subjected to high power microwave pulses and mass spectroscopic analysis of the gas in the cell were carried out throughout the life of the cell. Results from these experiments showed that throughout the life of the cell, water vapour was converted to hydrogen and oxygen through the action of the microwaves. Hydrogen was readily absorbed by the kovar of the TR cell window frame,

leaving the cell increasingly rich in oxygen and depleted of water vapour. Water vapour absorbed by the cell body earlier is released, to help prolong the cell lifetime. If the cell contained traces of carbon or nitrogen, however, the oxygen was rapidly converted into oxides of carbon or nitrogen.

In Chapter 6 a computer model of the microwave discharge in the TR cell has been established, using the available data on the reaction rates of argon and water vapour. Data is scarce for the reactions of argon and water vapour in a microwave discharge, so it has been adapted from similar systems, using the electron energy calculated for the microwave discharge. The model calculates the number densities of species present in the TR cell as a function of the number of microwave pulses. An estimate of the expected life of the cell is made, by calculating the time required for 5 torr water vapour to be lost from the discharge. The partial success of the model is due mainly to the unavailability of accurate data on reaction rates in microwave discharges. Clean-up in the TR cell is discussed, as is surface recombination of O, H and OH radicals. It has been shown that sufficient power can be released through recombination of these radicals on a glass surface to cause window failure in the TR cell.

In this thesis we have contributed to the existing information on the TR cell and its performance when subjected to microwave pulses.

Appendix 1

Physical Properties and Dimensions of the Materials in the TR Cell

X-Band TR Cell

Waveguide 16

Inside dimensions 2.286 cm x 1.016 cm

Outside dimensions 2.540 cm x 1.270 cm

Window Glass

Dimensions

Length 15.47 + 0.05 mm

Width 3.10 + 0.05 mm

Thickness 0.24 + 0.025 mm

Frame Kovar

Dimensions

Length 25.02 + 0.13 mm

Width 12.38 + 0.06 mm

Thickness 1.00 + 0.01 mm

Flange Steel

Dimensions

Length 41.28 + 0.25mm

Width 41.28 + 0.25 mm

Thickness 3.00 mm

Kovar

Thermal Conductivity k 17 W m<sup>-1</sup> K<sup>-1</sup>

Steel

Thermal Conductivity k 54 W m<sup>-1</sup> K<sup>-1</sup>

## Window Materials

### Glass

Specific Heat c	$0.837 \times 10^3 \text{ J kg}^{-1} \text{ K}^{-1}$
Thermal Conductivity k	$1.15 \text{ W m}^{-1} \text{ K}^{-1}$
Density	$2.28 \times 10^3 \text{ kg m}^{-3}$
Emissivity	0.93
Failure Temperature	800 K

### Glass Ceramic

Specific Heat c	$1.046 \times 10^3 \text{ J kg}^{-1} \text{ K}^{-1}$
Thermal Conductivity k	$2.51 \text{ W m}^{-1} \text{ K}^{-1}$
Density	$2.4 \times 10^3 \text{ kg m}^{-3}$
Failure Temperature	1373 K

### Alumina

Specific Heat c	$0.837 \times 10^3 \text{ J kg}^{-1} \text{ K}^{-1}$
Thermal Conductivity k	$13.0 \text{ W m}^{-1} \text{ K}^{-1}$
Density	$3.58 \times 10^3 \text{ kg m}^{-3}$
Failure Temperature	1400 K to 1700 K

### Corderite

Specific Heat c	$0.796 \times 10^3 \text{ J kg}^{-1} \text{ K}^{-1}$
Thermal Conductivity k	$2.93 \text{ W m}^{-1} \text{ K}^{-1}$
Density	$2.6 \times 10^3 \text{ kg m}^{-3}$
Failure Temperature	1573 K to 1623 K

Appendix 2

In this Appendix is listed the computer programme used in Chapter 3 to calculate the temperatures across a TR cell window having a chosen window material and chosen dimensions for a given power input.

The programme is written in Basic and is run on a Hewlett-Packard 9826A desk-top computer.

```
OPTION BASE 1
REAL A(20,20),B(20,20),C(20,1),D(20,1)
REAL E(20,1),F(20,1),Fr(20,1),G(20,1)
! D GIVES TEMP ALONG WINDOW CENTRE
! E GIVES TEMP ALONG WINDOW EDGE
! F GIVES TEMP ALONG FRAME/FLANGE BOUNDARY
! G GIVES TEMP ALONG FLANGE EDGE
Keys:ON KEY 0 LABEL "POWER" GOSUB Power
ON KEY 1 LABEL "MATERIAL" GOSUB Material
ON KEY 2 LABEL "LENGTH" GOSUB Length
ON KEY 3 LABEL "WIDTH" GOSUB Width
ON KEY 4 LABEL "THICKNESS" GOSUB Thickness
ON KEY 5 GOTO SPIN
ON KEY 6 GOTO SPIN
ON KEY 7 GOTO SPIN
ON KEY 8 GOTO Spin
ON KEY 9 LABEL "CALC" GOTO Calc
190 Spin:GOTO Spin !Wait for an input
!
Calc:N=INT((Le/(Wi/2))-1)
! N=NO OF POINTS ON WINDOW FOR WHICH THE
! TEMPERATURE IS TO BE CALCULATED
REDIM A(N,N),B(N,N),C(N,1),D(N,1),E(N,1),F(N,1),Fr(N,1),G(N,1)
FOR Ia=1 TO N
FOR Ib=1 TO N
A(Ia,Ib)=0
B(Ia,Ib)=0
NEXT Ib
C(Ia,1)=0
D(Ia,1)=0
E(Ia,1)=0
F(Ia,1)=0
Fr(Ia,1)=0
G(Ia,1)=0
NEXT Ia
W=(De*Sh*(Wi/2)^2*1.E-6)/Tk
!
! CALCULATION OF MATRIX A
FOR I=1 TO N
A(I,I)=-4-W
NEXT I
FOR J=1 TO N-1
A(J,J+1)=1
A(J+1,J)=1
NEXT J
MAT B= INV(A)
```

```
!
! CALC OF SPREAD OF POWER ON WINDOW
Z=INT(N/2)
IF N-2*Z=1 THEN Z=Z+1
FOR Ic=1 TO Z
Fr(Ic,1)=(S-Le+(Wi*Ic))/S
NEXT Ic
FOR Id=Z+1 TO N
Fr(Id,1)=Fr(N+1-Id,1)
NEXT Id
!
! CALC OF LINE MATRIX C AT TIME 0 SECONDS
! WINDOW AND FRAME AT 293 K AT 0 SECONDS
FOR K=2 TO N-1
C(K,1)=-(Wi*1.E+3*Pa*Fr(K,1))/(Tk*4*Le*Th)-586.-W*293.
NEXT K
C(1,1)=-(Wi*1.0E+3*Pa*Fr(1,1))/(Tk*4*Le*Th)-879.-W*293.
C(N,1)=C(1,1)
!
INPUT "HEATING TIME IN SECONDS",T1
FOR M=1 TO T1-1
MAT D= B*C
!
! CALC OF C FOR TIME T1>0
X=(Tk*(Q-Wi))/(17*Wi)
Y=(17*(S-Q))/(54*(Q-Wi))
V=(54*.03)/((S-Q)*.241)
FOR Ni=1 TO N
E(Ni,1)=(D(Ni,1)*X+293/(1+Y))/(1+X-Y/(1+Y))
F(Ni,1)=(E(Ni,1)*Y+293/(1+V))/(1+Y-V/(1+V))
G(Ni,1)=(F(Ni,1)*V+293)/(1+V)
NEXT Ni
FOR L=2 TO N-1
C(L,1)=-(Wi*1.E+3)/(4*Le*Th*Tk)*Fr(L,1)*Pa-D(L,1)*W-2*E(L,1)
NEXT L
C(1,1)=-(Wi*1.E+3/(Tk*4*Le*Th))*Fr(1,1)*Pa-D(1,1)*W-3*E(1,1)
C(N,1)=C(1,1)
!
NEXT M
PRINT "INPUT POWER IN WATTS IS";P
PRINT "HEATING TIME IN SECONDS IS";
PRINT USING "4D.D";T1
PRINT "TEMPERATURE AT SPECIFIED POINTS";Wi/2;"MM APART"
PRINT USING "5D.DD";D(*)
PRINT
PRINT "TEMPERATURES ALONG WINDOW EDGE"
PRINT USING "4D.2D";E(*)
PRINT
PRINT "TEMPERATURES ALONG FRAME/FLANGE BOUNDARY"
PRINT USING "4D.2D";F(*)
PRINT
PRINT "TEMPERATURES ALONG FLANGE EDGE"
PRINT USING "4D.2D";G(*)
PRINT
INPUT "CHANGE ANY VALUES?, 1=YES, 2=NO", R
ON R GOTO 190,1520
Power:INPUT "POWER IN WATTS", P
! Pa ARC LOSS = 0.8DB
```

```
Pa=((10^.08-1)*P)/10^.08
RETURN
Material:INPUT "WINDOW MATERIAL, 1=GLASS, 2=CERAMIC, 3=ALUMINA, 4=CORDERITE", Ma
ON Ma GOSUB G1, Gc, A1, Co
RETURN
! Tk=THERMAL CONDUCTIVITY, De=DENSITY, Sh=SPECIFIC HEAT
G1:Tk=1.15
De=2.28E+3
Sh=8.37E+2      !GLASS
RETURN
Gc:Tk=2.51
De=2.4E+3
Sh=1.046E+3    !CERAMIC
RETURN
A1:Tk=13.0
De=3.58E+3
Sh=8.37E+2     !ALUMINA
RETURN
Co:Tk=2.93
De=2.60E+3
Sh=7.955E+2    !CORDERITE
RETURN
Length:INPUT "WINDOW LENGTH IN mm", Le
RETURN
Width:INPUT "WIDTH IN mm (must be less than length)", Wi
RETURN
Thickness:INPUT "THICKNESS IN mm", Th
RETURN
1520 END
```

### Appendix 3

#### Magnetron

The microwave power source used to excite the discharge in the TR cell and for some pre-TR tube experiments is the magnetron. A magnetron is a diode with a cathode and anode in a cylindrical assembly. The anode may be split into two parts in a simple magnetron, or it may comprise multiple cavities which resonate at the operating frequency. The whole assembly is mounted in a magnetic field parallel to the axis of the electrodes. The magnet may be a close-fitting separate assembly, or a part of the valve. The axial field of the magnet causes the path of the electrons leaving the cathode to be curved. At a certain field strength the electrons fail to reach the anode and return to the cathode. The time taken for an electron to complete its orbital journey determines the oscillation frequency. The kinetic energy associated with the moving electrons is given up to the space around the cathode, transferred to the resonant cavities and coupled out into an associated waveguide by a loop and probe or by a windowed slot cut in the back of one of the cavities. The magnetron efficiency  $\eta$  is given by

$$\eta = (P_{in} - P_{loss}) / P_{in} = \mu_{lc} \mu_e \quad (A3.1)$$

where  $P_{in}$  is the power input to the magnetron,  $P_{loss}$  is the power lost,  $\mu_{lc}$  is the power available to the load (circuit efficiency) and  $\mu_e$  is the fraction of the input power converted to rf power (rf efficiency).

The magnetron supplied by EEV has the following operating characteristics.

Frequency	9.4 GHz
Pulse Repetition Frequency	3 kHz or 50 Hz
Pulse Length/microseconds	0.08 0.3 1.0
Maximum Mean Power/W	3.04 5.29 12.09

#### Appendix 4

##### The t-Test

The t-test is a statistical test on small (under 30) samples of data. We define t by

$$t = (x - \bar{x})(N - 1)^{.5}/s \quad , \quad (A4.1)$$

where  $x$  is the sample mean,  $s$  the sample standard deviation,  $\bar{x}$  the mean of the larger population from which the sample is drawn and  $N$  is the sample size (M R Spiegel (1972)).

The t-test may be performed on two random samples which are assumed to come from normal populations which have equal standard deviations. The samples have means  $x_1$  and  $x_2$ , respectively and standard deviations  $s_1$  and  $s_2$ , respectively. To test the hypothesis that the samples come from the same population, we calculate t for the two samples by

$$t = (x_1 - x_2)/((1/N_1 + 1/N_2)^{.5}) \quad , \quad (A4.2)$$

where

$$= ((N_1 s_1^2 + N_2 s_2^2)/(N_1 + N_2 - 2))^{.5} \quad . \quad (A4.3)$$

The distribution of t is Student's distribution, with  $N_1 + N_2 - 2$  degrees of freedom.

We calculated t for the distribution of intensities of the spectral lines from the microwave excited discharge in each cell for the two batches of cells. The value of t for 22 degrees of freedom for each spectral line was found to lie outside the 95% confidence level. So the probability that the two samples of cells

come from the same normal distribution of intensities of spectral lines of the cells is less than 95%. However, both batches of cells fulfilled their manufacturing requirements.

M R Spiegel (1972) Schaum's Outline of Theory and Problems of  
Statistics, McGraw-Hill Book Co, UK

Appendix 5

Computer Program to Analyse the Mass Spectra Data

- c This program fits the given mass spectrum for the given compounds
- c using a least square solution of linear simultaneous equations.
- c The cracking patterns are stored in f007.dat.

```
implicit real*8 (a-h,o-z)
integer ticurve
character*6 cname(30)
character*52 title
dimension height(50,50),b(50),massno(50),xht(10),
1      xmassht(50),lmassno(10),work(200),bx(50),
2      calcht(50),height2(50,50),massout(50),outht(50)
logical svd
c
c
write(5,555)
555 format(' data input, return 5 for terminal, 9 for for009 : '$)
read *, mdata
ngraph=0
write(5,556)
556 format(' return 1 if graph required: ', $)
read *, ngraph
if(ngraph.eq.1)open (unit=3,file='plotdata.dat',
1      status='new')
open(unit=12,file='specout.dat',status='new')
5 write(5,1)
1 format(' Spectrum No. and time: ', $)
read(mdata,*)title,ticurve
write(5,15)
15 format(' No. of peaks in the sample spectrum: '$)
read(mdata, *) n
write(5,25)
25 format(' Mass nos. and mass heights of sample spectrum: '$)
read (mdata,*) (massno(i),xmassht(i),i=1,n)
y=vmax(xmassht,n)
write (5,111)y
111 format(' Peak value in spectrum:'f8.2/)
write(5,112)title,ticurve
write(12,112)title,ticurve
112 format('//65('+'')/1x,a52,2x,'time:',i4,/)
if(ngraph.ne.1)go to 558
write(5,557)
557 format(' curveno, pointno: ', $)
read *, ncurve, npoint
558 write (5,279)(massno(i),xmassht(i),i=1,n)
write (12,279)(massno(i),xmassht(i),i=1,n)
279 format('/' m/e and magnitudes '//4(5x,i3,2x,1pg10.3))
do 6 i=1,50
do 6 j=1,50
b(i)=0.0
height(i,j)=0.0
6 continue
do 40 i=1,n
b(massno(i))=xmassht(i)
```

```
bx(massno(i))=xmassht(i)
40 continue
   jx=1
   rewind 7
50 read(7,65,end=100)cname(jx)
65 format(a6)
   read(7,375)(lmassno(i),i=1,10)
375 format(10(i3,1x))
   read(7,385)(xht(i),i=1,10)
385 format(10(f5.1,1x))
   do 300 i=1,10
   if(lmassno(i).eq.0)go to 300
   height(lmassno(i),jx)=xht(i)
   height2(lmassno(i),jx)=xht(i)
300 continue
   jx=jx+1
   go to 50
100 m=50
   jx=jx-1
   lwork=4*jx
   ifail=0
   nra=m
   tol=.00001
   call f04jgf(m,jx,height,m,b,tol,svd,sigma,irank,
1       work,lwork,ifail)
   if(ifail.ne.0)go to 150
   write(5,125)
   write(12,125)
   if(ngraph.eq.1)write(3,1250)ncurve,npoint,jx,ticurve
1250 format(5x,3i3,i4)
125 format(//' Compound',t15,'Calc value',t30,'Rel value')
   bmax=vmax(b,jx)
   do 51 i=1,jx
   if(ngraph.eq.1)write(3,1350)cname(i),b(i)
1350 format(5x,a6,e11.4)
   write(5,135)cname(i),b(i),b(i)/bmax
   write(12,135)cname(i),b(i),b(i)/bmax
135 format(5x,a6,3x,1pg10.3,5x,1pg10.3)
51 continue
   write(12,145)sigma,svd,irank
   write(5,145)sigma,svd,irank
145 format(//' Standard error:',1pg10.3,' SVD:',l3,4x,
1 ' IRANK:',i3,/'+'//)
   go to 140
   write(5,950)
   write(12,950)
950 format(//' Calculated(measured) mass spectrum, heights(in mm) < 5
1 omitted: '//)
   do 1156 mx=1,m
   calcht(mx)=0.
   do 1155 j=1,jx
   if(height2(mx,j).eq.0.)go to 1155
   calcht(mx)=calcht(mx)+height2(mx,j)*b(j)
1155 continue
   calcht(mx)=calcht(mx)*heht*1.0e-5
1156 continue
   jcount=1
   do 999 i=1,m
```

```
massout(jcount+1)=0.
outht(jcount+1)=0.
if(calcht(i).lt.5)go to 999
massout(jcount)=i
outht(jcount)=calcht(i)
jcount=jcount+1
999 continue
write(5,988)(massout(jc),outht(jc),
1bx(massout(jc)),jc=1,jcount)
write(12,988)(massout(jc),outht(jc),bx(massout(jc)),
1jc=1,jcount)
988 format(3(1x,i4,':',f8.3,'(',f6.1,')',2x))
go to 140
150 write(5,175)ifail
175 format(' ifail=',i2)
140 write(5,155)
155 format(' Type 0 to stop,
1 2 for fresh data:'$)
read *, ixx
if(ixx.eq.0) stop
if(ixx.eq.2) go to 5
close (unit=3)
close(unit=12)
stop
end
function vmax(array,n)
real*8 array(n),vmax,x
x=array(1)
do 10 i=2,n
10 if(x.lt.array(i))x=array(i)
vmax=x
return
end
```

This File contains the Cracking Pattern Data called in the above Program

H2  
002  
100.  
02  
032 016  
100.0 006.9  
N2  
028 014 029  
100. 004.7 000.7  
Ar  
040 020  
100.0 013.  
H2O  
018 017 016  
100.0 021.0 001.  
CO  
028 012 014 016 029  
100.0 005.0 001.0 002.0 001.13  
CO2  
044 032 028 016 022 012 029  
100.0 000.1 010.0 010.0 002.0 009.0 000.1  
NO  
030 014 015 016 031 032  
100.0 007.5 002.4 001.5 000.4 000.2  
N2O  
044 030 014 028 016 045 046 015 029 031  
100.0 014.1 003.0 014.0 014.0 000.7 000.2 000.1 000.1 000.1  
NO2  
030 046 016 014 047  
100.0 037.0 022.3 009.6 000.1  
CH4  
002 012 013 014 015 016 017  
003.0 002.4 007.7 015.6 085.8 100.0 001.2

Appendix 6 The Computer Program to Model the TR Cell Discharge

```
c  programme to solve series of 1st order rate equations
c  nag routine d02eaf - stiff equations
c  pulse + recovery time + interpulse period
c  file output included
c  O, H and OH recombination variable-input to program
c  rate Ar + e -> Ar+ +2e variable-input to program
c  H2O dissociation by electrons included
implicit none
real*8 x,w(15,68),y(15),xend,tol,c,e,ar,rec
real*8 x1,w1(15,68),z(15),xend1
real*8 x2,w2(15,68),v(15),xend2
integer s,u,ifail,i,iw,ir,n,j,k,iw1,n1,time,iw2,n2,r
      common ar,rec
external fcn,fcn1,fcn2
n=15
n1=15
      n2=15
      r=1
      s=1
      u=1
c  (1)=Ar (2)=Ar* (3)=Ar+ (4)=H2O (5)=H- (6)=H (7)=OH
c  (8)=e (9)=OH- (10)=O (11)=O2 (12)=H2 (13)=ArH+
c  (14)=H3O+ (15)= H2O+
write(6,44)
44 format(' number density')
read*,c
      y(3)=c
y(2)=c
write(6,30)
30 format(' electron density')
read*,e
      write (6,29)
29 format(' rate Ar+e ->Ar+')
read*,ar
      write (6,32)
32 format(' rate O,H,OH recombine')
read*,rec
y(1)=3.3e17
y(4)=3.3e17
      y(8)=e
do 15 i=5,7
y(i)=c
15 continue
do 10 i=9,15
y(i)=c
10 continue
iw=68
iw1=68
      iw2=68
      write(6,117)
117 format(1x,'time',9x,'Ar',11x,'Ar*',10x,'Ar+',10x,'H2O')
write (6,122)x,(y(i),i=1,4)
write(6,118)
118 format(1x,'H-',11x,'H',12x,'OH',11x,'e',12x,'OH-',10x,'O')
```

```
119  format(1x,'O2',11x,'H2',11x,'ArH+',9x,'H2O+',9x,'H3O+')
      write(6,123)(y(i),i=5,10)
      write(6,119)
124  format(1x,5(e12.6,1x))
      write(6,124)(y(i),i=11,15)
123  format(1x,6(e12.6,1x))
      write(6,55)
55  format(1x,' number of pulses')
      read*,time
      do 33 k=1,time
      x=0+1e-3*(k-1)
      tol=1.e-1
      xend=1e-6+1e-3*(k-1)
      y(8)=e
      call d02eaf(x,xend,n,y,tol,fcn,w,iw,ifail)
122  format(1x,5(e12.6,1x))
4    if (k-r*1000) 1,2,3
3    r=r+1
      go to 4
2    write(6,117)
      write(6,122)xend,(y(i),i=1,4)
      write(6,118)
      write(6,123)(y(i),i=5,10)
      write(6,119)
      write(6,124)(y(i),i=11,15)
      write(7,122)xend,(y(i),i=1,4)
      write(7,123)(y(i),i=5,10)
      write(7,124)(y(i),i=11,15)
      continue
1    continue
      do 20 i=1,15
      z(i)=y(i)
20  continue
      tol=1e-1
      x1=xend
      xend1=3e-6+1e-3*(k-1)
      call d02eaf(x1,xend1,n1,z,tol,fcn1,w1,iw1,ifail)
8    if (k-s*1000) 5,6,7
7    s=s+1
      goto 8
6    write(6,117)
      write(6,122)xend1,(z(i),i=1,4)
      write(6,118)
      write(6,123)(z(i),i=5,10)
      write(6,119)
      write(6,124)(z(i),i=11,15)
      write(7,122)xend1,(z(i),i=1,4)
      write(7,123)(z(i),i=5,10)
      write(7,124)(z(i),i=11,15)
      continue
5    continue
31  do 40 i=1,15
      v(i)=z(i)
40  continue
      tol=1e-1
      x2=xend1
      xend2=1e-3*k
      call d02eaf(x2,xend2,n2,v,tol,fcn2,w2,iw2,ifail)
```

```
11   if(k-u*1000) 12,13,14
14     u=u+1
      goto 11
13   write(6,117)
write(6,122)xend2,(v(i),i=1,4)
      write(6,118)
write(6,123)(v(i),i=5,10)
      write(6,119)
write(6,124)(v(i),i=11,15)
write(7,122)xend2,(v(i),i=1,4)
write(7,123)(v(i),i=5,10)
write(7,124)(v(i),i=11,15)
      continue
12   continue
      do 50 i=1,15
        y(i)=v(i)
50   continue
33  continue
      stop
      end
      subroutine fon(t,y,f)
      real*8 t,y(15),f(15),ar,rec
      common ar,rec
      f(1)=(-ar*y(1)*y(8))+1.5e-10*y(3)*y(4)
      * -2.1e-13*y(1)*y(8)+(y(2)**2)*1.2e-9+y(13)*y(4)*4.5e-9
      f(2)=y(1)*y(8)*2.1e-13-(y(2)**2)*1.2e-9
      f(3)=ar*y(1)*y(8)+(y(2)**2)*1.2e-9-y(3)*y(4)*1.45e-9
      f(4)=2.5e-12*(y(7)**2)-y(3)*y(4)*1.45e-9-y(13)*y(4)*4.5e-9
      * -y(15)*y(4)*1.3e-9+(y(7)**2)*rec-y(4)*y(8)*2e-9
      f(6)=2e-11*y(7)*y(10)-(y(6)**2)*rec+y(4)*y(8)*2e-9
      * +y(12)*y(8)*2e-9**2
      f(7)=-2.5e-12*(y(7)**2)-2e-11*y(7)*y(10)+y(3)*y(4)*1.3e-9
      * +y(4)*y(15)*1.3e-9-(y(7)**2)*rec+y(4)*y(8)*2e-9
      f(8)=1.2e-9*(y(2)**2)+ar*y(1)*y(8)
      f(10)=2.5e-12*(y(7)**2)-2e-11*y(7)*y(10)-(y(10)**2)*rec
      * +(y(7)**2)*rec+y(11)*y(8)*2e-9**2
      f(11)=2e-11*y(7)*y(10)+(y(10)**2)*rec-y(11)*y(8)*2e-9
      f(12)=rec*(y(6)**2)-y(12)*y(8)*2e-9
      f(13)=y(3)*y(4)*1.3e-9-y(13)*y(4)*4.5e-9
      f(14)=y(13)*y(4)*4.5e-9+y(15)*y(4)*1.3e-9
      f(15)=y(4)*y(3)*1.5e-10-y(4)*y(15)*1.3e-9
      return
      end
      subroutine fon1(t,z,f)
      real*8 t,z(15),f(15),ar,rec
      common ar,rec
      f(1)=2.8e-10*z(2)*z(8)+z(3)*z(8)*6e-10
      f(2)=-2.8e-10*z(2)*z(8)
      f(3)=-6e-10*z(3)*z(8)
      f(4)=-1.3e-13*z(4)*z(8)-3.8e-9*z(4)*z(5)+2.5e-12*(z(7)**2)
      * +z(6)*z(9)*1.0e-9+z(14)*z(8)*1.1e-6+z(15)*z(8)*4.1e-6
      * +(z(7)**2)*rec
      f(5)=1.3e-13*z(4)*z(8)-3.8e-9*z(4)*z(5)
      f(6)=3.8e-9*z(4)*z(5)**2+2e-11*z(7)*z(10)-(z(6)**2)*rec
      * -z(9)*z(6)*1.0e-9+1.1e-6*z(14)*z(8)
      f(7)=1.3e-13*z(4)*z(8)-2.5e-12*(z(7)**2)-2e-11*z(7)*z(10)
      * -(z(7)**2)*rec
      f(8)=z(6)*z(9)*1.0e-9-1.3e-13*z(4)*z(8)-6e-10*z(3)*z(8)
```

```

* -z(14)*z(8)*1.1e-6-z(15)*z(8)*4.1e-6
f(9)=3.8e-9*z(4)*z(5)-z(6)*z(9)*1.0e-9
f(10)=-rec*(z(10)**2)+2.5e-12*(z(7)**2)-2e-11*z(7)*z(10)
* +(z(7)**2)*rec
f(11)=2e-11*z(7)*z(10)+(z(10)**2)*rec
f(12)=(z(6)**2)*rec
f(14)=-z(14)*z(8)*1.1e-6
f(15)=-z(15)*z(8)*4.1e-6
return
end
subroutine fcn2(t,v,f)
real*8 t,v(15),f(15),ar,rec
common ar,rec
f(1)=2.8e-10*v(2)*v(8)+v(3)*v(8)*6e-10
f(2)=-2.8e-10*v(2)*v(8)
f(3)=-v(3)*v(8)*6e-10
f(4)=2.5e-12*(v(7)**2)+v(14)*v(8)*1.1e-6+v(15)*v(8)*4.1e-6
* +(v(7)**2)*rec
f(6)=2e-11*v(7)*v(10)-(v(6)**2)*rec+v(8)*v(14)*1.1e-6
f(7)=-2.5e-12*(v(7)**2)-2e-11*v(7)*v(10)-(v(7)**2)*rec
f(8)=-v(14)*v(8)*1.1e-6-v(3)*v(8)*6e-10-v(15)*v(8)*4.1e-6
f(10)=-2e-11*v(7)*v(10)+2.5e-12*(v(7)**2)-(v(10)**2)*rec
* +(v(7)**2)*rec
f(11)=2e-11*v(7)*v(10)+(v(10)**2)*rec
f(12)=(v(6)**2)*rec
f(14)=-v(14)*v(8)*1.1e-6
f(15)=-v(15)*v(8)*4.1e-6
return
end

```

Initial Values for the Variables Input to the Program

Species Number Density	$1 \times 10^3 \text{ cm}^{-3}$
Electron Number Density	$1 \times 10^9 \text{ cm}^{-3}$
Ionization Rate of Argon	$10^{-14} \text{ cm}^3 \text{ s}^{-1}$
Recombination Rate of	$10^{-10}$
O, H and OH Radicals	

Final Values for the Variables Input to the Program

Species Number Density	$1 \times 10^4 \text{ cm}^{-3}$
Electron Number Density	$1 \times 10^9 \text{ cm}^{-3}$
Ionization Rate of Argon	$10^{-15} \text{ cm}^3 \text{ s}^{-1}$
Recombination Rate of	$1.8 \times 10^{-10}$
O, H and OH Radicals	